CHEMICALLY MODIFIED CARBON-BASED ELECTRODES FOR THE DETECTION OF SOME SUBSTANCES OF ENVIRONMENTAL AND BIOMEDICAL SIGNIFICANCE

By

EMILY ANNE HUTTON

A Thesis Submitted for the Degree

of

Doctor of Philosophy

Dublin City University
Dublin 9, Ireland

National Institute of Chemistry
Ljubljana, Slovenia

September 2003

DECLARATION

I hereby declare that the contents of this thesis, except where otherwise stated, are based entirely on my own work, which was carried out in the National Centre for Sensor Research, School of Chemical Sciences, Dublin City University, Dublin, Ireland, and the Analytical Chemistry Laboratory, National Institute of Chemistry, Ljubljana, Slovenia.

Emily Hutton

Emily Anne Hutton

Prof. Malcolm R. Smyth
(supervisor)

Dr. Božidar Ogorevc
(supervisor)

Do mo thuismitheoirí, mo chlann agus Jure

Mojim staršem, družini in Juretu

ACKNOWLEDGEMENTS

I would like to sincerely thank my two supervisors Prof. Malcolm R. Smyth and Dr. Božidar Ogorevc for all their advice, help, encouragement and support.

Thanks also to Dr. Samo Hočevar for all his help, and to the whole MRS Research Group in DCU.

I would like to thank the National Centre for Sensor Research, Dublin City University for funding and the National Institute of Chemistry, Ljubljana for partial support.

I'm also grateful for the help of the technical staff in both Dublin City University and the National Institute of Chemistry.

Thanks to Dr. J.T. van Elteren for providing the soil extracts and ICP-MS results.

And last, but not least, I would like to thank my family, especially my parents, for all their support (financial and other!) over the whole course of my studies.

TABLE OF CONTENTS

		Page No.
Title page		i
Declaration		ii
Dedication		iii
Acknowledgements		iv
Table of Contents		v
List of publications, presentations and contributions		xii
Abstract		xv

CHAPTER 1: AN INTRODUCTION TO ELECTROANALYTICAL PRINCIPLES, CARBON-BASED ELECTRODES, AND ELECTRODE MODIFICATION

1.1	GENERAL INTRODUCTION	1
1.2	FUNDAMENTALS OF ELECTROANALYSIS	2
1.2.1	Introduction	2
1.2.2	Voltammetric Cell	2
1.2.3	Electrochemical Processes	5
1.2.4	Voltammetric, Amperometric, and Potentiometric Techniques	10
1.2.4.1	*Linear Sweep Voltammetry*	11
1.2.4.2	*Cyclic Voltammetry*	12
1.2.4.3	*Square Wave Voltammetry*	15
1.2.4.4	*Differential Pulse Voltammetry*	15
1.2.4.5	*Hydrodynamic Amperometry*	16
1.2.4.6	*Anodic Stripping Voltammetry and Potentiometric Stripping Analysis*	18
1.3	CARBON BASED ELECTRODES	20
1.3.1	Glassy Carbon Electrodes	20
1.3.1.1	*Composition and Features*	20
1.3.1.2	*Construction of Glassy Carbon Electrode*	20

1.3.2	Carbon Paste Electrodes	21
1.3.2.1	*Composition and Features*	21
1.3.3	Screen Printed Electrodes	22
1.3.3.1	*Composition and Features*	22
1.3.4	Microelectrodes	23
1.3.4.1	*Definition and Trends in Development*	23
1.3.4.2	*Intrinsic Voltammetric Advantages*	23
1.3.4.3	*Shapes, Responses and Fabrication*	28
1.3.4.4	*Carbon Fibre Microelectrodes*	30
1.4	ELECTRODE MODIFICATION	32
1.4.1	Definition and Purpose	32
1.4.2	Surface Modification Approaches	37
1.5	CONCLUSIONS	41
1.6	REFERENCES	42

CHAPTER 2: CATHODIC ELECTROCHEMICAL DETECTION OF NITROPHENOLS AT A BISMUTH FILM ELECTRODE

2.1	INTRODUCTION	46
2.2	NITROPHENOLS AND SIGNIFICANCE FOR MEASUREMENT	47
2.2.1	2-Nitrophenol	47
2.2.2	4-Nitrophenol	48
2.2.3	2,4-Dinitrophenol	49
2.3	DETECTION OF NITROPHENOLS	49
2.3.1	4-Aminoantipyrine Method	50
2.3.2	Gas Chromatographic and Capillary Electrophoretic Methods	50
2.3.3	Liquid Chromatographic Methods	51
2.3.4	Some Other Methods	54
2.4	ELECTROCHEMISTRY OF NITROPHENOLS	55
2.4.1	Electrochemical Behaviour of the Nitro Group	55
2.4.1.1	*Oxidation Reactions*	55

2.4.1.2	*Reduction Reactions*	56
2.4.2	Electrochemical Determination of Nitrophenols	59
2.5	BISMUTH FILM ELECTRODE	61
2.5.1	Introduction	61
2.5.2	Bismuth and Bismuth-Coated Electrodes – Analytical Performance	62
2.6	CATHODIC ELECTROCHEMICAL DETECTION OF NITROPHENOLS AT THE BISMUTH FILM ELECTRODE	63
2.6.1	Experimental	63
2.6.1.1	*Apparatus*	63
2.6.1.2	*Reagents and Materials*	64
2.6.1.3	*Preparation of BiFE, MFE and GCE*	64
2.7	RESULTS AND DISCUSSION	65
2.7.1	Preparation, Optimisation and Background Behaviour of the BiFE	65
2.7.2	Comparison of BiFE with GCE and MFE	68
2.7.3	Electrochemical Behaviour of Nitrophenols at BiFE	73
2.7.4	Influence of pH and Solution Composition	75
2.7.5	Calibration	79
2.7.6	Potential Effect on Response of BiFE and Hydrodynamic Amperometry	80
2.7.7	Flow Injection Analysis of Nitrophenols	82
2.8	CONCLUSIONS	85
2.9	REFERENCES	86

CHAPTER 3: THE BISMUTH FILM ELECTRODE FOR ADSORPTIVE STRIPPING VOLTAMMETRIC AND POTENTIOMENTRIC STRIPPING ANALYSIS OF TRACE COBALT AND NICKEL IN SOME LOW-VOLUME BODY FLUIDS, AND APPLICATION IN THE DETERMIATION OF SELECTED HEAVY METALS IN SOIL EXTRACTS

3.1	INTRODUCTION	90
3.2	COBALT, NICKEL AND HEAVY METALS AND SIGNIFICANCE FOR MEASUREMENT	92
3.2.1	Cobalt	92
3.2.1.1	*Introduction*	92
3.2.1.2	*Cobalt in the Environment and Human Body*	92
3.2.2	Nickel	94
3.2.2.1	*Introduction*	94
3.2.2.2	*Nickel in the Environment and Human Body*	94
3.2.3	Other Heavy Metals Measured in this Work	96
3.2.3.1	*Cadmium*	96
3.2.3.2	*Copper*	97
3.2.3.3	*Lead*	98
3.3	DETECTION OF HEAVY METALS	99
3.3.1	Non-Electrochemical Methods	99
3.3.2	Electrochemical Methods	103
3.3.2.1	*Introduction*	103
3.3.2.2	*Anodic Stripping Voltammetry*	106
3.3.2.3	*Cathodic Adsorptive Stripping Voltammetry and Potentiometric Stripping Analysis*	109
3.4	ADSORPTIVE STRIPPING VOLTAMMETRY AND POTENTIOMETRIC STRIPPING ANALYSIS OF TRACE COBALT AND NICKEL IN SOME LOW-VOLUME BODY FLUIDS	114
3.4.1	Experimental	114
3.4.1.1	*Apparatus*	114

3.4.1.2	*Reagents and Solutions*	114
3.4.1.3	*Preparation of GCE, MFE and BiFE*	115
3.4.1.4	*Procedures*	116
3.5	RESULTS AND DISCUSSION	116
3.5.1	Comparison of BiFE with GCE and MFE for Cobalt	116
3.5.2	Comparison of BiFE with MFE for Cobalt and Nickel	118
3.5.3	Optimisation of the Bismuth Film Electrode	120
3.5.4	Optimisation of Parameters for Trace Measurement of Cobalt	121
3.5.5	Investigation of Processes of Co and Co + Ni at BiFE	126
3.5.6	Comparison of Stripping Potential Scan Modes for Cobalt Measurement	130
3.5.7	Comparison of Stripping Potential Scan Modes for Simultaneous Cobalt and Nickel Measurement	132
3.5.8	Simultaneous Measurement of Cobalt and Nickel	134
3.5.9	Analytical Performance of BiFE for Cobalt and Nickel	136
3.5.10	Measurement of Trace Cobalt and Nickel in Some Low-Volume Artificial Body Fluids	138
3.6	APPLICATION OF BiFE IN THE DETERMINATION OF SELECTED HEAVY METALS IN SOIL EXTRACTS	143
3.6.1	Introduction	143
3.6.2	Experimental Procedures for Analysis of Soil Extracts	145
3.7	RESULTS AND DISCUSSION	146
3.7.1	Preliminary Investigation of Nickel in a Soil Extract Sample	146
3.7.2	Heavy Metal (Zn, Cd, Pb, Cu, Co, Ni) Measurements at a Preplated BiFE	148
3.7.3	Comparison of Adsorptive and Anodic Stripping Voltammetry Measurement of Heavy Metals in Soil Extracts at BiFE with ICP-MS	154
3.7.4	Use of Voltammetric and ICP-MS Results for Determination of K_D and a_o for Cadmium and Cobalt in Soil Extracts	158
3.8	CONCLUSIONS	160
3.9	REFERENCES	161

CHAPTER 4: AN ELECTROCHEMICAL MICROSENSOR FOR THE SELECTIVE DETERMINATION OF ASCORBIC ACID IN GASTRIC JUICE

4.1	INTRODUCTION	166
4.2	ASCORBIC ACID IN THE HUMAN BODY	168
4.2.1	Structure and Oxidation Reaction	168
4.2.2	Physiological Roles and Levels in Gastric Juice	169
4.2.3	Significance of Ascorbic Acid Measurement in Gastric Juice	171
4.3	METAL HEXACYANOFERRATES	172
4.3.1	Functions as Electrode Modifiers	172
4.3.2	Some Applications of Metal Hexacyanoferrate-Modified Electrodes	174
4.4	DETECTION OF ASCORBIC ACID	176
4.4.1	Non-Electrochemical Methods	177
4.4.2	Electrochemical Methods In Non-Physiological Media	179
4.4.3	Electrochemical Methods In Physiological Media	185
4.5	SELECTIVE DETERMINATION OF ASCORBIC ACID AT A NICKEL OXIDE,RUTHENIUM HEXACYANOFERRATE MODIFIED CARBON FIBRE MICROELECTRODE	187
4.5.1	Experimental	187
4.5.1.1	*Apparatus*	187
4.5.1.2	*Reagents and Solutions*	188
4.5.1.3	*Fabrication of Carbon Fibre Cylinder Microelectrodes*	188
4.5.1.4	*Modification of CFCMEs with Metal Hexacyanoferrates*	189
4.5.1.5	*Modification of CFCMEs with NiO,RuHCF and Variants*	190
4.5.1.6	*Further Modification of NiO,RuHCF-Modified Electrode*	190
4.6	RESULTS AND DISCUSSION	191
4.6.1	Some Preliminary Results for Ascorbic Acid Oxidation at Metal Hexacyanoferrate Modified CFCMEs	191
4.6.2	Preparation and Optimisation of the NiO,RuHCF Modified Microsensor	198

4.6.3	Preliminary Characterisation of the NiO,RuHCF Modified Microsensor	203
4.6.4	Electrochemical Oxidation of Ascorbic Acid at the NiO,RuHCF Modified Microsensor	206
4.6.5	Potential Effect on the Response of the Microsensor	207
4.6.6	Analytical Performance of the NiO,RuHCF Modified Microsensor Under Acidic Conditions	209
4.6.7	Performance of the NiO,RuHCF Modified Microsensor in Model Solution and Real Gastric Juice	213
4.7	CONCLUSIONS	225
4.8	REFERENCES	226

CHAPTER 5: CONCLUDING REMARKS AND SUGGESTIONS FOR FUTURE WORK

5.1	INTRODUCTION	231
5.2	CHAPTER TWO	232
5.3	CHAPTER THREE	233
5.4	CHAPTER FOUR	235
5.5	OTHER INTERESTING CONCEPTS CONSIDERED IN THE WORK	235
5.6	CONCLUSIONS	237
5.7	REFERENCES	237

LIST OF PUBLICATIONS, PRESENTATIONS AND CONTRIBUTIONS

Papers

- E.A. Hutton, B. Ogorevc, S.B. Hočevar, F. Weldon, M.R. Smyth, J. Wang
  An Introduction to Bismuth Film Electrode for use in Cathodic Electrochemical Detection
  Electrochemistry Communications **3** (2001) 707

- E.A. Hutton, S.B. Hočevar, B. Ogorevc, M.R. Smyth
  Bismuth Film Electrode for Simultaneous Adsorptive Stripping Analysis of Trace Cobalt and Nickel Using Constant Current Chronopotentiometric and Voltammetric Protocol
  Electrochemistry Communications **5** (2003) 765

- E.A. Hutton, B. Ogorevc, M.R. Smyth
  Bismuth Film Electrode for use in Continuous Flow Analysis of Nitrophenols
  Submitted (Electroanalysis)

- E.A. Hutton, J.T. van Elteren, B. Ogorevc, M.R. Smyth
  Validation of Bismuth Film Electrode for Determination of Cobalt and Cadmium in Soil Extracts using ICP-MS
  Submitted (Talanta)

- E.A. Hutton, S.B. Hočevar, B. Ogorevc, M.R. Smyth
  Application of Bismuth Film Electrode for Simultaneous Detection of Trace Cobalt and Nickel in Low-Volume Body Fluids
  In preparation

- E.A. Hutton, R. Pauliukaitė, B. Ogorevc, M.R. Smyth
  An Electrochemical Microsensor for the Selective Determination of Ascorbic Acid in Gastric Juice
  Draft of paper in preparation for submission

Presentations

- **8th Young Investigators Seminar on Analytical Chemistry, YISAC 2001**

University of Pardubice, Czech Republic, 2-5 July 2001; Oral Presentation

Cathodic Electrochemical Detection of Nitrophenols at a Bismuth Film Electrode

E.A. Hutton, B. Ogorevc, M.R. Smyth.

- **9th Young Investigators Seminar on Analytical Chemistry, YISAC 2002**

Jozef Stefan Institute, Ljubljana, Slovenia, 26-29 June 2002; Oral Presentation

A New Approach for Measuring Ascorbic Acid under Acidic Conditions using Microelectrodes Modified with Inorganic Films

E.A. Hutton, B. Ogorevc, M.R. Smyth

- **9th International Conference on Electroanalysis, ESEAC 2002**

University of Mining and Metallurgy, Cracow, Poland, 9-13 June 2002; Oral Pres.

An Electrochemical Microsensor for the Selective Determination of Ascorbic Acid in Gastric Juice

E.A. Hutton, R. Pauliukaitė, B. Ogorevc, M.R. Smyth

- **9th International Conference on Electroanalysis, ESEAC 2002**

University of Mining and Metallurgy, Cracow, Poland, 9-13 June 2002; Poster

Cathodic Electrochemical Detection of Nitrophenols at a Bismuth Film Electrode

E.A. Hutton, B. Ogorevc, M.R. Smyth

- **10th Young Investigators Seminar on Analytical Chemistry, YISAC 2003**

University of Venice, Venice, Italy, June 3-5, 2003; Oral Presentation

Determination of Some Heavy Metals in Soil Extracts Using Stripping Analysis at the Bismuth Film Electrode

E.A. Hutton, B. Ogorevc, M.R. Smyth

Other Contributions

(presenter name underlined)

- **Pittcon 2003**

Orlando, Florida, March 9-14, 2003; Oral Presentation

Bismuth Versus Mercury Electrodes in Modern Electrochemical Analysis

S.B. Hočevar, E.A. Hutton, B. Ogorevc, J. Wang

- **Modern Electrochemical Methods**

Jetřichovice, Czech Republic, 20-22 May, 2003

Can Bismuth Replace Mercury In Modern Electrochemical Analysis?

S.B. Hočevar, E.A. Hutton, I. Švancara, B. Ogorevc, K. Vytřas

Other

- **9th Young Investigators Seminar on Analytical Chemistry, YISAC 2002**

Jozef Stefan Institute, Ljubljana, Slovenia, 26-29 June 2002

Members Of Scientific And / Or Organizing Committee

V. Stibilj, M. Horvat, K. Kalcher, G. Knapp, B. Ogorevc, B. Pihlar, P. Ugo, K. Vytřas, P. Vreček, D. Mazej, P. Smrkolj, E.A. Hutton.

ABSTRACT

CHEMICALLY MODIFIED CARBON-BASED ELECTRODES FOR THE DETECTION OF SOME SUBSTANCES OF ENVIRONMENTAL AND BIOMEDICAL SIGNIFICANCE

The thesis opens with an introduction to some basic electroanalytical principles, and a brief description of carbon-based electrodes, with a particular focus on glassy carbon and carbon fibre microelectrodes. Also included is a review of the most commonly employed electrode modification procedures, with some examples of the analytical applications of modified electrodes.

The second chapter describes the use of the bismuth film electrode (BiFE), which consists of a bismuth film electrochemically deposited onto a glassy carbon substrate electrode, in the cathodic electrochemical detection of some reducible organic compounds. The electrochemical behaviour of nitrophenols at BiFE was investigated and the BiFE applied in flow injection analysis amperometric determination of these nitrophenolic compounds.

The application of the BiFE in adsorptive stripping voltammetric and potentiometric stripping analysis of cobalt and nickel in some low-volume body fluids is presented in Chapter Three. In addition, the BiFE was successfully applied in the determination of some selected trace heavy metals in soil extract samples, and the results obtained compared with those from ICP-MS measurements.

In Chapter Four, the development of a microsensor based on a nickel oxide,ruthenium hexacyanoferrate (NiO,RuHCF) inorganic layer, for the selective detection of ascorbic acid in acidic media is described. The modified microsensor is applied in measurement of ascorbic acid in model gastric juice solution. In addition, the modified microsensor, with a protective cellulose acetate membrane, is employed in the determination of ascorbic acid in real gastric juice solution.

The final chapter presents some possibilities for furthering the study, use and application of the modified electrodes used in the work.

1. AN INTRODUCTION TO ELECTROANALYTICAL PRINCIPLES, CARBON-BASED ELECTRODES, AND ELECTRODE MODIFICATION

1.1 General Introduction

Electrochemistry may be defined as the branch of chemistry that is concerned with electrolysis and other similar phenomena occurring when a current is passed through a solution of an electrolyte, or with the behaviour of ions in solution and the properties shown by these solutions [1]. It was discovered over 200 years ago (1791) in Bologna, Italy, where Luigi Galvani, upon dissecting a frog, noticed: "One of those who was assisting me touched lightly and by chance the point of his scalpel to the internal crural nerves of the frog (an electric machine was nearby), then suddenly all the muscles of its limbs were seen to be contracted..." [2]. Other particularly notable early events in the development of electrochemistry included Volta's discovery that if one used a pasteboard membrane to separate silver plates from zinc plates, and wetted the ensemble with salt water, an electric current flowed (1800), Faraday's discovery of the relation between the amount of electricity consumed and the amount of metal produced in a solid form from some invisible particles in solution (1834), and Tafel's discovery in 1905 that electric currents passing across metal-solution interfaces could be made to increase exponentially by changing the electric potential of the electrode across the surface of which they passed [2].

Today, following other considerable advances in the last century, such as the invention of the operational amplifier (1950's), the advent of cyclic voltammetry, pulse chronoamperometry, and rotating ring disc electrodes (1960's), the inception of chemically modified electrodes and photoelectrochemistry (1970's), and the introduction of microelectrodes (1990's), electrochemistry has become an extremely broad subject encompassing such diverse areas as batteries, fuel cells, corrosion, membrane potentials and electroanalytical chemistry [3]. It is the latter with which this thesis will be primarily concerned. Electroanalysis consists of techniques in which an essential or at least an indispensable role is played by electrochemistry. As a representative of wet-chemical methods, electroanalysis presents many attractive

advantages, such as selectivity and sensitivity, inexpensive equipment, ample choice of working electrode materials, and ability to attain real-time measurements. Indeed, electroanalysis has found a vast range of applications, including industrial quality control, environmental monitoring (e.g., trace heavy metal detection in waters), and biomedical analysis (e.g., pyrimidine and purine derivatives, amino acids, peptides and proteins, vitamins and coenzymes) [4,5]. This chapter will provide some insights into basic electrochemical principles in relation to electroanalytical chemistry, the most commonly used carbon-based electrodes (glassy carbon, carbon paste and screen-printed electrodes, and carbon fibre microelectrodes), and finally, an introduction to the possibilities for chemical modification of these carbon-based electrodes.

1.2 Fundamentals of Electroanalysis

1.2.1 Introduction

In contrast to many chemical measurements that involve homogeneous bulk solutions, electrochemical processes take place at the electrode-solution interface [4]. The type of electrical signal used for quantitation distinguishes the various electroanalytical techniques. There are two principle types of electroanalytical measurements: potentiometric and potentiostatic. Both types require at least two electrodes (conductors) and a contacting sample (electrolyte) solution, which constitute the electrochemical cell. The electrochemical (voltammetric) cell and the processes governing the electrode reactions will be discussed in more detail in the proceeding sections.

1.2.2 Voltammetric Cell

Electrochemical cells in which faradaic currents are flowing are classified as either *galvanic* or *electrolytic* cells. A *galvanic cell* is one in which reactions occur spontaneously at the electrodes when they are connected externally by a conductor, and are often employed in converting chemical energy into electrical energy [6]. An *electrolytic cell* is one in which reactions are effected by the imposition of an external voltage greater than the open-circuit potential of the cell. These cells are frequently

employed to carry out desired chemical reactions by expending electrical energy. *Electrolysis* is a term that is defined broadly as including chemical changes accompanying faradaic reactions (see Section 1.2.3) at electrodes in contact with electrolytes. The electrode at which reductions occur is termed the *cathode*, while the electrode at which oxidations occur is termed the *anode*. A current in which electrons cross the interface from the electrode to a species in solution is a *cathodic current*, while electron flow from a solution species into the electrode is an *anodic current*.

The electrochemical cell is most generally defined as two electrodes separated by at least one electrolyte phase. In general, there is a measurable difference in potential between the two electrodes whether the cell is passing a current or not. The overall chemical reaction taking place in a cell is made up of two independent *half-reactions*, which describe the real chemical changes at the two electrodes. Each half reaction responds to the interfacial potential difference at the corresponding electrode [7]. Usually, only one of these reactions is of interest, and the electrode at which it occurs is termed the *working* (or *indicator*) electrode. In order to focus on it, it is necessary to standardise the other half of the cell by using an electrode made up of phases of constant composition, the *reference* electrode. As this reference electrode is of stable composition, its potential is fixed and hence any changes that take place in the cell are ascribable to the working electrode. Thus, one can state that one observes the *potential* of the working electrode *with respect to* the reference electrode. A *counter* (or *auxiliary*) electrode is also employed in the cell, and functions to supply the current required by the working electrode without in any way limiting the measured response of the cell [8].

Designs of working electrodes for laboratory measurements are diverse. In general, it is a small sphere, small disc, or a short wire, but it can also be a metal foil, a single crystal of a semiconductor or metal, an evaporated thin film, or a powder pressed as discs or pellets [8]. An important feature is that the electrode should not react chemically with the solvent or solution components. Definition of the useful working range is difficult, as this depends on a number of factors such as hydrogen or oxygen evolution, oxide or complex formation, solvent decomposition, and the reactants and products of the system under investigation. The electrode area is generally small (< 0.25 cm^2; although microelectrodes, which will be discussed later, are considerably smaller than this), and the electrode surface should be clean and smooth, as the geometry and mass transport are thus better defined [8]. Some

examples of working electrode materials are gold, platinum, mercury, glassy carbon, carbon paste, and carbon fibre. Several of these will be discussed in greater detail in Section 1.3. Commonly used reference electrodes include mercury-mercurous chloride (calomel electrode), mercury-mercurous sulphate, mercury-mercuric oxide and silver-silver chloride, while the most common counter electrode material is platinum (wires, coils, gauzes) [8].

The electrolyte solution is the medium between the electrodes in the cell, and consists of a solvent with a high concentration of an ionised salt, as well as the electroactive species of interest. It may also contain other compounds, such as buffers or complexing agents. The choice of the solvent generally depends on the solubility of the analyte and its redox activity, and on solvent properties such as electrochemical and chemical activity and electrical conductivity [4]. It should not react with the analyte and should be stable over a wide potential range. Typical solvents include double-distilled water and organic solvents such as acetonitrile, methanol and dimethyl sulfoxide. The supporting electrolyte is required in controlled-potential experiments in order to decrease the solution resistance, to eliminate electromigration effects, and to maintain a constant ionic strength. The inert supporting electrolyte may be an inorganic salt (e.g., potassium chloride), a mineral acid or a buffer (e.g., acetate). A typical three-electrode voltammetric cell is shown in Figure 1.1 A, while Figure 1.1 B shows how the potentiostat (power supply) controls the cell potential.

In certain electrochemical experiments, a Faraday cage may be employed. The Faraday cage is a ruggedly constructed stainless steel cabinet designed to enclose the voltammetric cell and electrodes. When connected to the potentiostat ground terminal, the Faraday cage forms an extended electrical shield, reducing induced noise currents in the electrochemical cell from nearby electromagnetic field sources in the laboratory. The shield case is recommended for experiments in which current measurements are to be made routinely at levels below < 1 μA, for example when employing microelectrodes.

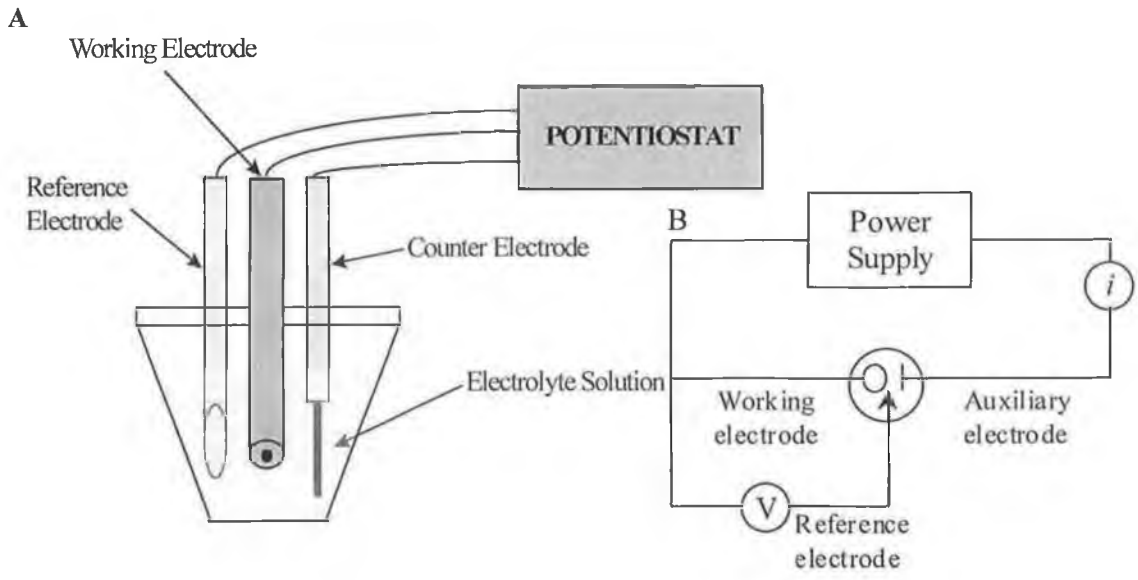

Figure 1.1: (A) Simple schematic of a typical 3-electrode voltammetric cell and (B) diagram showing how potentiostat (power supply) controls cell potential [6].

1.2.3 Electrochemical Processes

Four main types of electroanalytical measurements exist:

(a) conductimetric; where the concentration of charge is obtained through measurement of the solution resistance,

(b) amperometric; where a fixed potential is applied to the electrode, which causes the analyte of interest to react and a current to pass (controlled-potential technique),

(c) voltammetric; in which current is registered as a function of applied potential (controlled-potential technique), and

(d) potentiometric; in which the equilibrium potential of an indicator electrode is measured against a selected reference electrode using a high impedance voltmeter [9].

It is the latter three with which this work is concerned and hence these methods will be focussed on in the thesis.

The objective of controlled-potential experiments is to obtain a current response that is related to the concentration of the redox active target analyte. This is

achieved by monitoring the transfer of electron(s) during the redox process of the analyte:

$$O + ne^- \rightleftharpoons R \qquad (1.1)$$

where O and R are the oxidised and reduced forms, respectively, of the redox couple [4]. This reaction will proceed in a potential region that makes the electron transfer kinetically or thermodynamically favourable.

The current which results from a change in oxidation state of the analyte (electroactive species) is termed the *faradaic current* because it obeys Faraday's law i.e. the reaction of one mole of substance involves a change of n x F (where F is Faraday's constant; 96,487 coulombs). This current is a direct measure of the rate of the redox reaction and the resulting current-potential plot is known as a *voltammogram*. The shape and magnitude of the voltammetric response is governed by the processes involved in the electrode reaction, and the total current is the sum of the faradaic currents for the analyte and the blank solutions, and the *non-faradaic* charging background current, which is the current that results from the charging of the double-layer. The electrical double-layer is the array of charged particles and / or oriented dipoles that exist at every material surface. In electrochemistry, this layer represents the ionic zones formed in the solution to compensate for the excess of charge on the electrode. A negatively charged electrode thus attracts a layer of positive ions, and vice versa. As the interface must be neutral, a counterlayer of ions of opposite sign to that of the electrode is made. A schematic representation of the electrical double layer and the variation in potential across it is shown in Figure 1.2. When the overall reaction is controlled only by the rate at which the electroactive species reach the surface, the current is deemed mass transport limited, and it is known as a *Nernstian* or *reversible* reaction because it obeys thermodynamic conditions.

In potentiometry, information on the composition of a sample is obtained through the potential appearing between two electrodes. In systems that are controlled by the laws of thermodynamics (as in potentiometry), the potential of the electrode can be used to establish the concentration of the electroactive species at the surface [C_O and C_R] according to the Nernst equation:

$$E = E^{o} + \frac{2.3RT}{nF} \log_{10} \frac{C_O}{C_R} \qquad (1.2)$$

where E_o is the standard potential for the redox reaction, R is the universal gas constant (8.314 J/K/mol), T is the temperature in Kelvin, n is the number of electrons transferred in the reaction and F is the Faraday constant. On the negative side of E^{o}, the oxidised form thus tends to be reduced, and the forward reaction (i.e. reduction) is more favourable [4].

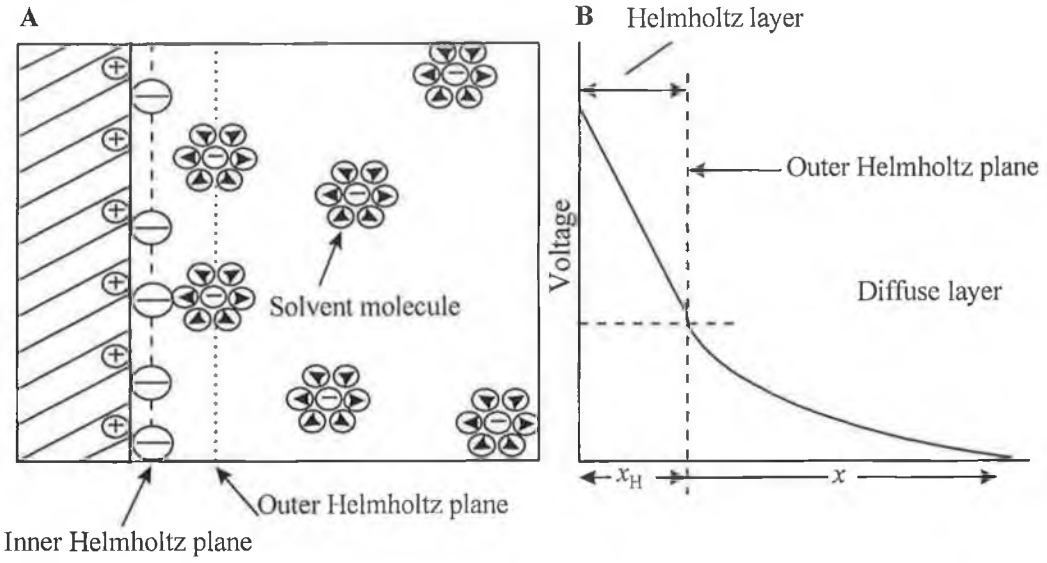

Figure 1.2: (A) Schematic representation of the electrical double layer and (B) variation of the potential across the electrical double layer (adapted from [4]).

These descriptions of the electrode reaction are in fact quite simplified, as the pathway can actually be quite complicated and take place in several steps. The simplest reactions involve only mass transfer of the electroactive species to the electrode surface, electron transfer across the interface, and transfer of the product back to the bulk solution [4]. In more complex reactions, additional chemical and surface reactions may occur either before or after the actual electron transfer. The slower process will then, obviously, be the rate-determining step. Mass transport to the electrode proceeds by three different processes:

(a) diffusion; the natural movement of species under a concentration gradient from a region of high to a region of low concentration so as to annul the concentration difference;

(b) convection; transport to the electrode by a gross physical movement; such fluid flow occurs with stirring or flow of the solution and with rotation or vibration of the electrode (i.e. forced convection) or due to density gradients (i.e. natural convection);

(c) migration; movement of charged particles along an electrical field (i.e. the charge is carried through the solution by ions according to their transference number). The three modes of mass transport are illustrated in Figure 1.3 [4,9].

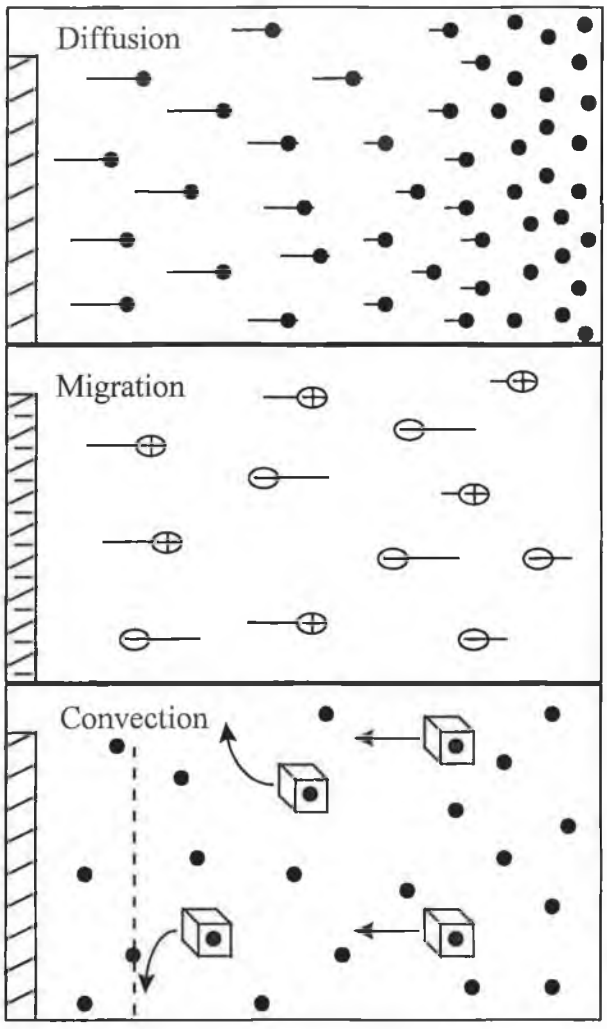

Figure 1.3: The three modes of mass transport (adapted from [4]).

The flux (J) is a common measure of the rate of mass transport at a fixed point. It is defined as the number of molecules penetrating a unit area of an imaginary plane in a unit of time (units = mol/cm^2/s). The flux to the electrode is described mathematically by a differential equation, known as the Nernst-Planck equation, given for one dimension by:

$$J(x, t) = -D \frac{\delta C(x, t)}{\delta x} - \frac{zFDC}{RT} \frac{\delta \phi(x, t)}{\delta x} + C(x, t)V(x, t) \qquad (1.3)$$

where D is the diffusion coefficient (cm^2/s), $\delta C(x, t)/\delta x$ is the concentration gradient (at distance x and time t), $\delta \phi(x, t)/\delta x$ is the potential gradient, z is the charge of the electroactive species, C is the concentration of the electroactive species, and $V(x, t)$ is the hydrodynamic velocity (in the x direction). In aqueous media, D usually ranges between 10^{-5} and 10^{-6} cm^2/s [4]. The current (i) is directly proportional to the flux:

$$i = -nFAJ \qquad (1.4)$$

where A is the area of the electrode. From equation 1.3, one can see that the situation is quite complex when all three processes occur at the same time, making it difficult to relate the current to the analyte concentration. These difficulties can be overcome by suppressing electromigration (through addition of excess inert salt) and / or convection (by using a quiescent solution). Hence, under these conditions, the movement of electroactive species in the solution is limited solely by diffusion. The reaction taking place at the surface generates a concentration gradient adjacent to the surface, which in turn results in a diffusional flux. The rate of diffusion is directly proportional to the slope of the concentration gradient according to *Fick's First Law*:

$$J(x, t) = -D \delta C(x, t) / \delta x \qquad (1.5)$$

Combination of equations 1.4 and 1.5 gives a general equation of the current response:

$$i = nFAD\ \delta C(x, t) / \delta x \qquad \textbf{(1.6)}$$

Thus, the current is proportional to the concentration gradient of the electroactive species. The diffusional flux is time dependent and this is described by *Fick's Second Law*:

$$\frac{\delta C(x, t)}{\delta t} = D\ \frac{\delta^2 C(x, t)}{\delta x^2} \qquad \textbf{(1.7)}$$

This equation reflects the rate of change of concentration between parallel planes at points x and $(x + dx)$ with time and is valid for planes parallel to one another and perpendicular to the direction of diffusion (linear diffusion). In cases where diffusion is towards a spherical electrode i.e. the lines of flux are not parallel but are perpendicular to segments of the sphere, *Fick's Second Law* takes the form:

$$\frac{\delta C}{\delta t} = D\left(\frac{\delta^2 C}{\delta r^2} + \frac{2}{r}\frac{\delta C}{\delta r}\right) \qquad \textbf{(1.8)}$$

where r is the distance from the centre of the electrode. Overall, Fick's laws describe the flux and the concentration of the electroactive species as functions of position and time [4].

1.2.4 Voltammetric, Amperometric, and Potentiometric Techniques

The following sections are by no means comprehensive descriptions of electroanalytical techniques, neither do they represent the entire range of techniques currently available with modern instrumentation. Rather, they represent the particular techniques that were employed throughout the course of this work.

1.2.4.1 Linear Sweep Voltammetry

Linear sweep voltammetry (LSV) is the simplest of the potential-time waveforms, in which the potential applied across the electrode-solution interface is scanned linearly from an initial value E_i to a final value E_f at a constant rate ν. An excursion in which the potential becomes increasingly positive i.e. going in the positive direction, is termed a positive scan. In LSV, one generally wants to initiate the potential scan at an E_i at which no reaction occurs and then scan through the standard electrode potential(s) of the species in solution. Hence, the composition of the reaction layer will not be altered at the beginning by application of E_i. LSV has a reasonable detection limit, down to 10^{-5} mol/L in some cases, which can be improved by increasing the scan rate [10]. Two important parameters in LSV are the peak potential E_p and the peak current i_p. For a reversible system the peak current is defined by the Randles-Sevcik equation:

$$i_p = (2.69 \times 10^5) n^{3/2} A D^{1/2} C^o \nu^{1/2} \qquad (1.9)$$

where i_p is the peak current (A), n is the number of electrons transferred, A is the electrode area (cm^2), D is the diffusion coefficient (cm^2/s), C^o is the concentration of species in the bulk solution, and ν is the scan rate (V/s) (at 25°C). The peak potential (for a reduction) is defined by:

$$E_p = E_{O,R}^{\ o} - 0.029 / n \qquad (1.10)$$

at 25°C and where E_p and $E_{O,R}^{\ o}$ are expressed in volts.

In the case of an irreversible system, the equation for i_p is given by:

$$i_p = (2.99 \times 10^5) n (\alpha n_a)^{1/2} A D^{1/2} C^o \nu^{1/2} \qquad (1.11)$$

where α is the transfer coefficient and n_a is the number of electrons transferred in the rate determining step of the electrode process. The peak current is still related to the bulk concentration, but will be lower in height (depending on the value of α). The peak potential is no longer independent of the scan rate, as shown in:

$$E_p = E^o - \frac{RT}{\alpha n_a F}\left[0.78 - \ln\frac{k_1}{D_o^{1/2}} + {}^1/_2 \ln\left(\frac{\alpha n_a F v}{RT}\right)\right] \qquad (1.12)$$

where k_1 is related to the heterogeneous rate constant of the electron transfer reaction [10]. Thus, E_p occurs at potentials higher than E^o, with the overpotential related to k^o and α. Independent of the value of k^o, such peak displacement can be compensated by an appropriate change of the scan rate. The peak potential and the half-peak potential (at 25°C) will differ by $48/\alpha n$ mV [4].

1.2.4.2 Cyclic Voltammetry

Cyclic voltammetry (CV) is the most widely used technique for acquiring qualitative information about electrochemical reactions. Its power derives from its ability to provide considerable information on the thermodynamics of redox processes, on the kinetics of heterogeneous electron-transfer reactions, and on coupled chemical reactions or adsorption processes in short times. As CV is a logical extension of linear sweep voltammetry, the theory and equations included in the previous section also apply to this method. Cyclic voltammetry is often the first experiment performed in an electroanalytical study, offering a convenient evaluation of the redox potentials of the redox species and a determination of the effect of media upon the redox process [4].

Cyclic voltammetry consists of scanning linearly the potential of a stationary working electrode (in a quiescent solution) using a triangular potential waveform. Single or multiple cycles can be performed depending on the information required. Figure 1.4 shows the potential-time excitation and resulting waveform for CV. The resulting plot of current versus potential is a *cyclic voltammogram* and is a complicated, time-dependent function of a large number of chemical and physical parameters. As in linear sweep voltammetry, the important parameters of a cyclic voltammogram are the magnitudes of the peak current(s), i_{pa} (anodic) and i_{pc} (cathodic), and the potentials at which the peaks occur, E_{pa} and E_{pc} (a reversible system will contain all of these parameters). The cyclic voltammogram can be an important method in determining whether a system is reversible or not. A redox couple in which both species (O and R) rapidly exchange electrons with the working

electrode is termed an electrochemically reversible couple, and can be identified from a cyclic voltammogram by the presence of two peaks and by measurement of the potential difference between the potentials of these two peaks:

$$\Delta E_p = E_{pa} - E_{pc} \approx 0.058/n \qquad (1.13)$$

where n is the number of electrons transferred. This $0.058/n$ V separation of peak potentials is independent of scan rate for a reversible couple, but is slightly dependent on switching potential and cycle number. The potential midway between the two peak potentials is termed the formal reduction potential of the couple [10]:

$$E^{o'} = E_{pa} + E_{pc} / 2 \qquad (1.14)$$

When the scan rate ν is increased, i_{pa} and i_{pc} both increase in proportion to $\nu^{1/2}$. For a reversible couple, plots of i_{pa} and i_{pc} versus $\nu^{1/2}$ should be linear with intercepts at the origin. The values of i_{pa} and i_{pc} are similar in magnitude for a reversible couple with no kinetic complications i.e.:

$$i_{pa} / i_{pc} \approx 1 \qquad (1.15)$$

This ratio, however, can be significantly influenced by chemical reactions coupled to the electrode process [10].

Electrochemical irreversibility is caused by slow electron exchange of the redox species with the working electrode and is characterised by a separation of peak potentials that is greater than $0.059/n$ V and that is dependent on the scan rate (see equations 1.11 and 1.12). In CV, the presence of only one peak (anodic or cathodic) can be an indication of irreversibility. For quasi-reversible systems, the current is controlled by both the charge transfer and mass transport. Overall, voltammograms of a quasi-reversible system are more drawn-out and exhibit a larger separation in peak potentials compared to those of a reversible system [4]. Figure 1.5 shows cyclic voltammograms for irreversible and quasi-reversible redox processes.

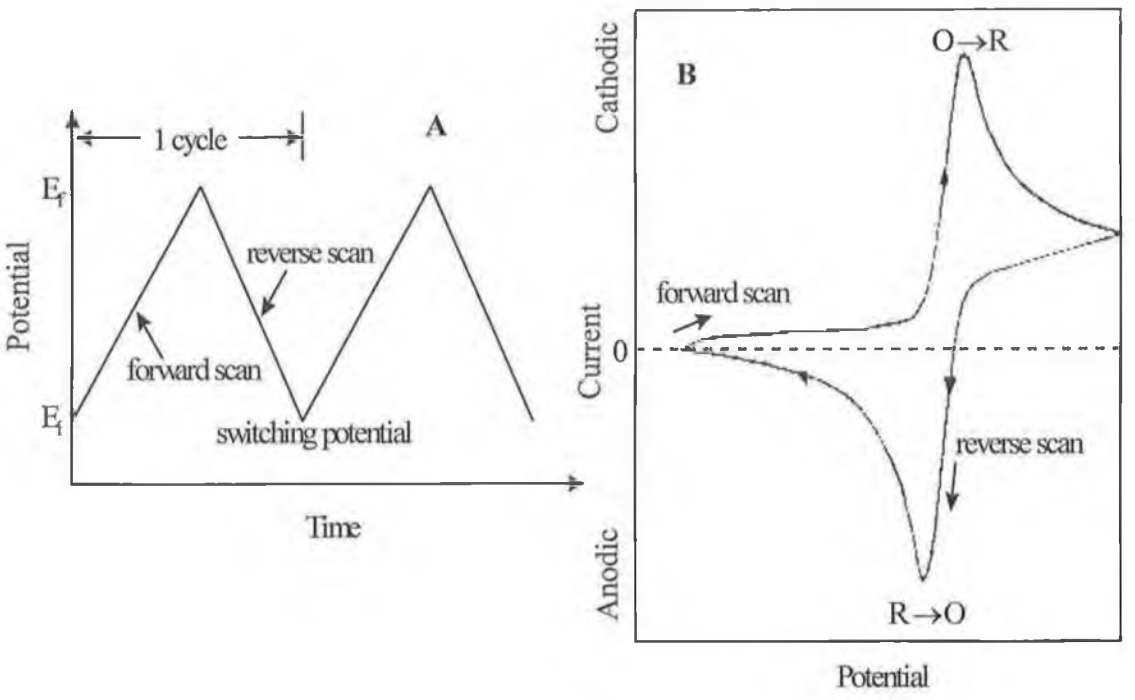

Figure 1.4: (A) Typical potential-time excitation signal for cyclic voltammetry, where E_i is the initial potential, and E_f the final potential, and (B) resulting voltammogram (both adapted from [4]).

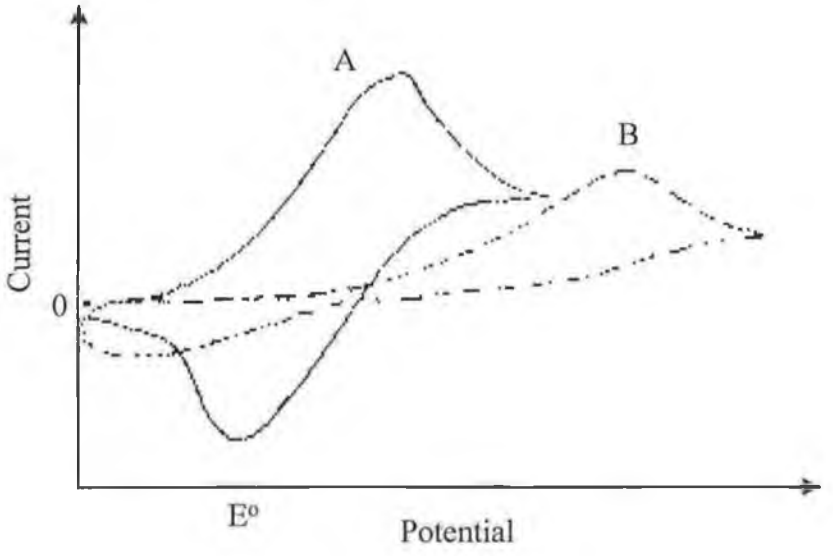

Figure 1.5: Cyclic voltammograms for quasi-reversible (curve A) and irreversible (curve B) redox processes (adapted from [4]).

1.2.4.3 Square Wave Voltammetry

The square wave voltammetric waveform consists of a square wave superimposed on a staircase. The currents at the end of the forward and reverse pulses are both registered as a function of staircase potential. The difference between them, the net current, is larger than either of its two component parts in the region of the peak, which is centred on the half-wave potential. Figure 1.6 shows the square wave waveform and the resulting voltammogram. Contributions from capacitative currents can be effectively discriminated against before they die away, since, over a small potential range between the forward and reverse pulses, the capacity is constant and is hence negated by subtraction. Detection limits lower than 10^{-8} mol/L are achievable employing SWV [9].

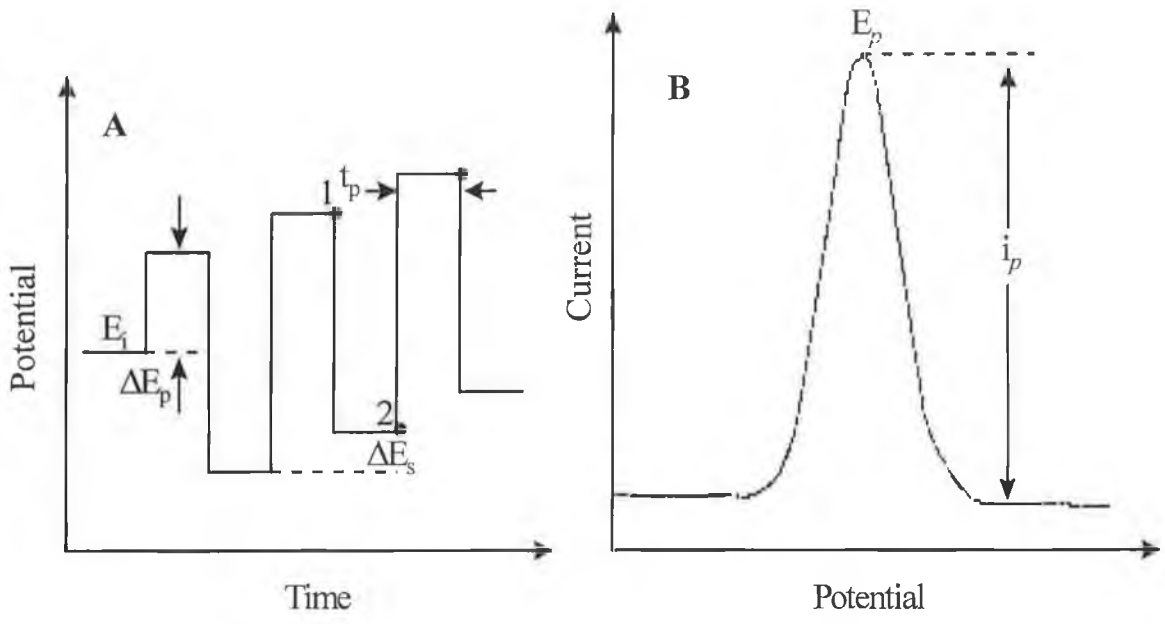

Figure 1.6: (A) Excitation waveform for square wave voltammetry, where t_p is the pulse width, ΔE_p the pulse amplitude, and ΔE_s the step height, and (B) response obtained in square wave voltammetry (adapted from [5]).

1.2.4.4 Differential Pulse Voltammetry

Differential pulse voltammetry (DPV) involves the application of fixed-magnitude pulses – superimposed on a linear potential ramp – to the working electrode. The current is sampled twice, just before the pulse application and again late in the pulse life, when the charging current has decayed. The first current is subtracted from the second, and this current difference plotted versus the applied potential. The resulting

differential pulse voltammogram consists of current peaks, the height of which are directly proportional to the concentration of the corresponding analytes. This method offers an effective correction of the charging background current and allows detection down to 10^{-8} mol/L [4]. See Figure 1.7 for the differential pulse waveform and voltammogram.

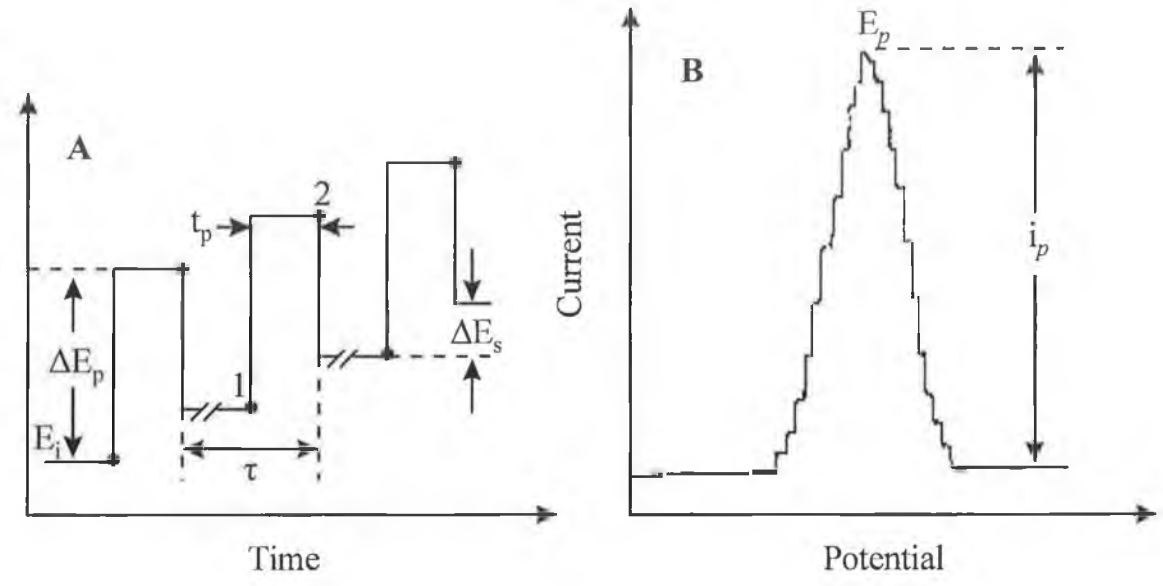

Figure 1.7: (A) Excitation signal for differential pulse voltammetry, where τ is the drop time (if polarography is used), and (B) schematic differential pulse voltammogram (adapted from [5]).

1.2.4.5 Hydrodynamic Amperometry

Several electroanalytical techniques involve hydrodynamic flow of electrolyte over the electrode surface. These methods take advantage of the enhanced sensitivity resulting from the increased mass transport of electroactive substance to the electrode that occurs under hydrodynamic conditions [10]. If a stationary electrode is employed with a stirred solution, three regions of solution flow result; (a) *turbulent flow* comprises the solution bulk, (b) as the electrode surface is approached, a transition to *laminar flow* (non-turbulent) occurs, and (c) the rate of this laminar flow decreases near the electrode due to frictional forces until a thin layer of *stagnant solution* is present beside the electrode surface (the Nernst diffusion layer).

Figure 1.8 shows the concentration-distance profiles for voltammetry in stirred solution; A illustrates this profile for O under the condition that its surface concentration has not been perturbed (the cell is either at open circuit, or a potential has been applied that has not been sufficient to alter the surface concentrations of the O, R couple). The profiles in B represent the situation in which a potential is applied that requires equal concentrations of O and R at the electrode surface to satisfy the Nernst equation. The electrode electrolyses O to R at the rate necessary to maintain equal levels of O and R at the electrode surface. If this potential is maintained, a continuous electrolysis of O to R is required to maintain surface concentrations because R diffuses away from the interface across the stagnant layer and is then swept away by the laminar flow. Figure 1.8 C shows the profiles that result when the applied potential is sufficiently negative that the concentration of O at the electrode surface is effectively zero. Here, all of O at the electrode surface must be electrolysed to R to satisfy the Nernst equation and hence O is converted to R as quickly as it can diffuse to the surface of the electrode. This is the limiting condition and application of even higher electrode potentials will have no effect on the profiles [10].

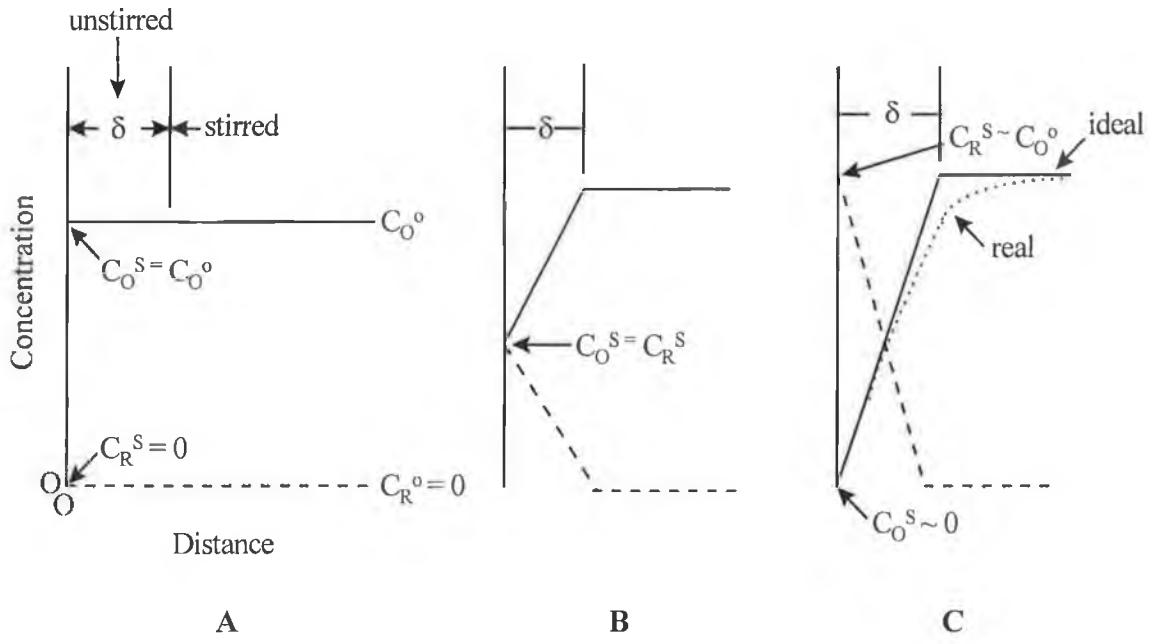

Figure 1.8: Concentration-distance profiles for voltammetry in stirred solution (adapted from [10]).

Direct-current amperometry (the measurement of electrochemical current in response to a fixed electrode potential) continues to be the most widely used finite-current electrochemical technique [11]. Its applications include endpoint detection in volumetric and coulometric titrations and measurement of the activity of redox enzymes. Amperometry is often carried out in stirred or flowing solutions or at a rotated electrode and is thus termed hydrodynamic amperometry. Current, the magnitude of which is proportional to the concentration of analyte, is measured as the electroactive species undergoes an oxidation or reduction at the working electrode, which is held at a fixed operating potential. Hydrodynamic voltammetry, a steady-state technique from which amperometry is derived, is used to select the optimum operating potential.

1.2.4.6 Anodic Stripping Voltammetry and Potentiometric Stripping Analysis

Stripping analysis is an extremely sensitive electrochemical technique for measuring trace metals (see also Section 3.3.2). Its remarkable sensitivity is attributed to the combination of an effective preconcentration step with advanced measurement procedures that generate an extremely favourable signal-to-background ratio [4]. Limits of detection down to 10^{-10} mol/L are achievable – up to 2 to 3 orders lower than those obtained using solution-phase voltammetric measurements. Stripping analysis is essentially a two-step procedure. The first step, deposition, involves the accumulation of the metal ions on the electrode surface. This is followed by the stripping (measurement) step, which involves the dissolution (stripping) of the deposit. Anodic stripping voltammetry (ASV), used in this work, is the most widely used stripping technique. Figure 1.9 illustrates the potential-time waveform and resulting voltammogram for ASV.

Adsorptive stripping techniques, which are also used in this work, greatly enhance the scope of stripping measurements toward numerous trace elements. These techniques involve the formation, adsorptive accumulation, and reduction of a surface-active complex of the metal. The accumulation and stripping steps in adsorptive stripping measurements are shown in Figure 1.10. In this work, both adsorptive stripping voltammetry (AdSV) and adsorptive stripping potentiometric analysis are employed. These methods greatly enhance the scope of stripping measurements by permitting the determination of those metals that cannot be measured using conventional stripping analysis. In AdSV, a negative-going potential scan is employed

for measuring the adsorbed complex, while potentiometric stripping analysis uses a constant cathodic current. The response of the surface-confined species is directly related to its surface concentration, with the adsorption isotherm providing the relationship between the surface and bulk concentrations of the adsorbate. As a result, calibration curves display non-linearity at high concentrations.

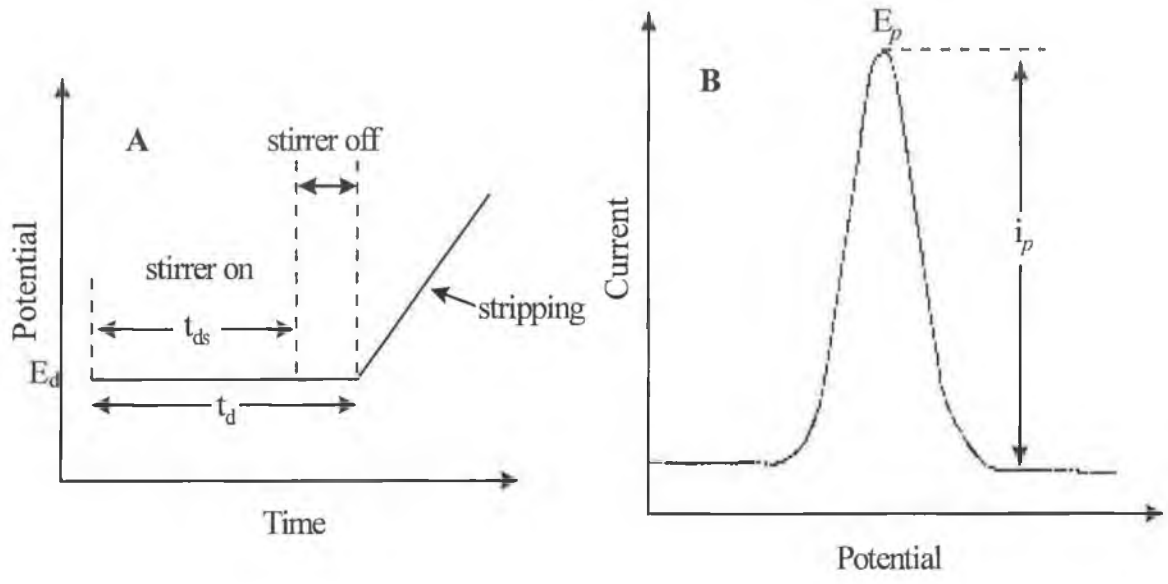

Figure 1.9: (A) Potential-time waveform for ASV, where t_d is the total time of the preconcentration step, t_{ds} is the deposition time with stirring, and E_d is the deposition potential, and (B) resulting voltammogram for ASV (adapted from [5]).

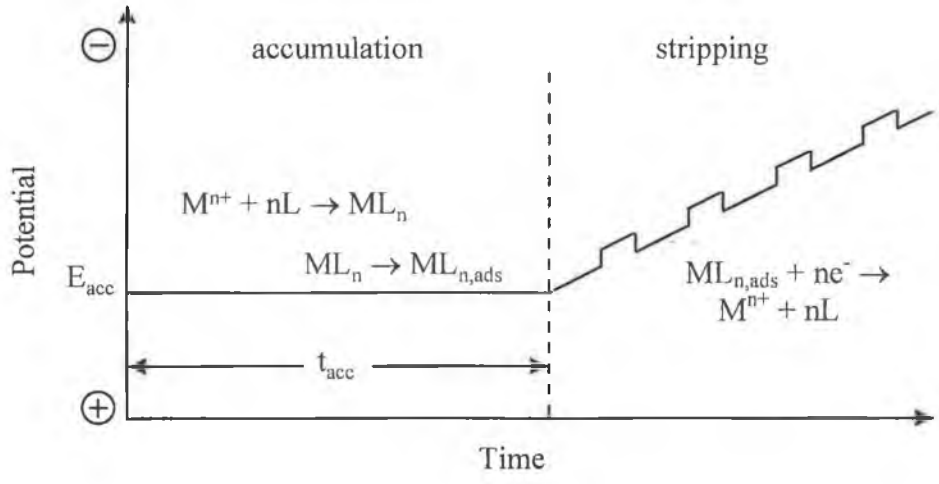

Figure 1.10: Accumulation and stripping steps in adsorptive stripping measurements of a metal ion (M^{n+}) in the presence of an appropriate chelating agent (L) (adapted from [4]).

1.3 Carbon-Based Electrodes

1.3.1 Glassy Carbon Electrodes

1.3.1.1 Composition and Features

Glassy carbon (GC) is made from a high-molecular weight carbonaceous polymer, often polyacrylonitrile, phenol/formaldehyde resin, etc. When such polymers are heated to 600-800°C, most of the non-carbon components are volatilised, while the polymer backbone remains intact [12]. After this initial heat treatment, the material is slowly heated under pressure to temperatures of 1000°C, 2000°C or 3000°C, producing different types of glassy carbon. GC is hard and impermeable to liquids and gases. The resistance of GC is low enough to be negligible in electroanalytical experiments, while for smooth, heat-treated GC, the observed capacitance is quite low. In general, the background current using glassy carbon tends to be larger than on graphite composites because the entire surface is active. A surface pretreatment is usually required in order to create active and reproducible GC electrodes and to enhance their analytical performance [4]. The pretreatment procedure usually involves polishing the surface to a shiny "mirror-like" appearance with successively decreasing alumina particles (down to 0.05 μm) on a polishing cloth. Other pretreatments such as electrochemical, chemical, heat or laser steps may also be employed. The improved electron-transfer reactivity of GC electrodes following these pretreatment techniques may be due to the removal of surface contaminants, exposure of fresh carbon edges, and an increase in the density of surface oxygen groups.

1.3.1.2 Construction of Glassy Carbon Electrode

Glassy carbon electrodes may be categorised as solid electrodes and can be stationary or rotating, usually in a planar disc configuration. They consist of a short cylindrical rod of the glassy carbon embedded in a tightly fitting tube of an insulating material (often Teflon) [4]. A schematic diagram and a photograph of a typical glassy carbon electrode are given in Figure 1.11. It is of critical importance to avoid crevices between the insulating material and the electrode material in order to prevent solution creeping and hence an increased background response. Electrical contact is provided at the rear face

of the electrode. Disc glassy carbon electrodes can also be used in flow analysis in connection with thin-layer or wall-jet detectors.

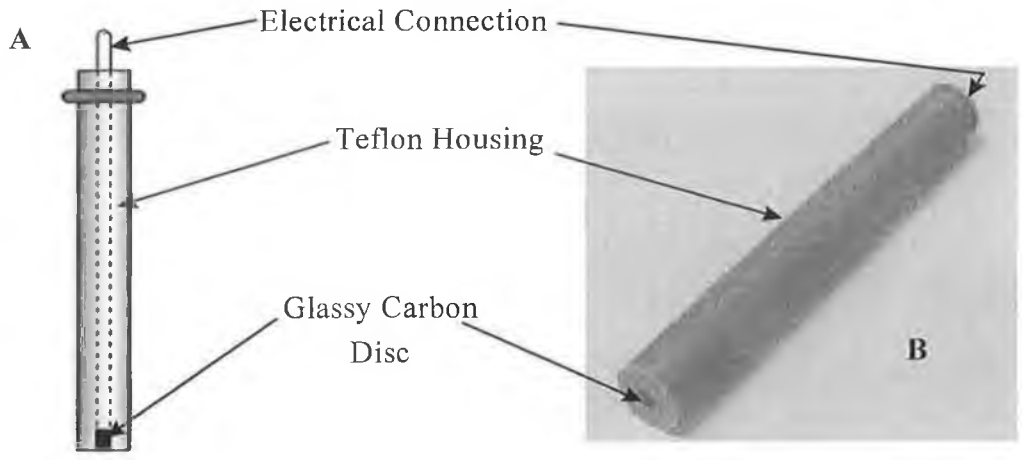

Figure 1.11: (A) Schematic of a glassy carbon electrode (from www.bioanalytical.com) and (B) photograph of a glassy carbon electrode.

1.3.2 Carbon Paste Electrodes

1.3.2.1 Composition and Features

Polycrystalline graphite (microcrystalline graphitic material with 3.354 Å interplanar spacing and 50 – 500 Å crystallites) is made by heat-treating high-molecular-weight petroleum fractions at high temperatures to bring about graphitization. When combined with a "heavy" hydrocarbon such as Nujol or hexadecane (typically ca. 70 % carbon by weight) and packed into an inert holder (e.g. Teflon), a carbon paste electrode results [12] (see Figure 1.12). Such electrodes provide an easily renewable and modifiable electrode surface, are of low cost and have very low background current contributions [4]. The paste composition greatly affects the electrode reactivity, with an increase in the pasting-liquid content decreasing electron-transfer rates as well as the background current contributions. Such electrodes have grown increasingly popular in recent years, although the exact behaviour of these electrodes is not fully understood. It is possible that some of the electrochemistry observed at these electrodes involves permeation of the pasting liquid layer by the electroactive species [4]. Modification of the carbon paste electrode is easily achieved by adding

the modifier(s) to the powdered graphite and binder, such as is the case with, for example, carbon-based biosensors containing enzymes [13].

Carbon paste electrodes have been employed in a number of applications such as determination of heavy metals, glucose, uric acid, dopamine and serotonin [14-17]. A great number of applications of carbon paste electrodes can be found in reference 13 and references therein.

1.3.3 Screen Printed Electrodes

1.3.3.1 Composition and Features

Production of screen printed electrodes involves several steps, including placement of an ink (both conducting and insulating) onto a patterned screen or stencil, followed by forcing it through the screen with the aid of a squeegee on to a planar substrate (plastic or ceramic), and then drying / curing the printed patterns [4]. Such a process yields mass-producible (uniform and disposable) electrodes of different shapes or sizes (see Figure 1.12). The electrochemical reactivity and overall performance of screen-printed electrodes are dependent upon the composition of the ink employed and on the printing and curing conditions (temperature, pressure, etc.)

Such carbon-based electrodes have found widespread use in many areas of electroanalytical chemistry, such as in the measurement of glucose, pesticides, lead, ethanol, and lactic acid [18-22].

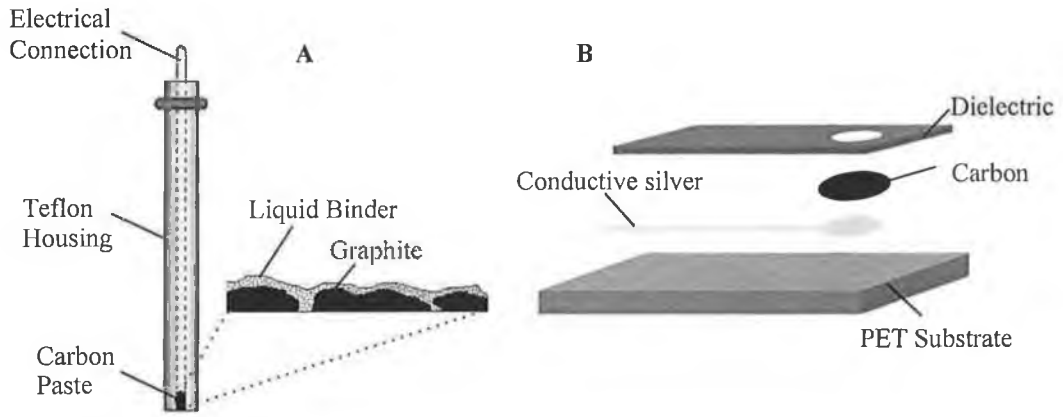

Figure 1.12: (A) Schematic of a carbon paste electrode and carbon paste surface and (B) schematic of a typical screen-printed electrode.

1.3.4 Microelectrodes

1.3.4.1 Definition and Trends in Development

Although the use of microelectrodes has become increasingly popular since the 1970s, there exists as yet no IUPAC nomenclature for such electrodes. Indeed, the term "microelectrodes" has several different meanings; in industrial usage, it is routinely the term for an electrode with centimetre dimensions [23]; Wang has called a carbon paste or graphite-epoxy electrode with a tip diameter of 50-200 μm a microelectrode [24]; while Bond has described a microelectrode as any electrode having at least one dimension with a size less than 25 μm [25]. The latter appears to be the most appropriate description of a microelectrode defined in terms of its size. The electrochemical behaviour of an electrode is an important criterion for determining whether or not it is a microelectrode. An electrode which exhibits steady-state or quasi-steady state cyclic voltammetric behaviour in a known and stable electrochemical system (e.g., 1 mmol/L potassium ferricyanide in a 0.1 mol/L KCl solution) at a reasonable time scale (e.g., at scan rates from 10 to 100 mV/s), is described as a microelectrode.

The earliest application of a true microelectrode was in 1942 in Davies and Brink's work on the measurement of oxygen concentrations in biological tissues [26]. In subsequent years, little attention was paid to the subject due to the lack of technology necessary to produce commercial devices and tools for measuring the small currents produced by these devices. In 1980, the theory for a semi-infinite linear (non-planar) diffusion profile more suitable to microelectrodes than the planar diffusion model of conventional electrodes (of mm dimensions) was established by Fleischmann's group (ref. 25 and reference therein). A year later, microelectrodes were introduced in several new areas that were inaccessible to conventional size electrodes [27]. Figure 1.13 illustrates the dramatic increase in publications reporting on microelectrodes.

1.3.4.2 Intrinsic Voltammetric Advantages

Numerous advantages arise from the physically small size (diameters from submicrometer to tens of micrometers) of microelectrodes. These include:

(a) Fast Mass Transport

At extremely small electrode surfaces, the diffusion process in the diffusion layer is dependent on the size and geometry of the electrode. In a stationary state, diffusion is primarily perpendicular to the surface of a conventional electrode (planar diffusion), whereas radial diffusion to the edges of the surface of a microelectrode becomes important and its contribution to the overall diffusion correspondingly greater. Hence, under identical conditions, the diffusion rate of electrochemically active species is significantly larger at a microelectrode than at a conventional electrode [28]. A steady-state response arises when the electrolysis rate is equal to the rate at which molecules diffuse to the surface and a steady-state voltammogram (sigmoidal voltammetric curve) results [29]. Equilibrium is more easily established at a microelectrode than at a conventional sized electrode, and hence, a sigmoidal voltammetric curve will result at the microelectrode, while a peak-shaped voltammogram is obtained at a conventional sized electrode. Figure 1.14 illustrates the near or quasi steady-state behaviour observed at a cylinder microelectrode and the typical peak-shaped cyclic voltammograms obtained under the same conditions at a conventional sized glassy carbon electrode. Near steady-state or steady-state current behaviour is actually obtainable at electrodes of all sizes, but the time scale (scan rate) required to reach this behaviour at conventional millimeter sized electrodes is far too long (too slow) to be of any practical use in experimental work [30].

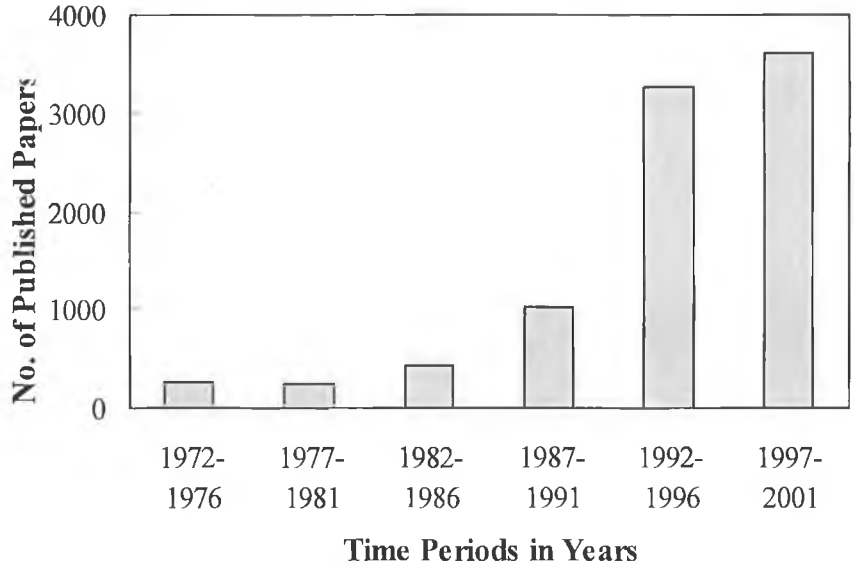

Figure 1.13: Trend in rate of publications on microelectrodes (from http://wos.izum.si).

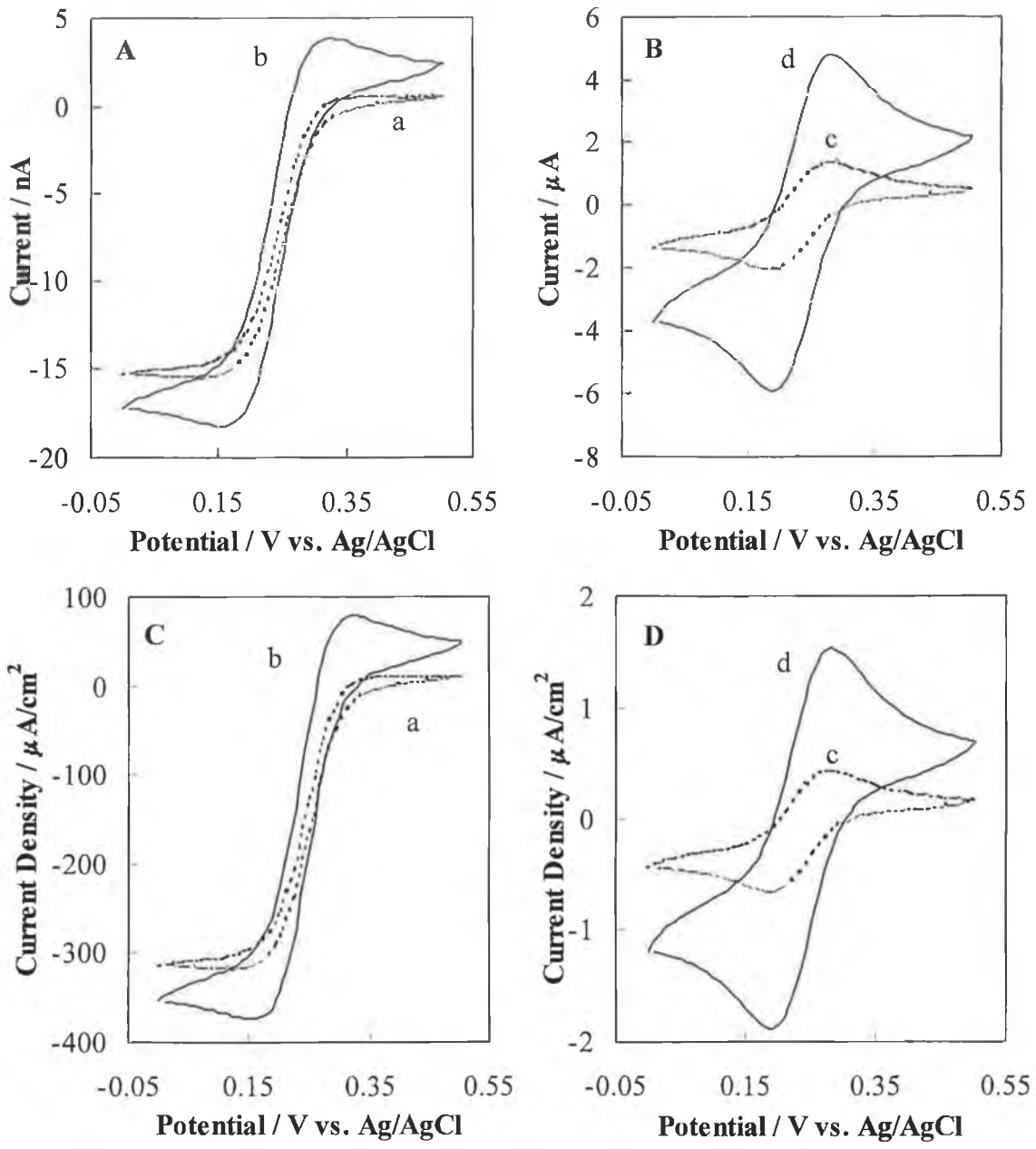

Figure 1.14: Cyclic voltammograms of 1 mmol/L potassium ferricyanide in 0.1 mol/L KCl solution at ((A) and (C)) a carbon fibre cylinder microelectrode (3.5 µm radius, 0.22 mm length) and at ((B) and (D)) a glassy carbon disc electrode (1.0 mm radius); scan rate: (a) and (c), 10 mV/s; (b) and (d), 100 mV/s. A and B: Current vs. Potential. C and D: Current Density µA/cm² vs. Potential.

(b) Decreased Capacitance and Enhanced Signal to Noise Ratio

The electrochemical double layer behaves like an electrolytic capacitor, i.e. when the applied potential is changed a current flows to charge the double layer capacitance. This process complicates the electrochemical measurement in two respects; the potential at the interface does not reach the applied potential until this charging process is complete, and the charging and faradaic currents are convolved at short times. Hence, it is desirable to minimise the magnitude of the charging current and the time it takes to charge the double layer [29]. From the equation:

$$\frac{i_f}{i_c} \approx \frac{1}{rC_d\nu} \qquad (1.16)$$

where r is the electrode radius, C_d is the double-layer capacitance, and ν is the scan rate, it is evident that reducing the electrode radius and / or lowering the scan rate will result in an enhanced signal-to-noise ratio. In addition, the reduced capacitance, which results from the reduced electrode size permits the usage of rapid scan rates (e.g., 10^5 V/s), hence permitting the exploration of very fast electrochemical reactions on a low microsecond or even a nanosecond timescale [29].

(c) Increased Current Density

For steady-state diffusion to a flat-plate electrode:

$$I_L = DCnF / \delta \qquad (1.17)$$

δ, which is the steady-state diffusion layer (cm), becomes constant after about 1 s of electrolysis due to the intervention of convection superimposed on diffusion, and has a value in a solution that is not artificially stirred of about 0.05 cm [31]. It was found that for a spherical electrode of radius less than the diffusion layer thickness, the maximum diffusion-controlled current is no longer DCF/r, but rather DC_iF/r. This opens the possibility of obtaining increased limiting diffusion currents and increasing the range of current densities at which reaction rates can be measured without disturbance by interfering diffusion of reactants to or from the electrode. Hence, by using a microelectrode, the maximum current density that remains free from transport control

can be increased by up to several thousand times [31]. This increase in current density is evident in Figure 1.14 (C and D), in which the current density for 0.1 mol/L KCl measured at the carbon fibre microelectrode is over 100 times greater than that at a glassy carbon electrode. In addition, the contribution to steady-state current by convection is not apparent at microelectrodes, thus making them particularly applicable for use in flowing systems [32, 33].

(d) Reduced Ohmic Effects

When faradaic and charging currents flow through a solution, they generate a potential that acts to weaken the applied potential by an amount iR, where i is the total current, and R is the cell resistance [29]. This can lead to distortions of the experimental responses. Microelectrodes reduce these ohmic effects considerably, as the faradaic currents observed are typically six orders of magnitude smaller than those at conventional size electrodes. These small currents may completely eliminate iR problems, even when working in resistive media such as organic solvents.

(e) High Temporal and Spatial Resolution

The small size of microelectrodes makes their use in micro-location and micro-volume measurements possible – a distinct advantage when compared to large, conventional size electrodes.

1.3.4.3 Shapes, Responses and Fabrication

Several microelectrode geometries exist; disc, band, cylinder, ring, cone, sphere, and array, with each form exhibiting its own distinct diffusion profile (see Figure 1.15). Of these geometries, disc and cylinder microelectrodes are the most commonly used. The most popular materials include platinum, carbon fibres, and gold, although mercury, iridium, nickel, silver, and superconducting ceramics have been used [34-40].

The surface of a disc microelectrode is not uniformly accessible, nor are all points equivalent as electroactive species are primarily depleted by electrolysis at the disc electrode boundary, thus inducing non-uniform diffusion and varying current densities. The total diffusion-limited current composed of the planar flux and radial flux diffusion components is:

$$i_{total} = i_{planar} + i_{radial} \tag{1.18}$$

where for a disc microelectrode, the general expression for the radial component is given by:

$$i_{radial} = arnFDC \tag{1.19}$$

where r is the radius of the electrode, a is a function of the electrode geometry (4, 4π and 2π for discs, spheres and hemispheres, respectively), D is the diffusion coefficient, and C is the concentration [4]. (Diffusion behaviour at spherical and ring electrodes is similar to this). The extent to which either predominates depends on the dimensions of the electrode and the diffusion layer. When the diffusion layer is larger than the electrode ($Dt/r_o^2 > 1$), the current approaches steady-state and sigmoidal voltammograms are obtained. Conversely, at small values of Dt/r_o^2, planar diffusion predominates and peak-shaped behaviour is observed [4].

The case for radial diffusion to a cylinder microelectrode differs slightly. Here, diffusion is identical at any cross-section plane perpendicular to the cylinder axis except at the end of a cylinder, which can be ignored. The limiting current of such an electrode is dependent on the length, and is often referred to as quasi-state current and is described by:

$$i_l = \frac{2\pi FDCL}{ln\,[2(Dt)^{1/2} / r]} \qquad (1.20)$$

where L and r are the length and radius of the cylinder, respectively. The electrochemical behaviour observed at a band microelectrode is similar to that obtained at cylinder microelectrodes.

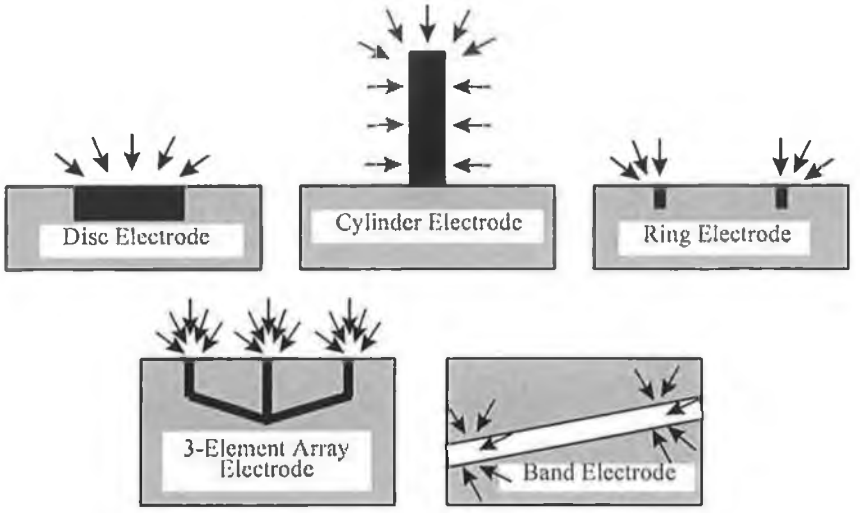

Figure 1.15: Illustrations of the most common microelectrode geometries and their corresponding diffusion fields (adapted from [29]).

Several techniques have been devised for constructing microelectrodes of the aforementioned geometries [41]. For each geometry, the dimension of the insulation layer surrounding the microelectrode has to be considered, as this will affect the overall size of the microelectrode and hence its potential applicability. The most common microelectrode form is the cylinder due to its relative ease of preparation and relatively large response signal. It is constructed by attaching a thin metal wire (e.g. platinum) or a carbon fibre to a copper wire and sealing this in a glassy capillary with the wire or fibre left protruding [26]. Disc electrodes can be fabricated by attaching conducting wires or sheets in either a large or small insulator. Disc electrodes contained in large housing are easily polished, while those contained in a thin insulation layer require some skill to prepare (e.g. tip cutting) or expensive equipment (e.g. a micro-beveller) [42]. Cone microelectrodes can be obtained by etching a carbon fibre or metal wire using ion-beam, flame, electrochemical, or chemical vapour deposition techniques.

Band array electrodes have been constructed using lithography [26, 43-46]. Microelectrodes with an integrated reference electrode have also been constructed [47, 48]. A more detailed description of the fabrication of carbon fibre cylinder microelectrodes will be given in Section 4.5.

1.3.4.4 Carbon Fibre Microelectrodes

Carbon fibres are long bundles of linked graphite plates and are commonly made from petroleum pitch or polyacrylonitrile, with a three step procedure of (a) stabilisation, (b) carbonisation and (c) graphitisation (heat treatment procedure similar to that of glassy carbon (see Section 1.3.1.1)). The carbon material is drawn out during the curing process to form filaments, with the process designed to orient the a axis along the fibre axis. The finished fibre has a cross-section of the "onion", "radial", or "random" type, and the fibre generally exhibits a high fraction of the edge plane [26]. There are two types of carbon fibre; nearly perfect oriented carbon fibres, which have high tensile strength, and disordered fibres, which have lower tensile strength and more defects on the cylindrical wall. Typical diameters of carbon fibres range from 5 – 15 μm. Figure 1.16 illustrates the structure of the carbon fibre cylinder microelectrodes employed in this work.

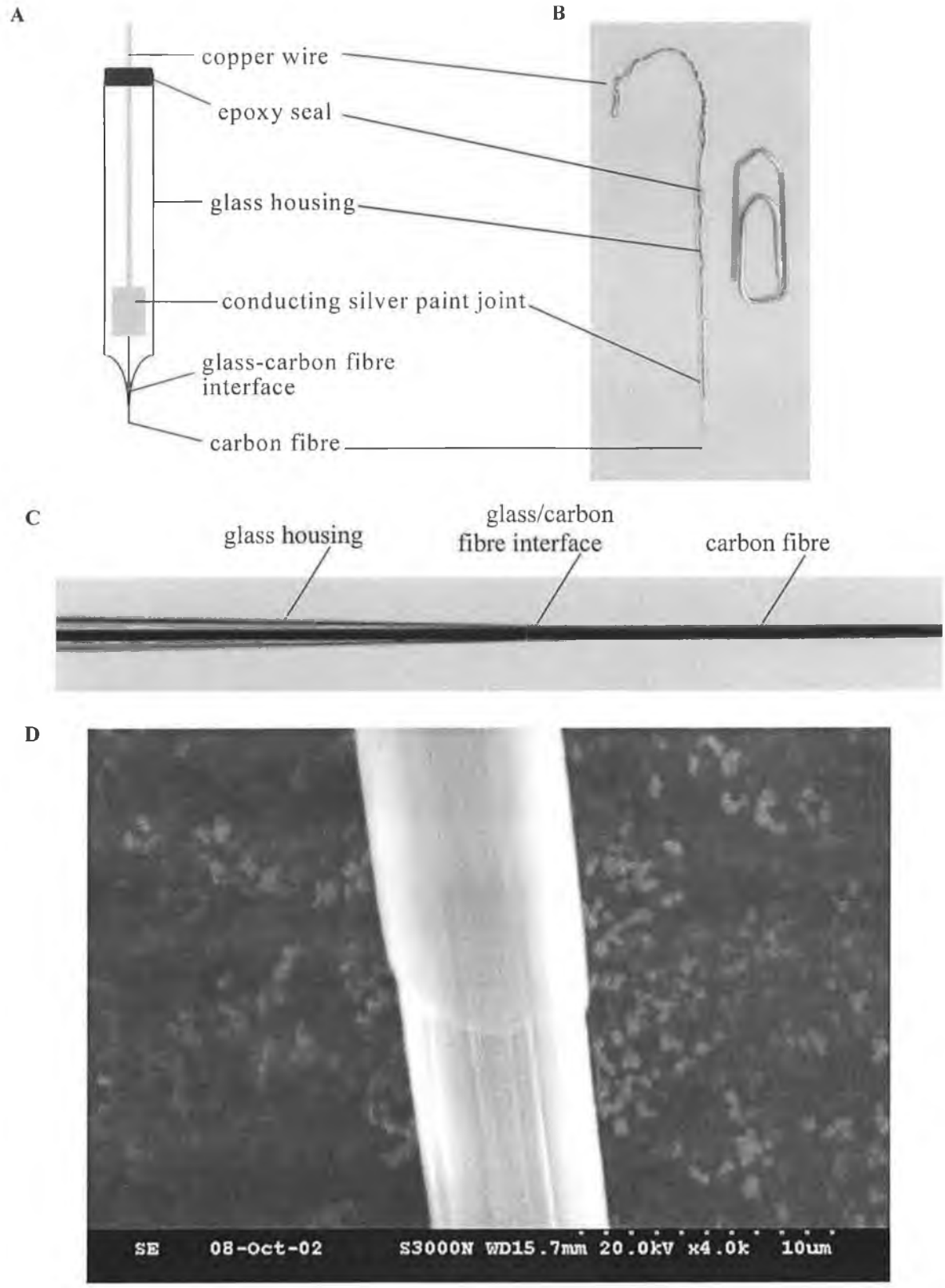

Figure 1.16: (A) Schematic of a CFCME, (B) Photograph of CFCME, (C) Optical microscopy image of the carbon fibre-glass interface and (D) SEM micrograph of carbon fibre-glass interface.

1.4 Electrode Modification

1.4.1 Purpose and Definition

Increasing requirements for versatility and accuracy of analysis have lead to much research and development in the field of analytical chemistry. Highly specific, sensitive and efficient analytical methods are necessary, especially for the analysis of trace components in complex samples [49]. Modern analytical instrumentation is a powerful tool for this purpose. However, the selective detection and / or separation of analytes are important to avoid errors due to matrix effects. A deliberate design of the analytical sensor can improve its abilities according to the needs of an analytical problem. Chemically modified electrodes (CMEs), as an example of this approach, have attracted considerable interest in recent decades as researchers have sought to exert more direct control over the chemical nature of an electrode [50]. For the analytical chemist, this means the preparation of a sensor that makes the desired electrochemical reaction simpler and more rapid.

A chemically modified electrode may be defined as *an electrode made of a conducting or semiconducting material that is coated with a selected monomolecular, multimolecular, ionic, or polymer film or a chemical modifier and that by means of faradaic (charge-transfer) reactions or interfacial potential differences (no new charge transfer) exhibits chemical, electrochemical, and / or optical properties of the film* [51]. When one component of the modification layer is a biological compound such as an enzyme, such a modified electrode is termed a biosensor. A CME consists of two parts – the substrate electrode and a layer of chemical modifier [49]. The choice of the parts is determined by the desired analytical features of the sensor. Figure 1.17 shows the strategy of sensor preparation.

Methods employed for the introduction of a modifier onto the surface of the substrate electrode are based on only a few approaches:

(i) direct irreversible adsorption,

(ii) covalent attachment to specific surface sites,

(iii) coating with a polymer film, and

(iv) mixing of the electrode substrate with a slightly soluble modifier and any further component (e.g., Nujol and epoxy resin) [49].

These and others will be discussed in more detail in the proceeding section. Many variations in the approach illustrated in Figure 1.17 exist, and there are numerous diverse methods for the attachment of the modifier. The most important criteria are the achievement of simple and reproducible fabrication procedures, resulting in robust CMEs. The level of modifier loading and modifier binding can be varied to achieve optimal mechanical and chemical stability. The activity of the modifier towards the analyte should be constant over a wide concentration range, and should exhibit low background current [49]. According to the chemical nature of the modifier and the thickness of the layer, the modified surfaces can be divided into three main categories:

(i) thin layers of materials with a low relative molecular mass,

(ii) polymer films, and

(iii) layers of inorganic materials.

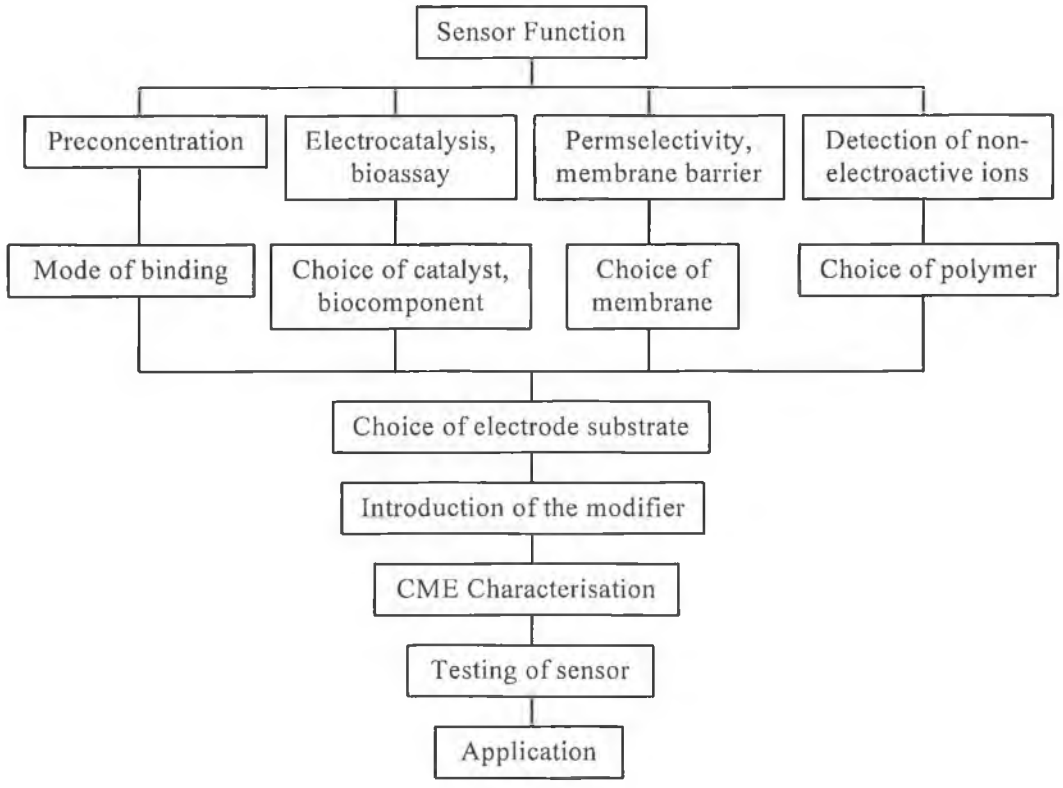

Figure 1.17: Strategy of CME sensor development (adapted from [49]).

The bare substrate electrode used for the CME preparation must exhibit certain necessary electrochemical parameters in order to yield satisfactory attachment of modifier. The most common substrate electrodes are solid electrodes such as gold, platinum, graphite, glassy carbon, etc. Microelectrodes have become increasingly

popular as substrates for CMEs. In general, the surface of the substrate electrode must be activated prior to modification. Physical, chemical and electrochemical cleaning, and adjustment of the oxygen level etc., are some of the most common approaches.

Chemical modification of the electrode may enhance the sensitivity and / or selectivity of the device towards a particular analyte(s) by exploiting several phenomena that occur at chemically modified electrodes. These include:

(i) *accumulation* of analytes from dilute solution, usually preceding detection, in order to improve detectability. The preferential accumulation of metallic as well as non-metallic species in the modifying layer represents an extensive application field of CMEs in inorganic and organic trace analysis. The method consists of three steps – accumulation, detection and regeneration, and is analogous to conventional stripping voltammetry. However, at CMEs, a non-electrochemical step is responsible for the accumulation (see Figure 1.18), thereby permitting the accumulation of analytes that cannot be preconcentrated electrolytically. A nontronite/cellulose acetate-coated glassy carbon electrode were found to exhibit good accumulation ability for Cu^{2+} in ammoniacal medium [52]. The modified electrode accumulated the $[Cu(NH_3)_4]^{2+}$ complex through the ion-exchange ability of nontronite, and permitted Cu^{2+} to be determined down to 1.73 μg/L.

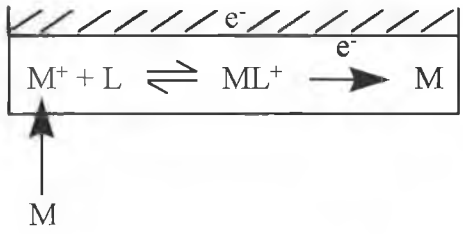

Figure 1.18: Scheme for metal (M) preconcentration; L = ligand (adapted from [49]).

(ii) *electrocatalysis* to mediate electron transfer between the electrode and the analyte, which otherwise undergoes very slow electrochemical reaction at the more commonly used bare electrodes. This process is shown in Figure 1.19. The reduced form of the mediator, M_{red}, is readily oxidised at the electrode. Its oxidised form M_{ox} then interacts in a chemical reaction with the substrate (S – the analyte) diffusing from the bulk of the solution, to yield a product (P) and regeneration of the catalyst M_{red} [49]. The reduced C-60-[dimethyl-(beta-cyclo-

dextrin)]$_2$/Nafion® CME was found to successfully catalyse the electrochemical response of norepinephrine [53]. A glassy carbon substrate electrode modified using the sol-gel technique with sol-gel glass thin films containing 12-molybdophosphoric acid was shown to exhibit a high electrocatalytic response for the reduction of iodate [54]. Iodate in table salt was determined down to 1 μmol/L. The application of organometallic mediators such as the ferrocenes, phthalocyanines, hexacyanoferrate, ruthenium oxide complexes and metalloporphyrins, and organic mediators including the phenoxazines, phenathiazines, phenazines, quinone-hydroquinones and tetrathiafulvalene, in the determination of a wide range of substances of biological importance is described in a thorough review by Wring *et al.* [55]. These mediators, which act as electrocatalysts, were used in the determination of substances such as glucose, hydrogen peroxide, cholesterol, galactose, carbohydrates, and dopamine, amongst others.

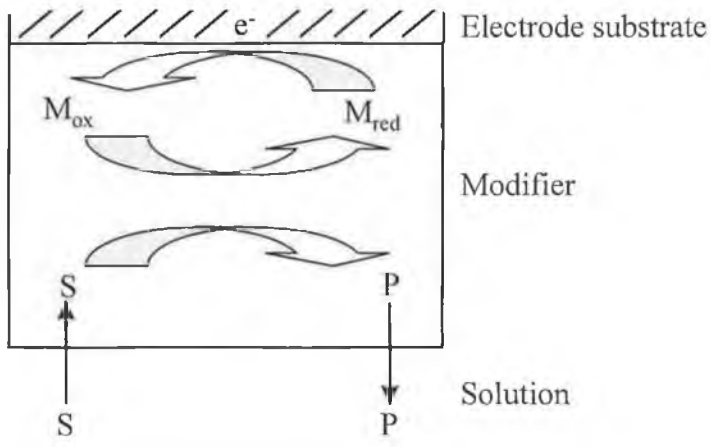

Figure 1.19: Scheme of mediated electrocatalysis (adapted from [49]).

(iii) *chemical transformation* in which an electroinactive analyte can be reacted with the appropriate reagent immobilised at the chemically modified electrode to yield an electroactive product suitable for electrochemical determination. This scheme is illustrated in Figure 1.20. A self-assembled monolayer was formed on a gold surface from a solution of thiolated alpha-cyclodextrin, creating an array of ultramicroelectrodes, which captured electroactive molecules such as those of ferrocene [56]. When the modified electrode was exposed to an electrochemically inactive compound, the ferrocene molecules were replaced by the electroinactive molecules via an equilibrium established between the two

compounds, lowering the current for ferrocene oxidation. The decrease in current was directly proportional to the amount of inactive compound added (in this case glucose). A conducting poly(3-methylthiophene) polymer modified platinum electrode was employed in the determination of some electroinactive anionic species such as nitrate, sulphate, and chloride [57].

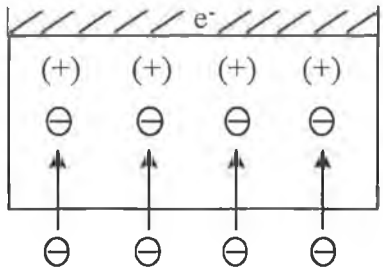

Figure 1.20: Principle of the detection of electroinactive ions (adapted from [49]).

(iv) *permeability*, which describes discriminative transport through a membrane coating that controls the access of analyte and interfering substances to the electrode surface i.e. an electrode coated with the permeable membrane is accessible to the target analyte while interfering substances are rejected or prevented from reaching the electrode surface. See Figure 1.21. Surfactant interference at the bismuth film electrode was circumvented by using a Nafion® coating [58]. Cellulose acetate was employed as an anti-interference barrier on screen-printed carbon electrodes, permitting the rapid and selective determination of paracetamol in urine, with a limit of detection of 13 μmol/L [59].

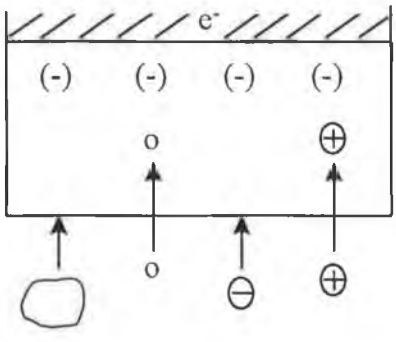

Figure 1.21: Scheme for a permselective coating (adapted from [49]).

(v) *ionic equilibria*, whereby an electrolyte solution containing an analyte ion is on one side of a selective ion-exchange membrane and a solid electrode on the other. A review of ion-exchange voltammetry at polymer-coated electrodes is given in [60].

(vi) *controlled-release* in which an analyte accumulated at the chemically modified electrode can undergo quantitative release to the test solution. Polypyrrole film modified electrodes were used as an electro-releasing reservoir [61]. The electrochemically controlled release of 5-fluorouracil from this modified electrode to aqueous electrolytes was studied, with the released amount controlled by the reduction potential and proportional to the thickness of the film.

In addition, modification of an electrode can reduce analysis times by eliminating the need for sample preparation / separation procedures.

1.4.2 Surface Modification Approaches

Several methods exist for the preparation of chemically modified electrodes, of which the most common will be briefly described here:

(a) Chemisorption / Self-Assembled Monolayers

Chemisorption (chemical adsorption) is an adsorptive interaction between a molecule and a surface in which electron density is shared by the adsorbed molecule and the surface [62]. This interaction requires direct contact between the chemisorbed molecule and the electrode surface; as a result, the highest coverage achievable is usually a monomolecular layer. In addition to this coverage limitation, chemisorption is rarely completely irreversible, with the chemisorbed molecules slowly leaching into the contacting solution phase during the duration of the experiment. Monolayers which have spontaneously adsorbed onto an electrode surface are commonly referred to as "self-assembled" monolayers (see Figure 1.22). This type of electrode modification is extremely suitable for studying fundamental aspects of electrochemistry, e.g., electron-transfer kinetics / mechanisms, adsorption processes, solvation effects, ion pairing and the effects of intermolecular interactions [63-67]. Sulphur containing groups (thiols, sulphides and disulphides) are popular chemisorption agents for the modification of

gold (and other) electrode surfaces. A self-assembled monolayer of a heterocyclic thiol, mercaptobenzimidazole, on a gold electrode was used in the voltammetric sensing of uric acid in the presence of 100 fold excess of ascorbic acid [68]. A gold electrode modified with a monolayer of an aromatic thiol, 4-aminothiophenol, showed electrocatalytic activity towards the oxidation of NADH, with an overpotential 600 mV lower than at the bare electrode [69].

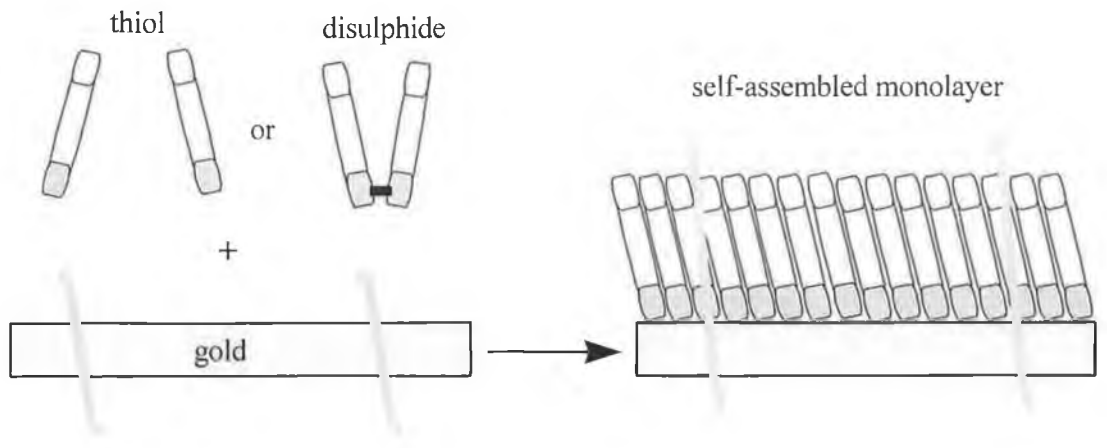

Figure 1.22: Formation of a self-assembled monolayer on a gold surface.

(b) Organic Polymers

Coating of an electrode with polymer films has proved to be one of the simplest and most versatile approaches for surface modification. An enormous number of polymers have been used to prepare chemically modified electrodes. These can be divided into three general categories: r*edox polymers*, which contain electroactive functionalities either within the main polymer chain or in side groups pendent to this chain (e.g., poly(vinylferrocene); *ion-exchange and coordination polymers*, which are not electroactive themselves, but can incorporate electroactive guest molecules (e.g. poly(vinylpyridine) and Nafion®); and *electronically conductive polymers*, where the polymer chains are themselves electroactive (e.g. polypyrrole) [62]. Several methods exist for the application of polymer films to the electrode surface. The simplest is dip-coating, which involves dipping the electrode surface into a solution of polymer, removing it, and allowing it to dry. This procedure can be repeated in order to achieve a thicker polymer film. A drawback of this method is that it is difficult to control the

amount of material that ends up on the electrode surface. Another method involves the application of a measured amount of solution to the surface, which allows more accurate control of the amount of material deposited. Spin-coating is used widely in the semi-conductor industry and yields very uniform film thicknesses. Finally, polymer films can be electropolymerised directly onto the electrode surface [62]. The range of applications for polymer modified electrodes is vast. An enzymatic biosensor based on a horseradish-peroxidase-ferrocene carbon paste modified electrode coated with a layer of electrochemically generated poly(o-aminophenol) was employed in the determination of hydrogen peroxide in milk [70]. Nitrite in commercial fertilizer was determined using an electrochemical sensor developed from a redox polymer $[Ru(bipy)_2(PVP)_{10}C]Cl$, where bipy is 2,2'=bipyridyl and PVP is poly-(4-vinylpyridine) [71]. The modified electrode was an efficient electrocatalyst for nitrite oxidation, providing a current amplification of at least three times compared to the unmodified electrodes. A Nafion® modified carbon paste electrode was employed in the determination of clenbuterol down to 1.02 nmol/L in bovine urine extracts [72]. Formaldehyde, after in situ conversion to an ionic derivative, was accumulated on a Nafion®-coated mercury film electrode, and detected at limits down to 34 nmol/L [73]. A platinum electrode modified by electropolymerisation of polypyrrole, using chloride as dopant, was employed for the detection of ammonia [74]. Following immobilisation of urease and creatinine iminohydrolase, the modified electrode was used as an internal detector in amperometric biosensors for urea and creatinine.

(c) Zeolites and Clays

Zeolites, clays and other microcrystalline-structured materials are of interest in electrode modification due to their ion-exchange properties. They also exhibit well-defined microstructures that can withstand high temperatures and highly oxidising solution environments [62]. For example, clays have a sheet-like structure, and zeolites contain pores and channels of well-defined diameter. One of the key points in the electrochemistry of these materials is the electrochemical accessibility of redox-active species within the zeolite framework. A nontronite clay-modified screen-printed carbon electrode was employed in the determination of codeine in pharmaceutical formulations [75]. Carbon paste electrodes modified with five different soils were prepared and their heavy metal ion uptake behaviour investigated using a model Cu(II) aqueous solution

[76]. Electrochemically preanodized clay-modified electrodes were used for the detection of uric acid or dopamine in the presence of a high concentration of ascorbic acid by square wave voltammetry [77]. Glucose oxidase was immobilized between two nontronite clay coatings on a glassy carbon electrode with methyl viologen as mediator, with the modified electrode being applied in the determination of glucose [78].

(d) Polymers of Transition Metal Complexes and Metal Oxides

These types of modifiers are classified into several categories: (i) ferrocene and related compounds, (ii) poly-cyanometallate (Prussian Blue and its analogues), (iii) phenanthroline complexes, (iv) pyridine complexes, (v) porphyrin complexes, (vi) phthalocyanine complexes, and (vii) metal oxides [28]. They are usually deposited onto the electrode surface from an appropriate solution containing precursor salts by using cyclic voltammetry in a suitable potential range. Films formed from poly-cyanometallates possess particularly interesting electrochemical and optical properties, exhibiting electrochromism – the ability of a material to change its colour upon a change in oxidation state [62]. A glassy carbon electrode modified with an electrochemically deposited ferrocene-modified polyaniline film, was used for determination of hydrogen peroxide at low potential [79]. A recent review describes the use of electrodes modified with supramolecular assemblies of ruthenium complexes and porphyrins in the determination of substances such as dopamine and ascorbic acid [80]. Metal hexacyanoferrates and their applications are reviewed more thoroughly in Section 4.3.

(e) Langmuir-Blodgett Methods

This method involves the use of a molecule with a polar "head group" (e.g., a carboxylate) and a hydrophobic "tail" (e.g., an alkyl chain). When such amphiphilic molecules (surfactants) are dispersed onto the surface of water, the head groups are oriented downwards due to their solvation by the water, and the tail groups point upwards [62]. This highly ordered monolayer is then transferred to a substrate surface. Both monolayer and multilayer films are achievable.

Some procedures for evaluating chemically modified electrodes include: *electrochemical measurements* (cyclic voltammetry, chronoamperometry, chronopotentiometry, impedance spectroscopy etc.), which enable the charge storage and transport, selectivity and dynamic properties of the modification layer to be investigated [81,82]; *electrochemical quartz crystal microbalance measurements*, which permit the simultaneous measurement of electrochemical parameters and mass changes at electrode surfaces [83,84]; *electrochemical microscopy techniques*, which provide insights into the microdistribution of electrochemical and chemical activity as well as the topography of a surface [85]; and *surface spectroscopy techniques*, (e.g., reflectance spectroscopy, Raman spectroscopy, ellipsometry), which offer dynamic and spatial resolution information on films interfaces and film formation [86, 87].

1.5 Conclusions

The purpose of this first chapter was to briefly describe some basic electrochemical / electroanalytical principles, outline the techniques employed in this work, describe carbon-based electrodes, and introduce the main approaches to electrode modification. The basic requirements of an electroanalytical experiment, such as electrodes and electrolyte solution were described, while an overview of the processes occurring in such an experiment was also provided. The main techniques used in this work, such as linear sweep voltammetry, cyclic voltammetry, square wave voltammetry etc. were described and their respective waveforms and responses illustrated. An introduction was also given to carbon-based electrodes, in particular glassy carbon, carbon paste, and screen-printed electrodes, with an additional introduction to microelectrodes. Finally, the possibilities for modification of electrodes were briefly described.

1.6 References

1. D.W.A. Sharp, *Dictionary of Chemistry*, Penguin Group, London, 1990, p. 148.
2. J.O'M. Bockris, A.K.N. Reddy, *Modern Electrochemistry 1, Ionics*, second ed., Plenum Press, New York, 1998, p.1.
3. P.T. Kissinger, W.R. Heineman (ed.s), *Laboratory Techniques in Electroanalytical Chemistry*, second ed., Marcel Dekker, Inc., New York, 1996, pp.iii-v.
4. J. Wang, *Analytical Electrochemistry*, second ed., Wiley-VCH, New York, 2000.
5. J.P. Hart, *Electroanalysis of Biologically Important Compounds*, Ellis Horwood, New York, 1990.
6. A.J. Bard, L.R. Faulkner, *Electrochemical Methods, Fundamentals and Applications*, second ed. John Wiley & Sons, Inc., 2001.
7. A.J. Bard, L.R. Faulkner, *Electrochemical Methods, Fundamentals and Applications*, John Wiley & Sons, Inc., 1980, Ch.1.
8. Southampton Electrochemistry Group, *Instrumental Methods in Electrochemistry*, Ellis Horwood, New York, 1990.
9. C.M.A. Brett, A.M.O. Brett, *Electroanalysis*, Oxford University Press, Oxford, 1998.
10. W.R. Heineman, P.T. Kissinger, in: P.T. Kissinger, W.R. Heineman (ed.s), *Laboratory Techniques in Electroanalytical Chemistry*, second ed., Marcel Dekker, Inc., New York, 1996, Ch.3.
11. S.M. Lunte, C.E. Lunte, P.T. Kissinger, in: P.T. Kissinger, W.R. Heineman (ed.s), *Laboratory Techniques in Electroanalytical Chemistry*, second ed., Marcel Dekker, Inc., New York, 1996, Ch.27.
12. R.L. McCreery, K.K. Cline, in: P.T. Kissinger, W.R. Heineman (ed.s), *Laboratory Techniques in Electroanalytical Chemistry*, second ed., Marcel Dekker, Inc., New York, 1996, Ch.10.
13. I. Svančara, K. Vytřas, J. Barek, J. Zima, *Crit. Rev. Anal. Chem.* **31** (2001) 311.
14. G.U. Flechsig, O. Korbout, S.B. Hočevar, S. Thongngamdee, B. Ogorevc, P. Grundler, J. Wang, *Electroanalysis* **14** (2002) 192.
15. J. Jezkova, E.I. Iwuoha, M.R. Smyth, K. Vytřas, *Electroanalysis* **9** (1997) 978.
16. E. Miland, A.J.M. Ordieres, P.T. Blanco, M.R. Smyth, C.O. Fagain, *Talanta* **43** (1996) 785.

17. J. Oni, T. Nyokong, *Anal. Chim. Acta* **434** (2001) 9.
18. M. Pravda, M.P. O'Halloran, M.P. Kreuzer, G.C. Guilbault, *Anal. Lett.* **35** (2002) 959.
19. S. Andreescu, T. Noguer, V. Magearu, J.L. Marty, *Talanta* **57** (2002) 169.
20. J. Wang, J.M. Lu, S.B. Hočevar, B. Ogorevc, *Electroanalysis* **13** (2001) 13.
21. M. Boujtita, J.P. Hart, R. Pittson, *Biosens. Bioelectr.* **15** (2000) 257.
22. S.D. Sprules, J.P. Hart, S.A. Wring, R. Pittson, *Anal. Chim. Acta* **304** (1995) 17.
23. R.M. Wightman, D.O. Wipf, in: A.J. Bard (ed.), *Electroanalytical Chemistry*, Vol. 15, Marcel Dekker, New York, 1989, pp. 267-353.
24. J. Wang, *Electroanalytical Techniques in Clinical Chemistry and Laboratory Medicine*, VCH, New York, 1988, p. 150.
25. A.M. Bond, *Analyst* **119** (1994) R1.
26. A.C. Michael, R.M. Wightman, in: P.T. Kissinger, W.R. Heinemann (ed.s), *Laboratory Techniques in Electroanalytical Chemistry*, second ed., Marcel Dekker, Inc., New York, 1996, Ch.12.
27. R.M. Wightman, *Anal. Chem.* **53** (1981) 1125.
28. J. Mo, *Doctoral Dissertation*, University of Ljubljana, Slovenia, 2000.
29. R.J. Forster, *Chem. Soc. Rev.* **23** (1994) 289.
30. C.G. Zoski, A.M. Bond, E.T. Allinson, K.B. Oldham, *Anal. Chem.* **62** (1990) 37.
31. J.O'M. Bockris, A.K.N. Reddy, M. Gamboa-Aldeca, *Modern Electrochemistry 2A, Fundamentals of Electrodics*, second ed., Plenum Press, New York, 1998, Ch. 7.
32. R.C. Matos, L. Angnes, M.C.U Araujo, T.C.B. Saldanha, *Analyst* **125** (2000) 2011.
33. K.A. Sagar, M.R. Smyth, M. Rodriguez, P.T. Blanco, *Talanta* **42** (1995) 235.
34. L. Keane, C. Hogan, R.J. Forster, *Langmuir* **18** (2002) 4826.
35. K.A. Sagar, M.R. Smyth, *J. Pharmaceut. Biomed. Anal.* **22** (2000) 613.
36. W.R. Jin, W. Li, Q. Xu, Q. Dong, *Electrophoresis* **21** (2000) 1409.
37. M.A. Baldo, S. Daniele, G.A. Mazzocchin, *Electrochim. Acta* **41** (1996) 811.
38. J. Wang, J.Y. Wang, W.K. Adeniyi, S.P. Kounaves, *Electroanalysis* **12** (2000) 44.
39. A.M. Fermier, L.A. Colon, *HRC-J High Res. Chrom.* **19** (1996) 613.
40. G.X. Li, Y.T. Long, H.Y. Chen, D.X. Zhu, *Fresen. J. Anal. Chem.* **356** (1996) 359.

41. C.G. Zoski, *Electroanalysis* **14** (2002) 1041.
42. X.J. Zhang, B. Ogorevc, *Anal. Chem.* **70** (1998) 1646.
43. X.J. Zhang, B. Ogorevc, J. Wang, *Anal. Chim. Acta* **452** (2002) 1.
44. W.H. Huang, D.W. Pang, H. Tong, Z.L. Wang, J.K. Cheng, *Anal. Chem.* **73** (2001) 1048.
45. S.L. Chen, A. Kucernak, *Electrochem. Commun.* **4** (2002) 80.
46. J.P. Bozon, D.M. Giolando, J.R. Kirchhoff, *Electroanalysis* **13** (2001) 911.
47. X.J. Zhang, B. Ogorevc, G. Tavčar, I. Grabec-Švegl, *Analyst* **121** (1996) 1817.
48. X.J. Zhang, J. Wang, B. Ogorevc, U.E. Spichiger, *Electroanalysis* **11** (1999) 945.
49. J. Labuda, *Selective Electrode Rev.* **14** (1992) 33.
50. IUPAC, *Pure Appl. Chem.* **70** (1988) 1301.
51. R.A. Durst, A.J. Bäumner, R.W. Murray, R.P. Buck, C.P. Andrieux, *Pure Appl. Chem.* **69** (1997) 1317.
52. J.M. Zen, H.F. Wang, A.S. Kumar, H.H. Yang, V. Dharuman, *Electroanalysis* **14** (2002) 99.
53. M. Wei, M.X. Li, N.Q. Li, Z.N. Gu, X. Duan, *Electrochim. Acta* **47** (2002) 2673.
54. W.B. Song, X. Chen, Y.X. Jiang, Y. Liu, C.Q. Sun, X.H. Wang, *Anal. Chim. Acta* **394** (1999) 73.
55. S.A. Wring, J.P. Hart, *Analyst* **117** (1992) 1215.
56. S.J. Choi, B.G. Choi, S.M. Park, *Anal. Chem.* **74** (2002) 1998.
57. E.A. Blubaugh, G. Russell, M. Racke, D. Blubaugh, T.H. Ridgway, H.B. Mark, *ACS Sym. Ser.* **556** (1994) 137.
58. J. Wang, R.P. Deo, S. Thongngamdee, B. Ogorevc, *Electroanalysis* **13** (2001) 1153.
59. M.A.T. Gilmartin, J.P Hart, *Analyst* **119** (1994) 2431.
60. P. Ugo, L.M. Moretto, *Electroanalysis* **7** (1995) 1105.
61. H. Huang, C.W. Liu, B.F. Liu, G.J. Cheng, S.J. Dong, *Electrochim. Acta* **43** (1998) 999.
62. C.R. Martin, C.A. Foss Jr., in: P.T. Kissinger, W.R. Heinemann (ed.s), *Laboratory Techniques in Electroanalytical Chemistry*, second ed., Marcel Dekker, Inc., New York, 1996, Ch.13.
63. K.V. Gobi, T. Okajima, K. Tokuda, T. Ohsaka, *Langmuir* **14** (1998) 1108.
64. M.A. Fox, M.D. Wooten, *Langmuir* **13** (1997) 7099.

65. S.E. Creager, G.K. Rowe, *J. Electroanal. Chem.* **420** (1997) 291.
66. R. Andreu, J.J. Calvente, W.R. Fawcett, M. Molero, *J. Phys. Chem. B* **101** (1997) 2884.
67. K. Aoki, T.J. Kakiuchi, *Electroanal. Chem.* **452** (1998) 187.
68. C.R. Raj, F. Kitamura, T. Ohsaka, *Analyst* **127** (2002) 1155.
69. C.R. Raj, T. Ohsaka, *Electrochem. Commun.* **3** (2001) 633.
70. M.A.V. Garcia, P.T. Blanco, A. Ivaska, *Electrochim. Acta* **43** (1998) 3533.
71. A.P. Doherty, M.A. Stanley, D. Leech, J.G. Vos, *Anal. Chim. Acta*, **319** (1996) 111.
72. S. Moane, M.R. Smyth, M. O'Keeffe, *Analyst* **121** (1996) 779.
73. W.H. Chan, H. Huang, *Analyst* **121** (1996) 1727.
74. M. Trojanowicz, A. Lewenstam, T.K.V. Krawczyk, I. Lahdesmaki, W. Szczepek, *Electroanalysis* **8** (1996) 233.
75. Y. Shih, J.M. Zen, H.H. Yang, *J. Pharmaceut. Biomed. Anal.* **29** (2002) 827.
76. I. Grabec-Švegl, B. Ogorevc, *Fres. J. Anal. Chem.* **367** (2000) 701.
77. J.M. Zen, P.J. Chen, *Anal. Chem.* **69** (1997) 5087.
78. J.M. Zen, C.W. Lo, *Anal. Chem.* **68** (1996) 2635.
79. A. Mulchandani, L.C. Barrows, *ASC Sym. Ser.* **613** (1995) 61.
80. H.E. Toma, K. Araki, *Coordin. Chem. Rev.* **196** (2000) 307.
81. J. Wang, B.Z. Zeng, C. Fang, F. He, X.Y. Zhou, *Electroanalysis* **11** (1999) 1345.
82. D.M. Kelly, J.G. Vos, *Electrochim. Acta* **41** (1996) 1825.
83. C.L. Lin, K.C. Ho, *J. Electroanal. Chem.* **524** (2002) 286.
84. G. Inzelt, E. Csahok, V. Kertesz, *Electrochim. Acta* **46** (2001) 3955.
85. J.Y. Ye, J.Y. Liu, Z.Q. Zhang, J.M. Hu, S.J. Dong, Y.H. Shao, *J. Electroanal. Chem.* **508** (2001) 123.
86. A.P. Taylor, J.A. Crayston, T.J. Dines, *Analyst* **123** (1998) 1913.
87. L.M. Abrantes, J.P. Correia, M. Savic, G. Jin, *Electrochim. Acta* **46** (2001) 3181.

2. CATHODIC ELECTROCHEMICAL DETECTION OF NITROPHENOLS AT THE BISMUTH FILM ELECTRODE

2.1 Introduction

The contaminants that enter water through human activities, such as detergents, plasticizers, pesticides, insecticides, herbicides, products of chlorination and industrial wastes are of great interest in water analysis programmes. Hundreds of such compounds have been identified and more than one hundred have been designated Priority Pollutants by the US Environmental Protection Agency. Of these, phenol and its nitro-, chloro- and methyl-substituted derivatives constitute a significant proportion, with approximately 20 being included. In addition, the EU has stated that the Maximum Admissible Concentration (MAC) of these compounds in potable water is 0.1 μg/L (individual) or 0.5 μg/L (collective).

Traditionally, these compounds have been determined by the oxidative coupling of phenols with 4-aminoantipyrine in alkaline solution, while other methods, such as gas and liquid chromatography, capillary electrophoresis, ELISA and optical methods have also been proposed. Nitrophenols also lend themselves well to electrochemical detection and this mode, along with the aforementioned techniques, will be reviewed in the chapter.

In this chapter, a new electrode surface design, the bismuth film electrode (BiFE), is presented as a promising alternative to mercury and other solid electrodes for the direct cathodic electrochemical detection of nitrophenols (2-nitrophenol; 2-NP, 4-nitrophenol; 4-NP and 2,4-dinitrophenol; 2,4-DNP). The preparation of the bismuth film, involving an *ex situ* electroplating of metallic bismuth onto a glassy carbon substrate electrode, was optimised. The useful negative potential windows of the BiFE at several pHs were determined. Cyclic voltammetry was employed to elucidate the nature of the electrochemical reduction process. The BiFE showed favourable voltammetric behaviour when compared to mercury and bare glassy carbon electrodes, and was successfully applied in voltammetric, amperometric and flow injection determination of nitrophenols.

2.2 *Nitrophenols and Significance for Measurement*

Nitrophenolic compounds, consisting of one or more nitro-groups bonded to a phenolic ring are of considerable interest due to their environmental and toxicological impact. The nitrophenols focused on in this work are 2-nitrophenol, 4-nitrophenol and 2,4-dinitrophenol and are illustrated in Figure 2.1.

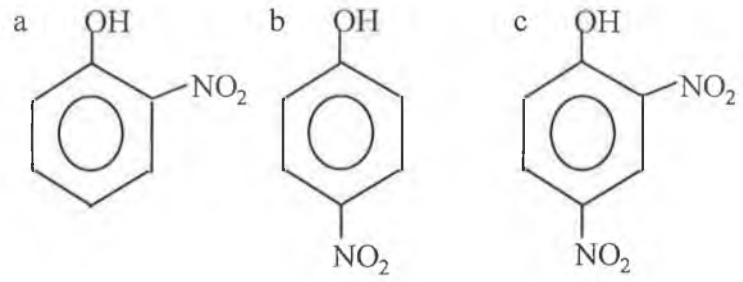

Figure 2.1: Structures of (a) 2-nitrophenol, (b) 4-nitrophenol and (c) 2,4-dinitrophenol.

2.2.1 2-Nitrophenol

2-nitrophenol, also known as *o*-nitrophenol or 2-hydroxynitrobenzene, occurs as light yellow needles or prisms, with a peculiar, aromatic odour [1]. It is used as a pH indicator and as an intermediate in the production of pigments, rubber chemicals, lumber preservatives, photographic chemicals and fungicide agents [2]. It is a water-soluble solid that is moderately acidic in water as a result of dissociation. Releases into the environment are primarily emissions into air, water, and soil from diffuse sources, such as vehicle traffic and hydrolytic and photolytic degradation of the respective pesticides [3]. The major transformation pathway for 2-NP emitted to the troposphere should be rapid nitration to 2,4-dinitrophenol, while it is enriched in the liquid phase of clouds. Although there is no evidence for the carcinogenicity of 2-nitrophenol, it is irritating to the skin and eyes, mucous membranes and the respiratory tract [1]. It may also cause central nervous system depression and dyspnoea, headache, and nausea. It also leads to the formation of methaemoglobin, which in sufficient concentration causes cyanosis (blue colour in the lips, ears, and fingernails).

2.2.2 4-Nitrophenol

4-nitrophenol is an odourless compound consisting of colourless to slightly yellow crystals, and is used in a variety of applications, including drug manufacture, fungicides, dyes and leather darkening [4]. It is a metabolite of parathion and a photooxidation product of aromatic hydrocarbons including benzene, toluene, phenanthrene, and nitrobenzene [1]. Figure 2.2 (A and B) illustrates the mechanism for the breakdown of the pesticides parathion and paraxon, to 4-NP.

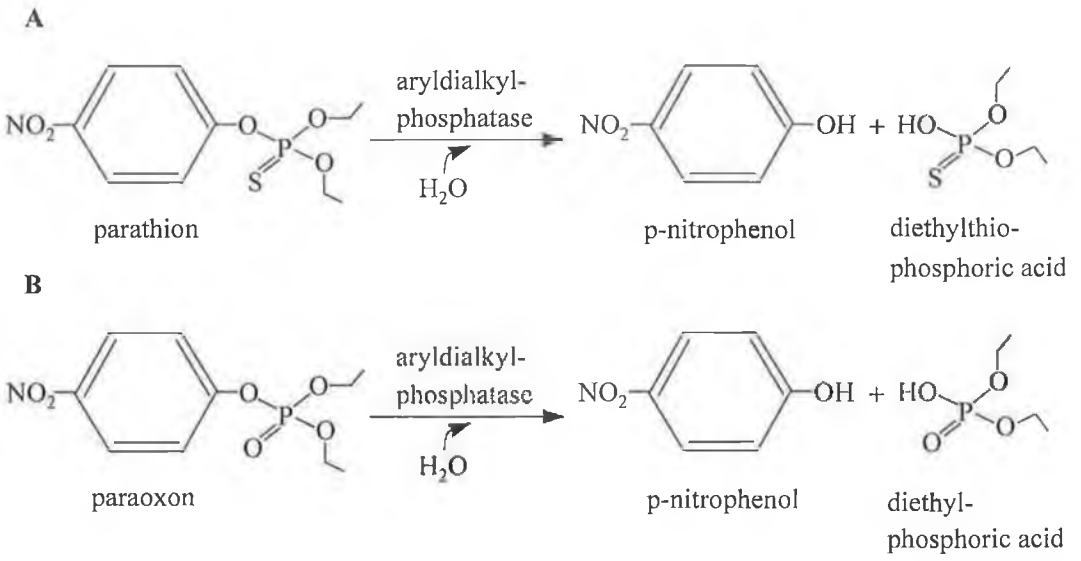

Figure 2.2: Breakdown of (A) parathion and (B) paraoxon to 4-nitrophenol (adapted from [5]).

Its release into the environment is by the same routes as that of 2-nitrophenol. 4-NP is found in the gas phase of clouds due to extensive binding to particles, with most of it removed from the air by wet and dry deposition [3]. Acute (short-term) inhalation or ingestion of 4-nitrophenol in humans or animals causes headaches, drowsiness, nausea and cyanosis. Contact with eyes causes irritation, while corneal opacity may occur upon inhalation. Tests involving acute exposure of animals, such as the LD_{50} test in rats (LD_{50} 250 mg/kg), have shown 4-nitrophenol to have high toxicity from oral and dermal exposure. Like 2-nitrophenol, 4-nitrophenol has not been classed as a carcinogen.

2.2.3 2,4-Dinitrophenol

2,4-Dinitrophenol is a yellow, odourless solid used in making dyes, wood preservatives, explosives, insect control substances and other chemicals, and as a photographic developer [6]. 2,4-DNP enters the air, soil and water during its manufacture and use, and can also be formed from the reaction of other chemicals in the air. It can be broken down slowly in water and soil by small organisms or by reacting with other chemicals. It sticks to particles in water, which will cause it to eventually settle to the bottom sediment. It also adheres to some types of soil particles, which may prevent it from moving very deep into the soil with rainwater [6]. It is considered to be highly toxic to humans, with a lethal oral dose of 14 to 43 mg/kg [4]. The acute (short-term) effects of 2,4-dinitrophenol in humans through oral exposure consist of nausea, vomiting, sweating, dizziness, headaches, and loss of weight. Long-term oral exposure to 2,4-DNP in humans has resulted in the formation of cataracts and skin lesions and has caused effects on bone marrow, and the central nervous and cardiovascular systems. As with the mononitrophenols, there is no evidence for the carcinogenicity of 2,4-dinitrophenol.

2.3 Detection of Nitrophenols

The toxicity of nitrophenols and their widespread use have necessitated the development of methods for their determination. The US Environmental Protection Agency (EPA) has included nitrophenols in their List of Priority Pollutants [7,8], while the European Union has stipulated that the maximum admissible concentration (MAC) of total phenols in water intended for human consumption, excluding those phenols which do not react with chlorine as 0.5 μg/L. The MAC for individual phenols is 0.1 μg/L [9]. Thus, several methods have been developed for the determination and quantification of phenolic substances, of which the most commonly employed, and their analytical performance, will be briefly described in the following sections.

2.3.1 4-Aminoantipyrine Method

The official standard methods in many countries are based on the oxidative coupling of phenols with 4-aminoantipyrine (4-AAP) in alkaline solution [10]. The phenols react with 4-AAP in the presence of potassium ferricyanide to form a coloured antipyrine dye (from yellow to red) [11]. The method, however, is non-specific, and coloured compounds are also formed with para-substituted phenols in which the substituent is a carboxyl, halogen, hydroxyl, methoxyl, or sulphonic acid group. For this reason, the determination with 4-aminoantipyrine is called the "phenol index". Some interferences can be eliminated by distillation and extraction with chloroform. The limit of detection tends to lie above 10 μg/L, therefore making the method unsuitable for samples where lower levels need to be determined [11].

2.3.2 Gas Chromatographic and Capillary Electrophoretic Methods

Gas chromatography (GC) permits speciation of the various substituted phenols after liquid-liquid extraction. The US EPA Method 604 for phenols (including 2- and 4-nitrophenol) involves the serial extraction of an acidified sample with methylene dichloride [12]. The extract is dried and concentrated, and exchanged to 2-propanol, after which the phenols are analysed by GC using a flame-ionisation detector. Alternatively, US EPA Method 625 for semivolatile compounds can also be used [13]. This method involves the serial extraction of a sample in methylene dichloride at a pH greater than 11 and again at pH less than 2. After drying the methylene dichloride extract, the sample is analysed by gas chromatography-mass spectrometry (GC-MS).

Kim and Kim have reported on the simultaneous determination of phenols using GC and GC-MS [14]. This method involved an extractive two-phase isobutoxycarbonyl derivatisation prior to analysis, where the phenolic hydroxy groups in acidic solution were allowed to react with isobutyl chloroformate present in the dichloromethane phase containing triethylamine. GC-MS with negative-ion chemical ionisation for the trace level determination of 11 phenols as pentafluorobenzyl derivatives was described by Nakamura *et al.* [15]. The derivatisation procedure involved a 5 hour reaction time at 80°C. The major limitation of these GC techniques is the extraction procedure, where losses can occur during extraction, concentration

and solvent exchange steps. The extraction can also be very labour intensive and often requires specialised glassware as well as the use of chlorinated solvents.

26 phenols included in the US EPA priority phenols were determined using non-aqueous capillary electrophoresis (CE) with UV detection [16]. The limits of detection achieved were, however, quite high; 109 μg/L for 2-nitrophenol, 168 μg/L for 4-nitrophenol and 28 μg/L for 2,4-dinitrophenol. Limits of detection of 5 – 10 μg/L were obtained using CE combined with off-column solid phase extraction and on-column field amplified injection [17]. These methods are advantageous as they allow the separation and detection of complex samples. However, the limits of detection obtained are higher than the required legislative levels.

2.3.3 Liquid Chromatographic Methods

Liquid chromatography (LC) finds widespread use in the separation of phenolic compounds. The primary advantages of using LC are that there is no requirement for precolumn derivatisation (as with GC) and the need for sample pretreatment is minimal. The main detection methods used with LC are UV, diode array or electrochemical detection, the latter of which will be discussed in more detail here. Nitrophenolic compounds exhibit a better response with a UV detector as compared to an electrochemical one (operated at oxidative potentials) [18]. Hence, these two detection methods are often used simultaneously for the detection of a range of phenolic substances. A range of phenols including 2-nitrophenol, 4-nitrophenol and 2,4-dinitrophenol were determined using LC with UV detection [19]. Limits of detection down to 0.2 μg/L were reached, which are suitable for analysis of surface water but not low enough to reach the levels required for tap water.

The aforementioned nitrophenols were determined at levels of < 0.04 μg/L following liquid-solid extraction and LC with UV detection at 280nm [20]. Determination of nitrophenols at levels below those required by EU regulations was carried out using LC with UV detection [21]. A comparative study of UV and electrochemical detection for the determination of priority phenols was performed [22]. Limits of detection down to 1 ng/L were obtained for all chlorinated phenolics with electrochemical detection. However, for the nitrophenols, the lowest limits of detection (< 0.1 μg/L) were obtained with the UV detector. Diode-array detection was employed in the detection of phenolic compounds following solid phase

extraction and liquid chromatography [23]. The nitrophenols were detected at levels between 2 and 30 μg/L with recoveries greater than 90%. These methods provide advantages over the GC and CE methods in that lower limits of detection are achieved, and, in contrast to GC, no complicated derivatisation procedures are required.

An overview of liquid chromatography with electrochemical detection is given here. The specifics of the electrochemistry of nitrophenols will be presented in the next section. Liquid chromatography in conjunction with electrochemical detection has also found widespread application in the determination of phenolic compounds. This method was used to determine 4-nitrophenol in landfill leachate (pre-concentrated and distilled) at a level of 7.0 μg/L [24]. The phenols were oxidised at a potential of +1.25 V (vs. Ag/AgCl) at a glassy carbon electrode. A similar electrode set-up, using a potential of +1.15 V was used by Paterson *et al.* to determine the eleven priority pollutant phenols [25]. Limits of detection between 0.1 and 7.8 μg/L were achieved for 2-nitrophenol, 4-nitrophenol and 2,4-dinitrophenol.

27 phenols and herbicides in water were determined by LC using an electrochemical detection system consisting of four coulometric array cell modules, each containing four electrochemical detector cells [26]. The detectors, porous graphite working sensors with palladium reference and counter electrodes, were arranged in series after the analytical column and operated in an increasingly positive potential along the array i.e. 0.00 V at electrode 1, 0.08 V at electrode 2, with increments of 0.08 V at each subsequent electrode until a value of +1.20 V was reached at electrode 16. The coulometric efficiency of each element in the array allows a complete voltammetric resolution of the analytes – even peaks that were unresolved by the chromatographic column were resolved by the detector. The three nitrophenols with which this work is concerned were detected at levels of between 0.08 and 0.22 ng/L, levels well below those required by legislation.

Similarly, low limits of detection (down to 2 ng/L for nitrophenols) were obtained using an electrochemical detector consisting of two glassy carbon electrodes operated in a "screen-out mode" or a "redox-mode" [27]. In the screen-out mode, the first electrode was set at low potentials to eliminate interferences and only the second one was used for analytical purposes. In the redox-mode, the first electrode was operated at high positive potentials to ensure oxidation of all the compounds of

interest. Afterwards the oxidation product was reduced in a second step. The redox-mode was, however, unsuitable for nitrophenols due to their lack of reversibility at these positive potentials.

Two electrodes were also used for the detection of total phenols in water and wastewater samples [28]. Interferences were oxidatively eliminated at a large surface area (coulometric) electrode and the phenols detected at an amperometric electrode operated at +0.78 V. All of the aforementioned electrochemical techniques involve the use of oxidative potentials; however, it is also possible to detect nitrophenols in the reductive mode. This method was employed for the detection of 4-nitrophenol using a dropping mercury electrode following separation by HPLC [29]. Using this detector, a limit of detection of 4.4 ng was determined for 4-nitrophenol. Limits of detection for nitrophenols (including 2-nitrophenol, 4-nitrophenol, and 2,4-dinitrophenol) down to 1 ng were obtained using LC with a dropping mercury electrode by sweeping the potential from –0.18 V to –0.66 V vs. Ag/AgCl in steps of –10 mV [30]. As can be seen from the literature, LC with electrochemical detection offers an attractive method for the determination of phenolic compounds at low levels.

Glassy carbon electrodes have found some use in the reduction of nitrophenols. One method employs a glassy carbon working electrode array in the wall-jet configuration, in which eight 1 mm electrodes are spaced radially around a 3 mm central electrode [31]. Different potentials were applied to the electrodes in order to selectively detect a specific phenol. In this mode, 2-nitrophenol and 4-nitrophenol were detected at potentials of –0.55 V and –0.85 V, respectively. This rather complicated set-up has the advantage of allowing nitrophenols to be determined cathodically rather than anodically, which although more commonly used, is less sensitive.

A glassy carbon electrode in the reductive mode was used for the electrochemical detection of 4-nitrophenol, 3-methyl-4-nitrophenol, 4,6-dinitro-*o*-cresol, parathion-methyl, fenitrothion and parathion-ethyl following their separation by liquid chromatography [32]. At the applied potentials (–0.80 to –1.60 V), however, the background current grew more than the peaks. In order to avoid this, the nitro group was detected indirectly i.e. by the oxidative detection of the coulometrically reduced organonitro compounds. Using this mode, limits of detection

< 0.20 μg/L were obtained for each of the nitro compounds. A major limitation associated with the use of glassy carbon electrodes is the difficulty in achieving simple surface renewal; in most cases, either a tedious mechanical initialisation (polishing) or a rigorous chemical and / or electrochemical surface regeneration is frequently required [33]. This applies especially when high oxidative potentials are used, as the oxidation of matrix components leads to significant fouling of the electrode surface.

2.3.4 Some Other Methods

Other techniques used for the determination of nitrophenols include ELISA and optical sensors. 4-Nitrophenol and 2,4-dinitrophenol were determined at levels of 0.61 μg/L and 0.26 μg/L respectively, using polyclonal antibody-based ELISAs [34,35]. An optode based on the fluorescence quenching of poly(2,5-dimethoxy-phenyldiacetylene) was developed for 2-NP with a linear range from 1.8×10^{-6} to 1.8×10^{-3} mol/L (0.25 to 250 mg/L) [36]. Another optical sensor, based on the fluorescence quenching of curcumin, with a detection limit of 8.0×10^{-5} mol/L (11.12 mg/L) was developed for 2-nitrophenol [37].

Nistor *et al.* reported on the use of a competitive flow immunoassay with fluorescence detection for the determination of 4-nitrophenol with a limit of detection of 0.5 μg/L [38]. This method showed little cross-reactivity for about 30 phenols and nitro-derivatives, with no major interferences except for 2,4-dinitrophenol and mercury(II) ions. Phenols, including 2-nitrophenol, were determined using a flow injection chemiluminescent quench method, using the ability of the phenols to quench the chemiluminescence of *p*-chlorobenzenediazonium fluoroborate in a medium of alkaline hydrogen peroxide [39]. The limit of detection for 2-nitrophenol was 20 μg/L.

2.4 *Electrochemistry of Nitrophenols*

2.4.1 Electrochemical Behaviour of Nitrophenols

2.4.1.1 Oxidation Reactions

The anodic oxidation mechanisms of phenol itself and substituted phenols are quite complex [40]. Hydroxylation reactions play a decisive role, but they are interwoven with another major reaction – oxidative coupling of phenoxy radicals producing dimeric and polymeric products. The relative importance of the two processes depends on applied potential, concentration and acidity etc. It has been shown that either one or two electrons are transferred in the electro-oxidation pathway of phenols, depending on the magnitude of the anodic potential [41]. Stepping the potential to just the foot of the phenol oxidation peak favours oxidation of phenol to the phenoxy radical, which very rapidly dimerizes to the corresponding 4,4'-biphenol, which is further oxidised to diphenoquinone (Figure 2.3 A). Conversely, stepping to more anodic potentials yields the phenoxonium cation, which undergoes rapid hydroxylation to hydroquinone, which in turn is further oxidised to *p*-benzoquinone (Figure 2.3 B) [41].

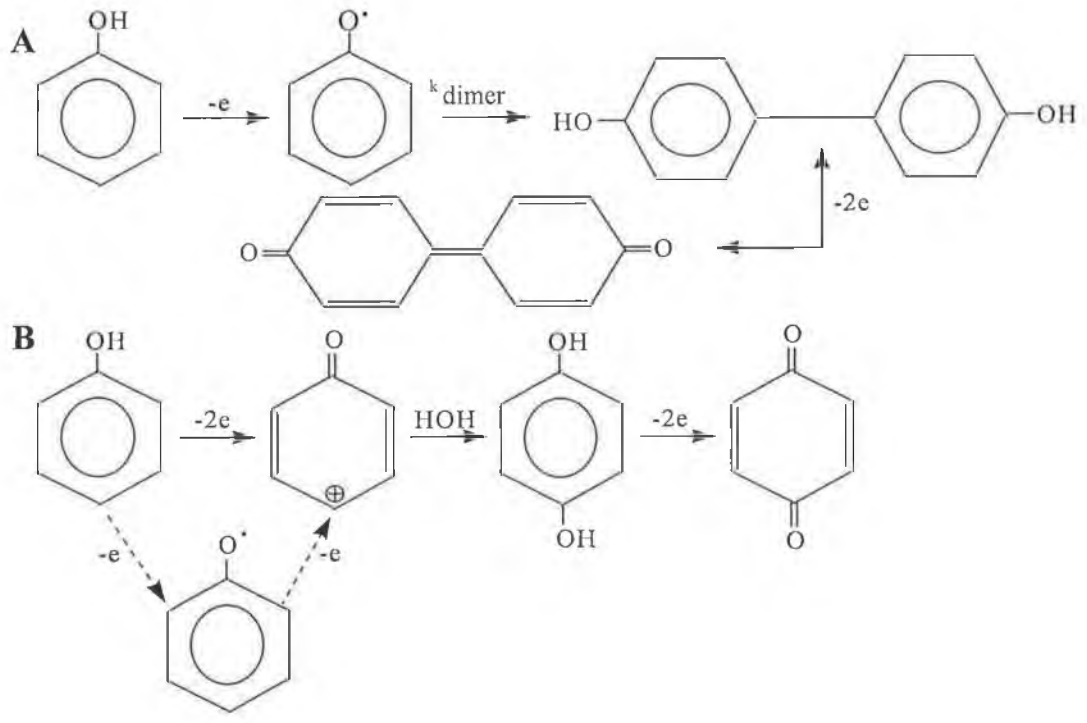

Figure 2.3: Oxidation pathways of phenol (adapted from [41]).

Electro-oxidation of nitro-substituted phenols will occur in a similar manner, with a hydroquinone intermediate and a benzoquinone end product. This can be seen in the following oxidation of 4-nitrophenol (Figure 2.4):

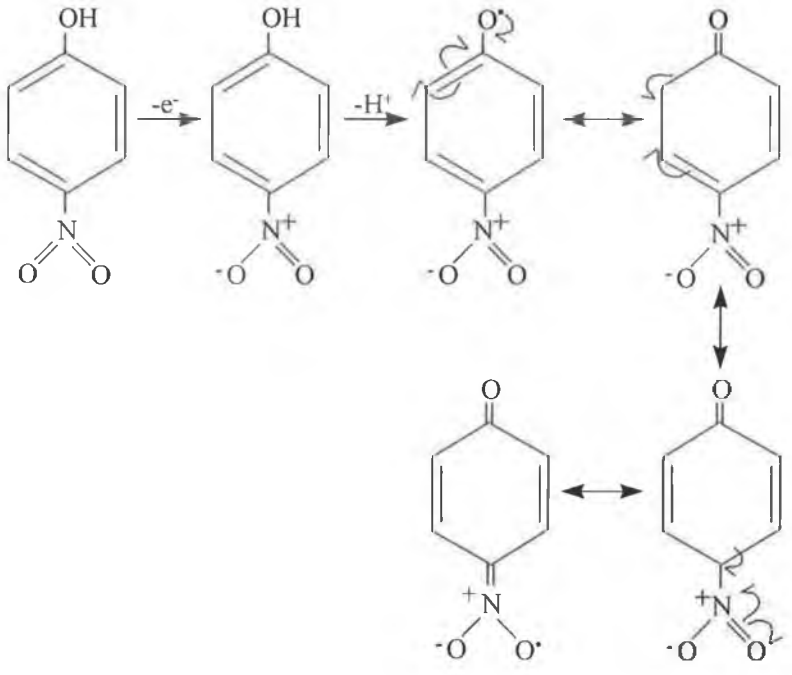

Figure 2.4: Oxidation pathway of 4-nitrophenol.

2.4.1.2 Reduction Reactions

The reduction of nitrophenols has been well documented in a number of excellent texts and reviews [42-46]. The reduction of the nitro group, although influenced by the nature of its environment, follows a generalised pattern [44]. In acidic solution, reduction to the hydroxylamine only, to the hydroxylamine and then to the amine in two steps, or directly to the amine in one step can occur. In instances where two waves occur, the largest wave occurs at a small negative potential and has been shown to involve four electrons. This wave is generally well-defined and constant in height over a wide pH range. In solutions of less than pH 4, a smaller two electron reduction wave occurs at more negative potentials and disappears in neutral and alkaline solutions. The largest wave occurs at the least negative potential and is due to the irreversible electrochemical reduction of the nitro group to a hydroxylamine. The following reaction is involved in this reduction process:

$$R\text{-}NO_2 + 4H^+ + 4e^- \longrightarrow R\text{-}NHOH + H_2O \quad (2.1)$$

Although this reduction process is normally observed as a single four-electron reduction step, it is really a combination of two separate reduction steps with a short lived intermediate. The reduction of the nitro group to a nitroso group constitutes the first stage. Nitroso compounds are generally reduced at more positive potentials than nitro groups, thus the nitroso compound is not isolated but reduced immediately to the hydroxylamine in a fast two-electron process. The main wave is therefore a combination of the following reactions [44]:

$$R\text{-}NO_2 + 2H^+ + 2e^- \longrightarrow R\text{-}NO + H_2O \ (Slow) \quad (2.2)$$

$$R\text{-}NO + 2H^+ + 2e^- \longrightarrow R\text{-}NHOH \ (Fast) \quad (2.3)$$

In general, these two waves are combined to give a single four-electron polarographic reduction wave. The polarographic behaviour of this nitro group is not constant for all nitro compounds, but is dependant on a number of parameters including molecular structure, composition and pH of supporting electrolyte and, in the case of a dropping mercury electrode, the drop time.

The main reduction wave of the nitro group is useful in the polarographic analysis of nitro compounds for the number of reasons:

1. The determination of nitro compounds enjoys a certain selectivity in polarographic analysis as only a limited number of other polarographic reactions occur at the small negative potential of these substances.
2. The polarographic determination of nitro compounds tends to be quite sensitive due to the relatively large wave / peak height of the four-electron reduction process.
3. The wave / peak height is unaffected by minor changes in pH.

The smaller secondary wave, which occurs at more negative potentials during the reduction of nitro compounds, involves a two-electron reduction step [44]. In general, this corresponds to the reducible protonated hydroxylamine. The unionised

hydroxylamine tends to be polarographically inactive, while the cation is reduced to the corresponding amine in a two-electron step:

$$R\text{-}N^{+}H_2OH + 2H^{+} + 2e^{-} \longrightarrow RN^{+}H_3 + H_2O \qquad (2.4)$$

In the analysis of drugs, for example, the most useful polarographic wave is the four-electron reduction wave, which generally occurs in the range $E_{1/2}$ –0.1 V → –0.4 V (vs. s.c.e.) where many other compounds are polarographically inactive [44]. The exact reduction potential is dependant on the pH of the supporting electrolyte, which for analytical purposes, is usually a buffer solution in the pH range of 3.5 to 5.5.

For the mononitrophenols in particular, all three exhibit two steps at low pH values [43]. The total height of the two steps occurring below pH 4.0 was found to correspond to a six-electron reduction (see Figure 2.5). Similarly, the reduction of the 2- and 4-nitrophenols in alkaline solution involves six electrons, although only the para- compound forms a double step, the height of the second step increasing progressively with increasing pH. The reduction of 3-nitrophenol in alkaline solution produces a single step involving four electrons, but above pH 12 the single step is replaced by a double step.

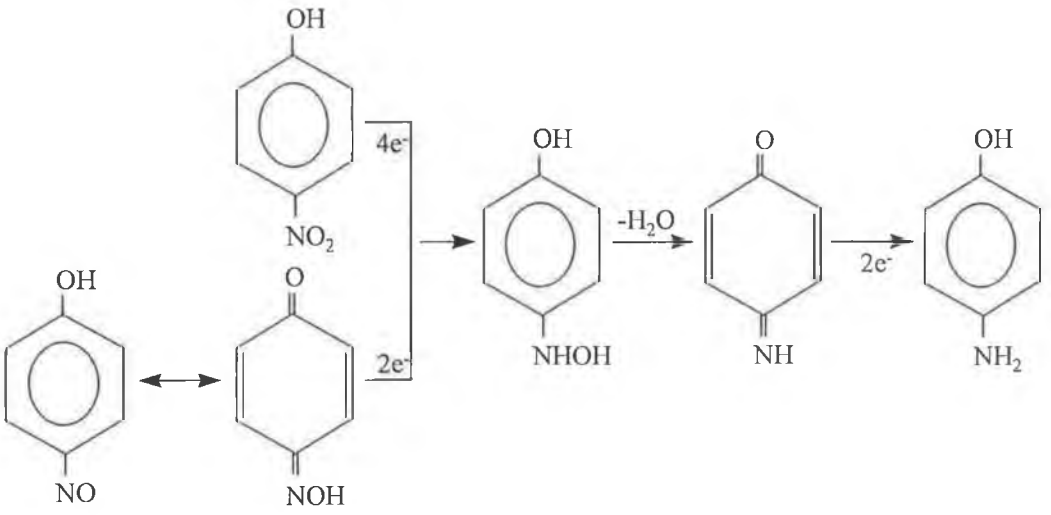

Figure 2.5: Reduction pathways of 4-nitrophenol.

2.4.2 Electrochemical Detection of Nitrophenols

As mentioned in the previous section, electrochemical studies of nitrophenols were, in general, carried out at mercury electrodes. Mercury is a very attractive choice of electrode material because it has a high hydrogen overvoltage that greatly extends the cathodic potential window (compared to solid electrode materials) and possesses a highly reproducible, readily renewable, and smooth surface [33]. There are several types of mercury electrodes. Of these, the dropping mercury electrode (DME), the mercury film electrode (MFE) and the hanging mercury drop electrode (HMDE) are the most commonly used [33,47-50]. Disadvantages of the use of mercury are its limited anodic range (due to the oxidation of mercury), its instability, and its well-documented toxicity [51-53].

Ni *et al.* described the simultaneous determination of nitrobenzene and nitro-substituted phenols by differential pulse voltammetry using a hanging mercury drop electrode [54]. The mononitrophenols, 2-, 3- and 4-nitrophenol, had well-defined voltammetric reduction waves, with peak potentials at –0.284 V, –0.292 V and –0.376 V, respectively. 2,4-Dinitrophenol exhibited two peaks at –0.240 V and –0.364 V (all vs. Ag/AgCl). Chemometric methods of data analysis were applied to resolve the overlapped voltammograms obtained when a mixture of these compounds was analysed. Limits of detection between 0.8 μg/L and 2.7 μg/L were obtained. This method is advantageous in that resolution of overlapped voltammograms within ±10% of the target value was achieved.

A hanging mercury drop electrode was used in the determination of 2-nitrophenol, 4-nitrophenol, 2-methoxy-5-nitrophenol and 2,4-dinitrophenol by differential pulse voltammetry (DPV) and adsorptive stripping voltammetry (AdSV) [55]. DPV was used in order to study the dependence of the behaviour of the nitrophenols on Britton Robinson (BR) buffer pH. BR buffer pH 5 was chosen as the optimum. AdSV provided a decrease in the limit of determination, allowing the nitrophenols to be determined at levels < 3.9 μg/L. The voltammetric behaviour of 2,4-dinitrophenol was studied at a HMDE in view of its use as a universal label in immunoelectrochemical assays [56]. The electrochemical behaviour of 2,4-DNP, albumin and 2,4-DNP-albumin was compared. The limit of detection (after an accumulation time of 120 s) for 2,4-DNP was determined to be 0.09 μg/L, which is actually below the desired legislative level.

Carbon paste electrodes (CPE) have found some use in the detection of nitrophenols. These electrodes, which use graphite powder mixed with various water-immiscible organic binders offer advantages such as an easily renewable and modifiable surface, low cost, and very low background current contributions [33] (see Section 1.3.2). Bentonite, an impure montmorillonite (clay) capable of adsorbing electroactive species for their direct determination, has found some use in the modification of carbon paste electrodes for determination of nitrophenolic substances. Such an electrode was employed in the determination of 2-nitrophenol [57]. 5% bentonite was added to the carbon paste, which was packed into an electrode and the surface smoothed. After each measurement it was necessary to remove the paste and clean and dry the cavity of the electrode. The limit of detection achieved was a rather high 30 μg/L.

This electrode was also applied for the determination of 2-nitrophenol in a flow system by differential pulse voltammetry [58]. 2-Nitrophenol exhibited a single, well-defined peak at approximately –0.575 V (vs. Ag/AgCl) in a formic acid / sodium formate buffer solution of pH 4. The results obtained here were favourable – it was not necessary to remove the paste from the electrode after each new injection as the surface of the electrode was continuously washed with the carrier liquid and exposed to relatively short analyte zones, in contrast to batch experiments. However, as with the previous study, quite a high detection limit of 20 μg/L was obtained. This electrode was again applied to the analysis of phenolic compounds, this time in the analysis of some chloro-, methyl- and nitrophenols by differential pulse voltammetry [59]. An advantage of this bentonite-modified carbon paste electrode is its ability to be used in both anodic and cathodic modes. The former was applied in the analysis of pentachlorophenol, 4-chloro-3-methylphenol and 2,4-dimethylphenol, while 2,4-dinitrophenol and 2-methyl-4,6-dinitrophenol were determined cathodically. No significant decrease in peak intensity was observed for the nitrophenols upon repeated injections. However, the peak height for the chlorophenols decreased after each new injection. No information regarding limits of detection was given.

A zeolite-modified carbon paste electrode was employed in the differential pulse voltammetric determination of 4-nitrophenol [60]. The zeolites are mixed aluminosilicates containing $(Si,Al)_nO_{2n}$ frameworks with cations added to maintain charge balance. These minerals contain cavities that are large enough for other

molecules to enter and are able to absorb electroactive species for their direct determination. When the 5% zeolite-modified CPE was used an increase in peak height (7-8 times) over that obtained at an unmodified electrode was observed. Despite this increase, the limit of detection achieved, 40 μg/L, was quite high. This electrode was applied to the determination of 4-nitrophenol in a seawater sample, whereby the sample was spiked with 0.1 mg/L 4-nitrophenol and a recovery of 98% obtained.

A C_{18} modified carbon paste electrode was used for the voltammteric determination of methyl parathion (MPT) and ortho-, meta-, and para-nitrophenol (ONP, MNP and PNP) [61]. The use of chromatographic column filling materials (gas and liquid columns) produces an effective preconcentration of organic substances in a wide range of matrices, thus facilitating methods for selective and sensitive determination by oxidation and reduction of different molecules with electroactive functional groups. Here, the carbon paste was modified with 50% C_{18} and the influence of pH and accumulation time on i_p investigated. BR buffer was employed as supporting electrolyte and the optimum pH values were determined to be pH 4 for ONP, pH 6 for MNP and PNP, and pH 2-4 for MPT. For all four compounds, i_p was found to increase with increasing accumulation time, up to a set time, after which there was no noticeable difference, due to saturation of the electrode. Limits of detection < 7.9 μg/L were determined and it was possible to decipher the reduction waves when a mixture of MNP, PNP and MPT was analysed, but when all four compounds were present, the ONP overshadowed the MPT and MNP peaks. This method is therefore advantageous in that a mixture of nitro compounds can be measured, although the limits of detection achieved are rather high.

2.5 Bismuth Film Electrode (BiFE)

2.5.1 Introduction

Since its inception as an electrode material in 1903 [62] and its application by Heyrovský in the original polarographic apparatus [63], mercury has been one of the most widely used electrode surfaces in the field of electroanalytical chemistry. Its advantages and disadvantages have already been mentioned in the previous section,

and due to its particular disadvantages, a constant search for new alternatives has been underway, particularly with respect to stripping analysis. Different bare carbon, gold or iridium electrodes have been used, although none of these approached mercury electrodes due to low cathodic potential limit, multiple peaks, or large background contributions [64-66]. Recently, bismuth coated electrodes were introduced in stripping analysis of various metal ions including Cd, Pb, Zn, Cu, Tl and In, which involves *in situ* deposition of the non-toxic bismuth [67] onto carbon substrate electrodes with subsequent stripping detection of the accumulated analyte [68-73]. More information regarding the application of the bismuth film electrode in stripping analysis of heavy metals is provided in Chapter 3. The promising results achieved in stripping analysis prompted consideration of the use of BiFE as an electrode surface in cathodic electrochemical detection of some organic compounds (particularly nitrophenols), which will be described in the following sections.

2.5.2 Bismuth and Bismuth-Coated Electrodes - Analytical Performance

Bismuth, Bi, is a member of Group VA of the periodic table in the same sub-group as arsenic and antimony [74]. Its electron configuration is [Xe] $4f^{14}$ $5d^{10}$ $6s^2$ $6p^3$ [67]. The only natural isotope is ^{209}Bi. Bismuth is a heavy, lustrous, silver-white metal with a slightly pink cast. If solidification is slow, large brittle crystals form. The major source of bismuth is as a by-product from the treatment of lead and copper ores. Some bismuth is also found associated with molybdenum, gold, silver, tin, tungsten, and zinc ores [74]. Bismuth is the most diamagnetic of all the metals, with a mass susceptibility of -1.35×10^6 and only liquid mercury has a lower thermal conductivity. Bismuth is not very reactive; generally, it is less reactive than lead and more reactive than silver [67]. The principal uses of bismuth are in pharmaceutical manufacture, fusible alloys (low melting; bismuth can form a number of binary, ternary, quaternary and quinary alloys melting in the range of 47 - 262°C), and as metallurgical additives. They are involved in the manufacture of a diverse range of products from autoclaves to drugs for the treatment of gastric diseases.

Several studies have been conducted regarding the electrochemical and interfacial behaviour of bismuth, including the formation of Bi_2O_3 film under anodic conditions [75], and the adsorption of organic molecules on the bismuth single plane [76-78]. With particular regard to electroanalytical applications, bismuth has shown great promise; bismuth coated carbon electrodes were successfully employed in

anodic stripping detection of several metal ions, with well-defined peaks, low background contributions, improved selectivity compared to mercury electrodes due to changes in peak potentials, detection limits in the low μg/L range, and importantly, the use of non-toxic bismuth [68-73]. The bismuth film electrode has also been employed in the cathodic electrochemical detection of some organic compounds, showing promising results compared to glassy carbon and mercury electrodes [79]. Bismuth modified carbon paste electrodes have also been used in voltammetric stripping analysis of some heavy metals [80] and a bulk bismuth electrode has been introduced recently for possible use in electrochemical studies and electroanalytical applications [81].

2.6 Cathodic Electrochemical Detection of Nitrophenols at the Bismuth Film Electrode

2.6.1 Experimental

2.6.1.1 Apparatus

Cyclic, linear sweep, differential, square wave (CV, LSV, DPV, SWV) and amperometric measurements were performed using a modular electrochemical system (Autolab, Eco Chemie, The Netherlands), equipped with a potentiostat PGSTAT10 and driven by GPES 4.8 software (Eco Chemie). For bulk voltammetric experiments, a bare or (mercury or bismuth coated) glassy-carbon disk (2 or 6 mm in diameter) served as the working electrode, with an Ag/AgCl(satd. KCl) and a platinum coil acting as the reference and auxiliary electrodes, respectively.

The flow system was composed of an LC pump (ConstaMetric-III, Milton Roy, Philadelphia, PA, USA), a 20 μL sample loop injector (Rheodyne), which was filled manually using a syringe, and a Model CC-5 thin-layer electrochemical cell (Bioanalytical Systems, Inc., Indiana, USA). A bismuth coated glassy-carbon electrode (3 mm in diameter) served as the working electrode, with an Ag/AgCl(satd. KCl) working electrode and an in-built counter electrode. For the flow injection-amperometric detection (FI-AD) measurements, the flow rate was 0.5 mL/min and the operating potential was set at –1.0 V vs. Ag/AgCl(satd. KCl).

Prior to electrochemical measurements, the solutions were deoxygenated by purging with pure nitrogen unless otherwise stated. All experiments were performed at room temperature (23 ± 2 °C). All potentials in this work are referred to Ag/AgCl(satd.) as reference.

2.6.1.2 Reagents and Solutions

All chemicals used were of analytical grade purity and were used as received. Aqueous solutions were prepared with de-ionised water further purified via a Milli-Q unit (Millipore, Bedford, MA, USA). The bismuth stock solution (1000 mg/L in 5 wt. % nitric acid), 4-nitrophenol and 2,4-dinitrophenol were obtained from Aldrich (Dorset, UK), and diluted as required. Bromofenoxim (3,5-dibromo-4-hydroxybenz-aldehyde-2,4-dinitrophenyloxime) and 2-nitrophenol were obtained from Riedel-de-Haën (Germany). Stock solutions of 50 mmol/L of the nitrophenols and 0.6 mmol/L bromofenoxim were prepared by dissolving an appropriate amount of the compound in methanol. They were stored in a refrigerator when not in use and protected from daylight during use in the laboratory.

The supporting electrolyte for bulk electrochemical measurements was Britton-Robinson (BR) buffer stock solution, which was made 0.04 mol/L in acetic, boric and orthophosphoric acid with appropriate additions of 0.2 mol/L NaOH to obtain the desired pH. The electrolyte-carrier solution in flow injection experiments was BR buffer, which was made 0.1 mol/L in acetic, boric and orthophosphoric acid with appropriate addition of 1 mol/L NaOH to pH 4.0, and methanol (20+80). Working solutions for flow analysis were diluted with this carrier solution. An acetate buffer solution (0.05 mol/L, pH 4.5) served as the electrolyte for plating of the bismuth onto the GC electrode in both bulk measurements and flow analysis.

2.6.1.3 Preparation of BiFE, MFE and GCE

The glassy carbon (GC) surface was hand-polished using alumina slurry of consecutively decreasing particle size (0.3, 0.1 and 0.05 μm), with washing and sonication for 2 min in methanol between each step. This polishing procedure was carried out each time the bare GC electrode was used for measurements, whereas when GC served as a substrate for BiFE, it was performed only occasionally (after the glassy carbon electrode was not in use and stored in air for a period of more than two

days). In bulk experiments, the bismuth film was deposited from a separate acetate buffer solution (*ex situ* deposition), in the presence of dissolved oxygen, containing 5 mg/L Bi(III) by electrolysis at –1.0 V vs. Ag/AgCl for 60s while stirring the solution. The same plating solution and electrochemical parameters were used for electrodeposition of the bismuth film onto the GC electrode under flow conditions with an applied flow rate of 1.0 mL/min (instead of stirring). Mercury was plated *ex situ* following a standard procedure in a solution containing 1 x 10^{-3} mol/L $Hg(NO_3)_2$, 0.1 mol/L KNO_3 and 1 x 10^{-2} mol/L HNO_3 at –1.1 V for 5 min [82].

2.7 Results and Discussion

2.7.1 Preparation, Optimisation and Background Behaviour of the BiFE

Due to the particular requirements for *ex situ* BiFE preparation from a separate plating solution (in contrast to *in situ* films used in stripping analysis [68]), and enhanced robustness of the bismuth film for flow detection purposes, which necessitates deposition of thicker films in the shortest possible times, the parameters for bismuth plating onto the GC substrate electrode (plating time and bismuth concentration) were optimised using 2-nitrophenol as a test signal. Figure 2.6 shows the results of the optimisation experiments. From Figure 2.6 A, it is evident that 30 and 60 s provide the optimum signal for the reduction of 2-nitrophenol. However, 60 s was chosen as this will provide a thicker bismuth film, which is necessary considering the application of the BiFE under hydrodynamic conditions. 5 and 10 mg/L of bismuth exhibit quite similar results, so 5 mg/L was chosen in order to minimise consumption of reagents. Hence, the optimum parameters were determined to be –1.0 V deposition potential, 60 s deposition time and 5 mg/L Bi(III) concentration, applying 0.05 mol/L acetate buffer pH 4.5 as supporting electrolyte. Acetate buffer has previously been shown to be suitable for *in situ* bismuth film formation for voltammetric stripping analysis of heavy metals [68], and so it was also employed in this work. For the removal of the bismuth film, a simple electrochemical clean-up step was carried out by applying a fixed potential of +0.3 V for 15 s, after which a new bismuth film can be immediately deposited.

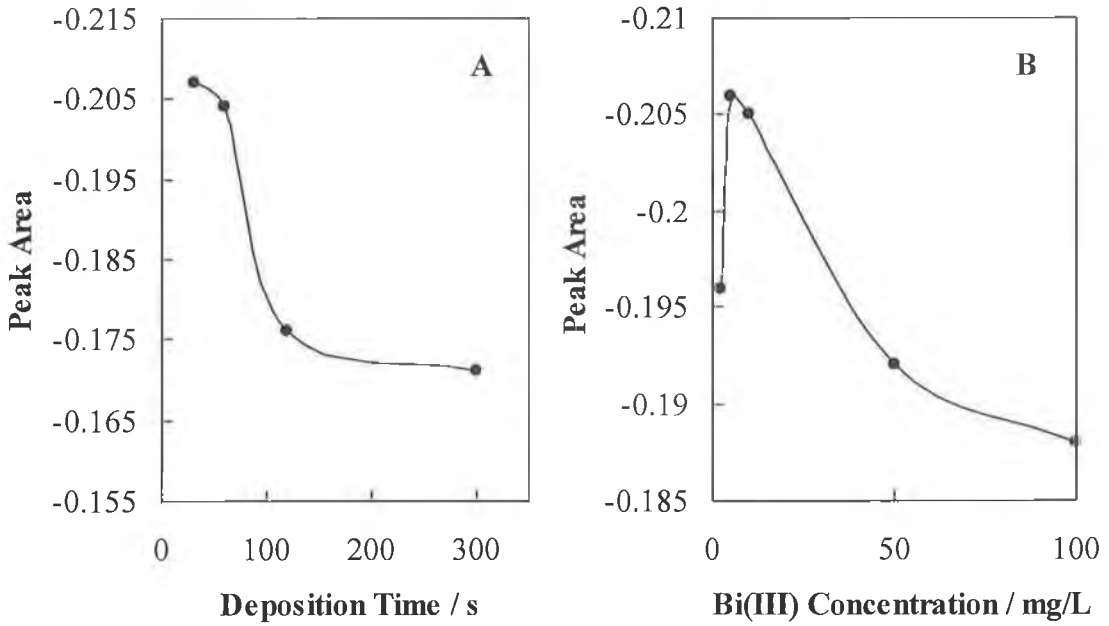

Figure 2.6: Optimisation of (A) deposition time and (B) bismuth concentration with respect to 2-nitrophenol as a test signal. Conditions: deposition potential –1.0 V; SWV settings; step potential 5 mV, amplitude 25 mV; electrode radius 3 mm.

An important parameter in the investigation of a new electrode surface is its useful potential window, i.e. the range of potentials over which it can be employed. In order to assess the useful potential window of the BiFE, its response on employing LSV in several blank buffer solutions covering the pH range of approximately 1 to 10 was examined in Figure 2.7. Systems used were 0.1 mol/L HCl (pH 1.1), 0.05 mol/L acetate buffer (pH 4.0), 0.1 mol/L phosphate buffer (pH 7.3), and 0.1 mol/L ammonia/ammonium chloride (pH 9.7). The positive (least negative) limit of the BiFE represents the re-oxidation of the deposited metallic bismuth which occurs at potentials less negative than –0.2 V, as can be seen from curve (a) in Figure 2.7. By taking a strict criterion of raising the current response due to the background discharge (commencement of hydrogen evolution) above –1 μA (-3.54 μA/cm^2), the following negative potential limits of the *ex situ* prepared bismuth film electrode were determined: –0.82 V at pH 1.1, –1.17 V at pH 4.0, –1.30 V at pH 7.3 and –1.49 V at pH 9.7. The background current level of the BiFE was also determined from the recordings shown in Figure 2.7. The average background current level of the BiFE was calculated to be approximately 0.1 μA. This relatively low background level

observed in solutions of varying composition and the sufficiently wide negative potential window available make the BiFE suitable for the detection of nitrophenolic compounds, as their reduction potentials lie in this range.

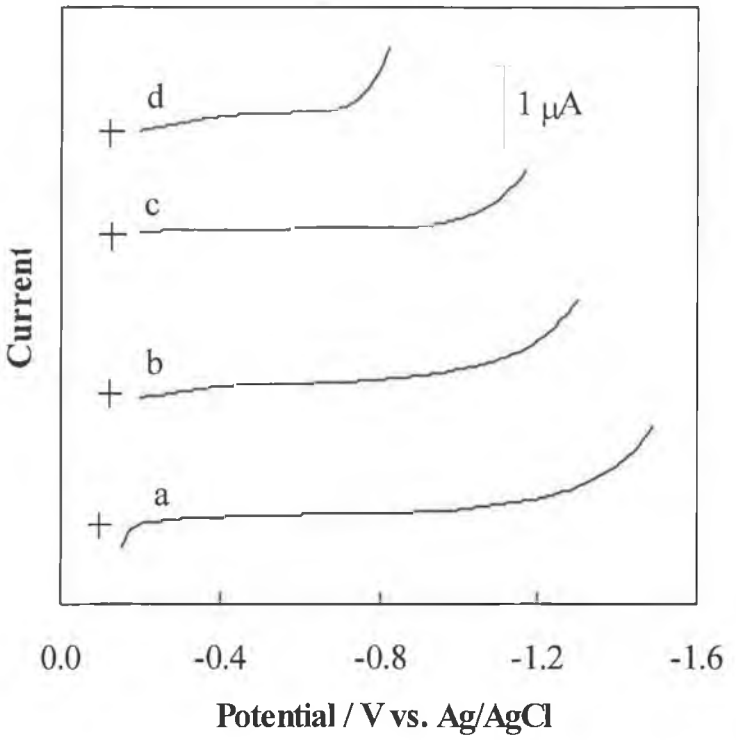

Figure 2.7: Available potential windows of the BiFE at different pHs: (a) 9.7 (0.1 mol/L ammonia/ammonium chloride), (b) 7.3 (0.1 mol/L phosphate buffer), (c) 4.0 (0.05 mol/L acetate buffer), and (d) 1.1 (0.1 mol/L HCl). LSV scan rate: 50 mV/s; electrode radius: 1 mm; initial potential: (a) –0.16 V, (b) – (d) –0.20 V; + assigns a zero-current position.

As expected, the presence of dissolved oxygen affected the cyclic voltammetric current performance at the bismuth film electrode, causing two weak and broad cathodic peaks at approximately –0.4 and –0.9 V (in pH 4 Britton Robinson buffer), which diminished upon increasing the deaeration time. Therefore, appropriate deaeration of the measurement solution is required for total oxygen removal. In addition, a blanket of nitrogen was maintained over the measurement solutions during experimentation. This interference of dissolved oxygen in reduction of the nitrophenols at the bismuth film electrode was in stark contrast to the behaviour of the BiFE in stripping voltammetry, in which dissolved oxygen caused no interference (see

Chapter 3). Further studies to investigate the kinetics of the reduction of dissolved oxygen at the bismuth film electrode, which are beyond the scope of this work, are required.

2.7.2 Comparison of BiFE with GCE and MFE

As the bismuth film electrode is considered as a possible alternative to toxic mercury electrodes and glassy carbon electrodes, which need to be cleaned regularly, the behaviour of the BiFE was compared to both of these electrodes. A preliminary experiment involved the measurement of bromofenoxim (3,5-dibromo-4-hydroxy-benzaldehyde-2,4-dinitrophenyloxime), a foliar acting herbicide and major pesticide of various crops, and which is regarded as particularly difficult to determine, at the bismuth film electrode. Bromofenoxim, according to its structure (Figure 2.8), possesses two readily reducible nitro groups (also present in nitrophenols). Bromofenoxim was previously found to exhibit a voltammetric cathodic signal at mercury electrodes alone (*no response* was observed at bulk platinum and gold, bare glassy carbon and carbon paste electrodes) [82].

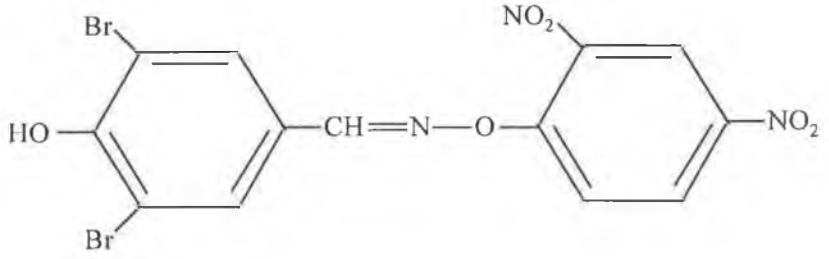

Figure 2.8: Structure of Bromofenoxim.

In a preliminary experiment to investigate the possibility of detecting reducible nitro-groups at the bismuth film electrode, cyclic voltammograms of bromofenoxim in BR buffer pH 7 were obtained. These are shown in Figure 2.9. The reduction of bromofenoxim elicited a strong response at the BiFE. The behaviour, however, was somewhat different to that observed at the MFE [82]. At the MFE, the peaks for the two nitro groups were well separated, while here, the peak at approximately –0.54 V appeared as a "side-peak" on the peak at –0.66 V. The corresponding peak potentials at the MFE were –0.38 V and –0.54 V, respectively. This difference in peak

potentials may be attributed to slower reaction kinetics at the BiFE. The different behaviour regarding the peak separation may be due to the different initial potentials employed at the two electrode surfaces; –0.1 V at MFE and –0.25 V at BiFE.

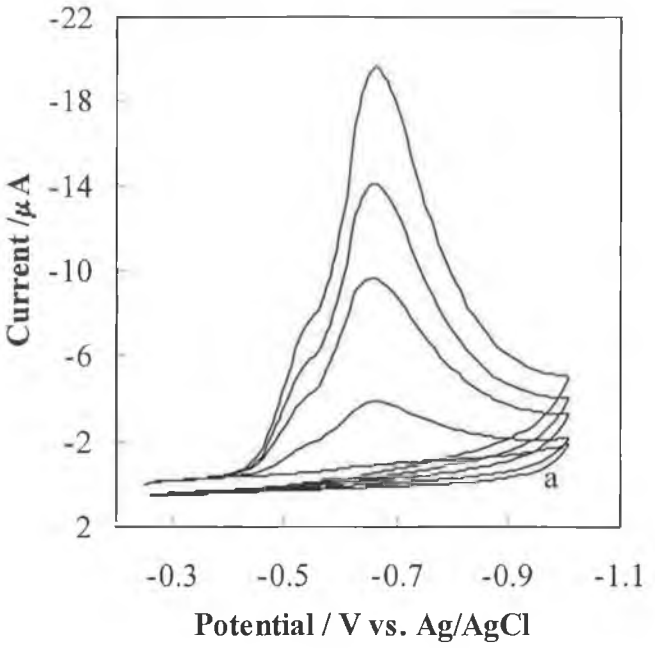

Figure 2.9: Cyclic voltammograms of (a) BR buffer pH 7 with subsequent increments of 0.5 mg/L (1.12 x 10^{-6} mol/L) bromofenoxim; scan rate 100 mV/s; initial potential – 0.25 V; vertex potential –1.0 V.

Differential pulse voltammetry further indicated the suitability of the BiFE for use in the electrochemical detection of bromofenoxim and other reducible organic compounds. The results of this are displayed in Figure 2.10 A. When DPV was employed, the peak separation was much improved when compared to cyclic voltammetry. In addition, in a preliminary investigation into the potential applicability of the bismuth film electrode in electrochemical detection under hydrodynamic conditions, the hydrodynamic amperometric behaviour of bromofenoxim was examined. Relatively high concentrations were employed here in order to elicit a strong response and demonstrate the potential use of the bismuth film electrode under hydrodynamic conditions. Figure 2.10 B displays a hydrodynamic amperometric recording obtained at the BiFE by increasing the bromofenoxim concentration in 1 mg/L increments at an operating potential of –0.7 V. The current response at the BiFE exhibited good linearity with increasing bromofenoxim

concentration, with a correlation coefficient (r) of 0.999. Some noise was observed in the amperogram; this may be attributed to perturbations of the double layer and not to the actual electrode surface, as the noise was reduced when the electrodes were positioned so as to minimise disturbances around the working electrode. These results indicate that the bismuth film electrode offers a suitable electrode surface for cathodic electrochemical detection under both quiescent and hydrodynamic conditions.

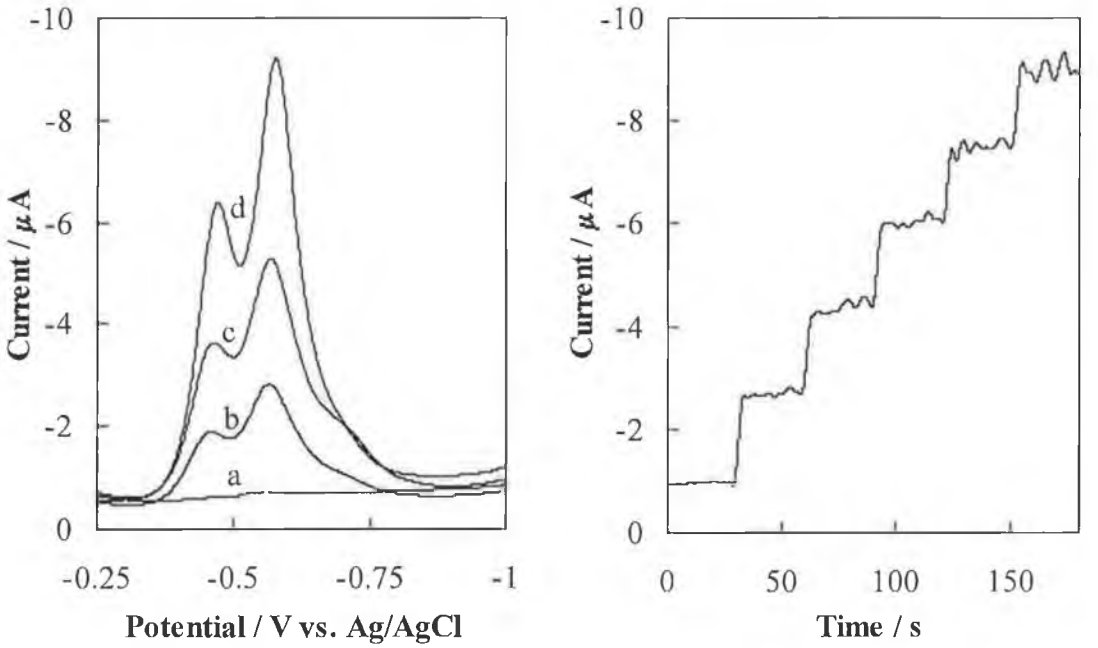

Figure 2.10: (A) DPV recording of (a) BR buffer, pH 7.0, (b), (c), and (d) a + 2 mg/L, + 5 mg/L, and + 8 mg/L bromofenoxim, respectively; scan rate 20 mV/s, modulation time 0.05 s, modulation amplitude 50 mV and (B) hydrodynamic amperogram obtained at BiFE on increasing the bromofenoxim concentration in 1 mg/L increments in BR buffer, pH 7.0; operating potential –0.7 V; electrode radius 3 mm.

The performance of the BiFE was compared to a bare glassy carbon electrode (GCE) and a mercury film electrode (MFE). Figure 2.11 displays cyclic voltammetric recordings of 2-nitrophenol at the BiFE and a mirror-polished bare GCE. As is clearly evident from this figure, the 2-nitrophenol reduction behaviour is analogous to, and even slightly advantageous over, that observed at the bare GCE under identical conditions, as the peak potential is about 20 mV less negative, the peak current is about 10% higher, and the peak is narrower with the BiFE. These results suggest that

the electrochemical reaction at both electrodes is the same, although its rate seems very slightly higher at the BiFE. Notably, the baseline behaviour at both electrodes is almost identical.

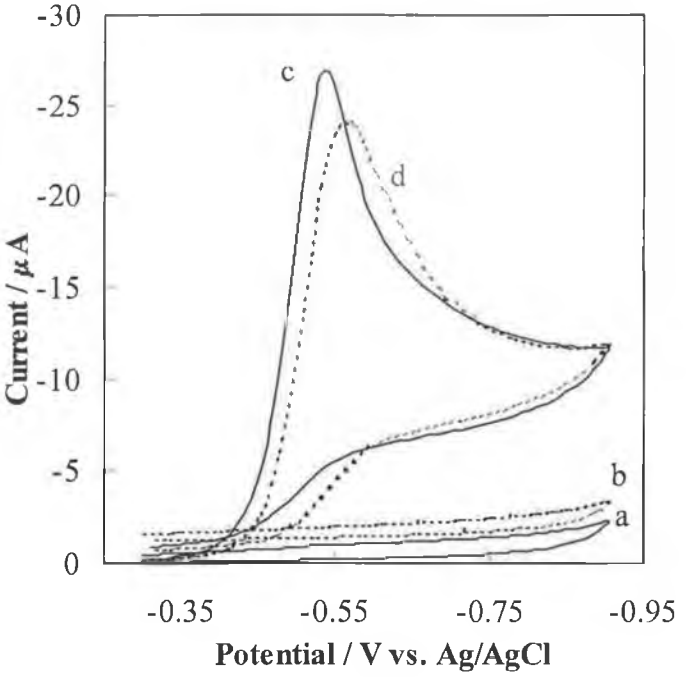

Figure 2.11: Cyclic voltammograms obtained at the BiFE (a, c) and at a bare GCE (b, d); solutions (a, b) blank Britton-Robinson buffer, pH 4.0, (c, d) Britton-Robinson buffer, pH 4.0 + 10 mg/L 2-nitrophenol. The baselines (curves a and b) are offset by 3.5 and 1.50 μA for the sake of clarity. Scan rate 100 mV/s; initial and final potential –0.3 V; vertex potential –0.9 V; electrode radius 3 mm.

The reproducibility of measurements at the BiFE reveal that for eight measurements (such as those in Figure 2.11), the variability (relative standard deviation, r.s.d.) of the recorded reduction peak current was 0.7% (mean i_p = 22.3 μA), of the reduction peak potential was 0.7% (mean E_p = –0.543 V) and of the half-peak width 2.7% (mean 130 mV). The corresponding values for the bare GC were; mean i_p = 19.4 μA (r.s.d. = 0.8%), mean E_p = –0.560 V (r.s.d. = 0.6%), and mean half-peak width = 150 mV (r.s.d. = 2.4%). The similarity in these results again indicate that the reduction reaction at the BiFE and bare GCE is similar.

In a similar manner, the BiFE was compared to a MFE under identical conditions, and with the same glassy carbon electrode serving as the substrate surface. Similarly as in the previous case, the CV recordings in Figure 2.12 reveal that the peak current for 2-nitrophenol reduction at the BiFE is about 10% higher and the peak is narrower when compared to that observed at the MFE (note that the analyte concentration is higher here than in Figure 2.11). However, the peak potential is shifted negatively for approximately 170 mV with the BiFE.

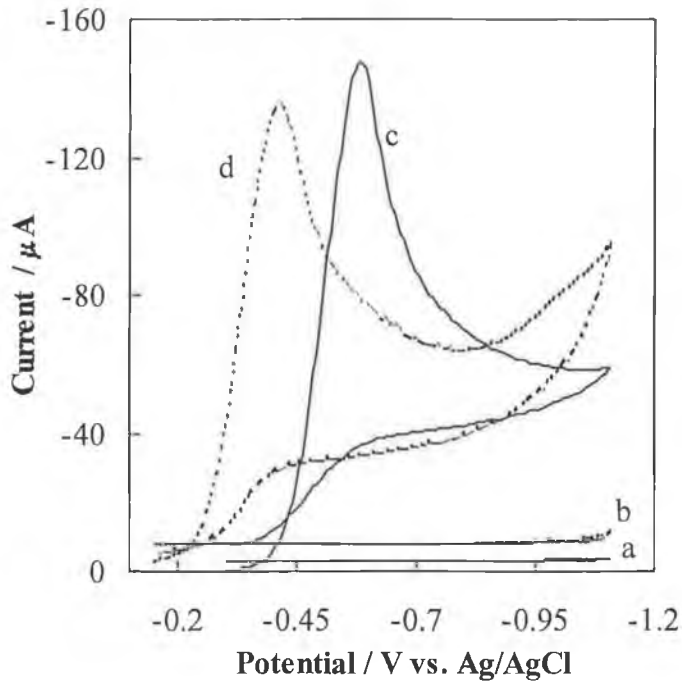

Figure 2.12: Cyclic voltammograms obtained at the BiFE (a, c) and at a MFE (b, d); solutions: (a, b) blank Britton-Robinson buffer, pH 4.0, (c, d) Britton Robinson buffer, pH 4.0 + 69.5 mg/L 2-nitrophenol. The baselines (curves a and b) are offset by 3.0 and 8.0 μA for the sake of clarity. Scan rate 100 mV/s; initial and final potential -0.15 for MFE and –0.3 V for BiFE; vertex potential –1.1 V for both electrodes; electrode radius 3 mm.

This implies slower electron transfer kinetics and / or differences in the double layer regions of the BiFE, when compared with the MFE (more detail about the possible reaction mechanism at the BiFE will be provided in the following section). Also notable in Figure 2.12 is the behaviour of both electrodes at potentials more negative that about –0.8 V in the presence of 2-nitrophenol (curves c and d) in comparison to

the corresponding baselines (curves a and b). For the MFE, an increase in current contribution possibly due to electrolyte discharge at higher negative potentials was observed, whereas the BiFE does not show such an increase in signal. However, it is more likely that this increase at the MFE is be due to the beginning of a further two electron reduction reaction to hydroxylamine (see Equation 2.4).

2.7.3 Electrochemical Behaviour of Nitrophenols at BiFE

Cyclic voltammetry was used initially to elucidate the nature of the electrochemical process occurring at the bismuth film electrode for 2-nitrophenol, 4-nitrophenol and 2,4-dinitrophenol. Typical cyclic voltammograms of the three compounds at concentrations of 5 mg/L are shown in Figure 2.13.

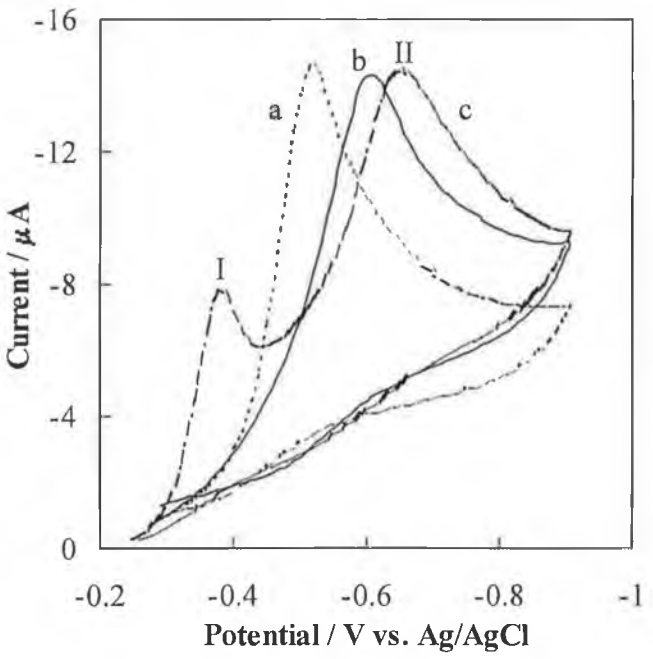

Figure 2.13: Cyclic voltammograms of 5 mg/L (a) 2-nitrophenol, (b) 4-nitrophenol and (c) 2,4-dinitrophenol, obtained at the BiFE; supporting electrolyte 0.04 mol/L Britton-Robinson buffer pH 4.0; scan rate 100 mV/s; initial and final potential –0.3 V (–0.25 V for 2,4-dinitrophenol); vertex potential –0.9 V.

2-Nitrophenol exhibits one well-defined reduction peak at –0.54 V (a) with 4-nitrophenol also exhibiting a single peak at –0.61 V (b). 2,4-Dinitrophenol exhibits two well-defined reduction peaks at –0.38 V and –0.65 V (c,I and c,II, respectively).

The presence of one peak for the mononitrophenols and two peaks for 2,4-dinitrophenol is consistent with results obtained at mercury electrodes [54,55]. For 2,4-dinitrophenol, the first peak corresponds to the reduction of the nitro group in the *ortho* position, while the second peak corresponds to the reduction of the nitro group in the *para* position. However, the peak potentials for the nitrophenols at BiFE are shifted to more negative values. As mentioned previously, this may be attributed to slower reaction kinetics at the BiFE as compared to mercury and / or differences in the double layer regions of both electrodes.

The reduction of the nitrophenols at the BiFE is an irreversible process (i.e. occurs with sluggish electron exchange). The first and most obvious proof of this is the absence of a peak in the reverse scan i.e. no oxidation peak(s) corresponding to the reduction peak(s) for the nitrophenols. A shift in peak potential was also observed with a change in scan rate (from 5 mV/s to 500 mV/s) for 2-nitrophenol (see Figure 2.14), which is typical of an irreversible process [33].

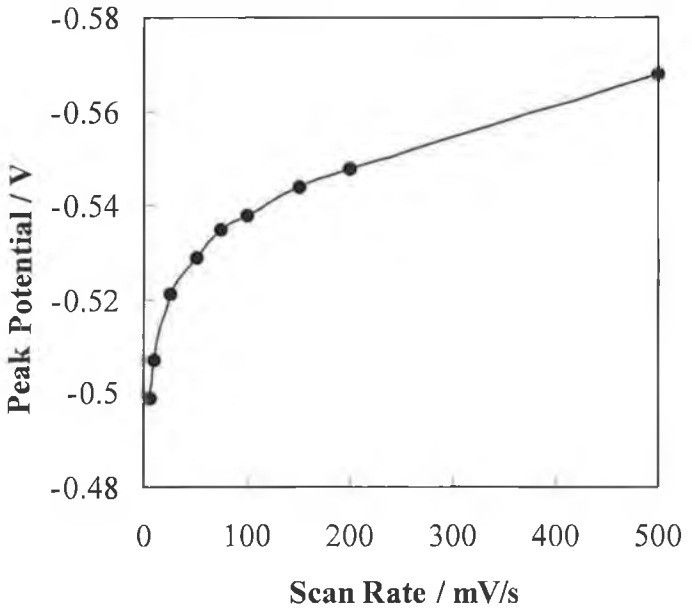

Figure 2.14: Influence of CV scan rate on peak potential for 10 mg/L 2-nitrophenol in Britton-Robinson buffer pH 4.0.

The peaks for each of the nitrophenols were observed to decrease upon second and subsequent scans at the same bismuth film, indicating an adsorptive nature of the analytes. Similar adsorptive behaviour has also been reported for aromatic nitro

compounds at mercury electrodes [46,82]. Figure 2.15 A and B shows the influence of scan rate on peak current. A plot of current vs. the square root of scan rate yielded a straight line over the entire range (5 mV/s to 500 mV/s), pointing to a diffusion-controlled process. Interestingly, stirring the solution between scans was found to considerably affect the current response, whereby the r.s.d. (n = 8) between scans of a solution of 10 mg/L 2-NP for 4, 6, 8, 10 and 15 s stirring was 9.5, 4.0, 1.3, 0.7 and 0.7%, respectively. These results seem to suggest that reduction product adsorption on the electrode causes the decrease in signal, with stirring for 10 s removing this product from the surface and returning it to its original state. Overall, these results suggest that during the reduction of nitrophenols at the BiFE, the process is controlled by diffusion, although some weak adsorption of the reduction product on the electrode surface occurs.

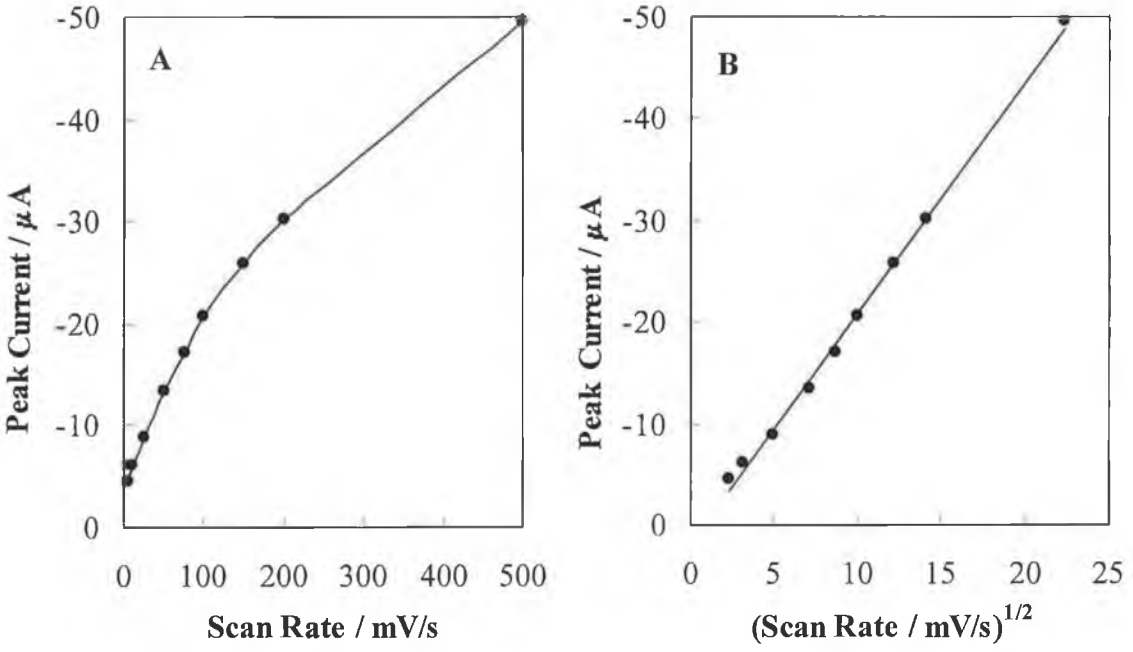

Figure 2.15: (A) Influence of scan rate and (B) influence of square root of scan rate on reduction of 10 mg/L 2-nitrophenol in Britton-Robinson buffer pH 4.0.

2.7.4 Influence of pH and Solution Composition

Cyclic voltammograms were recorded in BR buffers in the pH range 2-10 in order to study the pH dependence of peak potential and peak current of the three nitrophenols. Consistent with results obtained at mercury electrode for the dependence of peak potential on pH [54,56], a linear shift towards more negative peak potentials is

observed for all three compounds with increasing pH as shown in Figure 2.16. The predicted rate of increase of potential with increasing pH in a reaction involving a 1:1 ratio of protons to electrons is approximately 59 mV per pH unit [43,56]. In the pH range covered in this study, the following slope values were obtained for the nitrophenols: 45 mV/pH for 2-nitrophenol (a), 52 mV/pH for 4-nitrophenol (b) and 72 mV/pH for 2,4-dinitrophenol (first process; c) and 58 mV/pH for 2,4-dinitrophenol (second process; d). The corresponding correlation coefficients are all > 0.997. These results indicate that the reduction of the nitrophenols involves a 1:1 ratio of protons to electrons, as determined at the mercury electrode. The peak currents of the nitrophenols exhibited a change in sensitivity over the pH range, as expected in a reaction involving protonation (see Figure 2.17). Variations in the current response with pH were also observed for nitrophenols at mercury and modified carbon paste electrodes [54,60,61]. The pH of maximum response for 2-NP and 2,4-DNP was determined to be pH 4.0, while that of 4-NP was pH 5.0. Britton Robinson buffer pH 4.0 was chosen as supporting electrolyte as this pH provided the highest sensitivity for 2-nitrophenol and 2,4-dinitrophenol, while still providing a well-defined peak for 4-nitrophenol.

In addition to investigating the effect of solution pH on the reduction of nitrophenols at the BiFE, the influence of the supporting electrolyte composition on the reduction of 2-nitrophenol was also investigated. The supporting electrolytes used were 0.05 mol/L and 0.1 mol/L acetate buffer, 0.05 mol/L and 0.1 mol/L formate buffer. In addition, the BiFE response to 2-nitrophenol in partially non-aqueous medium (acetonitrile + 20 mmol/L ammonium acetate (3 + 1) at pH 4 and 7.8), relevant for use in conjunction with chromatographic / preconcentration methodologies, was also examined. The results of these measurements are shown in Figure 2.18.

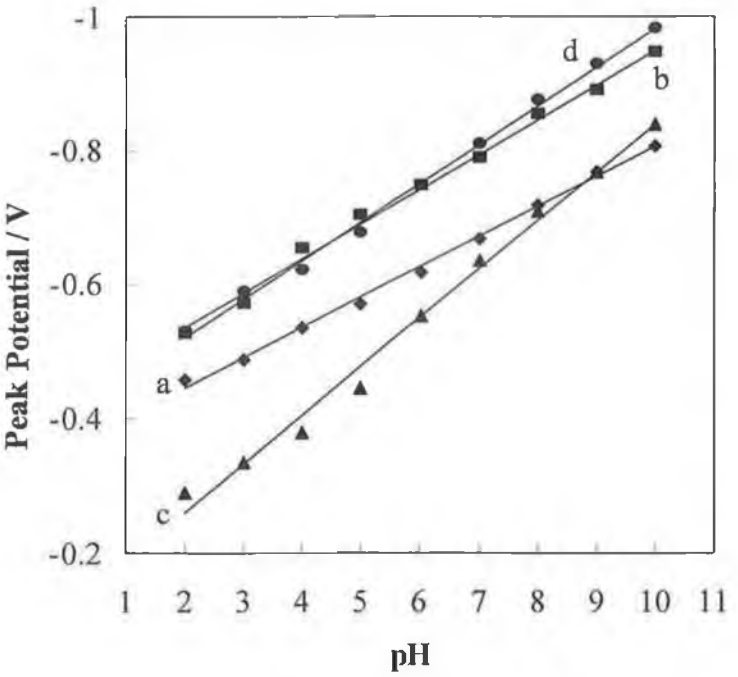

Figure 2.16: Influence of pH of the Britton-Robinson buffer on peak potential for 10 mg/L (a) 2-NP, (b) 4-NP, (c, d) 2,4-DNP (processes I and II, respectively); supporting electrolyte 0.04 mol/L BR buffer (pH 2.0 to 10.0); CV scan rate 100 mV/s.

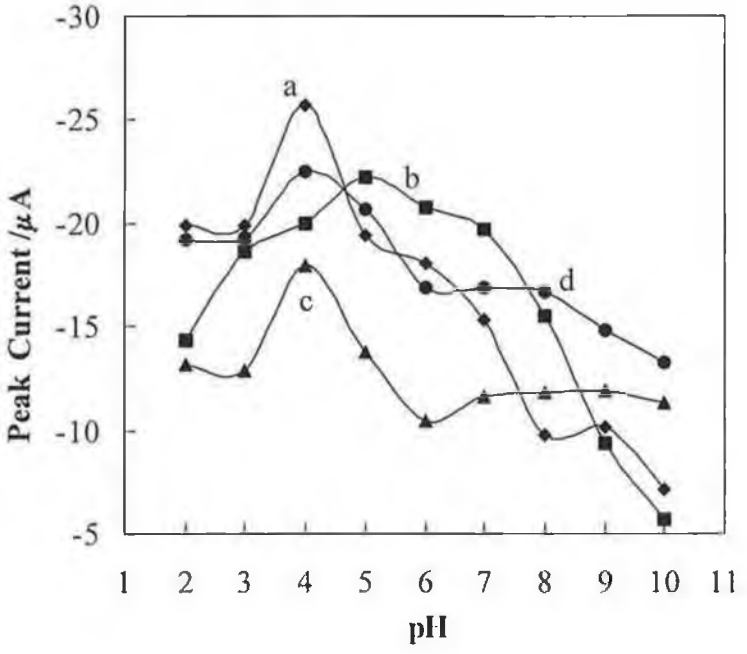

Figure 2.17: Influence of pH of the Britton-Robinson buffer on peak current for nitrophenols; all conditions as in Figure 2.16.

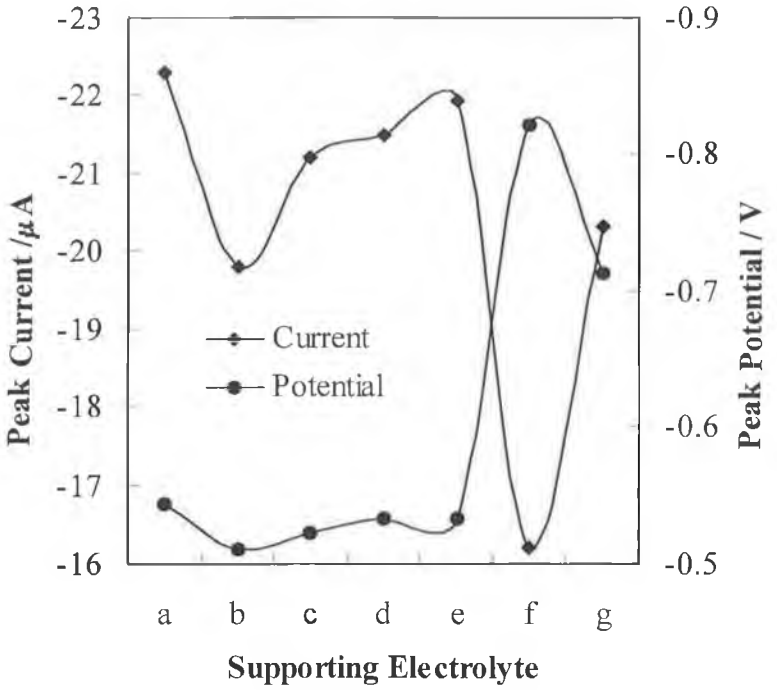

Figure 2.18: Influence of supporting electrolyte composition on current and potential response for 10 mg/L 2NP; (a) 0.04 mol/L BR buffer pH 4, (b, c) 0.05 mol/L and 0.1 mol/L acetate buffer pH 4, respectively, (d, e) 0.05 mol/L and 0.1 mol/L formate buffer, respectively, (f, g) acetonitrile+20 mmol/L ammonium acetate (3 + 1) pH 7.8 and pH 4, respectively; CV scan rate 100 mV/s.

From Figure 2.18, it is evident that 0.04 mol/L Britton Robinson buffer provided that optimum conditions for reduction of 2-nitrophenol as the current was highest here when compared to that obtained with the other solutions. However, a strong response was obtained for reduction of 2-nitrophenol in each of the other media. In addition, in aqueous media, the peak potentials were almost the same. As expected, the behaviour in non-aqueous medium was considerably different to that in completely aqueous media. At pH 7.8, the current response was the lowest, although on adjusting the pH to the optimum of 4.0, the current increased considerably. The peak potential in acetonitrile + 20 mmol/L ammonium acetate (3 + 1) pH 7.8 was shifted to more negative values by approximately 280 mV. This was partly attributed to the change from protic to aprotic medium and thus to a variation in pH. However, a contribution of the unknown liquid junction potential due to the use of an all-aqueous reference electrode was also anticipated. This seemed likely, as even when the pH was adjusted to pH 4, the difference in peak potentials was approximately 170

mV. These results show that the reduction of 2-nitrophenol at the BiFE is possible in various media, including those commonly employed in solid phase extraction and chromatographic methodologies i.e. non-aqueous media.

2.7.5 Calibration

Table 2.1 shows the calibration data for each of the nitrophenols obtained employing square wave voltammetry. As can be seen, the dependence of the SWV peak height on the analyte concentration is linear over a wide range, with low limits of detection being achieved for each compound. The relative standard deviations (n = 9) for a 5 μg/L solution of 2-NP, and a 10 μg/L solution of 4-NP, were 6.3% and 8.7% respectively, while for a 25 μg/L solution of 2,4-DNP the r.s.d.s (n = 8) were 10.6% and 10.4%, for the first and second processes, respectively. For concentrations of 1 mg/L solutions of 2-nitrophenol, 4-nitrophenol and 2,4-dinitrophenol (processes one and two) the r.s.d.s (n = 9) were 0.7%, 1.8% and 2.8% and 3.4%, respectively. Figure 2.19 shows square wave voltammograms obtained for BR buffer pH 4 and 1 and 5 μg/L 2-nitrophenol at the BiFE. Here the sensitive response of the BiFE to 2-nitrophenol reduction can be clearly observed, indicating the potential usefulness of this electrode for determinations at low μg/L levels.

Substance	*Linear Range / μg/L*	r^a	*LoD / μg/L*
2-NP	10 – 10000	0.999	0.44
4-NP	10 – 5000	0.999	1.37
2,4-DNP[b]	10 – 10000	0.997	7.96
2,4-DNP[c]	25 - 10000	0.999	6.66

[a] correlation coefficient, [b] first peak, [c] second peak

Table 2.1: Calibration data for nitrophenols.

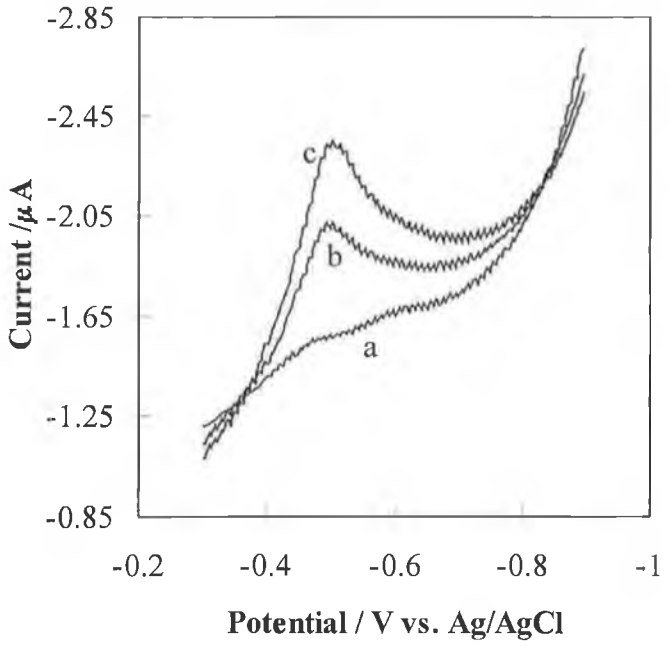

Figure 2.19: Square wave voltammograms of (a) 0.04 mol/L Britton Robinson buffer pH 4.0, (b) a + 1 μg/L 2-nitrophenol and (c) a + 5 μg/L 2-nitrophenol; SWV settings; initial potential -0.3 V; final potential -0.9 V; amplitude 25 mV; frequency 20 Hz, step potential 5 mV.

2.7.6 Potential Effect on Response of BiFE and Hydrodynamic Amperometry

As expected, the applied potential in hydrodynamic amperometry exerted a significant effect on the reduction of the nitrophenols. Figure 2.20 shows hydrodynamic voltammograms obtained for each of the three nitrophenols. As expected, the inflection point in the hydrodynamic voltammogram for 2-nitrophenol was lower than that for 4-nitrophenol, due to its lower reduction potential. The hydrodynamic voltammogram for 2,4-dinitrophenol exhibited two inflection points. The presence of two inflection points can be explained by the fact that two nitro groups are reduced in 2,4-dinitrophenol. The first inflection point most likely is attributed to the reduction of the first nitro group, which the second corresponds to the reduction of the second nitro group. The possibility of using a rotating BiFE in the reduction of 2-nitrophenol was also investigated. Here, the bismuth film was plated onto the substrate glassy carbon electrode as usual and the electrode then rotated at 500 r.p.m. The resulting amperogram is shown in Figure 2.21. These results suggest the possibility of employing a rotating electrode in detection of nitrophenols at the BiFE.

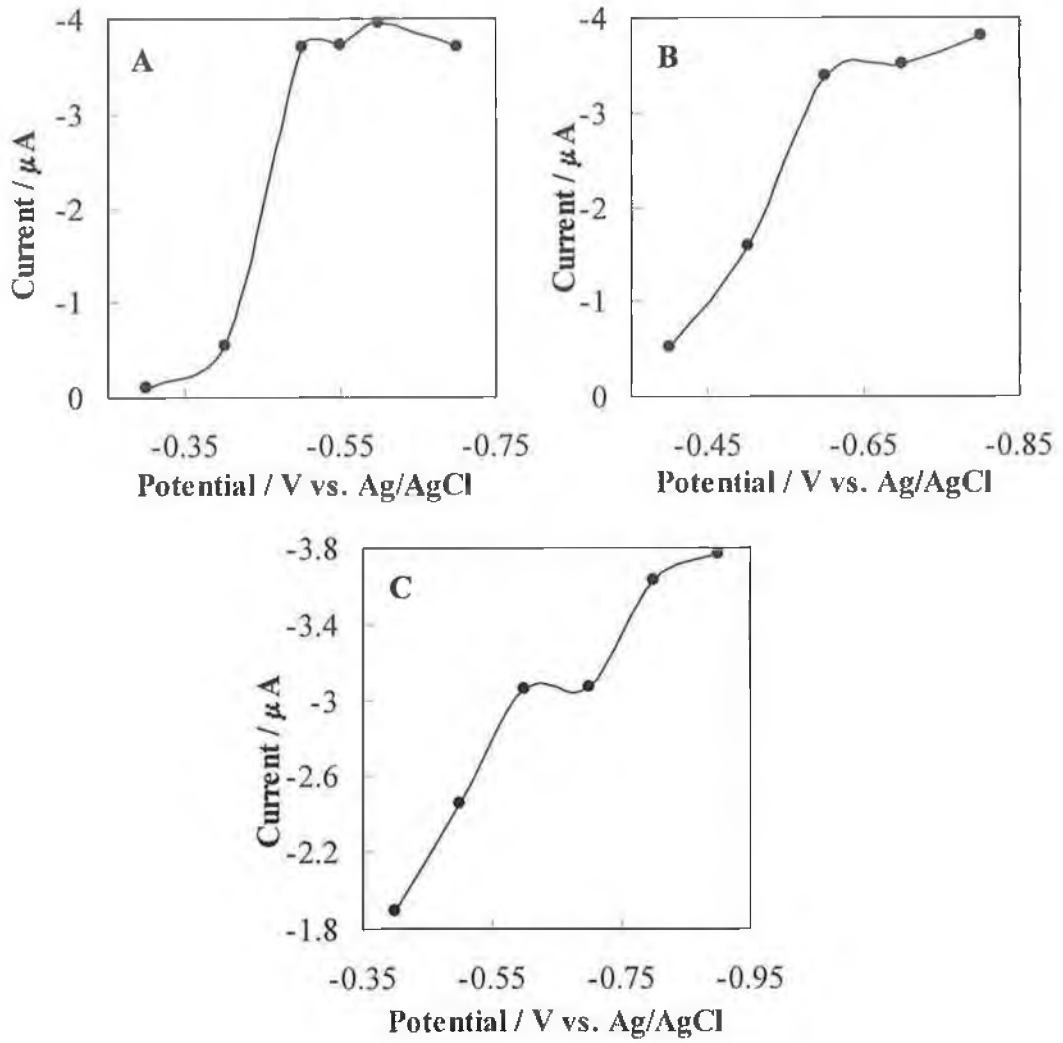

Figure 2.20: Hydrodynamic voltammograms obtained for additions of (A) 2-nitrophenol, (B) 4-nitrophenol and (C) 2,4-dinitrophenol to 0.04 mol/L Britton-Robinson buffer pH 4.0 under stirring conditions.

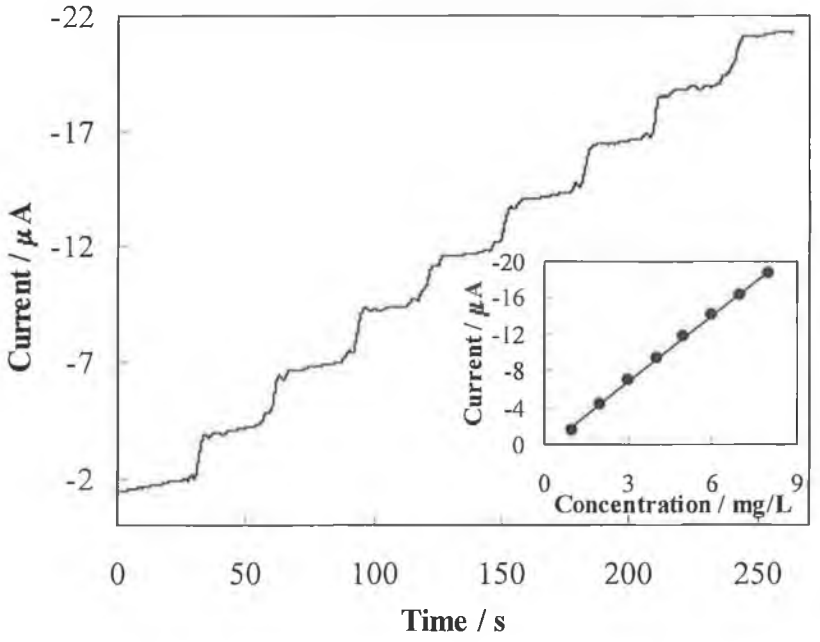

Figure 2.21: Hydrodynamic amperogram obtained for 1 mg/L additions of 2-nitrophenol to 0.04 mol/L Britton-Robinson buffer pH 4.0 at a rotating disc electrode at 500 r.p.m.; operating potential +0.6 V; inset: corresponding data.

2.7.7 Flow Injection Analysis of Nitrophenols

As described in Section 2.3.3, reducible substances such as nitrophenols are often separated employing liquid chromatography, and detected with an electrochemical detector comprising a working electrode of mercury or glassy carbon. In this study we considered employing the bismuth film electrode as a new solid electrode surface suitable for use in such an application. The advantages of using such an electrode include replacement of toxic mercury with non-toxic bismuth and elimination of the necessity for regular electrode cleaning, which is necessary with glassy carbon electrodes, as the bismuth film can be quickly and easily regenerated with an electrochemical cleaning and re-deposition step. As the suitability of the BiFE in the detection of nitrophenols (and bromofenoxim) under hydrodynamic conditions was previously proved (Section 2.7.2 and 2.7.6), its application in a flow injection analysis system was investigated. While 0.04 mol/L Britton Robinson buffer pH 4.0 was suitable for bulk electrochemical measurements, it was decided to alter the electrolyte for flow measurements in order to assess its potential usage with solid phase extraction preconcentration and chromatographic separation methodologies [22,23].

The BR concentration was increased to 0.1 mol/L in order to improve conductivity, and methanol (80%) was added as this proportion of organic solvent closely relates to amounts used in the aforementioned procedures; a potential of –1.0 V was found to be suitable under these conditions for determinations of the nitrophenol compounds at low μg/L levels. Plating of the bismuth film "in-line" was successfully accomplished and confirmed by plating a bismuth film under flowing conditions, removing the electrode from the flow-through cell and stripping the film off in blank acetate buffer solution. The stripping behavior of the "in-line" plated bismuth was determined to be the same as that of a film plated by bulk electrolysis, indicating that the "in-line" plated BiFE is the same as a film plated under bulk conditions. Removal of the bismuth film simply involves the application of +0.3 V for 15 s after which a new bismuth film can be plated, without any requirement for polishing. Figure 2.22 shows an amperogram obtained under flowing conditions for repeat injections (x 3 each) of (a) 1, (b) 5, (c) 10 and (d) 1 μg/L concentrations of 2-nitrophenol at the BiFE. Here the BiFE is demonstrated to be extremely sensitive for the measurement of 2-nitrophenol, with the electrode responding to increasing concentrations of 2-NP and in turn to a decrease in concentration injected.

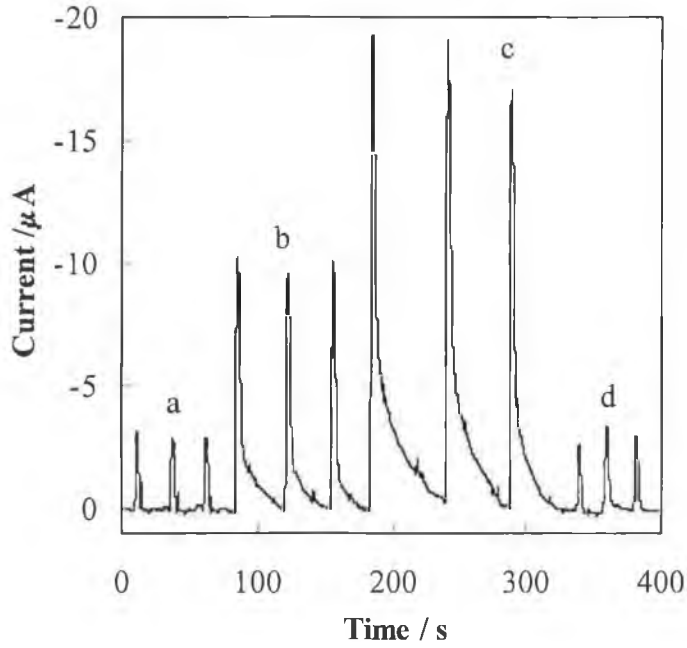

Figure 2.22: Flow injection-amperometric detection measurements for 1 (a), 5 (b), 10 (c) and 1 (d) μg/L injections of 2-NP. Conditions: carrier solution; 0.1 mol/L BR buffer-methanol (20+80) pH 4.0; operating potential –1.0 V; flow rate 0.5 mL/min.

Figure 2.23 displays 3 recordings for 3 injections of 1 μg/L 2-nitrophenol obtained at three different bismuth films. These results in particular demonstrate the potential applicability of the BiFE for flow injection measurements whereby reproducible results, at low concentrations, are obtainable at different films following simple electrochemical deposition and renewal of the bismuth film. The repeatability obtained for 8 repeat injections of 1 μg/L 2-nitrophenol at the same film is 8.5%, illustrating that the BiFE is also extremely suitable for repeat measurements of low concentrations. The linear range for 2-nitrophenol is 1 to 10 μg/L (r = 0.997), with a limit of detection (S/N = 3) of 0.25 μg/L. The limit of detection (S/N = 3) of 4-nitrophenol is 0.56 μg/L, with a linear range of 1 to 10 μg/L (r = 0.998). The linear range for 2,4-dinitrophenol extends from 1 to 20 μg/L (r = 0.993), with a limit of detection (S/N = 3) of 0.73 μg/L.

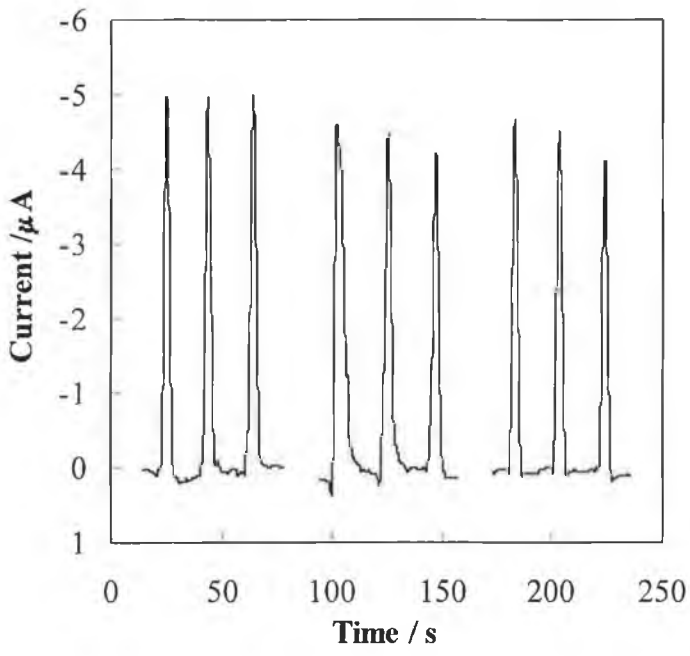

Figure 2.23: Triplicate flow injection-amperometric detection recordings of 3 injections of 2 μg/L 2-nitrophenol at 3 different successively plated bismuth films; Conditions: carrier solution; 0.1 mol/L BR buffer-methanol (20+80) pH 4.0; operating potential –1.0 V; flow rate 0.5 mL/min.

2.8 Conclusions

The cathodic electrochemical detection of some reducible organic compounds (bromofenoxim, 2-nitrophenol, 4-nitrophenol and 2,4-dinitrophenol) at a bismuth film electrode is presented, with the study focusing on the latter three. The results revealed that the BiFE is an attractive solid electrode surface for the detection of the priority pollutants 2-nitrophenol, 4-nitrophenol and 2,4-dinitrophenol, providing low limits of detection and eliminating the need for regular polishing of the electrode surface due to the easy electrochemical renewal of the bismuth film. Its suitability to the bulk electrochemical detection of nitrophenols has been demonstrated, allowing excellent limits of detection in the low μg/L range to be achieved using square wave voltammetry. In addition, flow injection measurements have revealed that the BiFE shows excellent promise in terms of achieving full automation (film preparation-measurement-electrode regeneration cycle) and its suitability for use with a non-aqueous carrier solution indicates its potential for coupling to a solid phase extraction / chromatographic procedure. Under such conditions it was found to be extremely sensitive to the detection of nitrophenols, whereby excellent limits of detection < 1 μg/L were obtained for each compound. Employing a suitable preconcentration (e.g. solid phase extraction) procedure should easily facilitate the determination of these compounds at limits < 0.1 μg/L, the current regulatory limits.

2.9 References

1. M.L. Richardson and S. Gangolli (eds), *The Dictionary of Substances and Their Effects*, Vol. 6, N-R, The Royal Society of Chemistry (1994).
2. Agency for Toxic Substances and Disease Registry (ATSDR), *Toxicological Profile for Nitrophenols: 2-Nitrophenol and 4-Nitrophenol*, Atlanta, GA, USA, Department of Health and Human Services, Public Health Service (1992).
3. *Concise International Chemical Assessment Document on Mononitrophenols, No. 20,* Fraunhofer Institute for Toxicology and Aerosol Research, Hanover, Germany (2000).
4. *EPA Health Effects Notebook for Hazardous Air Pollutants* – Draft, EPA-452/D-95-00, PB95-503579, Dec. (1994).
5. D.M. Munnecke, D.P. Hsieh, *Appl. Environ. Microbiol.* **31** (1976) 63.
6. Agency for Toxic Substances and Disease Registry (ATSDR). *Toxicological Profile for Dinitrophenols*, Atlanta, GA, USA, Department of Health and Human Services, Public Health Service (1995).
7. U.S. Environmental Protection Agency, *Fed. Regist.* **44** (1979) 233.
8. U.S. Environmental Protection Agency, *Fed. Regist.* **52** (1989) 131.
9. *EC Directive Relating to the Quality of Water Intended for Human Consumption, 80/778/EEC*, Office for Official Publications of the European Communities, 2 rue Mercier, L-2985, Luxembourg (1982).
10. W. Frenzel, S. Krekler, *Anal. Chim. Acta* **310** (1995) 437.
11. J.R. Dojlido and G.A. Best, *Chemistry of Water and Water Pollution*, Ellis Horwood Series in Water and Wastewater Technology, Ellis Horwood, New York, London (1993) pp. 301.
12. US Environmental Protection Agency Method 604 – Phenols, 40 CFR Part 136, 43290; Federal Register 49, No. 209 (1984).
13. US Environmental Protection Agency Method 625 – Base/Neutrals and Acids, 40 CFR Part 136, 43385; Federal Register 49, No. 209 (1984).
14. K.R. Kim and H. Kim, *J. Chromat. A* **866** (2000) 87.
15. S. Nakamura, M. Takino, S. Daishima, *Analyst* **126** (2001) 835.
16. S. Morales and R. Cela, *J. Chromat. A* **896** (2000) 95.
17. Y. He and H.K. Lee, *J. Liq. Chrom. Rel. Tech.* **21** (1998) 725.

18. N. Masqué, E. Pocurull, R.M. Marcé, F. Borrull, *Chromatographia* **47** (1998) 176.
19. N. Masqué, M. Galià, R.M. Marcé, F. Borrull, *J. Chromat. A* **771** (1997) 55.
20. M. Castillo, D. Puig, D. Barceló, *J. Chromat. A* **778** (1997) 301.
21. D. Puig, D. Barceló, *J. Chromat. A* **773** (1996) 371.
22. D. Puig, D. Barceló, *Anal. Chim. Acta* **311** (1995) 63.
23. E. Pocurull, M. Calull, R.M. Marcé, F. Borrull, *J. Chromat. A* **719** (1996) 105.
24. G. Carrieri, S. Cavalli, P.P. Ragone, N. Cardellicchio, *Ann. Chim.* **88** (1998) 619.
25. B. Paterson, C.E. Cowie, P.E. Jackson, *J. Chromat. A* **731** (1996) 95.
26. G. Achilli, G.P. Cellerino, G.M. d'Eril, S. Bird, *J. Chromat. A* **697** (1995) 357.
27. D. Puig, D Barceló, *J. Chromat. A* **778** (1997) 313.
28. M.J. Christopherson, T.J. Cardwell, *Anal. Chim. Acta* **323** (1996) 39.
29. L. Michel, A. Zatke, *Anal. Chim. Acta* **105** (1979) 109.
30. J. J. Scanlon, P.A. Flaquer, G.W. Robinson, G.E. O'Brien, P.E. Sturrock, *Anal. Chim. Acta* **158** (1984) 169.
31. T. McCreedy, P.R. Fielden, *Analyst* **120** (1995) 2343.
32. T. Galeano-Díaz, A. Guiberteau-Cabanillas, N. Mora-Díez, P. Parrilla-Vázquez, F. Salinas-López, *J. Agric. Food Chem.* **48** (2000) 4508.
33. J. Wang, *Analytical Electrochemistry*, second ed., Wiley-VCH, New York (2000).
34. A. Oubina, B. Ballesteros, R. Galve, D. Barcelo, M.P. Marco, *Anal. Chim. Acta* **387** (1999) 255.
35. A. Oubina, D. Barceló, M.P. Marco, *Anal. Chim. Acta* **387** (1999) 267.
36. H.M. Huang, K.M. Wang, D. Xiao, R.H. Yang, X.H. Yang, *Anal. Chim. Acta* **439** (2001) 55.
37. W. Ying, K.M. Wang, G.L. Shen, R.Q. Yu, *Talanta* **44** (1997) 1319.
38. C. Nistor, A. Oubina, M.P. Marco, D. Barcelo, J. Emneus, *Anal. Chim. Acta* **426** (2001) 185.
39. H.S. Zhuang, F. Zhang, Q.E. Wang, *Analyst* **120** (1995) 121.
40. L. Papouchado, G. Petrie, R.N. Adams, *J. Electroanal. Chem.* **38** (1972) 389.
41. L. Papouchado, R.W. Sandford, G. Petrie, R.N. Adams, *J. Electroanal. Chem.* **65** (1975) 275.
42. I.M. Koltoff, J.J. Lingane, *Polarography*, Interscience Publishers, New York (1952) pp. 748.

43. G.W.C. Milner, *The Principles and Applications of Polarography and Other Electroanalytical Processes*, Longmans, London (1962) pp. 553.
44. J.T. Browne, *Polarography of Molecules of Biological Significance*, Ed. W.F. Smyth, Academic Press, London (1979) pp. 111.
45. A.M. Bond, *Modern Polarographic Methods in Analytical Chemistry*, Marcel Dekker, Inc., New York (1980) pp. 42.
46. M.R. Smyth, W.F. Smyth, *Analyst* **103** (1978) 529.
47. P. Zuman, *Microchem. J.* **57** (1997) 4.
48. Z. Galus, in: P.T. Kissinger and W.R. Heinemann (Eds.), *Laboratory Techniques in Electroanalytical Chemistry*, 2nd ed., Marcel Dekker, Inc., New York (1996) Ch. 14.
49. P. Zuman, *Electroanalysis* **12** (2000) 1187.
50. P. Zuman, *Anal. Lett.* **33** (2000) 163.
51. K.A. Graeme, C.V. Pollack Jr., *J. Emerg. Med.* **16** (1998) 45.
52. N.J. Langford, R.E. Ferner, *J. Hum. Hypertens.* **13** (1999) 651.
53. A.S. Boyd, D. Seger, S. Vannucci, M. Langley, J.L. Abraham, L.E. King, *J. Am. Acad. Dermatol.* **43** (2000) 81.
54. Y. Ni, L. Wang, S. Kokot, *Anal. Chim. Acta* **431** (2001) 101.
55. J. Barek, H. Ebertová, V. Mejstřík, J. Zima, *Collect. Czech. Chem. Commun.* **59** (1994) 1761.
56. A. Costa-García, M.T. Fernández-Abedul, P. Tuñón-Blanco, *Talanta* **41** (1994) 1191.
57. I. Naranjo Rodríguez, M. Barea Zamora, J.M Barberá, J.A. Muñoz Leyva, M.P. Hernandez-Artiga, J.L. Hidalgo Hidalgo de Cisneros, *Mikrochim. Acta* **126** (1997) 87.
58. I. Naranjo Rodríguez, J.A. Muñoz Leyva, J.L. Hidalgo Hidalgo de Cisneros, *Anal. Chim. Acta* **344** (1997) 167.
59. I. Naranjo Rodríguez, J.A. Muñoz Leyva, J.L. Hidalgo Hidalgo de Cisneros, *Analyst* **122** (1997) 601.
60. M. del Mar Cordero-Rando, M. Barea-Zamora, J.M. Barberá-Salvador, I. Naranjo Rodríguez, J.A. Muñoz Leyva, .L. Hidalgo Hidalgo de Cisneros, *Microchim. Acta* **132**, (1999) 7.
61. L. Hernández, P. Hernández, J. Vicente, *Fresenius J. Anal. Chem.* **345** (1993) 712.

62. B. Kucera, *Ann. Phys.* **11** (1903) 529.
63. J. Heyrovský, *Chem. Listy* **16** (1922) 256; *Philos. Mag. J. Sci.* **45** (1923) 303.
64. T.H. Lu, H.Y. Yang, I.W. Sun, *Talanta* **49** (1999) 59.
65. J. Wang, B. Tian, *Anal. Chem.* **65** (1993) 1529.
66. E.P. Achterberg, C. Braungardt, *Anal. Chim. Acta* **400** (1999) 381.
67. *Ullman's Encyclopedia of Industrial Chemistry*, fifth ed., Vol. A4, W. Gerhartz (Ed.), Benzoyl Alcohol to Calcium Sulfate, VCH Verlagsgesellschaft, Germany, 1985, pp. 171.
68. J. Wang, J. Lu, S.B. Hočevar, P.A.M. Farias, B. Ogorevc, *Anal. Chem.* **72** (2000) 3218.
69. J. Wang, J.M. Lu., *Electrochem. Commun.* **2** (2000) 390.
70. J. Wang, J. Lu, U.A. Kurgoz, S.B. Hočevar, B. Ogorevc, *Anal. Chim. Acta* **434** (2001) 29.
71. J. Wang, J. Lu, S.B. Hočevar, B. Ogorevc, *Electroanalysis* **13** (2001) 13.
72. G.U. Flechsig, O. Korbut, S.B. Hočevar, S. Thongngamdee, B. Ogorevc, P. Gründler, J. Wang, *Electroanalysis* **14** (2002) 192.
73. S.B. Hočevar, J. Wang, R.P. Deo, B. Ogorevc, *Electroanalysis* **14** (2002) 112.
74. *Kirk-Othmer, Encyclopedia of Chemical Technology*, third ed., Vol. 3, H.F. Mark (ed.), Antibiotics (Phenazines) to Bleaching Agents, John Wiley and Sons, 1978, pp. 913.
75. D.E. Williams, G.A. Wright, *Electrochim. Acta* **21** (1976) 1009.
76. A. Janes, E Lust, *Electrochim. Acta* **47** (2001) 967.
77. M.D. Maciá, E. Herrero, J.M. Feliu, A. Aldaz, *J. Electroanal. Chem.* **500** (2001) 498.
78. E. Lust, A. Janes, *J. Electroanal. Chem.* **413** (1996) 175.
79. E.A. Hutton, B. Ogorevc, S.B. Hočevar, F. Weldon, M.R. Smyth, J. Wang, *Electrochem. Commun.* **3** (2001) 707.
80. A. Królicka, R. Pauliukaitė, I. Švancara, R. Metelka, A. Bobrowski, E. Norkus, K. Vytřas, *Electrochem. Commun.* **4** (2002) 193.
81. R. Pauliukaitė, S.B. Hočevar, B. Ogorevc, J. Wang, *Electroanalysis*, in press.
82. X. Cai, B. Ogorevc, E. Benfenati, K. Kalcher, M. Novič, I. Grabec, *Anal. Chim. Acta* **310** (1995) 153.

3. THE BISMUTH FILM ELECTRODE FOR ADSORPTIVE STRIPPING VOLTAMMETRIC AND POTENTIOMETRIC STRIPPING ANALYSIS OF TRACE COBALT AND NICKEL IN SOME LOW-VOLUME BODY FLUIDS, AND APPLICATION IN THE DETERMINATION OF SELECTED HEAVY METALS IN SOIL EXTRACTS

3.1 Introduction

Metals have played an important, yet dual role in the history of man. On the one hand, their increased industrial use has contributed substantially to technological development, and on the other, they have long been recognised as potential hazards to human health [1]. While many metals have been acknowledged as essential (e.g. boron, iron, selenium, zinc), toxic effects on living material can be expected from all elements. The toxicology of an element is dependent on the kinetics of the interaction of the element in ionised form or as an organic compound of the element with the human organism. The potential toxic character or the final toxicity depends on the result of this interaction, in which both the element concerned and the organism, with its anatomical and physiological characteristics, have a mutual influence. Toxicokinetics can be considered in three stages: (1) a stage of entry and resorption, (2) a stage in the organism where transport, distribution, accumulation, biotransformation and the effect take place, and (3) a stage in which the chemical leaves the organism. In each of these stages, the element is found in a suitable chemical and physical form to interact with the anatomical characteristics and the physiological properties of the organs or systems [1].

The possible contacts of man with potentially toxic metals and their compounds differ widely. Toxic elements such as Pb, Hg, Cd, As, Cr and Ni occur in very different concentrations in nature, air, water, soil, food, and beverages, so that the background concentrations differ throughout the world. The health effects associated with metal toxicity in mammals include early mortality, growth retardation, impaired reproduction with mortality of offspring, depression or physiologic

parameters, neoplasms, and chronic disease symptoms [2]. At the cellular level, derangement of cell-membrane permeability and anti-metabolite activity are the effects of metal toxicity. Metals can interact with a protein, leading to an allosteric effect, or with DNA or RNA to stop normal metabolism, or with unknown compounds, leading to a change in physiologic processes, to a change in behaviour, or even to a change in an ecological system. Changes in rates of the catalytic decomposition of essential metabolites, enzyme inhibition, and irreversible conformation changes in macromolecular structure are some of the effects of metal toxicity at the molecular level [2].

The inherent toxicity of a metal and its compounds in biologic systems depends on its electrochemical character and oxidation state, its absorption and transport in the body tissues, the stability and solubility of its compounds in body fluids, its ease of excretion, and its reaction with functioning tissues and organelles and with essential metabolites and other metals [2]. Toxicity due to metal compounds under acute and moderately severe chronic conditions can be distinguished by outward clinical symptoms. Postmortem examination and analysis of the tissues and internal organs indicate the extent of intoxication and the distribution of metal toxicants in the body. Toxicity due to chronic exposure to very low doses of metallic toxicants is difficult to diagnose, especially when clinical or outward symptoms are not well pronounced. Under these conditions, blood, cerebrospinal fluids, and available excretory products of metabolism such as faeces, urine, skin, nails, and hair are analysed to identify and assess the dosage of the toxicant [2]. Other samples in which metals may be measured include saliva and sweat. In addition, it is of interest to measure these elements and compounds in samples such as marine, river and tap waters, air, soils and foods as these represent possible routes for exposure.

Considering the widespread availability of toxic metals, and the hazards associated with contact with them, methods suitable for their determination in a variety of samples are highly desirable. Many methods have been developed for this purpose, including atomic absorption spectrometry, atomic emission spectrometry, x-ray fluorescence, gas-liquid chromatography, neutron activation analysis and electrochemical methods [2]. It is the latter with which this work is concerned and further information about several of these techniques is included in the following sections.

3.2 Cobalt, Nickel and Heavy Metals and Significance for Measurement

3.2.1 Cobalt

3.2.1.1 Introduction

Cobalt is a member of the iron triad in the eighth group of the periodic table, with atomic number 27 (atomic configuration; [Ar].$3d^7.4s^2$) and atomic weight 58.93 g/mol [3]. The electrochemical behaviour of cobalt is usually intermediate between that of iron and nickel, with a standard electrode potential at 25°C for $Co \rightarrow Co^{2+}$ of +0.278 V. Cobalt exhibits a valency of 2 or 3, the bivalent being the stable state for the simple ion when not co-coordinated to anything but water [3]. The simple trivalent cobaltic (Co(III)) ion is unstable; cobalt occupies an intermediate position between iron, where the trivalent ion is the stable state, and nickel, where trivalent ions probably do not exist. There are a great number of co-ordination compounds of Co(III). The Co(III) ion readily forms six-coordinate, octahedral complexes such as the cobaltammines, whose parent ion is hexamminecobalt(III), $[Co(NH_3)_6]^{3+}$, in which six ammonia molecules are bonded, through their nitrogen atoms, to the central cobalt atom. There are also a number of complexes of cobalt(II). Divalent cobalt in complexes has a coordination number of either four or six, whereas that of the Co(III) ion is invariably six.

3.2.1.2 Cobalt in the Environment and Human Body

Cobalt is not an abundant element (earth abundance ~ 20 ppm), but it is widely diffused in nature, occurring in rocks, sea water, mineral water, coal, meteorites, the Sun and stellar atmospheres, soils, plants and animals [1]. Its uses are varied and include its utility in the ceramic and glass industries, cemented carbides, driers, catalysts, magnetic, wear-resistant, corrosion-resistant, or heat resistant alloys, and in such diverse fields as radiography, pigment manufacture, electroplating, tracers, and animal nutrition. Many cobalt minerals have been described, but the important ones are sulphides, arsenides, and oxidised compounds.

While cobalt is an essential element in humans and animals as a constituent of vitamin B_{12}, and has also been used in the treatment of anaemia due to its ability to stimulate red blood cell production, exposure to this element results in some quite

serious health effects [4]. Chronic inhalation exposure to cobalt includes effects on the respiratory system such as respiratory irritation, wheezing, asthma, decreased lung function, pneumonia, and fibrosis. Other effects noted in humans from inhalation exposure include cardiac effects, such as functional effects on the ventricles and enlargement of the heart, congestion of the liver, kidneys and conjunctiva, and immunological effects that include cobalt sensitisation, which can precipitate an asthma attack in sensitised individuals [4]. Cardiovascular effects were observed in people who consumed large quantities of beer over a period of several years, which contained cobalt sulphate as a foam stabiliser (average concentration of cobalt ingested 0.04 mg/kg/day to 0.14 mg/kg/day). Gastrointestinal effects (nausea, vomiting, and diarrhoea), effects on the blood, liver injury and allergic dermatitis have also been reported in humans from oral exposure to cobalt [4]. Animal studies have reported respiratory, cardiovascular, and central nervous system effects, decreased body weight, necrosis of the thymus, and effects on the blood, liver, and kidneys from inhalation exposure to cobalt. The most common sources of exposure are through air, drinking water, and food. The average concentration of cobalt in ambient air in the US is approximately 0.0004 $\mu g/m^3$, while the level in one industrial site was found to be 0.61 $\mu g/m^3$. Average levels in drinking water were found to be 2 $\mu g/L$, but values up to 107 $\mu g/L$ have been measured. The average daily intake of cobalt from food is estimated to be 5 to 40 μg/day [2]. Increased exposure occurs in those working in the production of cobalt powders and in metal workers. Excretion of cobalt occurs mainly via urine.

The 2001 CERCLA (Comprehensive Environmental Response, Compensation, and Liability Act) Priority List of Hazardous Substances, which prioritises substances based on their frequency, toxicity, and potential for exposure at National Priorities List (a prioritised list of the USA's worst hazardous waste sites, developed by the USEPA, which identifies and informs the public about releases of hazardous substances, pollutants, and contaminants [5]) sites, ranks cobalt in 49th position [6]. In another prioritisation of the toxicity of certain compounds, the Agency for Toxic Substances and Disease Registry (ATDSR) developed the Minimal Risk Level (MRL) for hazardous substances, which is an estimate of the daily human exposure to a hazardous substance that is likely to be without appreciable risk of adverse non-cancer health effects over a specified duration of exposure [7]. The

toxicological profiles include an examination, summary, and interpretation of available toxicological information and epidemiological evaluations of a hazardous substance. The MRLs for cobalt are shown in Table 3.1. Considering the health effects associated with exposure to cobalt and its widespread occurrence and use, methods suitable for its determination at low (μg/L) levels are extremely desirable. Currently used methods, and the newly introduced measurement of cobalt at the bismuth film electrode will be described in the proceeding sections.

3.2.2 Nickel

3.2.2.1 Introduction

Nickel is a silvery white, hard metal that is very tenacious, malleable and ductile [8]. It can take a high polish so that it reflects a large proportion of the light falling on a polished surface. Its atomic number is 28 (atomic configuration; $[Ar].3d^8.4s^2$) and atomic weight 58.71 g/mol. In the ionic form, nickel usually has the oxidation state of two, but unstable compounds having the oxidation states of one and three are known. The highly toxic compound nickel carbonyl exhibits the oxidation state of zero. The standard oxidation potential for $Ni \rightarrow Ni^{2+}$ is +0.250 V. Nickel forms many complexes. These include nickel(II) cyanides of the type $M_2Ni(CN)_4$, nickel(II) amines, and chelates of nickel with dioximes. The latter are employed in its determination.

3.2.2.2 Nickel in the Environment and Human Body

Nickel is more widely distributed in nature than cobalt (80 ppm vs. 20 ppm). It is found in the Earth's core, deep-sea nodules, meteorites, seawater, soils, coal, and crude oil [9]. Intermediate uses of nickel include steel production, the production of other alloys, and electroplating. The most important end-uses are in transportation, the chemical industry, electrical equipment, and construction. It is also found in coinage, jewellery, household appliances, and as a component of dental and orthopaedic devices. The burning of residual and fuel oils, nickel mining and refining, and municipal waste incineration are the main anthropogenic sources of nickel emissions to the atmosphere, and account for approximately 90% of the total global emission.

Nickel is an essential element in some animal species, and it has been suggested that it may be essential for human nutrition, being found in numerous foodstuffs including cocoa, chocolate, dried fruit, nuts, and several grains, fruits, and vegetables. Food is the main source of nickel exposure, with an average intake for adults estimated to be approximately 100 to 300 μg/day [10]. Small amounts of nickel are also found in water, soil and air. Because of the large number of nickel-releasing sources, the nickel concentration in ambient air may show considerable variation. For example, in a remote area (Canadian Arctic), levels of 0.38 – 0.62 ng/m^3 were recorded, as compared to 124 ng/m^3 in the vicinity of a nickel smelter [9]. Nickel concentrations in drinking water in European countries of 2-13 μg/L have been reported. In most food products, the nickel content is less that 0.5 mg/kg fresh weight. Nickel ranks 53rd in the CERCLA Priority List of Hazardous Substances [6]. Its MRL data are included in Table 3.1.

Dermatitis is the most common effect in humans from chronic dermal exposure to nickel. Cases of nickel dermatitis have been reported following occupational and non-occupational exposure, with symptoms of eczema of the fingers, hands, wrists and forearms [10]. Chronic inhalation exposure to nickel also results in respiratory effects, including a type of asthma specific to nickel, decreased lung function, and bronchitis. Human studies have reported an increased risk of lung and nasal cancers among nickel refinery workers exposed to nickel refinery dust. The EPA has classified nickel carbonyl as a Group B2, probable human carcinogen [10]. Methods for the measurement of nickel will be described in the following sections.

Name	*Route*	*Duration*	*MRL**	*Endpoint*
Cadmium	Oral	Chronic[a]	0.0002 mg/kg/day	Renal
Cobalt	Inhalation	Chronic	0.0001 mg/m^3	Respiratory
	Oral	Intermediate[b]	0.01mg/kg/day	Haematological
Copper	Oral	Acute[c]	0.02 mg/kg/day	Gastrointestinal
		Chronic	1 mSv/yr	Other
Nickel	Inhalation	Chronic	0.0002 mg/m^3	Respiratory

*MRL = minimum risk level, [a]≥ 365 days, [b]>14-364 days, [c]1-14 days

Table 3.1: MRLs associated with cadmium, cobalt, copper and nickel (from [7]).

3.2.3 Other Heavy Metals Measured in this Work

While the main focus of this Section of the work is the measurement of nickel(II) and cobalt(II) as their dimethylglyoximate complexes using adsorptive stripping voltammetry and adsorptive potentiometric stripping analysis at the bismuth film electrode, the final part of this Section deals with the measurement of some other heavy metals in soil extracts. Hence, a brief summary of some of the characteristics and effects of these metals is provided here.

3.2.3.1 Cadmium

Cadmium is a soft, bluish-white metal which is easily cut with a knife [11]. In the Periodic Table of the elements, it lies below zinc and above mercury: its atomic number is 48, its atomic weight 112.41 g/mol, and its electronic configuration [Kr].$4d^{10}.5s^2$. Its common oxidation state is +2, although it can also form some very unstable oxidation state +1 compounds. It forms chlorides, bromides, iodides and fluorides and also organic compounds of the type R_2Cd.

Cadmium is used in the manufacture of pigments and batteries, and in the metal plating and plastics industries. The average cadmium content of the earth's crust is estimated to be about 0.1 mg/kg. Weathering of minerals in geological periods has lead to Cd enrichment of sediments by a factor of 2-3. Phosphates show a broad range of Cd contents with an average of about 15 mg/kg. Soils generally contain < 5 mg/kg, with higher levels being attributed to anthropogenic sources [11]. The largest sources of airborne cadmium in the environment are the burning of fossil fuels and incineration of municipal waste materials [12]. It may also be emitted from zinc, lead, or copper smelters. Smoking is another important source of cadmium exposure, with smokers having approximately twice the amount of cadmium in their bodies than non-smokers. For non-smokers, food is generally the largest source of cadmium exposure. The average intake of Cd in most European countries, the US and New Zealand is estimated to be in the 10-30 μg/day range, while levels of up to 400 μg/day have been reported in Japan [11]. Cadmium occupies 7th place in the CERCLA Priority List of Hazardous Substances [6]. Its MRL data are included in Table 3.1.

Chronic inhalation and oral exposure of humans to cadmium results in an accumulation of cadmium in the kidneys that can cause kidney disease [12]. Other

effects noted in occupational settings include effects on the lungs, including bronchitis. Human developmental studies on cadmium are limited, although there is some evidence that maternal cadmium exposure may result in decreased birth-weights. Occupational studies have reported an excess risk of lung cancer in humans from exposure to cadmium, and although the evidence is rather limited, the USEPA considers cadmium to be a probable human carcinogen. Measurements of cadmium in blood or urine using atomic absorption spectrometry, or in liver or kidney using neutron activation analysis, are used as indicators of cadmium exposure [12].

3.2.3.2 Copper

Copper, atomic number 29, atomic mass 63.55 g/mol, and electronic configuration [Ar].$3d^{10}.4s^{1}$, is the 26th most abundant element in the earth's crust [13]. It has been known for about 10,000 years and occurs in pure form as a "semi-precious" metal or in compounds as Cu(I) or Cu(II). After silver, copper is the best common conductor of heat and electricity, hence its widespread use in electrical wiring. Other uses include water piping, stills, roofing material, kitchenware, and chemical equipment. Notable alloys of copper include bronze (with tin) and brass (with zinc). Copper salts are used as fungicides and also as growth promoters in animal (swine and poultry) feed [13].

Exposure to copper is usually through ingestion, inhalation or skin contact with copper-containing substances [14]. The concentration of copper in air ranges from a few ng/m^3 to about 200 ng/m^3, while the concentration near copper smelters may reach 5,000 ng/m^3. The average concentration of copper in lakes and rivers is 4 μg/L, while slightly higher levels may be encountered in groundwater. Ingestion exposure to copper may be increased if there are high levels of soluble copper in corrosive drinking water, which also flows through copper piping and brass water fixtures, with levels reaching as high as 1 mg/L. The average daily intake of copper through eating and drinking is approximately 1 mg/day. The MRL data for copper are included in Table 3.1.

Copper is one of the several heavy metals that have essential as well as toxic properties. It is toxic to many bacteria and viruses, but for plants, copper toxicity is virtually unknown. In humans, copper is an essential part of several enzymes including ferroxidases, cytochrome oxidase, superoxide dismutase, and amine

oxidases. Excess copper ingested in the diet of man and animals is usually deactivated or eliminated by various biochemical mechanisms, thus under normal conditions no toxic actions occur. Toxicity may occur if one of these mechanisms is defective [13]. Chronic copper exposure in industry (e.g., inhalation of copper fumes), may lead to various health effects such as respiratory symptoms, gastrointestinal disturbances, nervous dysfunctions, and dermatological and hematological changes. The CERCLA Priority List of Hazardous Substances ranks copper in 129th position [6]. Copper levels in body fluids and tissue are routinely measured using flame or graphite furnace atomic absorption spectrometry [13].

3.2.3.3 Lead

Lead is a soft metal having little tensile strength, and is the heaviest of the common metals excepting gold and mercury, indeed its name is derived from the Latin "plumbum", meaning heavy [15]. It has a metallic lustre when freshly cut but quickly acquires a dull grey colour when exposed to air. Its atomic number is 82, its atomic weight 207.2 g/mol and its electronic configuration $[Xe].4f^{14}.5d^{10}.6s^2.6p^2$. Lead occurs naturally in small quantities in the earth's crust and is present in a variety of compounds such as lead acetate, lead chloride, lead chromate, lead nitrate and lead oxide [16]. Its primary use is in the manufacture of batteries, also being used in the production of meal products such as sheet lead, solder, pipes, and in ceramic glazes, paint, and ammunition. It was formerly used in the tetraethyl form for addition to petrol to increase the octane rating, until lead additives were phased out and eventually banned.

The largest source of lead in the atmosphere was from leaded petrol combustion, but with the prohibition of lead in petrol, air lead levels have decreased considerably. Other airborne sources include combustion of solid waste, coal, oils, emissions from iron and steel production and lead smelters, and tobacco smoke [16]. Exposure to lead can also occur from food and soil. Until 1978, lead-based paints were commonly used, with flaking paint, paint chips and weathered paint powder being a major source of lead exposure. Lead in drinking water is primarily due to the presence of lead in certain pipes, solder and fixtures. The CERCLA Priority List of Hazardous Substances ranks lead in 2nd position, which indicates its high risk [6]. Death from lead poisoning may occur in children who have blood levels greater than

125 μg/dL. Chronic exposure to lead in humans can affect the blood causing anaemia. It also affects the nervous system, slowing nerve conduction in peripheral nerves. Other effects of chronic lead exposure include effects on blood pressure, kidney function, interference with vitamin D metabolism, spontaneous abortion in pregnant women, low birthweight and impaired mental development in the human foetus, and decreased IQ scores in children. The EPA considers lead as a probable human carcinogen [16]. From the viewpoint of occupational and environmental toxicology the determination of lead in blood is of greatest importance, since the concentration of lead in whole blood is considered to be the best indicator of current lead exposure in humans and mammals. The most commonly employed methods include anodic stripping voltammetry and flame or graphite furnace atomic absorption spectrometry [17].

3.3 Detection of Heavy Metals

3.3.1 Non-Electrochemical Methods

Some of the most popular non-electrochemical techniques used in the determination of heavy metals in samples are atomic absorption spectrometry (AAS) and inductively coupled plasma-mass spectrometry (ICP-MS), and to a lesser extent, neutron activation analysis (NAA). A brief description of these techniques and some of their many applications in the measurement of various heavy metals will be provided in this section.

Atomic absorption has as its basis the tendency of a population of unexcited atoms to absorb strongly the radiation emitted by excited atoms of the same element [18]. In practice, an atomiser-burner is used to aspirate a fine mist of the sample into a flame. This is the basic technique – flame-AAS, which is widespread and has an acceptable level of accuracy for most analytes. Most of the atoms of the sample remain in their ground states in the inner cone and are thus available to absorb selected wavelengths of radiation from a suitable source. One of these wavelengths is isolated with a monochromator; its power is measured with a detector. A relationship analogous to the Beer-Lambert law exists between the power of this radiation before and after interaction with the atoms of the sample. The most popular variation of

AAS, which allows for better sensitivity and more control of the chemical environment of the analyte, involves electrothermal atomisation (also known as graphite furnace), in which samples are deposited in a small graphite tube, which is then heated to vapourise the sample.

ICP-MS is one of the fastest growing methods for trace element determinations. Its power lies in its ability to measure a wide variety of elements at low concentrations. The sample, which must be in a liquid form, is pumped at 1 mL/min, usually with a peristaltic pump into a nebulizer, where it is converted into a fine aerosol with argon gas at about 1 L/min. The fine droplets of the aerosol, which represent only 1-2% of the sample, are separated from larger droplets by means of a spray chamber. The fine aerosol then emerges from the exit tube of the spray chamber and is transported into the plasma torch via a sample injector. Once the ions are produced in the plasma, they are directed into the mass spectrometer via the interface region, which is maintained at a vacuum of 1-2 torr with a mechanical roughing pump. This interface region consists of two metallic cones (usually nickel), each with a small orifice (0.6-1.2 mm) to allow the ions to pass through to the ion optics, where they are guided into the mass separation device [19].

About 70% of the elements have properties suitable for measurement by neutron activation analysis. This sensitive technique involves a number of steps, as follows. When a neutron interacts with the target nucleus via a non-elastic collision, a compound nucleus forms in an excited state. The excitation energy of the compound nucleus is due to the binding energy of the neutron with the nucleus. The compound nucleus will almost instantaneously de-excite into a more stable configuration through emission of one or more characteristic prompt gamma rays. In many cases, this new configuration yields a radioactive nucleus which also de-excites (or decays) by emission of one or more characteristic delayed gamma rays, but at a much slower rate according to the unique half-life of the radioactive nucleus. Depending upon the particular radioactive species, half-lives can range from fractions of a second to several years. In principle, therefore, with respect to the time of measurement, NAA falls into two categories: (1) prompt gamma-ray neutron activation analysis, where measurements take place during irradiation, or (2) delayed gamma-ray neutron activation analysis, where the measurements follow radioactive decay. The latter operational mode is more common; thus, when one mentions NAA it is generally assumed that measurement of the delayed gamma rays is intended [20].

While the above methods are extremely sensitive and offer the possibility of detecting a wide range of elements, they suffer from certain disadvantages. ICP-MS and AAS can suffer from plasma and matrix interferences, respectively. In NAA, if the target element has a long half-life, analysis may take a considerable amount of time. Certainly, one of the biggest drawbacks of these techniques is their cost, which will inevitably preclude their use in many laboratories.

Atomic absorption spectrometry is often used in studies to determine the levels of heavy metals in the environment, or in studies of the levels of and hence effects of heavy metals in a variety of biological matrices. One such study involved the use of AAS in investigation of the levels of Pb, Cu, Mn, Cr, Cd, Zn and Hg in the hair, blood and urine of child and adult subjects with alopecia (hair loss of unknown cause, characterised by round patches of complete baldness) [21]. Electrothermal-AAS (ET-AAS) following thermal decomposition of proteins in the samples was employed in the direct determination of nickel in human blood serum and urine. The limits of detection were 0.2 μg/L for both samples, with linear ranges from 0.5 – 2.0 μg/L and 0.5 – 2.5 μg/L for serum and urine samples, respectively [22]. The levels of a number of heavy metals in human colostrum were determined using ET-AAS, following wet-ashing of the samples. The levels of lead, cadmium, nickel, chromium, manganese, copper, zinc and iron in the samples were found to be 14.6, 2.8, 27.8, 8.6, 43.2, 278, 12.9 and 3.5 μg/L, respectively [23].

AAS was employed to determine the role of proteins in affecting elemental release from a variety of clinically available dental casting alloys by immersing the alloys in saline or saline-protein solutions [24]. Levels of Ag, Cu, Ni, Pd and Zn were measured based the ratio of μg of mass released to square centimetre alloy surface area exposed to solution. The AAS results showed that more element release occurred when the saline solutions contained protein. AAS was also used to measure Zn, Cu, Mn, Cd, Ni and Al in the sweat samples of 15 healthy subjects [25]. The mean sweat levels of the aforementioned metals were 358.1, 486.8, 3.1, 1.9, 69.9 and 15.0 μg/L, respectively, indicating that substantial quantities of these trace elements are excreted in this manner. ET-AAS was used in the determination of cobalt in serum and urine following sample mineralisation by wet acid digestion, with the procedure providing a detection limit of 0.11 μg/L cobalt in both matrices [26]. Arsenic, lead and mercury were determined in mg/L to μg/L levels in environmental

and biological samples using flow injection hydride generation and cold vapour flow injection AAS, with limits of detection of 1.8, 2.0, and 1.5 μg/L, respectively [27].

AAS has also found widespread use in the measurement of heavy metals in matrices other than biological fluids. It was used in an investigation of the content of heavy metals (Cd, Cr, Pb, Hg) in food packaging paper boards, such as those used as packaging materials for pasta and cereal products, with the results showing that most of the samples contained amounts higher than those permitted by the European Council [28]. Flow injection on-line preconcentration and flame AAS were used in the determination of copper, cadmium and lead in marine sediment samples [29]. Following preconcentration, sensitivity enhancement in the order of 80, 90 and 60 times, and corresponding detection limits of 1.2, 0.6 and 3.0 μg/L were found for Cu, Cd and Pb, respectively. Lead was determined in soil samples by in-valve solid-phase extraction flow injection flame atomic absorption spectrometry [30].

Although used to a lesser extent than AAS in trace heavy metal determinations, ICP-MS finds widespread use in their measurement in a variety of samples and matrices. Numerous heavy metals were determined in artificial and real seawater samples using on-line column preconcentration inductively coupled-mass spectrometry [31]. In artificial seawater, the detection limits of for example, cobalt, nickel, copper and lead, were 0.014, 0.029, 0.099, and 0.007 μg/L, respectively. ICP-MS coupled to HPLC and in conjunction with an isotope dilution mass spectrometric method, was developed for the simultaneous determination of the complexes of 11 heavy metals with humic substances, and was applied in the analysis of brown water, ground water, sewage and seepage waters. The detection limits were very low, in the 5 to 100 ng/L range [32]. On-site ICP-MS analyses on drinking and vadose waters at a disused industrial / mining site revealed several "hot spots" of high heavy metal concentrations, with maximum concentrations of for example, 12,000 μg/L of zinc, 126 μg/L of nickel, and 184 μg/L lead [33]. An automated on-line sample pretreatment system combining microwave digestion with sample preconcentration / matrix separation coupled with ICP-MS was used in the determination of some heavy metals in blood and serum samples [34]. Limits of detection for Fe, Ni, Cu, Zn and Pb, were 68, 0.34, 3.5, 13.4, and 0.22 μg/L, respectively.

Neutron activation analysis was employed in determination of the elemental composition of sediment samples [35]. The aim of the study was to determine

whether less common elements like the rare earths or the actinides are associated with contaminant metals such as zinc. While high concentrations of zinc were measured (1000 μg/g), no evidence of any association between the zinc and other potential contaminants was identified. In a study to relate toenail zinc concentrations to the risk of myocardial infarction, the average zinc concentration was found to be 106.0 mg/kg using NAA [36]. Tin was determined in human serum using neutron activation analysis following dry-ashing of the samples at levels of approximately 0.50 μg/L [37].

The above examples have revealed, in addition to use of atomic absorption spectrometry, inductively coupled plasma-mass spectrometry and neutron activation analysis in heavy metal determination, the wide range of samples and matrices in which heavy metals are found. Each of the mentioned techniques permit the analysis of a wide variety of elements at high sensitivity, although a sample preparation step is necessary when analysing many matrices in order to prevent signal interference and fouling of the respective instruments. The next Section will deal with some of the many studies carried out on heavy metal detection employing electrochemical techniques.

3.3.2 Electrochemical Methods

3.3.2.1 Introduction

Stripping voltammetric techniques (anodic stripping voltammetry; ASV and cathodic adsorptive stripping voltammetry; CAdSV) have made an important contribution to fields such as marine chemistry, food analysis, soil science and bioanalysis. The selectivity and extremely low detection limits have made stripping voltammetry a widely used technique for trace metal speciation and trace metal distribution measurements in a variety of sample matrices. A description of these techniques was given in Section 1.2.4.6, and this will be expanded upon in this Section.

Historically, the most popular working electrodes for environmental trace metal analysis have been the hanging mercury drop electrode (HMDE) and the mercury film electrode (MFE). The use of mercury electrodes in the determination of nitrophenols has been described in the preceding chapter – a more complete description of their application in trace heavy metal determinations will be provided

here. Due to the aforementioned disadvantages associated with mercury electrodes (see Section 2.4.2), a constant search has been underway for mercury electrode substitutes. Other electrode surfaces such as gold or various carbon substrates have been used for electrochemical measurements of trace metals [38]. Such solid electrodes are suitable for the determination of Cu, Hg and Pb, and elements which have oxidation potentials more positive than Hg (e.g., Ag, Au, Se and Te). The surface of these electrodes is often poorly defined and the capacitance current is higher than for mercury electrodes. Consequently, the voltammetric analysis of trace metals with solid electrodes is less sensitive and reproducible compared with the HDME or MFE. In recent years, much progress has been made in the field of microelectrodes (see Section 1.3.4 and Chapter 4). Such electrodes may have a bare or coated surface. Successful applications of trace metal determination in natural waters have been reported for gold microelectrodes, Hg plated carbon fibre microelectrodes, and Hg plated iridium microelectrodes [38 and references therein]. Recently, as described in the previous chapter, bismuth has been introduced in stripping analysis and cathodic electrochemical detection as a promising alternative to mercury electrodes.

Further to the descriptions of stripping analysis provided in Section 1.2.4.6, some more detail about these techniques is provided here. During ASV analysis, a deposition, or preconcentration step is carried out under conditions of forced convection, at deposition potentials approximately 0.3 – 0.4 V more negative than the reduction potential of the metal. During the deposition step metal ions are collected in the mercury by reduction (to a metallic state) and amalgamation with the Hg, as follows:

$$M^{n+} + ne^- + Hg \leftrightarrow M(Hg) \qquad (3.1)$$

Only a small fraction of the metal is actually being deposited during the deposition step. Rather than amalgams, it is believed that bismuth forms alloys with the target heavy metals [39]. The deposition is followed by a voltammetric scan towards more positive potentials during which the metal in the Hg (or alloyed with bismuth) is oxidised and the current produced is determined. The resultant current-potential

stripping voltammogram provides both quantitative and qualitative information about the sample being analysed [38].

Cathodic adsorptive stripping voltammetry exploits the ability of those metals that cannot be determined using ASV to be complexed with a particular specific added ligand, to be adsorbed onto the mercury (or bismuth) surface and then to be stripped off the surface, thus providing quantitative and qualitative information about the sample under investigation. The formation of the metal-ligand complex is pH dependent, hence a buffer is used to control the pH of the sample [38]. The adsorption potential is carefully chosen to be approximately 0.1 V (or more) more positive than the reduction of the metal-ligand complex. The potential is then scanned in the negative direction and the resulting current is measured. The current produced is the result of the reduction of a reducible group on the ligand or of the metal itself in the adsorbed complex. The chosen ligand must obey two criteria – the ability to form a complex with the element of interest and electroactivity i.e. the capability to adsorb onto the surface of the mercury (or bismuth). Figure 3.1 shows the Periodic Table with those elements that can be determined employing stripping voltammetry or adsorptive stripping voltammetry highlighted. The target elements of this study are also noted.

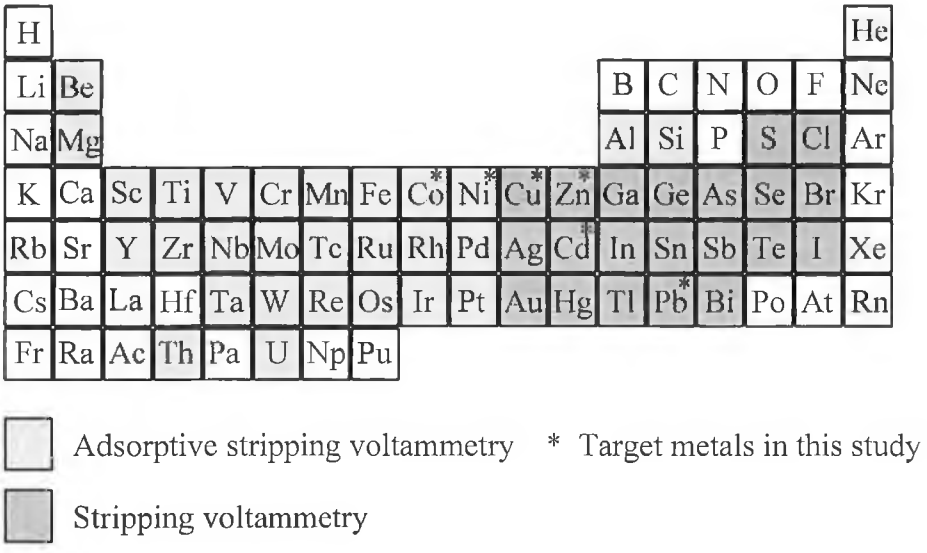

Figure 3.1: Elements measurable by adsorptive stripping voltammetry or stripping voltammetry, and target metals of this study.

3.3.2.2 Anodic Stripping Voltammetry

Anodic stripping voltammetry at a hanging mercury drop electrode was employed in the simultaneous determination of lead and cadmium in TiO_2 and titanium dioxide containing cosmetics (sun-screen products) [40]. Triethanolamine was employed to remove titanium interference following TiO_2 acidic digestion, with a detection limit of 1 μg/L being achieved for both metals. The results obtained compared favourably with those obtained using ET-AAS. A range of heavy metals were determined at 10^{-9} mol/L levels in environmental matrices using stripping voltammetry at a stationary mercury electrode [41]. A standard addition procedure was found to improve the resolution of the voltammetric technique. Differential pulse stripping voltammetry in various modes, with a HMDE, was used in the direct simultaneous determination of Cd, Pb, Cu, Sb, Bi, Se, Zn, Mn, Ni, Co, and Fe in water samples [42]. Low detection limits ranging from 1.1×10^{-10} to 1.05×10^{-9} mol/L were found for each element, and the method was applied for the determination of these elements in some ground water samples. Selenium and lead contents in milk samples were quantified employing differential pulse cathodic stripping and anodic stripping voltammetry [43]. Following wet-digestion of the samples, selenium and lead were determined using the method of standard additions at levels of 21.5 – 69.4 μg/L and 22.1 – 59.2 μg/L, respectively.

A significant problem in using mercury films is the difficulty in achieving reproducible films. The presence of thiocyanate in the mercury film was found to result in more reproducible mercury films and more sensitive determination of lead and cadmium in lake waters and certified seawater after UV digestion [44]. Employing a very negative potential of –1.5 V resulted in a 10-fold and 3-fold increase in the sensitivity of the procedure for cadmium and lead, respectively. ASV at the MFE and HDME was applied in the determination of trace amounts of lead (0.1 – 25 μg/L), cadmium (0.015 – 0.44 μg/L), zinc (0.07 – 1.06 μg/L) and copper (0.14 – 0.4 μg/L) leached from ceramic plates by 4% acetic acid solution, with the concentrations measured dependent on the kind of plate and manufacture [45].

As mentioned previously, lead represents a serious threat to human health and its level in blood is seen as the best indicator of exposure. An automated electrochemical method, using flow injection analysis with a wall-jet detector, in conjunction with a MFE is described for the measurement of lead in blood [46].

Electrode poisoning by proteins present in the blood samples was suppressed by using a Nafion®-membrane coating, and lead was measured at levels of 0.05 mg/L with an accuracy of about 10%. Trace amounts of zinc, cadmium and lead were determined in refined beet sugar by differential pulse ASV at a HMDE [47]. The samples were digested and the metals determined at the 10 – 80 μg/kg level, and the results compared with those obtained by ET-AAS. Results obtained using ASV were found to show better accuracy than those of ET-AAS measurements. The influence of sample pretreatment procedures on the determination of lead and copper in wine was assessed using ASV at mercury microelectrodes [48]. Three different procedures were employed in pretreatment of the wine samples; (a) the samples were added to conc. HCl at pH 1.5, (b) 30% H_2O_2 was added to the samples (1:2.5 v/v) and UV irradiation applied for 2 hours, and (c) the wine plus conc. HCl at pH 1.5 were UV irradiated for 4 hours. The results showed that the pretreatments ranked b > c > a, with the results obtained using pretreatment (b) being more comparable to AAS measurement results.

As mentioned previously, the bismuth film electrode (BiFE) was recently introduced in anodic stripping voltammetry of several heavy metals [49]. The anodic stripping voltammetry performance of the bismuth film was compared with that of a mercury film electrode for the heavy metals Pb, Cd, Zn and Tl. The stripping voltammetry measurements of μg/L quantities of the aforementioned metals at the bismuth film electrode yielded well-defined peaks, along with a low background, following short deposition periods. The BiFE was found to exhibit favourable stripping behaviour compared to the MFE with particular reference to the measurement of thallium. The quantitation of thallium in the presence of cadmium and lead represents a common problem in stripping voltammetry at the MFE due to overlapping signals. In contrast, these three peaks are well-defined and well-separated at the BiFE. A further advantage of the BiFE over the MFE is presented with regard to the measurement of copper [39]. The standard potential of copper is more positive than bismuth, unlike those of Pb, Cd, Zn and Tl, and its signals are often distorted at the mercury electrode. While a split peak for copper was observed at the BiFE at low concentrations, a sharp peak with a potential approximately 210 mV more positive than that of bismuth appeared at concentrations > 20 μg/L. Upon increasing the copper concentration, a simultaneous decrease in the bismuth

peak was observed, reflecting competition of the electrodeposited copper and bismuth for surface sites. Similar to the MFE, the formation of Cu-Zn intermetallic compounds was observed at the BiFE, with the problem being overcome by the addition of gallium, which preferentially forms a Cu-Ga intermetallic compound, thereby permitting quantification of zinc.

In a further study on the newly introduced bismuth film electrode, its operational parameters were studied in order to provide new insights into the influence of key parameters such as substrate electrode, electrolyte ionic strength and pH, potential scan mode, temperature and the presence of potential interferents on the stripping voltammetry signals of trace heavy metals [50]. It was determined that the most suitable supporting electrode materials were carbon-based (glassy carbon and carbon fibre). The optimum pH range was between 4 and 5 for both cadmium and lead, while for the same two elements, the most suitable supporting electrolyte was 0.1 mol/L acetate buffer. The stripping performance of cadmium and lead was found to be temperature dependent, with the stripping current response increasing almost linearly with increasing temperature. This was attributed to increased mass transport and enhanced electrochemical reaction kinetics. This feature was also observed in further studies of the BiFE, in which it was shown that by elevating the temperature during the deposition step at a heated BiFE, signals for Zn, Cd, and Pb were enhanced by a factor of 10 to 16 [51].

The bismuth film has also been applied to screen-printed electrodes for stripping voltammetry measurements of trace lead, with a view to creating disposable "one-shot" decentralised lead testing [52]. The main difference between this and the aforementioned applications at the BiFE, was that this sensor relied on a preplated bismuth film. Following 10 minutes of deposition, a very low limit of detection of 0.3 μg/L was achieved. The sensor was also applied in the measurement of lead in a drinking water sample, with a value of 1.8 μg/L obtained using the method of standard additions. In another variation, carbon paste electrodes were bulk-modified with bismuth oxide and applied in the stripping voltammetry determination of lead, cadmium and copper [53]. Zinc and lead levels in drinking water samples were measured employing this electrode, with the results obtained comparing favourably with those of an AAS reference method.

3.3.2.3 Cathodic Adsorptive Stripping Voltammetry and Potentiometric Stripping Analysis

Cathodic adsorptive stripping voltammetry measurement of cobalt as its dimethylglyoxime (DMG) complex in connection to the mercury electrode has been known for approximately four decades [54]. The structures of DMG and the metal-dimethylglyoxime complex are shown in Figure 3.2. In the past two decades, much work was carried out on the determination of cobalt and nickel as their DMG complexes at mercury film electrodes.

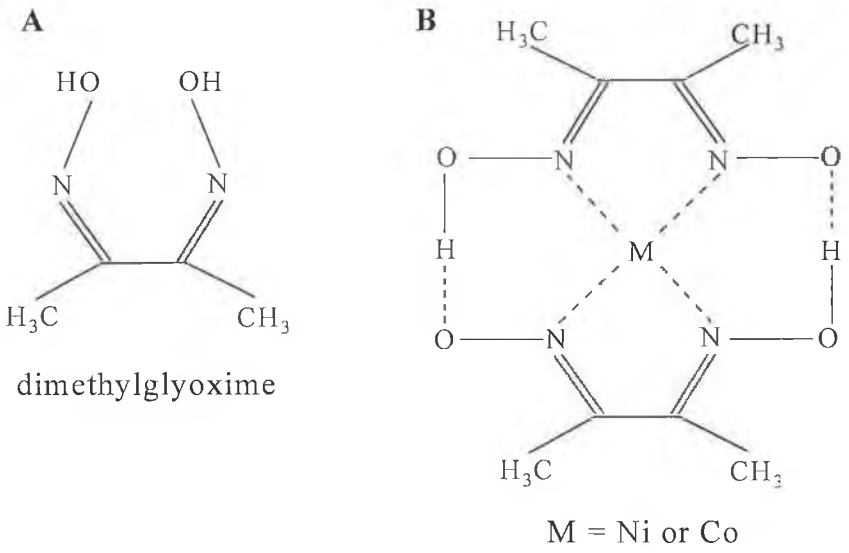

Figure 3.2: Structures of (A) DMG and (B) metal-dimethylglyoxime complex.

For example, Eskilsson *et al.* describe the determination of nickel and cobalt in natural waters and biological material by reductive chronopotentiometric stripping analysis in a flow system [55]. The flow set-up consisted of a six-way valve system, in which various solutions were pumped through a thin-layer cell, with each solution representing a separate step in the procedure, i.e., (i) mercury film deposition, (ii) adsorption of nickel and cobalt as their DMG complexes onto the mercury film electrode (iii) reduction of the metals in 5 mol/L $CaCl_2$, (iv) removal of the mercury film, (v) cleaning of the glassy carbon electrode with ethanol and (vi) with sodium hydroxide. The detection limits of the system after 60 s deposition were 9 and 11 ng/L for nickel and cobalt, respectively. Results obtained in natural waters and digested biological material were in excellent agreement with those obtained using AAS. The possibility of modifying a graphite paste electrode with DMG and then

employing this electrode in the potentiometric stripping determination of nickel was also investigated [56]. In contrast to other methods, the electrode was not polarised during the preconcentration step. The preconcentration time (under stirring conditions) was found to increase the signal up to times of 3 minutes, after which no appreciable increase in current was observed. In the potentiometric stripping step, hydrogen peroxide, potassium persulphate and atmospheric oxygen were investigated as oxidants, with the latter proving to be most suitable. The limit of detection was found to be 8.2 μg/L following 3 minutes preconcentration, which is somewhat higher than that achieved by other authors. However, the use of oxygen as oxidant obviates the need to de-aerate the working solution, a step which is generally necessary when using mercury electrodes.

A similar working electrode to that in the previous example was employed in the simultaneous cathodic stripping voltammetry determination of Hg, Co, Ni and Pd [57]. In order to simultaneously determine all four metal ions, the sample solution had to be maintained at pHs between 4 and 6. As expected, pH 8-9 was optimum for the measurement of cobalt and nickel. The method was employed in the simultaneous determination of each element in human hair, tea and rice samples. The application of the rotating disc MFE for square-wave adsorptive stripping voltammetry of cobalt and nickel was shown to provide extremely low limits of detection of 12 ng/L and 14 ng/L for each metal, respectively [58]. The method was applied to the measurement of nickel and cobalt in a high-purity iron reference sample and in a laboratory-prepared standard. The results were comparable to the certified values (iron sample) and the added amounts (laboratory-prepared sample), reflecting the accuracy of the method. A constant current potentiometry method was optimised for cobalt and nickel and the method tested against reference values for both metals in soil and biological samples [59,60]. This method, like those previously described, employed a mercury film electrode. A certain disadvantage of this technique involved the necessity of removing the working solution after every three measurements and replacing it with the mercury plating solution for at least one minute in order to regenerate the MFE. Following optimisation of parameters such as DMG concentration, buffer composition, deposition time and adsorption time, the method was successfully applied in the measurement of both heavy metals in industrial solutions, mussels, algae and standard reference materials [59].

Two procedures were investigated to measure nickel in zinc plant electrolyte as its DMG complex at a hanging mercury drop electrode [61]. The first was an on-line method which utilised *in situ* matrix exchange in order to minimise interferences found from variable cobalt concentrations and large excesses of zinc. While this method was suitable for continuous monitoring of levels of nickel down to 60 μg/L, in highly pure electrolyte, where nickel concentrations do not affect the refining process, a second, more sensitive off-line procedure was necessary. Here, following a nickel-DMG solvent-extraction scheme to remove interference from zinc, nickel was measured by AdSV at levels down to 1 μg/L. Differential pulse AdSV was used to determine nickel and aluminium concentrations in electrolyser cell liquors (solutions of NaCl and KCl brines and NaOH and KOH solutions of various concentrations) [61]. Nickel was complexed with DMG and aluminium with 1,2-dihydroxyanthro-quinone-3-sulphonic acid. Following 60 s and 30 s of accumulation, the limits of detection were 0.1 μg/L and 0.2 μg/L, respectively. As is common with mercury electrodes, it was necessary to remove interference from free chlorine prior to analysis. This was accomplished using hydrazinium sulphate.

Ni and Co were determined simultaneously by means of CAdSV at a MFE in connection with a computerised flow injection system [63]. In this study, the cleaning and regeneration of the MFE is described in detail. This step is necessary after prolonged use of an MFE, as surface active compounds become adsorbed on the active mercury surface, resulting in fouling of the surface over time. After each measurement, the mercury film was reactivated by polarisation at –1.4 V for 40 to 60 s in a flowing stream of ammonia solution. This procedure was deemed to be advantageous to the plating of a new mercury film before each measurement as the "between-film" reproducibility for the Ni and Co stripping peaks was very poor. The proposed method of film cleaning / regeneration resulted in a much lower "within-film" uncertainty. The method was applied in the measurement of cobalt and nickel in a standard reference material of high purity iron and the results compared well with the stated certified contents.

Nickel was determined voltammetrically in natural waters as its DMG complex at a mercury drop electrode [64]. In order to eliminate potential interference from surfactants present in natural waters, high negative deposition potentials of –1.35 V or –1.65 V were applied. Application of such potentials increases the

efficiency of the nickel deposition, probably due to a simultaneous reduction of the hydrogen ions on Ni clusters formed on the mercury surface. Following 120 s deposition at –1.35 V, the limit of detection was found to be 2 x 10^{-10} mol/L (0.012 μg/L). A recent publication describes a continuous flow system for simultaneous determination of heavy metals (Zn, Cd, Pb, Cu, Ni, Co, Cr) in river water samples [65]. The flow system consisted of a mercury film electrode in the wall-jet configuration with a six-way valve system. In order to successfully determine each element, different solutions of appropriate composition i.e. cleaning solutions and different electrolytes / solutions containing an appropriate complexing agent (if necessary) and mercury. Using potentiometric stripping analysis, limits of detection in the 0.01 to 0.11 μg/L range were obtained and the method was successfully used in the measurement of these heavy metals in river water. The results also compared favourably with those obtained using an ICP-MS procedure.

In an article published by Wang *et al.*, the first application of the bismuth film electrode in adsorptive stripping voltammetry of nickel was described [66]. Again, the bismuth film electrode showed great promise for the replacement of toxic mercury electrodes. The performance of the BiFE in CAdSV of nickel compared favourably with that of the MFE, with the added advantage of yielding well-defined signals even in the presence of dissolved oxygen. The operating parameters for measurement of trace nickel at the BiFE were similar to those required for mercury electrodes, for example, adsorption of nickel at the BiFE as its dimethylglyoxime complex at alkaline pH at negative potentials. The scope of this work will be further expanded in this work, with results shown for the determination of cobalt and a mixture of cobalt and nickel as their DMG complexes at the BiFE.

Different electrode systems / complexing agents have also been used in the determination of nickel and cobalt. In one such method, nickel- and cobalt-xanthate (potassium propyl xanthate) were adsorptively accumulated on a hanging mercury electrode following extraction into methyl isobutyl ketone [67]. Following optimisation of the parameters of the procedure, Ni and Co were determined in soils and leafy vegetables, with a lower detection limit of 0.35 μg/L and 0.30 μg/L, respectively. A carbon paste electrode modified with a H^+ ion exchanger was used to determine nickel by anodic adsorptive stripping voltammetry [68]. The procedure involved a pre-concentration step at open circuit conditions, followed by a deposition

step and finally stripping of the metals from the surface. For 12 minutes of accumulation and 5 minutes of deposition, the detection limit was 0.005 μg/L at a linear potential scan of 200 mV/s. The method was applied for measurement of nickel in tap and mineral water and the results compared favourably with those obtained by ICP-AES.

Adsorptive stripping voltammetry has also been applied in the measurement of elements other than nickel and cobalt. Some examples are presented here. Iridium-based mercury electrodes were shown to be suitable for the determination of chromium and uranium in the presence of DTPA and propyl gallate complexing agents [69]. Following 10 minutes accumulation, detection limits of 0.4 μg/L uranium and 0.5 μg/L chromium were obtained. An electrochemical "cleaning" step was applied to remove the adsorbed metal chelate at the end of each measurement, which provided excellent reproducibility over a prolonged period. Trace amounts of copper were determined by CAdSV, based on a procedure involving adsorptive accumulation of the copper as its Alizarin Red A complex on a HDME [70]. Following accumulation of the complex for 60 s, the limit of detection was 0.05 μg/L. The same author proposed a method for the selective catalytic adsorptive stripping voltammetry of cobalt as its methyl thymol blue complex on the surface of a hanging mercury drop electrode [71]. The reduction current was enhanced catalytically by the addition of nitrite, with a detection limit of 0.005 μg/L obtained following an accumulation time of 60 s. Such a catalytic effect of nitrite on the determination of cobalt as its DMG complex at a mercury electrode has been reported [72]. A laboratory made chelating agent, 2-mercapto-5-phenil-amino-1,3,4-thiadiazole, was used in AdSV of cadmium on a mercury drop electrode [73]. A limit of detection of 4.67×10^{-10} mol/L (~ 0.05 μg/L) of cadmium was obtained under optimised conditions. Copper was selectively accumulated on a HMDE as its 2-mercaptobenzimidazole complex and the stripping step carried out using differential pulse voltammetry [74].

From the brief literature review given above, it is evident that there is an on-going search for even more selective, sensitive and convenient methods for the determination of the toxic heavy metals. While ICP-MS, AAS and NAA provide excellent sensitivity over a wide range of elements, stripping voltammetry exhibits equal if not better sensitivity for many elements and the possibility of measuring a

wide range of metals using instrumentation that costs a fraction of the above techniques. Although the toxic mercury film and hanging mercury drop electrodes continue to be used by many laboratories, their use in others is extremely limited or even prohibited. The recent introduction of the bismuth film electrode has opened new possibilities for stripping detection of heavy metals in anodic stripping and cathodic adsorptive stripping voltammetric modes. The reader is referred to Sections 2.5 and 3.3.2 for a description of the bismuth film electrode and its applications.

3.4 Adsorptive Stripping Voltammetry and Potentiometric Stripping Analysis of Trace Cobalt and Nickel in Some Low-Volume Body Fluids

3.4.1 Experimental

3.4.1.1 Apparatus

Voltammetric (cyclic: CV, linear sweep: LSV, differential pulse: DPV, square wave: SWV, and sampled DC: SDC) and potentiometric stripping analysis (PSA) measurements were performed using a modular electrochemical system (Autolab, Eco Chemie, The Netherlands), equipped with a potentiostat PSTAT10 and driven by GPES 4.8 software (Eco Chemie). For all voltammetric and potentiometric experiments, a bare or (mercury or bismuth coated) glassy-carbon disk (2 mm in diameter) served as the working electrode, with an Ag/AgCl(satd. KCl) and a platinum coil acting as the reference and auxiliary electrodes, respectively. All measurements were performed in a 20 mL or 5 mL electrochemical cell, which was placed in a laboratory-made Faraday cage. All experiments were performed at room temperature (23 ± 2 °C). Measurements were carried out in non-deaerated solutions. All potentials in this work are referred to Ag/AgCl(satd. KCl) as reference.

3.4.1.2 Reagents and Solutions

The bismuth(III), cobalt(II) and nickel(II) stock solutions (1000 mg/L in 5 wt.% HNO_3), ammonia solution (25%), ammonium chloride, and dimethylglyoxime were

supplied by Merck (Darmstadt, Germany), while sodium acetate and acetic acid were supplied by Kemika (Zagreb, Croatia). Lactic acid sodium salt was obtained from Fluka (Switzerland). All chemicals employed in this work were of analytical grade purity and used as received. Water used to prepare all solutions throughout the work was first deionised and then further purified via a Milli-Q unit (Millipore, Bedford, USA). Acetate buffer solution (0.1 mol/L, pH 4.5) was prepared by mixing appropriate amounts of acetic acid and sodium acetate, while ammonia buffer solution (0.01 mol/L, pH 9.2) was made using ammonia solution (25%) and ammonium acetate. DMG was made 0.01 mol/L in 95% ethanol. Synthetic sweat adjusted to a pH of 6.5 with 25 % ammonia solution, was prepared with 0.5 % NaCl, 0.1 % lactic acid sodium salt and 0.1 % urea [75]. Artificial saliva (pH 6.7) was prepared using 5.3×10^{-5} mol/L KSCN, 1.5×10^{-2} mol/L $NaHCO_3$, 2×10^{-2} mol/L KCl, 1.4×10^{-3} mol/L NaH_2PO_4 and 1×10^{-2} mol/L lactic acid sodium salt [76]. Nickel was extracted from soil using doubly distilled water and acidified to pH 2 with nitric acid. The heavy metals (in Section 3.7) were extracted from the soil samples using 0.1 mol/L HNO_3 using the "end-over-end" shaking extraction technique. If required, working solutions were adjusted to alkaline pH with 25 % ammonia solution.

3.4.1.3 Preparation of GCE, MFE and BiFE

Before use, the glassy carbon electrode (GCE), which served as either the working or the supporting electrode for all experiments, was thoroughly polished with 0.05 μm alumina powder on a polishing pad. The electrode was then rinsed thoroughly with Milli-Q water and placed in a sonicator for two minutes. It was then ready to use. For preparation of the BiFE, the electrode was placed in 0.1 mol/L acetate buffer, pH 4.5 containing 100 mg/L Bi(III) ions, whereupon a potential of –1.0 V was applied for 5 minutes under stirring conditions. After modification and rinsing in water, the electrode was ready to use. The mercury film electrode was prepared in a similar manner. The polished glassy carbon substrate electrode was placed in a 0.1 M HCl solution containing 100 mg/L Hg(II) ions and a potential of –0.6 V applied for 8 minutes, according to a previously reported procedure [66].

3.4.1.4 Procedures

All potentiometric and voltammetric measurements were carried out in 0.01 mol/L ammonia buffer solution, pH 9.2, containing either 1 x 10^{-5} or 5 x 10^{-5} mol/L dimethylglyoxime as complexing agent, unless otherwise stated. A deposition potential of –0.7 V was applied in all measurements, unless otherwise stated. During the deposition step, the solution was stirred and following 15 s equilibration time, the voltammogram or potentiogram were recorded by applying a negative-going potential scan or a reductive constant current, respectively. Where different stripping modes or conditions were employed, the appropriate conditions will be provided in the text.

3.5 Results and Discussion

3.5.1 Comparison of BiFE with GCE and MFE for Cobalt

Figure 3.3 compares the adsorptive stripping voltammetric responses of the bare glassy carbon, mercury film and bismuth film electrodes to 20 μg/L cobalt following 90 s accumulation from non-deaerated solutions. The corresponding data are shown in Table 3.2. As expected, no response was observed at the bare glassy carbon electrode. The process at approximately –0.8 V in both the blank and sample solutions was attributed to oxygen reduction. Hydrogen evolution was observed at potentials above approximately –1 V, as expected at the bare glassy carbon electrode. The response at the mercury film electrode is characterised by a typically high contribution from oxygen, occurring at –1 V and –0.9 V in the blank and sample solutions, respectively. For this reason, it is necessary to carry out deoxygenation of all solutions when employing such electrodes, and also to maintain a blanket of nitrogen or argon over the working solution during measurements. In stark contrast, the bismuth film electrode displays a well-defined and sharp stripping peak, even in oxygen-containing solution. This is possibly attributed to slower reaction kinetics for oxygen reduction at the BiFE. In addition, it is also of interest to note the similar behaviour of both the BiFE and MFE regarding the commencement of hydrogen reduction at approximately –1.2 V. Overall, Figure 3.3 and Table 3.2 indicate that the adsorptive stripping behaviour of the bismuth film electrode for determination of cobalt compares favourably with and even surpasses that of the mercury film

electrode. The signal at the BiFE is almost twice as high as that at the MFE, while the BiFE isn't susceptible to oxygen interference.

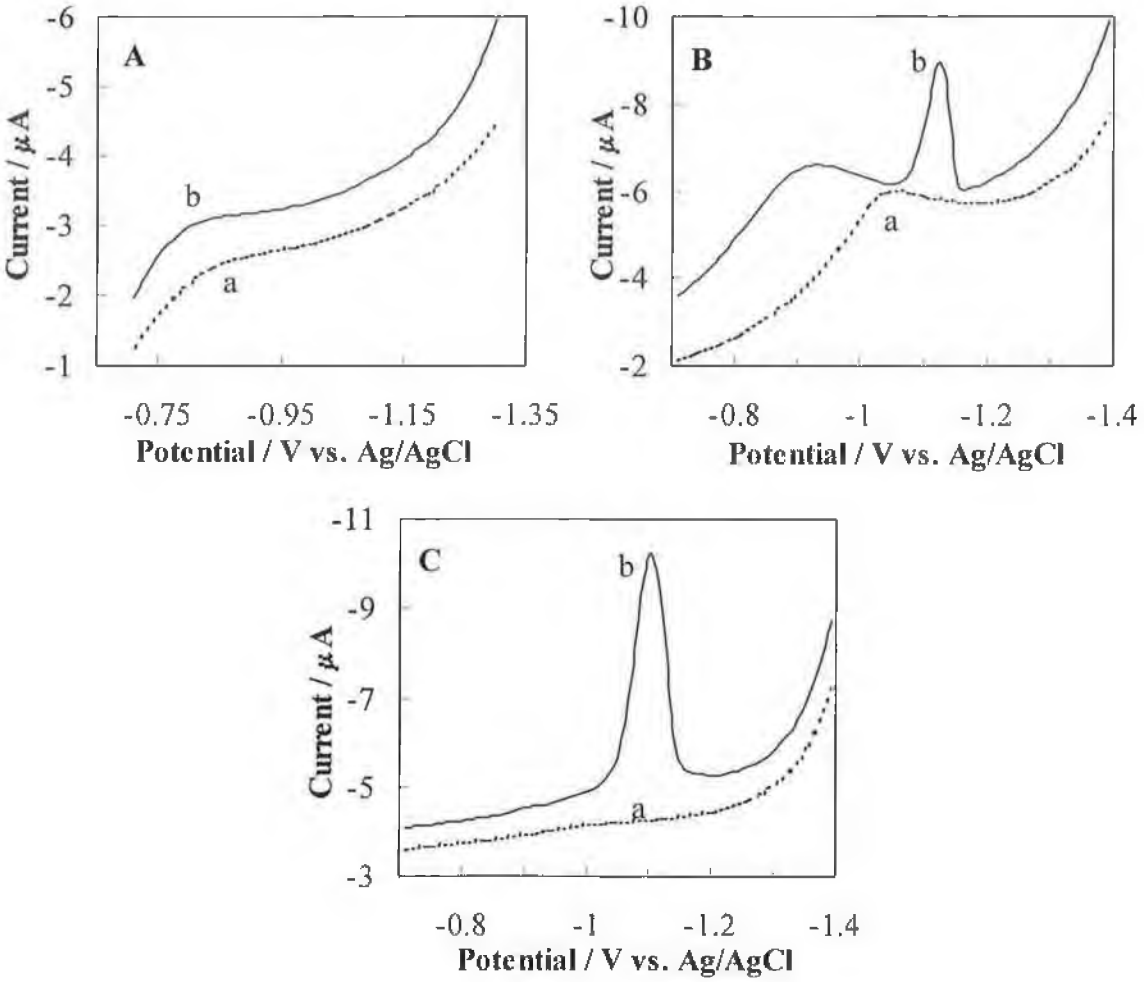

Figure 3.3: Linear sweep voltammograms obtained at the bare GCE (A), MFE (B) and BiFE (C); solutions: (a) blank solution of 0.01 mol/L ammonia buffer (pH 9.2) containing 1 x 10^{-5} mol/L DMG, and (b) a + 20 µg/L cobalt; accumulation conditions: -0.7 V for 90 s; scan rate: 50 mV/s; initial and final potential: –0.7 V and –1.4 V (–1.3 V for A).

Electrode Surface	*Peak Potential / V*	*Peak Current / μA*	$W_{1/2}$ / *mV*
BiFE	-1.123	5.21	50
MFE	-1.103	2.88	40

Table 3.2: Comparison of BiFE and MFE for measurement of 20 μg/L cobalt. Conditions as in Figure 3.3.

3.5.2 Comparison of BiFE with MFE for Cobalt and Nickel

As the bismuth film was proven to be suitable for trace cobalt (above) and nickel detection [66], it was decided to investigate their simultaneous measurement at the bismuth film electrode. The results of this experiment are displayed in Figure 3.4, which compares the response of the bare glassy carbon, mercury film and bismuth film electrodes to a solution containing 20 μg/L each of cobalt and nickel. Again, as expected, the response of the GC electrode was poor, although a small peak, possibly attributable to nickel, was observed at approximately –1.1 V. Similar to the above results regarding the adsorptive stripping measurement of cobalt, both the MFE and BiFE display well-defined and well-separated stripping peaks for both cobalt and nickel (ΔE_p = 91 mV for both). The MFE again showed typical interference from oxygen present in the measurement solution. In contrast the background at the BiFE is almost flat.

The behaviour of the bismuth film electrode and mercury film electrode regarding the individual elements in the sample is considerably different. At the BiFE, the peak currents for both cobalt and nickel are quite similar in magnitude. At the MFE, the signal for nickel is over 2-fold higher than that of cobalt. Similar behaviour has been reported in previous studies [59 and reference therein]. It was shown that upon increasing the DMG concentration from 2.5 x 10^{-5} mol/L to 10^{-3} mol/L, the cobalt peak increased while the peak for nickel reached a maximum at approximately 10^{-4} mol/L. This behaviour is probably due to more favourable formation of the nickel-DMG complex and hence its greater adsorption on the mercury surface. Increasing the concentration of dimethylglyoxime appears to result in more favourable complexation / adsorption for cobalt. Regarding the results featured here, it is expected that the nickel and cobalt peaks would be more similar in magnitude to each other at higher DMG concentrations. Adsorption of both

complexes on the surface of the BiFE appears to be equally favourable, as evidenced by the similarity in the peaks. This feature suggests a possible advantage over the MFE as regards the measurement of each heavy metal in the presence of an excess of the other. Table 3.3 shows the results obtained for the MFE and BiFE.

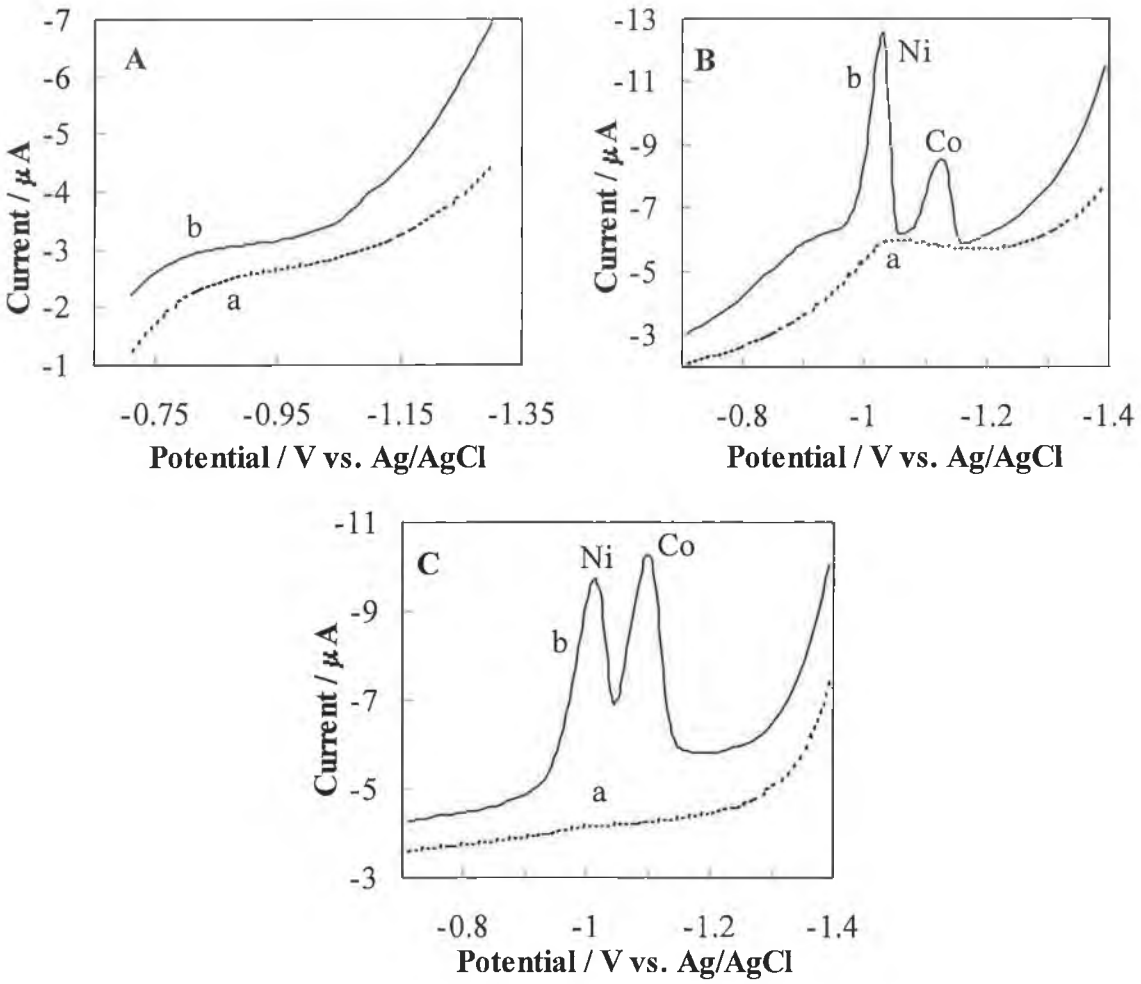

Figure 3.4: Linear sweep voltammograms obtained at the bare GCE (A), MFE (B) and BiFE (C); solutions: (a) blank solution of 0.01 mol/L ammonia buffer (pH 9.2) containing 1 x 10^{-5} mol/L DMG, and (b) a + 20 μg/L cobalt and 20 μg/L nickel; other conditions as in Figure 3.3.

Electrode Surface	*Peak Potential / V*	*Peak Current / μA*	$W_{1/2}$ / *mV*
BiFE: ***Ni / Co***	-1.012 / -1.103	3.40 / 3.69	50 / 50
MFE: ***Ni / Co***	-1.032 / -1.123	6.20 / 2.55	40 / 40

Table 3.3: Comparison of BiFE and MFE for measurement of 20 μg/L cobalt. Conditions as in Figure 3.4.

3.5.3 Optimisation of the Bismuth Film Electrode

Following establishment of the suitability of the BiFE for the measurement of trace amounts of cobalt and nickel, some important experimental parameters were optimised. The procedure for trace measurement of cobalt and nickel was modelled on that of Wang *et al.* [66]. Here, the bismuth film deposition conditions were application of a potential of –1.0 V for 8 minutes using a plating solution composed of 100 mg/L Bi(III) ions in 0.1 mol/L acetate buffer, pH 4.5. While this provided a suitable film for determination of nickel, it was decided to investigate whether application of a different film would provide more optimal conditions for trace measurement of cobalt. As 0.1 mol/L acetate buffer was previously found to be optimum for *in situ* deposition of the bismuth film electrode [50], it was decided to investigate the effect of bismuth deposition time on the response for cobalt.

The bismuth film was deposited from 100 mg/L Bi(III) in 0.1 mol/L acetate buffer pH 4.5 for 1, 3, 5, 7 and 10 minutes. Cobalt was added in μg/L quantities to a working solution of 0.01 mol/L ammonia buffer containing 1 x 10^{-3} mol/L DMG, and the slope from the resulting graph used to determine the optimum plating time. The correlation coefficients (r) in each case were greater than 0.992. In addition, the signal for 20 μg/L cobalt was plotted against the deposition time to obtain further information about the optimum plating time. Figure 3.5 (A and B) shows the results obtained in this optimisation procedure. From these results it can be clearly seen that 5 minutes deposition time provides the optimum response for measurement of trace cobalt. From Figure 3.5 A, it is evident that 1 and 3 minutes deposition time do not provide an adequate amount of bismuth for adsorptive accumulation of the cobalt-dimethylglyoxime complex, as the slopes of the response are low (0.14 μA·L/μg and 0.19 μA·L/μg, respectively). Use of 5 minutes as the deposition time provided the optimum response, with the highest slope being attained (0.83 μA·L/μg). Although

the signals were still quite high, a decrease in current response for cobalt was observed at longer deposition times of 7 and 10 minutes (slope = 0.68 μA·L/μg for each time). This could possibly be attributed to the formation of a "too thick" bismuth film with lower conductivity, thus resulting in slightly lower current signals. Again, from Figure 3.5 B, it is evident that 5 minutes of bismuth film deposition provided the optimum conditions for trace cobalt measurement as the current vs. deposition time curve is observed to increase substantially up to 5 minutes and to decrease after this time. Hence, in all further measurements, a bismuth deposition time of 5 minutes was employed.

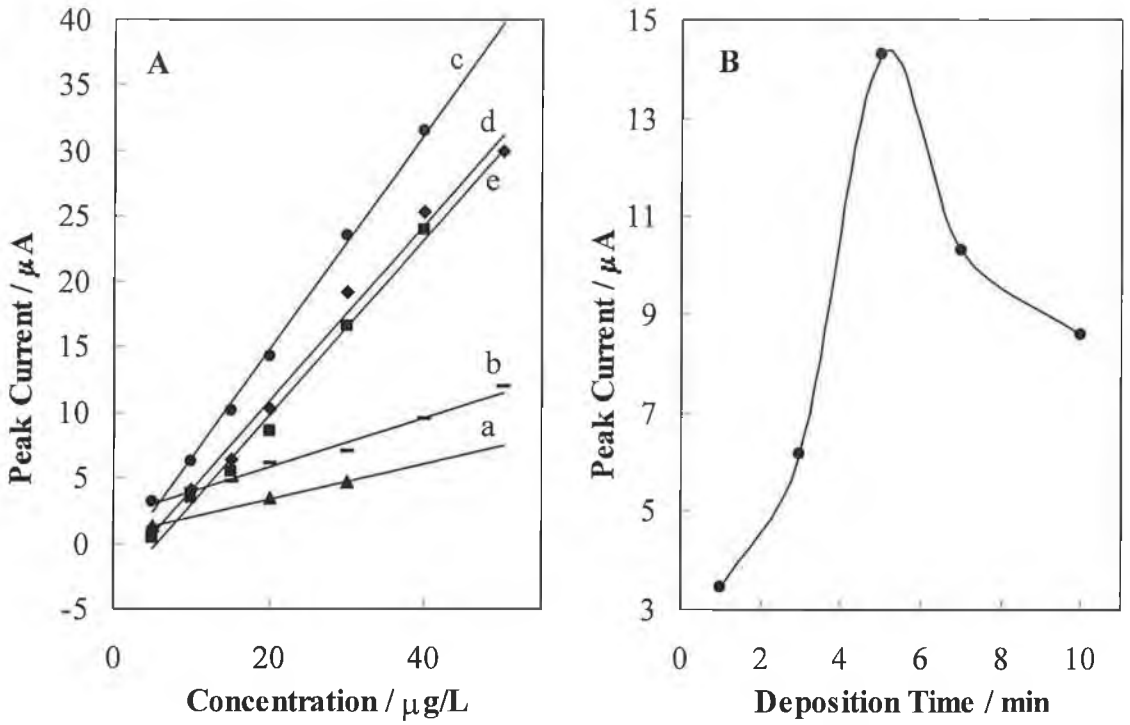

Figure 3.5: (A) Effect of bismuth film deposition times of 1 (a), 3 (b), 5 (c), 7 (d) and 10 (e) minutes upon the adsorptive stripping voltammetric response of increasing additions of cobalt and (B) Effect of bismuth deposition time on the adsorptive stripping voltammetric response of 20 μg/L cobalt; solutions: 0.01 mol/L ammonia buffer (pH 9.2) containing 1 x 10^{-3} mol/L DMG; accumulation conditions: –0.7 V for 60 s.

3.5.4 Optimisation of Parameters for Trace Measurement of Cobalt

The conditions for determining cobalt (and nickel) as its DMG complex on mercury electrodes by adsorptive stripping analysis have been optimised previously. Although

the BiFE has shown consistently to be similar in behaviour to these mercury electrodes, it was necessary to optimise the same conditions, as the BiFE is still a relatively new and incompletely investigated electrode surface. Hence, some optimisation procedures were carried out in this work. The determination of cobalt by CAdSV of its DMG complex is threatened by interferences unless the solution pH is properly adjusted. A pH 9.2 ammonia-ammonium chloride medium has been shown to be the best choice when employing mercury electrodes [59]. It has also been shown to be suitable when employing CAdSV at the bismuth film electrode [66]. The appropriate choice of ammonia buffer concentration is a critical point in determinations (especially simultaneous) of cobalt and nickel by adsorptive stripping, since it affects peak resolution, and moreover its contamination by nickel is in most cases the major source of a nickel blank signal [59]. This last fact makes it desirable to operate with a minimum buffer concentration, but it cannot be decreased to a point where pH control of the solution becomes impossible during the experiment. In other works, at both MFE and BiFE, the appropriate buffer concentration was 0.01 mol/L [59,66]. Hence, it was decided to employ the same buffer composition and pH in these measurements.

The influence of DMG concentration was checked in the range 1 x 10^{-5} mol/L to 1.4 x 10^{-3} mol/L on a sample containing 35 μg/L cobalt in 0.01 mol/L ammonia buffer solution pH 9.2. As shown in Figure 3.6, the peak height of the cobalt signal increases considerably with increasing DMG concentration, reflecting the efficiency of the complexation / adsorption process. The increase of the cobalt peak height with increasing concentrations of DMG is consistent with previous results [59]. The current increases almost linearly from 1 – 10 x 10^{-5} mol/L, with the increase slowing at higher concentrations. Above a DMG concentration of 1 x 10^{-3} mol/L, the current response of cobalt was observed to plateau. This is probably due to saturation of the electrode surface with the cobalt-DMG complex. The cobalt peak width was also observed to increase upon increasing the concentration of DMG, for example from 50 mV at 1 x 10^{-5} mol/L to 80 mV at 1 x 10^{-3} mol/L. This increase in peak width is indicative of some change in the reversibility of the reaction, possibly due to the increased time required for stripping of the cobalt-DMG complex from the electrode surface.

From Figure 3.6, it is evident that at high ratios of DMG to cobalt a large signal is obtained for cobalt. However, it was deemed impractical to employ such high concentrations of DMG as it was difficult to polish the glassy carbon substrate electrode following such measurements. Also, lower concentrations still provided excellent current signals. Hence, in subsequent measurements, a DMG concentration of 1 x 10^{-5} or 5 x 10^{-5} mol/L was employed.

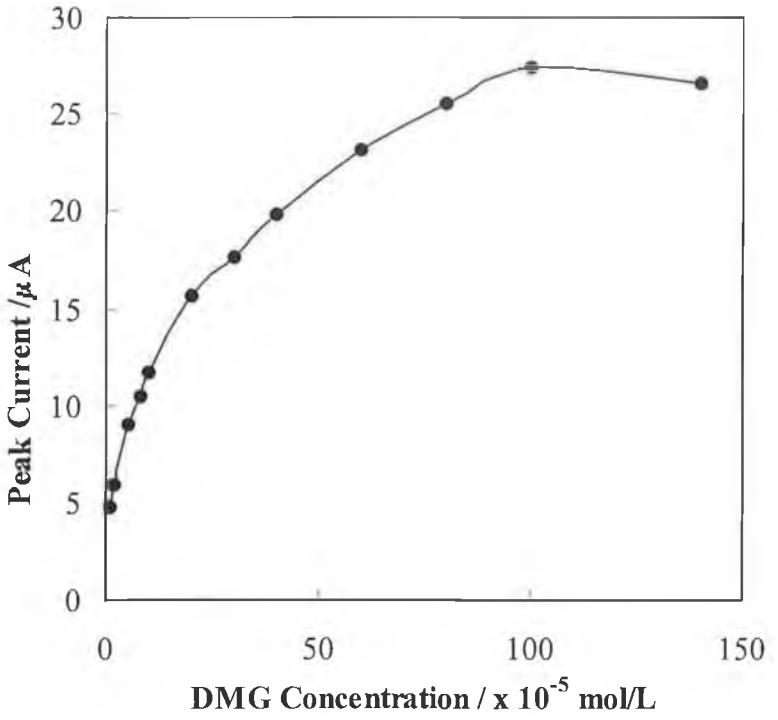

Figure 3.6: Influence of DMG concentration on the adsorptive stripping voltammetric response of 35 μg/L cobalt in 0.01 mol/L ammonia buffer (pH 9.2); accumulation conditions: –0.7 V for 60 s.

Subsequently, some important operating parameters were investigated. The first of these was the effect of the deposition potential on the adsorption of the cobalt-dimethylglyoxime complex. The results of this investigation are shown in Figure 3.7. The deposition potential was varied from –0.4 V to –0.9 V in 0.1 V increments in a solution containing 20 μg/L cobalt. The adsorption of the Co-DMG complex increased rapidly as the potential was increased from –0.4 to –0.6 V, and more slowly from –0.6 V to –0.9 V. Cobalt-DMG has been reported to adsorb on the surface of a mercury film electrode as a positively charged species [58]. As a result, the

adsorption of the Co-DMG is more favoured at more negative potentials. Considering the similarity in behaviour here, it is assumed that the Co-DMG complex is also adsorbed as a positively charged species at the BiFE. In further measurements, a deposition potential of -0.7 V was employed. This is also in agreement with other previously reported studies [58,66].

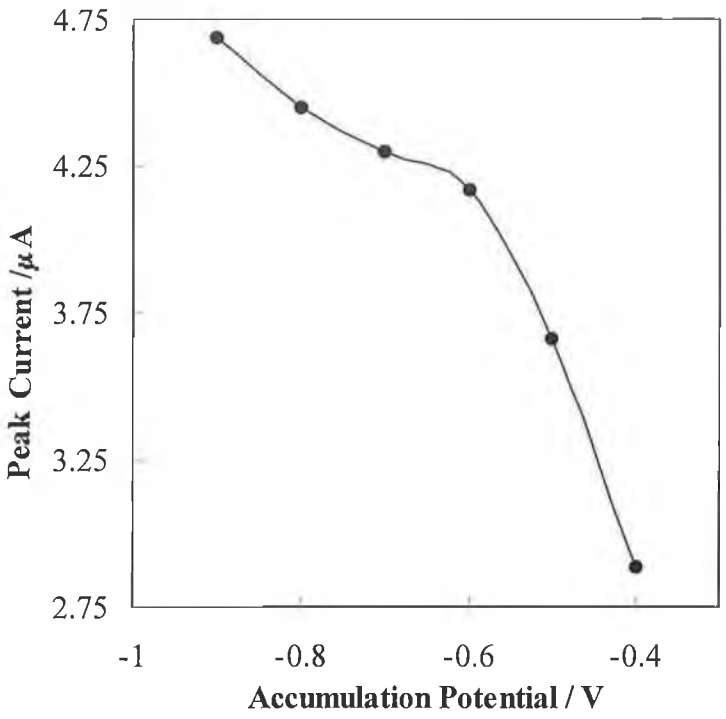

Figure 3.7: Influence of the adsorption potential on the peak current of 20 μg/L cobalt in 0.01 mol/L ammonia buffer (pH 9.2) containing 1 x 10^{-5} mol/L DMG; accumulation time: 60 s.

The next experimental parameter to be investigated was the accumulation time. The effect of increasing the accumulation time from 0 to 120 s on the signal for 10 μg/L cobalt is shown in Figure 3.8. As expected for adsorptive stripping experiments, the response of the bismuth film electrode increases rapidly with the accumulation time. The response of a surface-confined species is directly related to its surface concentration, with an adsorption isotherm (commonly that of Langmuir), providing a relationship between the surface and bulk concentrations of the adsorbate. Hence, calibration curves display non-linearity at high concentrations [77]. The behaviour observed when increasing the accumulation time is analogous to this i.e. non-linearity is observed at higher accumulation times. This is evident in Figure 3.8

in which a linear increase of signal is observed between 0 and 60 s (straight line with r = 0.999). However, between 60 s and 120 s, the signal is observed to level off, due to saturation of the electrode surface. In subsequent experiments, the accumulation time was varied in accordance with the concentration of cobalt (or nickel) in the sample, for example, at lower concentrations higher accumulation times were used.

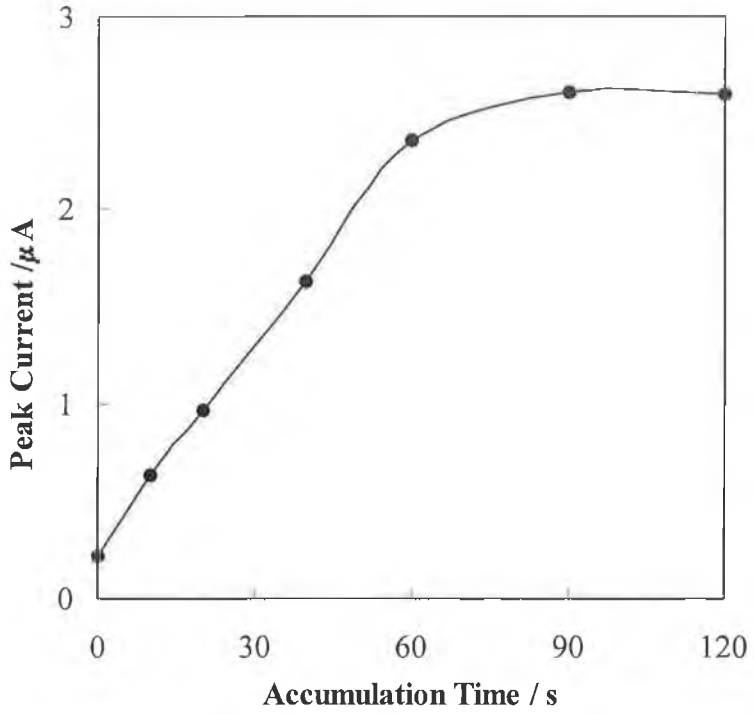

Figure 3.8: Influence of the adsorption time on the peak current of 10 μg/L cobalt in 0.01 mol/L ammonia buffer (pH 9.2) containing 1 x 10^{-5} mol/L DMG; accumulation potential: –0.7 V.

As mentioned in earlier sections, constant current potentiometric stripping analysis was also employed in this study. The most important operating parameter in this method is the stripping current, hence its influence in the range –5 μA to –50 μA on the signal for 5 μg/L cobalt at the bismuth film electrode was investigated. These results are presented in Figure 3.9. From Figure 3.9 A, it is evident that the stripping current exerts a considerable effect on the signal for cobalt, with a stripping current of –5 μA producing by far the highest response for cobalt. Between –5 and –10 μA the response decreased considerably, with a slower increase observed between –10 μA and –30 μA. At stripping currents more negative than –30 μA, the response was very

low. While –5 μA would appear to be the optimum stripping current for all measurements, the use of such a low current increases the measurement time considerably. Hence, for most experiments, a compromise between response and measurement time was reached by employing a stripping current of –10 μA. Only in those instances where the concentrations measured were extremely low (< 1 μg/L), was a stripping current of –5 μA applied. Figure 3.9 B shows the stripping potentiograms obtained with stripping currents of –5 μA and –10 μA. The peaks are well-defined and as with voltammetric measurements, characterised by a low background current contribution.

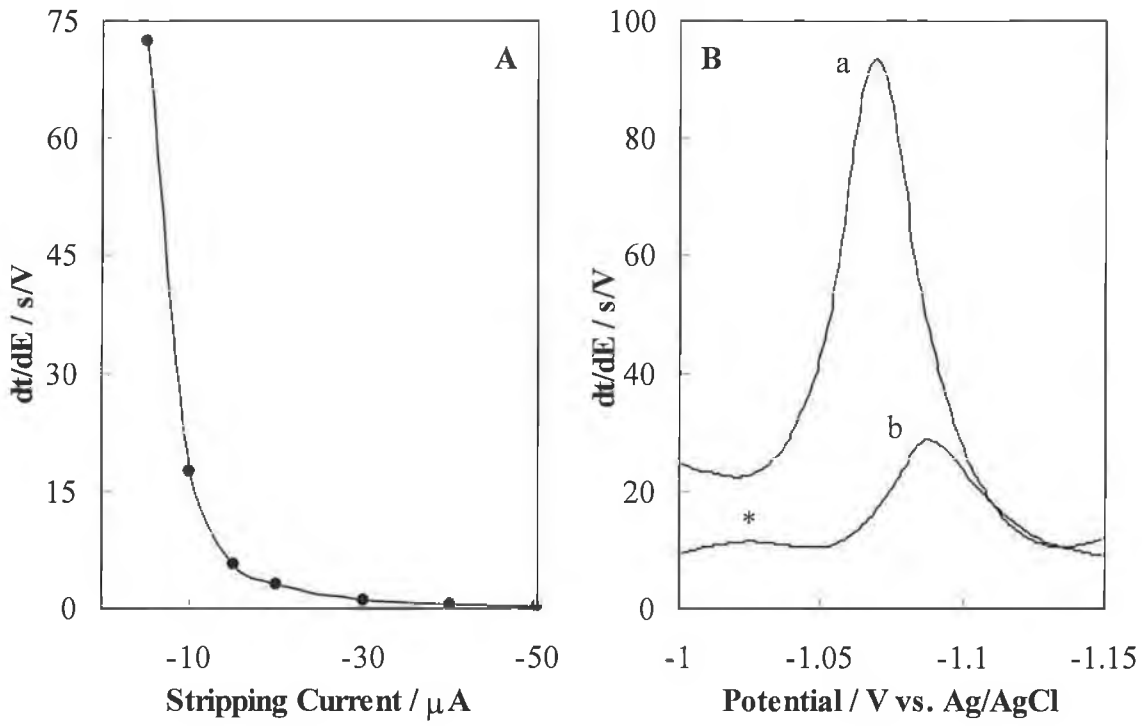

*Figure 3.9: (A) Influence of stripping current on response of 5 μg/L cobalt in 0.01 mol/L ammonia buffer (pH 9.2) containing 1 x 10^{-5} mol/L DMG; accumulation conditions: –0.7 V for 60 s and (B) Stripping potentiograms of 5 μg/L cobalt at (a) –5 and (b) –10 μA; conditions as in A. * Possible nickel impurity peak.*

3.5.5 Investigation of Processes of Co and Co + Ni at BiFE

Cyclic voltammetry was employed to provide further insights into the interfacial and redox processes of the Co-DMG and Ni-DMG chelates at the bismuth film electrode. Figure 3.10 displays repetitive cyclic voltammograms for 20 μg/L cobalt recorded

without (A) and with (B) 60 s accumulation at –0.7 V. In both cases, a well-defined cathodic peak due to the reduction of the chelate was observed in the first scan. No oxidation peaks were observed upon scanning in the anodic direction. The reduction peak following the accumulation was approximately 5-fold larger than that with no accumulation step. Subsequent scans exhibited considerably smaller cathodic peaks, reflecting the desorption of the chelate. Similar behaviour was observed for the simultaneous measurement of cobalt and nickel at the BiFE, with an increase in the cathodic peaks of 8 and 4 times for cobalt and nickel, respectively, following 60 s accumulation at –0.7 V. This is shown in Figure 3.11.

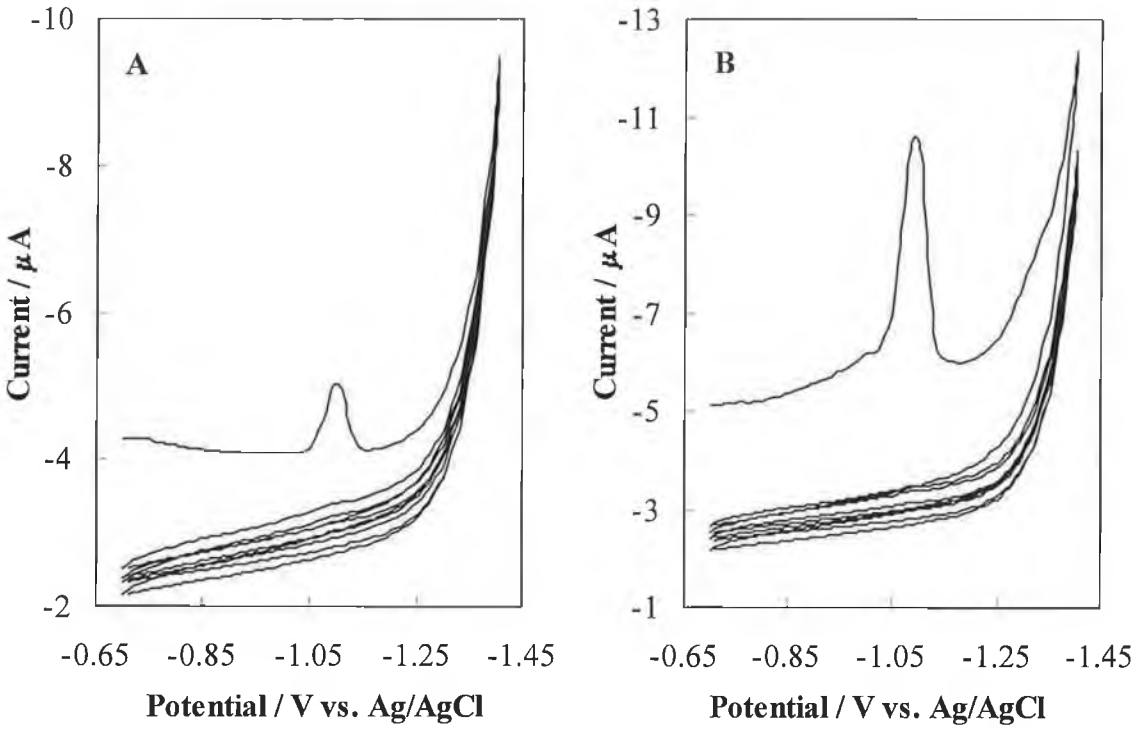

Figure 3.10: Repetitive cyclic voltammograms of the Co-DMG complex at the BiFE for 20 μg/L cobalt with (A) 0 s and (B) 60 s accumulation. Other conditions as in Figure 3.3.

Further proof that the process occurring involving Co-DMG displays irreversible behaviour is provided in Figure 3.12. In potentiometric stripping analysis, the influence of stripping current upon the peak potential was also examined. This is illustrated in Figure 3.12, in which peak potentials are plotted against the applied stripping current. It can be clearly seen that increasing the magnitude of the stripping

current from –5 μA to –50 μA causes a gradual shift of the peak potentials in the negative direction from –1.06 V to –1.19 V. This behaviour suggests the irreversible nature of the reduction of the cobalt-DMG complex [78].

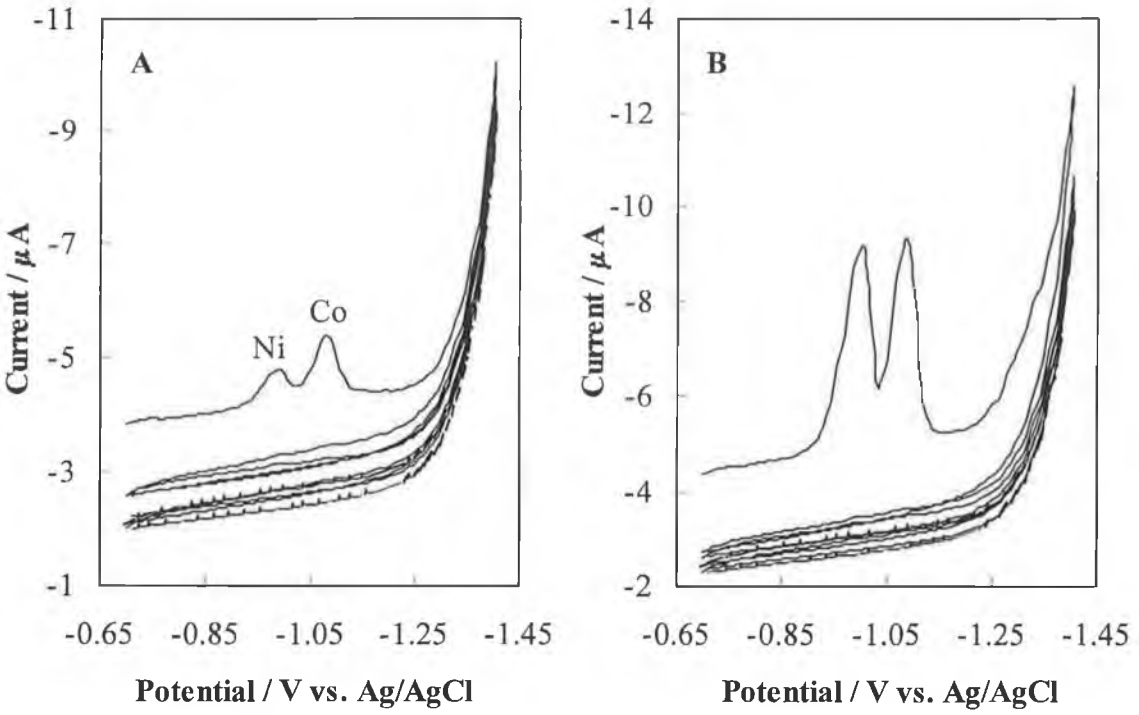

Figure 3.11: Repetitive CVs of the Co-DMG complex at the BiFE for 20 μg/L Co and Ni with (A) 0 s and (B) 60 s accumulation. Other conditions as in Figure 3.4.

Some further insights into the redox process of the cobalt-DMG complex occurring at the bismuth film electrode were obtained by observing the change in current signal upon altering the scan rate. Figure 3.13 illustrates the results of these measurements. As expected, upon increasing the scan rate in linear sweep voltammetry, a corresponding increase in the peak current for cobalt was observed. When this increase was plotted as a function of the square root of the scan rate, a linear relationship was obtained ($r = 0.999$). This indicates that while the accumulation process is governed by adsorption processes, the stripping process involves diffusion.

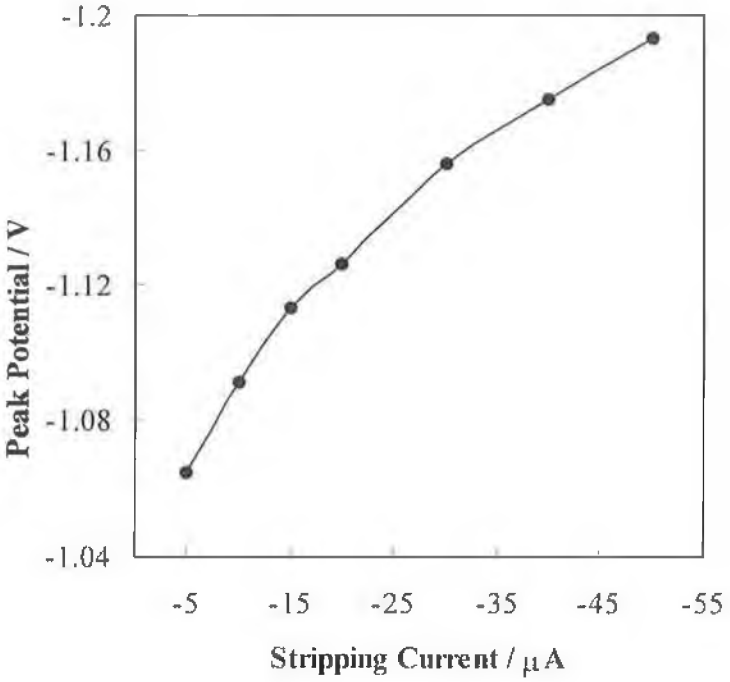

Figure 3.12: Influence of stripping current on response of 5 μg/L cobalt. Conditions as in Figure 3.9.

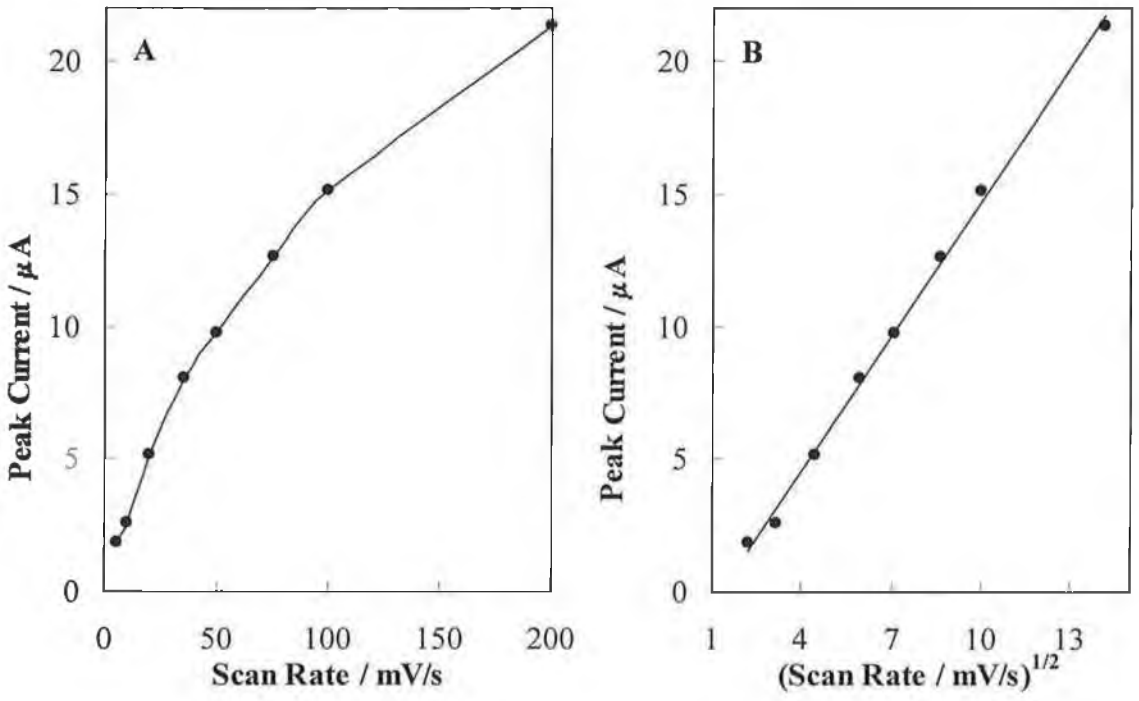

Figure 3.13: (A) Influence of scan rate and (B) influence of square root of scan rate on adsorptive stripping voltammetric response of 15 μg/L cobalt in 0.01 mol/L ammonia buffer containing 5 x 10^{-5} mol/L DMG; accumulation conditions: –0.7 V for 60 s.

3.5.6 Comparison of Stripping Potential Scan Modes for Cobalt Measurement

The adsorptive stripping voltammetric performance of cobalt at the bismuth film electrode was compared by applying five different simple and pulsed potential ramps. The resulting voltammograms are shown in Figure 3.14 and the corresponding data presented in Table 3.4. From this figure one can clearly see that each mode provides a sharp and well-defined peak for cobalt. In contrast to the behaviour observed for anodic stripping voltammetry at the *in situ* prepared BiFE [49], normal pulse voltammetry provided a distinct signal in AdSV. Indeed, the signal for cobalt here was the highest, but was accompanied by a correspondingly high background current contribution, due to its specific excitation mode. The responses in the other modes are very similar (the difference in the current between LSV, SWV, DPV and SDC may be attributed to the higher scan rates – 50 mV/s for the former two and 25 mV/s for the latter two). As found in previous experiments, the background contribution is very low despite the presence of dissolved oxygen. Although each mode was suitable for cobalt measurement, LSV was employed in most of the subsequent experiments.

Technique	*Peak Potential / V*	*Peak Current / μA*	$W_{1/2}$ */ mV*
Linear Sweep Voltammetry	-1.103	-9.78	50
Square-Wave Voltammetry	-1.105	-10.4	63
Normal Pulse Voltammetry	-1.154	-20.0	73
Different. Pulse Voltammetry	-1.071	-4.34	59
Sampled DC Voltammetry	-1.086	-4.02	49

Table 3.4: Data regarding the voltammograms in Figure 3.14. All conditions as in Figure 3.14 (below).

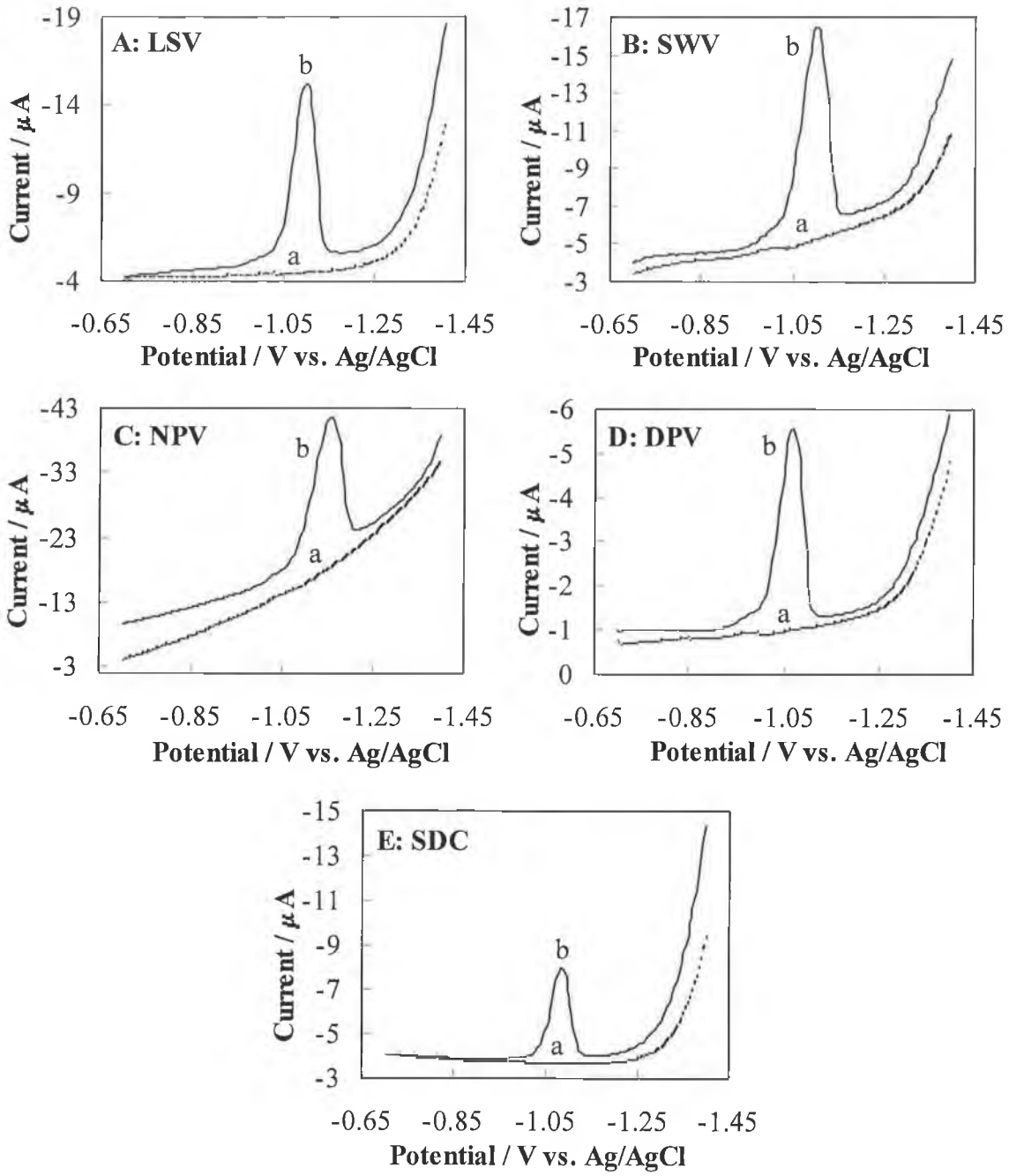

Figure 3.14: Adsorptive stripping voltammograms of (a) 0.01 mol/L ammonia buffer (pH 9.2) containing 5 x 10^{-5} mol/L DMG and (b) a + 15 µg/L Co at BiFE using (A) linear sweep (LSV), (B) square wave (SWV), (C) normal pulse (NPV), (D) differential pulse (DPV) and (E) sampled DC (SDC) potential scans; accumulation conditions: – 0.7 V for 60 s; settings: LSV: scan rate 50 mV/s; SWV: frequency 10 Hz, potential step 5 mV, pulse amplitude 25 mV; NPV and DPV: pulse duration time 60 ms, interval time 0.2 s, potential step 5 mV; SDC: interval time 0.2 s, step potential 5 mV.

3.5.7 Comparison of Stripping Potential Scan Modes for Simultaneous Cobalt and Nickel Measurement

In a similar experiment to that described in the preceding Section, various voltammetric potential scan modes were compared for their behaviour towards a solution containing both cobalt and nickel. In addition, the potentiometric stripping analysis mode was compared to that of voltammetry. The results for this are shown in Figure 3.15 and the corresponding data shown in Table 3.5. While each mode exhibited well-defined and well-separated peaks for cobalt and nickel, amongst the voltammetric methods, LSV yielded slightly better peak resolution than the other modes. However, it was observed that PSA provided the best overall resolution of the cobalt and nickel peaks. SWV provided the optimum current response for both cobalt and nickel. As expected with the BiFE, each voltammogram and the potentiogram exhibited excellent signal to background ratios, even in the presence of dissolved oxygen. Considering the strong signal (dt/dE) for potentiometric stripping analysis and the superior resolution between the cobalt and nickel peaks, the method was employed in certain subsequent measurements.

Technique	*Peak Potential / V*	*ΔE_p / mV*	*Peak Current / μA*
Linear Sweep Voltammetry: Co / Ni	-1.083 / -0.992	91	1.94 / 1.92
Square Wave Voltammetry: Co / Ni	-1.076 / -0.988	88	3.14 / 3.42
Normal Pulse Voltammetry: Co / Ni	-1.110 / -1.022	88	4.24 / 4.17
Differential Pulse Voltammetry: Co / Ni	-1.057 / -0.969	88	1.06 / 1.16
Sampled DC Voltammetry: Co / Ni	-1.071 / -0.983	88	1.18 / 0.98
Potentiometric Stripping Analysis: Co / Ni	-1.071 / -0.985	86	35.58 / 35.38*

*Table 3.5: Data regarding the voltammograms in Figure 3.15. All conditions as in Figure 3.15 (below). * dt/dE / s/V rather than current.*

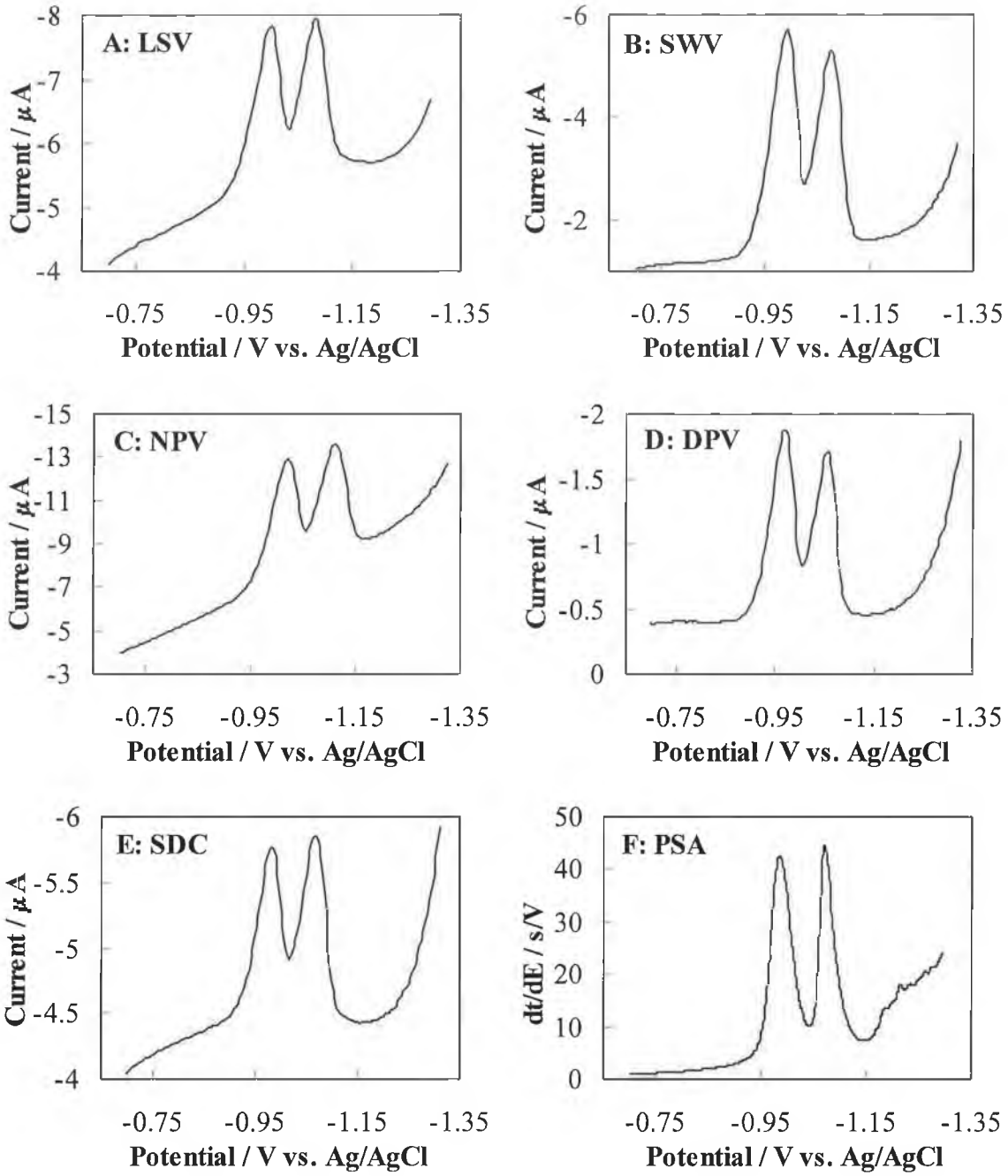

Figure 3.15: Adsorptive stripping voltammograms of 20 µg/L Co + 20 µg/L Ni in 0.01 mol/L ammonia buffer pH 9.4 containing 1 x 10^{-5} mol/L DMG at BiFE using (A) linear sweep (LSV), (B) square wave (SWV), (C) normal pulse (NPV), (D) differential pulse (DPV), (E) sample DC (SDC) and (F) potentiometric stripping analysis (PSA) modes; accumulation conditions: –0.7 V for 60 s; settings: LSV: scan rate 50 mV/s; SWV: frequency 10 Hz, potential step 5 mV, pulse amplitude 25 mV; NPV and DPV: pulse duration time 60 ms, interval time 0.2 s, potential step 5 mV; SDC: interval time 0.2 s, step potential 5 mV; PSA: stripping current –10 µA.

3.5.8 Simultaneous Measurement of Cobalt and Nickel

It is unlikely that cobalt and nickel will appear in any sample in a fixed and constant ratio. Hence, it was decided to investigate the possibility of measuring each heavy metal in an excess of the other. In the first case, cobalt was held at a constant concentration of 2 μg/L, while nickel was added in increments of 2 μg/L, and in the second instance, nickel was held at a constant concentration while increasing amounts of cobalt were added to the working solution. The results of the former are presented in Figure 3.16, and the latter in Figure 3.17. Also included in each figure are the relevant data regarding the respective analyte. Regarding Figure 3.16, in which cobalt is maintained at 2 μg/L and nickel is added from 2 to 10 μg/L, it was evident that the addition of nickel didn't interfere with the cobalt peak as the peak current remained almost constant. In addition, the presence of cobalt in the measuring solution didn't affect the response obtained upon adding nickel as evidenced by the excellent correlation coefficient (r) of 0.999 for the nickel additions. Similarly, addition of increments of cobalt to a solution containing nickel caused no significant influence on the peak height for nickel (Figure 3.17). Also, the correlation coefficient for the cobalt additions was 0.997. In both cases, the peaks remained well-defined and well-resolved, thus demonstrating the excellent performance of the bismuth film electrode in simultaneous measurement of cobalt and nickel.

Considering the superior resolution of cobalt and nickel signals when employing potentiometric stripping analysis (see Section 3.6.7), one of the above experiments, in which linear sweep voltammetry was employed, was repeated. Here, cobalt was held at a constant concentration while successively higher concentrations of nickel were added to the working solution. These results are illustrated in Figure 3.18. Upon comparison of these results, the superiority of the PSA technique in resolution of the peaks is again revealed. The correlation coefficient here is 0.997.

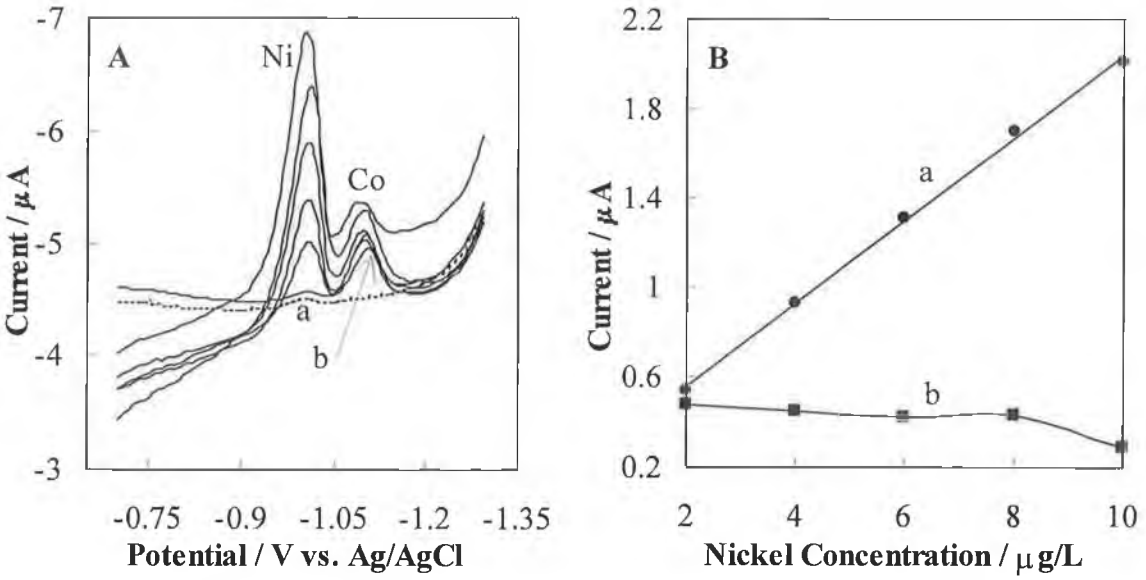

Figure 3.16: (A) Adsorptive stripping voltammograms of (a) 0.01 mol/L ammonia buffer (pH 9.2) containing 1 x 10^{-5} mol/L DMG, (b) a + 2 μg/L cobalt; subsequent scans b + 2 μg/L nickel increments; accumulation conditions: –0.7 V for 60 s; and (B) corresponding data for (A); (a) nickel, (b) cobalt.

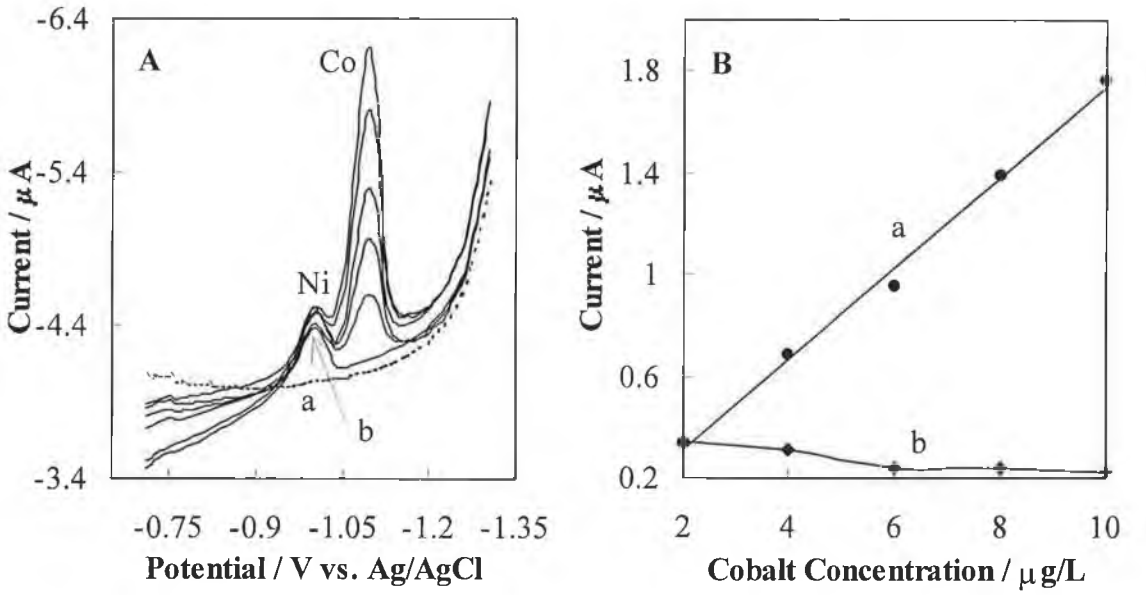

Figure 3.17: (A) Adsorptive stripping voltammograms of (a) 0.01 mol/L ammonia buffer (pH 9.2) containing 1 x 10^{-5} mol/L DMG, (b) a + 2 μg/L nickel; subsequent scans b + 2 μg/L cobalt increments; accumulation conditions: –0.7 V for 60 s; and (B) corresponding data for (A); (a) cobalt, (b) nickel.

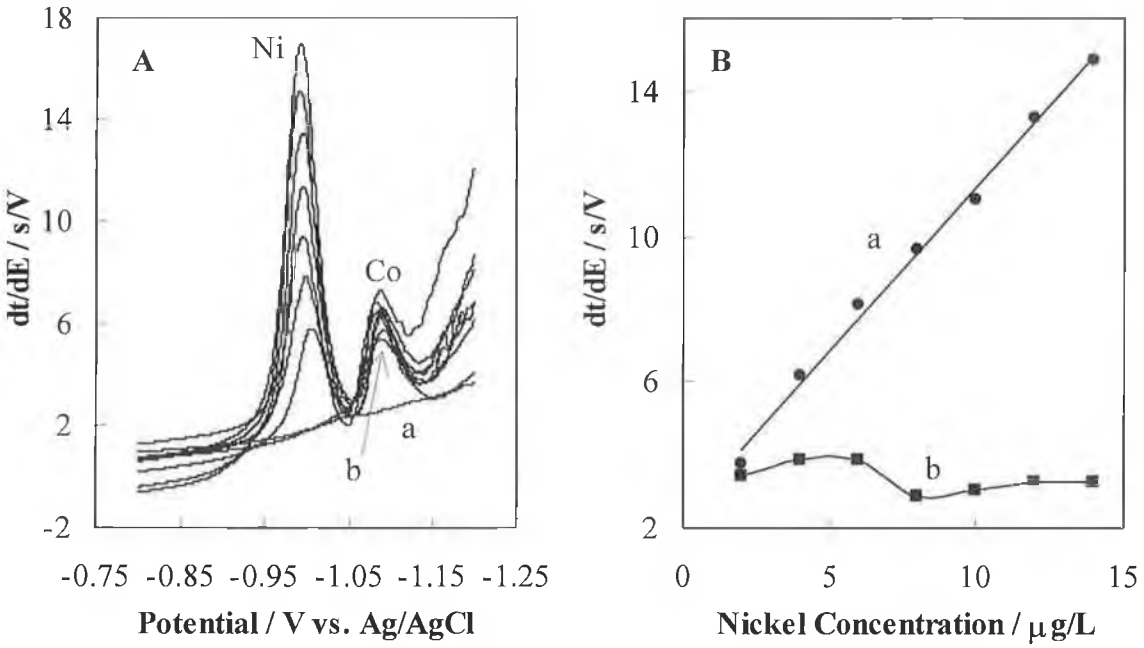

Figure 3.18: (A) Adsorptive stripping potentiograms for 2 µg/L cobalt and increasing concentrations of nickel and (B) corresponding data for (a) nickel and (b) cobalt. All data as in Figure 3.16, except stripping current –10 µA.

3.5.9 Analytical Performance of BiFE for Cobalt and Nickel

As seen from previous results regarding the adsorptive stripping voltammetry and potentiometric stripping analysis of cobalt and nickel, the BiFE exhibits excellent sensitivity and selectivity towards both elements. Further studies were carried out into the analytical performance of the BiFE for determinations of trace amounts of these particular heavy metals. The limit of detection and linear range in such adsorptive stripping measurements is extremely dependent on two parameters, namely the concentration of DMG in the sample solution and the accumulation time. Hence, different calibration curves (and limits of detection) were obtained when varying conditions were employed. Employing LSV, cobalt exhibited a linear dependence on concentration over the range 2-16 µg/L, with a slope of 0.54 µA·L/µg and correlation coefficient (r) of 0.998. Here, the accumulation time was 40 s and the concentration of DMG, 5×10^{-5} mol/L. Above a concentration of 16 µg/L, a typical curvature in the calibration curve was observed due to saturation of the electrode surface. As cobalt is frequently present in sub µg/L levels in samples, the possibility of measuring cobalt at these concentrations was investigated. The results using both LSV and PSA were very promising. Employing a DMG concentration of 5×10^{-5} mol/L and an

accumulation time of 120 s (LSV), there was a linear correlation between cobalt signal over the range 0.1 to 0.8 μg/L, with a slope of 2.17 μA·L/μg and correlation coefficient (r) of 0.999. From these two examples, it is evident that calibration data differ depending on the conditions used. Using potentiometric stripping analysis with a stripping current of –5 μA, a DMG concentration of 1 x 10^{-5} mol/L and an accumulation time of 120 s, the response to cobalt was linear over the range 0.1 to 0.9 μg/L, with a slope of 16.33 s·L/V·μg and a correlation coefficient (r) of 0.997. The potentiograms obtained in these measurements and the resulting data regarding peak magnitude are presented in Figure 3.19. Data were also obtained for the simultaneous calibration of nickel and cobalt using LSV. The linear ranges were both from 1 to 9 μg/L with slopes of 0.12 μA·L/μg and correlation coefficients (r) > 0.996 for each element.

The reproducibility of measurements of both elements at the BiFE was also determined using both linear sweep voltammetry and potentiometric stripping analysis. Employing the former, a relative standard deviation (r.s.d) of 4.2 % was obtained for 12 measurements of 1 μg/L cobalt, while for cobalt and nickel at a concentration of 5 μg/L each in the measuring solution, the r.s.d.s (for 12 measurements) were 7.7 and 4.2 %, respectively. Using PSA, for 10 repeat measurements of a solution containing 2 μg/L of each heavy metal individually, the r.s.d.s were 1.4 % and 4.3 %, respectively. These data signify another advantage of BiFE over MFE regarding the possibility of carrying out many measurements at the same BiFE, obviating the need for a film regeneration step as is required with mercury electrodes [59,60,63].

As noted above, the detection limit varies depending on the applied operational parameters. Using PSA, the detection limits (S/N = 3) for cobalt and nickel were determined to be 0.08 and 0.26 μg/L, respectively, employing a DMG concentration of 1 x 10^{-5} mol/L, an accumulation time of 60 s and a stripping current of –10 μA. The extremely low limits of detection achievable in adsorptive stripping analysis of these elements can be attributed to the fact that the reduction of the metal-DMG complex involves the transfer of 10 electrons [79]. These calibration data reveal the excellent sensitivity of the bismuth film electrode in the adsorptive stripping voltammetry and potentiometric stripping analysis of trace cobalt and nickel,

with the possibility of further reduction of the detection limit for both elements upon varying the appropriate parameters.

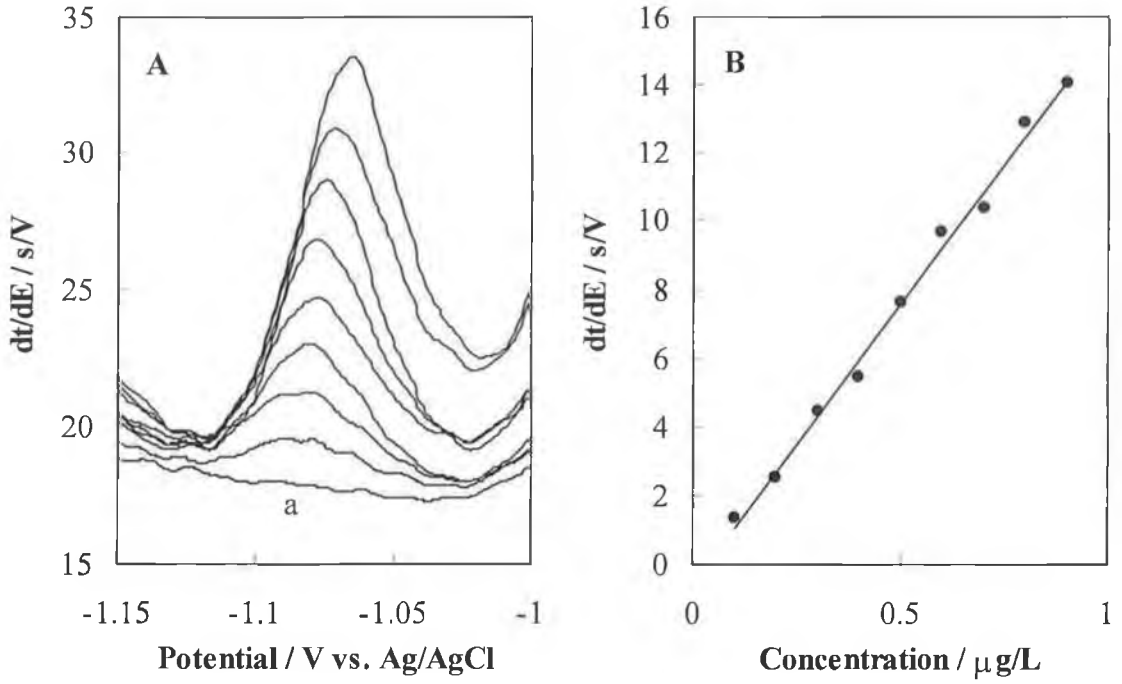

Figure 3.19: (A) Stripping potentiograms obtained upon adding cobalt in 0.1 μg/L increments to (a) 0.01 mol/L ammonia buffer pH 9.2 containing 1 x 10^{-5} mol/L; accumulation conditions:-0.7 V for 120 s; stripping current: -5 μA and (B) resulting data.

3.5.10 Measurement of Trace Cobalt and Nickel in Some Low-Volume Artificial Body Fluids

Following optimisation of the relevant parameters, and investigation of the analytical parameters for trace measurement of cobalt and nickel at the BiFE, both heavy metals were measured in a variety of low-volume body fluid samples. The samples selected were artificial saliva and synthetic sweat.

Cobalt- and nickel-based alloys have been used widely and successfully in dental, orthodontic and orthopaedic materials, although concerns exist regarding the release of metal ions from these alloys to surrounding tissues. Studies have revealed decreases in cellular proliferation and inhibition of various enzymes of cultured cells when exposed to these alloys [80]. Release of potentially toxic metal ions into saliva from amalgam fillings and orthodontic appliances is of considerable concern in

dentistry [81]. Hence, it is of great interest to quantify such releases in the saliva of patients fitted with such dental materials, and also to measure the effect of saliva components upon the release of these elements. Natural saliva is a mixture of fluids secreted by the parotid, submaxillary and sublingual glands that have been shown to differ from each other in composition and volume [82]. Being an extremely complex system with numerous constituents, and variable according to the time of day, exact duplication is impossible. Hence, in many studies, artificial saliva is employed. The release of metal ions from dental amalgam occurs in two stages, *short-time release*, which is the period ranging from a few hours to a few weeks after completion of the dental application, and *long-term release*, which occurs when metals diffuse from the bulk to the surface of the amalgam and oxidise, the oxides gradually dissolving when the saliva pH goes below a certain value [76]. Hence, the metals present in these alloys will be present at varying, but low concentrations. For example, nickel has been found at levels of 0.5 to 2.0 μg/L in saliva using ET-AAS [83], and was released into synthetic saliva in amounts between 0.4 and 4.1 μg/L from nickel-containing orthodontic arch wires [84]. These levels suggest the necessity for extremely sensitive techniques for measurement of nickel in this matrix. Common nickel-chromium-beryllium alloys, which have been used in dental appliances are being replaced by cobalt-chromium alloys [85]. Considering the already described hazards associated with cobalt exposure (Section 3.2), it is apparent that methods are also required for measuring cobalt in saliva.

Adsorptive stripping voltammetry and potentiometric stripping analysis at the bismuth film has proved to be suitable for measurement of trace levels of cobalt and nickel, hence it was decided to investigate the possibility of determining these trace elements in saliva matrix. Figure 3.20 shows adsorptive stripping potentiograms obtained upon adding 1 μg/L amounts of cobalt to an artificial saliva solution. The peak in the blank solution of artificial saliva (pH 9.4) containing 5 x 10^{-5} mol/L DMG is more than likely due to the presence of trace impurity nickel (*) in one or more of the five salts used in making up the artificial saliva solution. Use of suprapure chemicals in more detailed studies should result in a "clean" blank solution. However, despite the presence of nickel in the blank solution, it is evident that adsorptive stripping potentiometric analysis at the BiFE is a potentially suitable method for determination of nickel, as its presence in trace amounts elicits a strong

signal response. Furthermore, a strong response is also obtained upon addition of two 1 μg/L increments of cobalt to the artificial saliva sample.

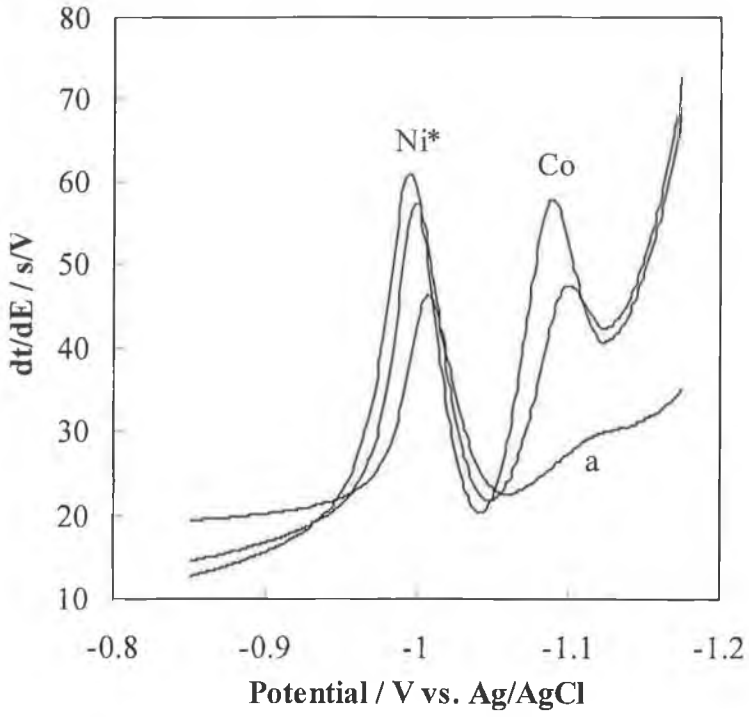

*Figure 3.20: Adsorptive stripping potentiograms of (a) artificial saliva, pH adjusted to 9.4, containing 5 x 10^{-5} mol/l DMG, subsequent potentiograms a + 1 μg/L cobalt each; accumulation conditions: –0.7 V for 90 s; stripping current: -10 μA. * Nickel impurity in the artificial saliva.*

In performing their main function of thermoregulation, the sweat glands excrete a variety of solutes. The results of nutritional balance studies indicate that nutrients are lost in sweat in such amounts that allowances have to be made for such losses in the calculation of daily requirements [25]. It is widely known that skin contact with nickel-containing objects (alloys) causes allergic reactions in sensitised individuals. Sweat is an important parameter in the corrosion of such objects, hence studies are carried out to investigate the effect of sweat on the quantity of nickel liberated from nickel-containing alloys [86]. It is therefore of interest to quantify the amount of nickel and other trace essential elements in this sample matrix. Atomic emission spectrometry and atomic absorption spectrometry have been used for this purpose [25,86], with mean concentrations of nickel found in sweat of 69.9 μg/L [25].

It also seems likely that cobalt will be excreted in the sweat of cobalt-exposed individuals.

In this study, adsorptive stripping voltammetry at the bismuth film electrode was investigated as a possible method for determination of trace levels of cobalt and nickel in sweat. Figures 3.21 and 3.22 show the results of these experiments. In both Figure 3.21 and 3.22, as in Figure 3.20, a nickel impurity peak (*) from one of the components of the artificial sweat matrix is observed in the blank. Again, use of suprapur chemicals should eliminate such an impurity. Figure 3.21 A shows voltammograms obtained upon adding 10 μg/L increments of nickel to an artificial sweat solution (pH 9.4) containing 1 x 10^{-5} mol/L DMG.

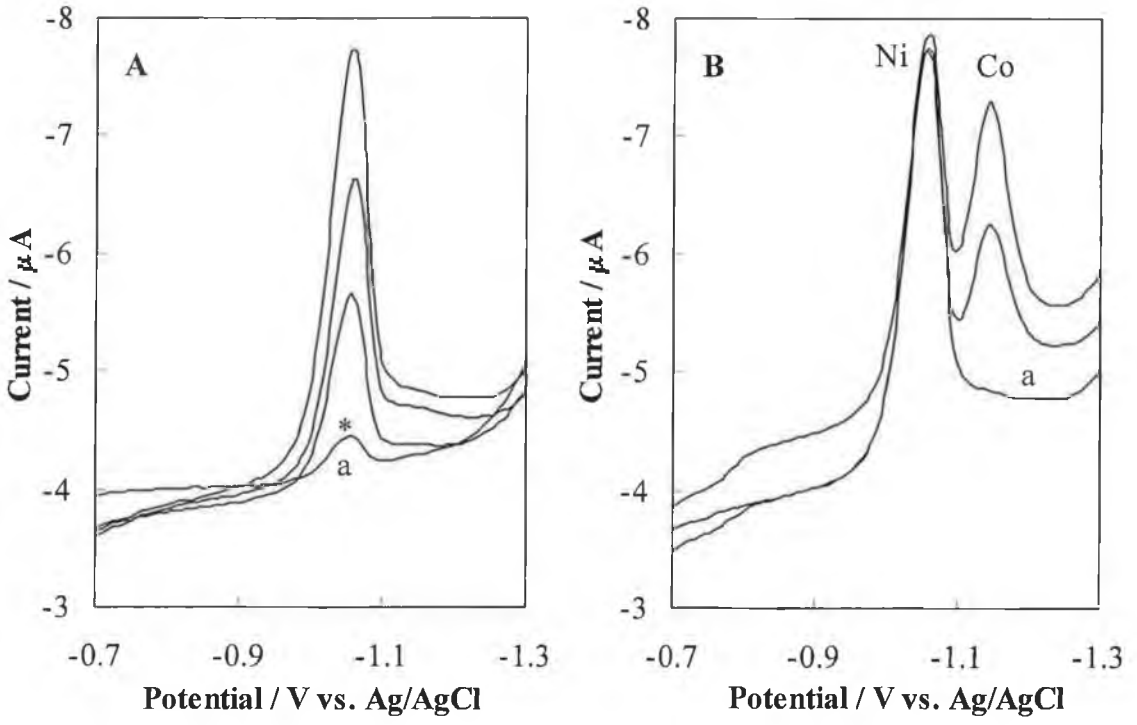

*Figure 3.21: (A) Adsorptive stripping voltammograms of 10 μg/L additions of nickel to (a) synthetic sweat solution, (pH 9.4) containing 1 x 10^{-5} mol/L DMG; and (B) adsorptive stripping voltammograms of 10 μg/L additions of cobalt to (a) synthetic sweat solution, (pH 9.4) containing 1 x 10^{-5} mol/L DMG and 30 μg/L nickel; accumulation conditions: -0.7 V for 30 s. * Nickel impurity in the synthetic sweat.*

Applying an accumulation time of just 30 s, a strong signal response was obtained for nickel. Considering a mean concentration of nickel in sweat of approximately 70 μg/L (according to [25]), routine adsorptive stripping voltammetry detection of nickel at the BiFE seems feasible as the technique is extremely fast and sensitive. Indeed, if the concentration of nickel is as high as 70 μg/L, very short accumulation times could be employed. In addition to these measurements, cobalt was added in increasing increments to a solution containing 30 μg/L of nickel (Figure 3.21 B). Strong stripping peaks were obtained for the cobalt additions. Employing PSA would likely permit improved resolution of the nickel and cobalt peaks. Figure 3.22 (A and B) show "reciprocal" voltammograms to Figure 3.21, whereby cobalt was added to an artificial sweat solution (pH 9.4) containing 1 x 10^{-5} mol/L DMG (A) and nickel was added in 10 μg/L increments to a solution containing 30 μg/L cobalt (B).

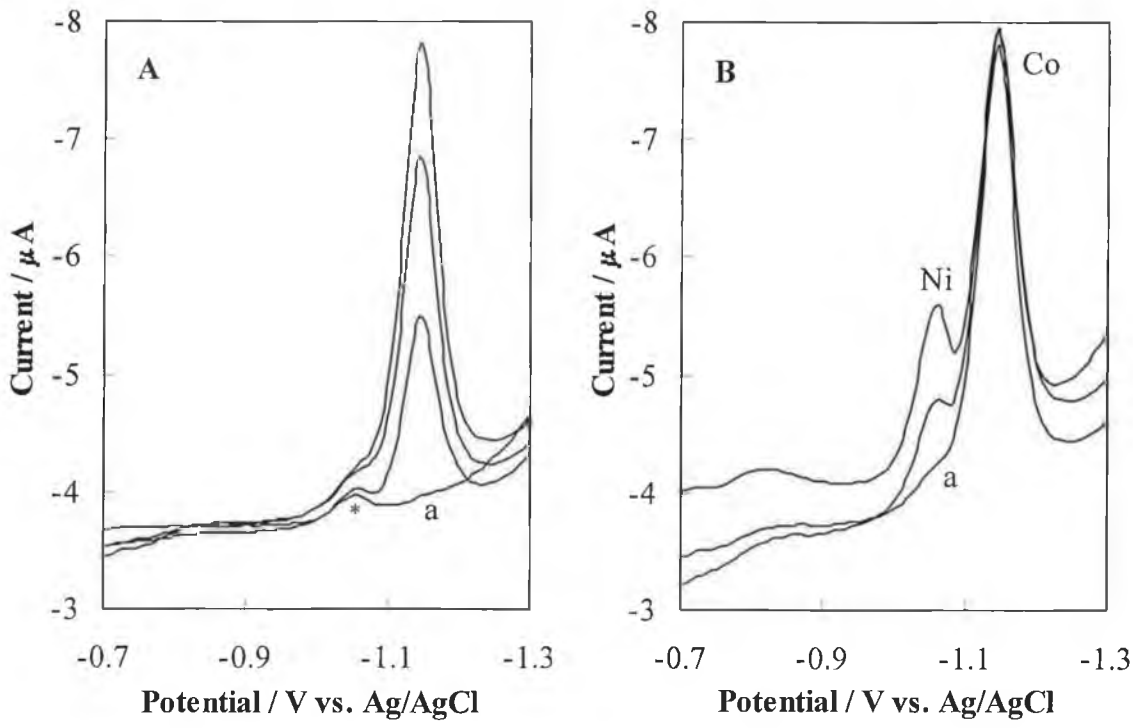

*Figure 3.22: (A) Adsorptive stripping voltammograms of 10 μg/L additions of cobalt to (a) synthetic sweat solution (pH 9.4) containing 1 x 10^{-5} mol/L DMG, (B) adsorptive stripping voltammograms of 10 μg/L additions of nickel to (a) synthetic sweat solution, pH 9.4 containing 1 x 10^{-5} mol/L DMG and 30 μg/L cobalt; accumulation conditions: -0.7 V for 30 s. * Nickel impurity in the synthetic sweat.*

Similar to the behaviour of nickel in Figure 3.21, cobalt exhibits strong stripping peaks in the synthetic sweat matrix. In contrast, however, upon adding nickel to the solution containing 30 μg/L cobalt, the signal for nickel is significantly smaller than that of the cobalt signal. This might be attributable to some interaction of the cobalt-DMG complex and the sweat matrix, causing favourable adsorption of cobalt-DMG over nickel-DMG on the bismuth film electrode. However, it is apparent that adsorptive stripping methodologies at the bismuth film electrode are suitable for trace nickel and cobalt measurements in a sweat matrix, suggesting its possible future use in studies of trace element excretion.

3.6 Application of BiFE in the Determination of Selected Heavy Metals in Soil Extracts

3.6.1 Introduction

The ecotoxicity and mobility of heavy metals in the environment depend strongly on their specific chemical forms or method of binding [87]. Consequently, toxic effects and biogeochemical pathways can only be studied on the basis of the determination of these forms. The determination of heavy metal species is often difficult in soil and sediment matrices. In practice, environmental studies involving soil and sediment analysis are often based on the use of leaching or extraction procedures (e.g. single or sequential extraction schemes), which enable broader forms or phases to be measured (e.g. "bioavailable" forms of elements). In an extraction involving a single extractant, a relative empirical assessment of heavy metal availability for plant uptake from different components of the soil is made [88]. Heavy metals brought into the extract solution are either defined as "plant available" or attributed to a soil phase such as carbonates, which may or may not be available for root uptake. Sequential extraction procedures, in which the sample is subjected to a series of extractions using different extractants, provide insights into the partitioning of trace metals in soils and their phase associations, e.g. exchangeable, bound to carbonates, bound to iron and manganese oxides, bound to organic matter and residual [89].

However, the actual environmental availability is the metal fraction directly accessible by the solution surrounding the soil via various processes, for example,

ion-exchange, complexation, precipitation, dissolution, accumulation, oxidation, reduction etc. [90]. The extractability of a metal is directly related to the partitioning coefficient, K_D, which assumes a proportionality between the metal concentration in solid and the metal concentration in liquid via a linear adsorption isotherm. In work by van Elteren [90], a batch-type experimental approach was employed to derive the environmental availability of trace metals. In order to permit extraction of the environmentally available fraction from a soil sample, a high volume to mass ratio (V/m) of soil to extractant may be required, depending on the K_D. In such a case, the resulting metal concentration may be too low to be detected. To avoid such a problem, the concentration of metal in the extract may be measured as a function of the V/m ratio, and from the resulting relationship, the environmentally available metal concentration in soil be deduced. A brief description of the "model" on which this is based is presented as follows. The adsorption of a metal on a "pure" solid may be modelled with a linear adsorption isotherm:

$$a_1 = K_D \, x \, c_1 \qquad \textbf{(3.2)}$$

where a_1 is the metal concentration in the solid after equilibration (mg/kg), c_1 the metal concentration in the liquid after equilibration (mg/L) and K_D the partitioning coefficient (L/kg) [91]. It seems justified to apply a linear adsorption isotherm to describe the sorption of exchangeable metals on soils and sediments. It should be noted that the K_D value is dependent on the liquid composition and therefore only a constant if the liquid composition has a defined ionic strength and pH. Extraction is the reverse of sorption and under thermodynamic conditions, i.e. reversible conditions, the mass balance for extraction of exchangeable metals from soils and sediments may be written as:

$$m \, x \, a_0 = c_1 \, x \, V + m \, x \, a_1 \qquad \textbf{(3.3)}$$

where a_0 is the initial exchangeable metal concentration in the solid (mg/kg), V the volume of the extractant (L) and m the mass of the solid (kg). Substitution of Equation 3.2 in 3.3 gives:

$$c_1 = \frac{a_0}{V/m + K_D} \tag{3.4}$$

The reciprocal of Equation 3.4 gives:

$$\frac{1}{c_1} = \frac{1}{a_0} x \frac{V}{m} + \frac{K_D}{a_0} \tag{3.5}$$

Hence, a plot of $1/c_1$ vs. V/m gives a straight line with an intercept of K_D/a_0 and a slope of $1/a_0$, from which the partitioning coefficient, K_D and the available fraction, a_0 can be calculated.

The most commonly employed methods in determination of heavy metals in soil extracts are ICP-MS and AAS. As mentioned previously, their high cost may preclude their use in some laboratories, prompting other techniques such as stripping voltammetry to be employed. In addition, in cases were no standard reference materials are available for a particular analysis, employing two techniques is recommended to ensure more accurate results. In a study under consideration in our laboratory, heavy metals are determined in soil extracts using ICP-MS. The purpose of this study is to use the batch-mode extraction technique with different extractants in order to gain insights into the environmental availability of certain heavy metals. No standard reference materials are available, hence it was decided to investigate the possibility of using stripping voltammetry at the BiFE as a complimentary tool to ICP-MS in the measurement of several heavy metals in soil extracts, and from these results determine the partitioning coefficient and environmental availability of these elements in the soils.

3.6.2 Experimental Procedures for Analysis of Soil Extracts

The procedures involved in this section are slightly different to those described in Section 3.5. Following some preliminary investigations (results below), it was determined that an *in situ* plated film was more suitable for determination of lead, cadmium and copper using anodic stripping voltammetry at the BiFE. The previously used preplated BiFE was employed in CAdSV measurements of cobalt and nickel.

The *in situ* formed BiFE was formed by simply adding 1 mg/L Bi(III) to the sample solution, and then performing an accumulation and stripping step.

Preparation of the soil sample extracts for determination of lead, cadmium and copper simply involved diluting the sample appropriately with 0.1 mol/L acetate buffer pH 4.5, and adding 1 mg/L Bi(III). As acidic conditions are suitable for anodic stripping voltammetry at the BiFE, no pH adjustment was required. The samples were then analysed. On the contrary, when preparing the samples for determination of nickel and cobalt, following appropriate dilution with 0.01 mol/L ammonium buffer, the pH was adjusted to approximately 9.2 – 9.6 with 25 % ammonia solution. In the case of the sample containing only nickel at very low levels, ammonium chloride was added to the sample to a final concentration of 0.01 mol/L. Dimethylglyoxime was then added and the samples analysed. The method of standard additions was employed in determination of the concentrations of heavy metals present in the soil extract samples.

In CAdSV measurements, the applied potential during the accumulation step was –0.7 V, while in ASV measurements, the applied potential was –1.0 V.

3.7 Results and Discussion

3.7.1 Preliminary Measurement of Nickel in a Soil Extract Sample

A series of three soil extracts were selected in order to conduct a preliminary investigation into the possibility of measuring nickel (and / or cobalt) in such a matrix using the bismuth film electrode. All of the soils in this study were from an urban area of Ljubljana. In this example, the heavy metals were extracted using deionised water. Following addition of ammonium chloride and 5×10^{-5} mol/L DMG, and pH adjustment to 9.4, nickel was accumulated at the BiFE for 90 s at –0.7 V. The results of these measurements are presented in Figure 3.23 in a critical comparison with the ICP-MS results using the "least squares analysis" method. In this technique, the results obtained using each technique are plotted against each other, and the resulting plot used as a method for basic comparison of the two sets of results.

From Figure 3.23, it is evident that a correlation exists between the ICP-MS and AdSV techniques. The dashed line shows the situation in which a perfect

correlation between two methods is obtained; the slope is 1, the correlation coefficient is 1 and the line intercepts the origin. The equation for the line obtained with the real results gives a slope of 1.005, an intercept of 0.49 and a correlation coefficient (r) of 0.998. The slope of 1.005 is very close to the ideal of 1, and the correlation is quite good. The intercept of 0.49 suggests a systematic error / difference between the two techniques. This could be due to the following reasons:

(a) differences in the techniques employed for determination of the amount of nickel in the samples i.e., the method of standard additions with voltammetry and from a calibration curve with ICP-MS. It should be noted here that over time (several hours) the peak magnitudes in ICP-MS decreased considerably, hence an internal standard was injected periodically, which the samples were compared to. This may have resulted in another source of error.

(b) as the samples were not pretreated, dissolved organic matter present in the soil samples could have caused interference in both methods – in the plasma of the ICP-MS or through adsorption on the electrode surface.

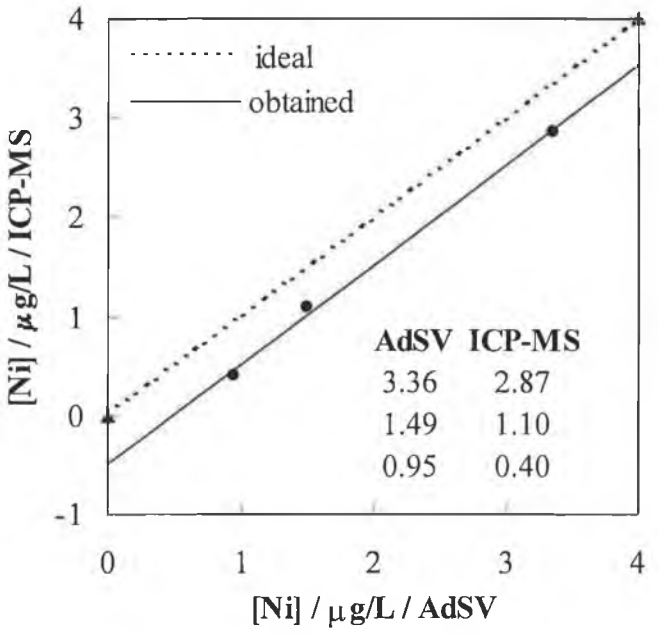

Figure 3.23: Comparison of results obtained using ICP-MS and adsorptive stripping voltammetry for measurement of nickel in a soil extract; nickel was extracted with Milli-Q water; AdSV parameters in text. Inset: Actual values obtained.

These promising results led us to consider stripping voltammetry at the BiFE in determination of heavy metals in soil extract samples.

3.7.2 Heavy Metal (Zn, Cd, Pb, Cu, Co, Ni) Measurements at a Preplated BiFE

It should first be noted that at the start of this study, determination of Zn, Cd, Pb, Co and Ni was considered. Following some preliminary experiments, it was considered more appropriate to analyse the soil extract samples for Cd, Pb, Cu, Co and Ni, for reasons which will be outlined below.

It was considered that measurement of all the target heavy metals – Zn, Cd, Pb, Co and Ni – would be simplest and most convenient employing the same BiFE. As determination of cobalt and nickel can only be performed at a preplated BiFE, this electrode surface was investigated for the possibility of measuring Zn, Cd, Pb, Co and Ni. In a preliminary experiment, the BiFE was plated as usual i.e. for 5 minutes at –1.0 V from a solution containing 100 mg/L Bi(III) in 0.1 mol/L acetate buffer pH 4.5. A solution of 0.05 mol/L acetate buffer pH 4.5 was then chosen as the electrolyte solution, as a compromise between 0.1 mol/L acetate buffer necessary for Cd, Pb and Zn and 0.01 mol/L ammonia buffer necessary for Co and Ni. 20 μg/L each of the target metals was added to this solution. In the first part of this experiment, Zn, Cd and Pb were accumulated at the BiFE at a potential of –1.4 V for 2 minutes and then stripped off the electrode surface. The results are presented in Figure 3.24 A. In the second part of this experiment, the pH of the working solution was adjusted to pH 9.6 and 1 x 10^{-5} mol/L DMG added. Accumulation of the cobalt-DMG and nickel-DMG complexes was carried out at –0.7 V for 60 s. The resulting voltammogram is displayed in Figure 3.24 B.

Figure 3.24 A and B reveal that the preplated BiFE can be employed in the determination of lead, cadmium, nickel and cobalt, with well-defined and well-resolved peaks obtained for each element. However, there was no peak at approximately –1 V, where the stripping peak for zinc was expected. This wasn't expected, as from previous work [49], it was possible to measure Zn, Cd and Pb at the same (*in situ*) BiFE. Hence, it was assumed that some interaction between zinc and nickel or cobalt occurred. Further evidence pointing to such an interaction is seen in Figure 3.24 B. Considering that 20 μg/L of cobalt and nickel were determined simultaneously under conditions similar to those in Figure 3.4, it was expected that

both voltammograms would be similar. However, while the peak currents were similar in Figure 3.4, the nickel peak in Figure 3.24 is approximately four and a half times that of cobalt, suggestive of some difference in the behaviour of cobalt and / or nickel in the presence of zinc. In order to investigate this further, an experiment was carried out in which a stripping voltammogram was obtained for zinc, cadmium and lead, with nickel subsequently added to the working solution and another voltammogram recorded. The results for this are displayed in Figure 3.25.

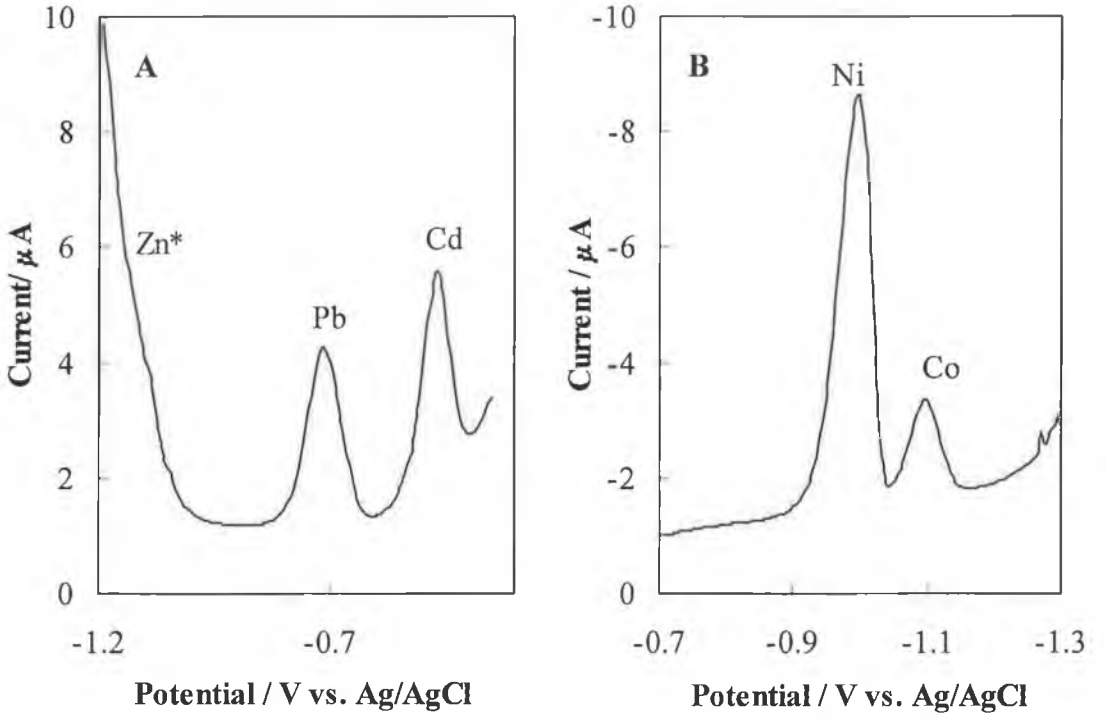

*Figure 3.24: Square wave voltammograms of five heavy metals at the same preplated BiFE. (A) ASV of 20 µg/L Zn, Pb and Cd in 0.05 mol/L acetate buffer (pH 4.5) containing also 20 µg/L Co and Ni; accumulation conditions: -1.4 V for 120 s; initial potential: –1.4 V; final potential: -0.35 V (-1.2 V to –0.35 V shown for the sake of clarity); and (B) CAdSV of 20 µg/L Co and Ni in the above solution adjusted to pH 9.6 and containing 1 x 10^{-5} mol/L DMG; accumulation conditions: -0.7 V for 60 s; settings for A and B: frequency 20 Hz, potential step 5 mV, pulse amplitude 25 mV. * Expected Zn peak position.*

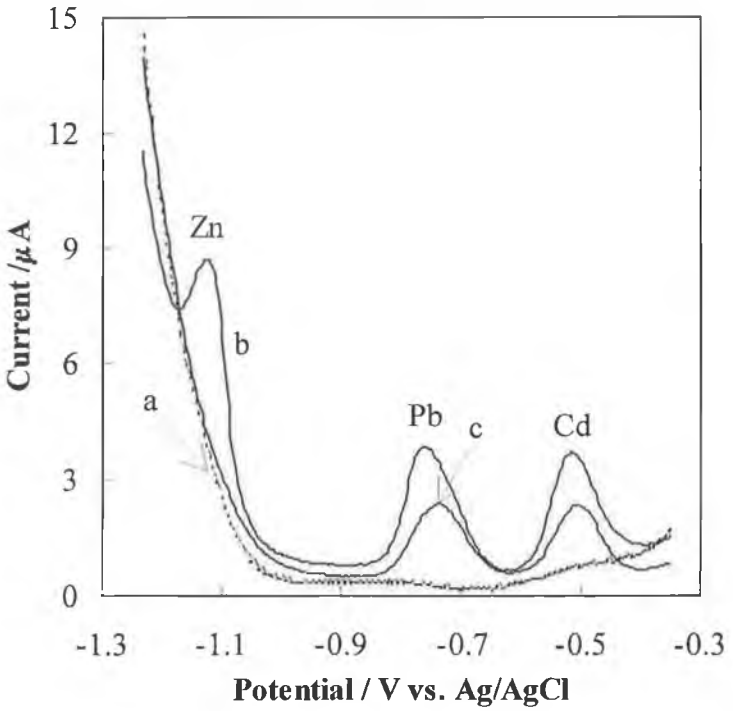

Figure 3.25: Square wave voltammograms of (a) 0.1 mol/L acetate buffer (pH 4.5), (b) a + 50 μg/L Zn, Pb, Cd and (c) b + 50 μg/L Ni. Other conditions as in Figure 3.24.

From Figure 3.25 (b), peaks for Zn, Cd and Pb are observed. Following this, nickel was added to the solution and another voltammogram recorded (Figure 3.25 (c)). Here, it can be clearly seen that addition of nickel to the solution causes the zinc peak to disappear and also the lead and cadmium peaks to decrease. Almost identical results were obtained when the same experiment was carried out with cobalt.

The reasons for the obvious effects of nickel and cobalt on the stripping signals for the other elements, especially zinc, require much in-depth study. Some preliminary assumptions about these interactions can be made, e.g., formation of some zinc-cobalt, zinc-nickel or zinc-nickel-cobalt alloys, or interaction of the three heavy metals with the bismuth film. However, these are assumptions and further investigations in order to prove them are necessary. In order to eliminate / prove the interaction of the elements with the BiFE, a comparative study at the MFE should be undertaken. Here it would be possible to see if this effect on Zn occurs at both surfaces under the same conditions or not. It would also be interesting to note the

effect of varying Zn:Ni and Zn:Co ratios on the stripping response of the BiFE to zinc.

Although it was shown above that cadmium, lead, cobalt and nickel could be determined at the same BiFE, it was decided that in analysis of the soil extracts, an *in situ* BiFE would be employed in ASV and a preplated BiFE in CAdSV. One of the reasons for this is that unpretreated samples were employed in this study, which could lead to fouling of the preplated electrode surface over time, hence leading to erroneous results. Indeed, visual inspection of the samples revealed a distinct "cloudiness" of some of the samples, due possibly, to the presence of dissolved organic matter. In addition, following the recording of an anodic stripping voltammogram of sample "K7A", at the *in situ* BiFE, it was obvious that a high concentration of copper was present in the sample (see Figure 3.26). The ICP-MS results revealed that the concentrations of zinc and copper in this soil extract were 500 and 262 μg/L, respectively. The presence of such a small peak for zinc (at ~ -1 V) points to the formation of a Zn-Cu alloy at the applied deposition potential of –1.4 V. As there was no method with which to prevent the formation of such an alloy (gallium was unavailable), only measurement of copper was possible, since application of potentials sufficiently negative for stripping of analysis of zinc ($\geq$ –1.2 V) will lead to the formation of the Zn-Cu alloy. A potential of –1 V was applied in the deposition step, thus eliminating zinc from the reaction. Copper's re-oxidation potential is more positive that of bismuth's, hence it is necessary to strip bismuth from the surface of the substrate electrode to determine copper. Such a step precludes use of the preplated BiFE in copper measurements. Hence, in all determinations of Cd, Pb and Cu, the *in situ* BiFE was employed.

Figure 3.27 shows some typical stripping voltammograms obtained for the five target heavy metals in some of the soil extract samples. The first voltammogram (a) in each represents the soil extract (appropriately diluted, with pH adjustment if necessary), with the subsequent voltammograms representing standard additions of the respective metal to the sample solution. In each set of voltammograms, the excellent performance of the BiFE in the unpretreated samples is evident, with well-defined peaks obtained for each element in the μg/L concentration range.

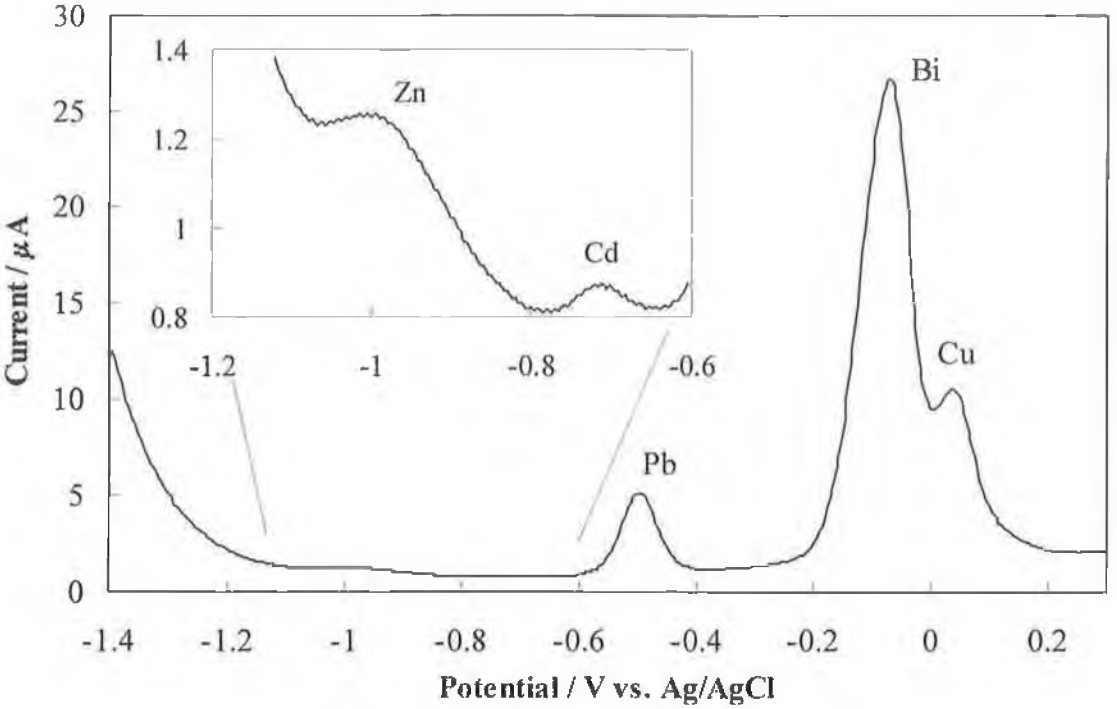

Figure 3.26: Anodic stripping voltammogram of a soil extract sample diluted 1 + 3 (v/v) with 0.1 mol/L acetate buffer (pH 4.5) and containing 1 mg/L Bi(III); accumulation conditions: –1.4 V for 120 s; stripping from –1.4 V to + 0.3 V; inset: magnification of potentials between –1.2 V and –0.6 V; heavy metals extracted using 0.1 mol/L HNO_3.

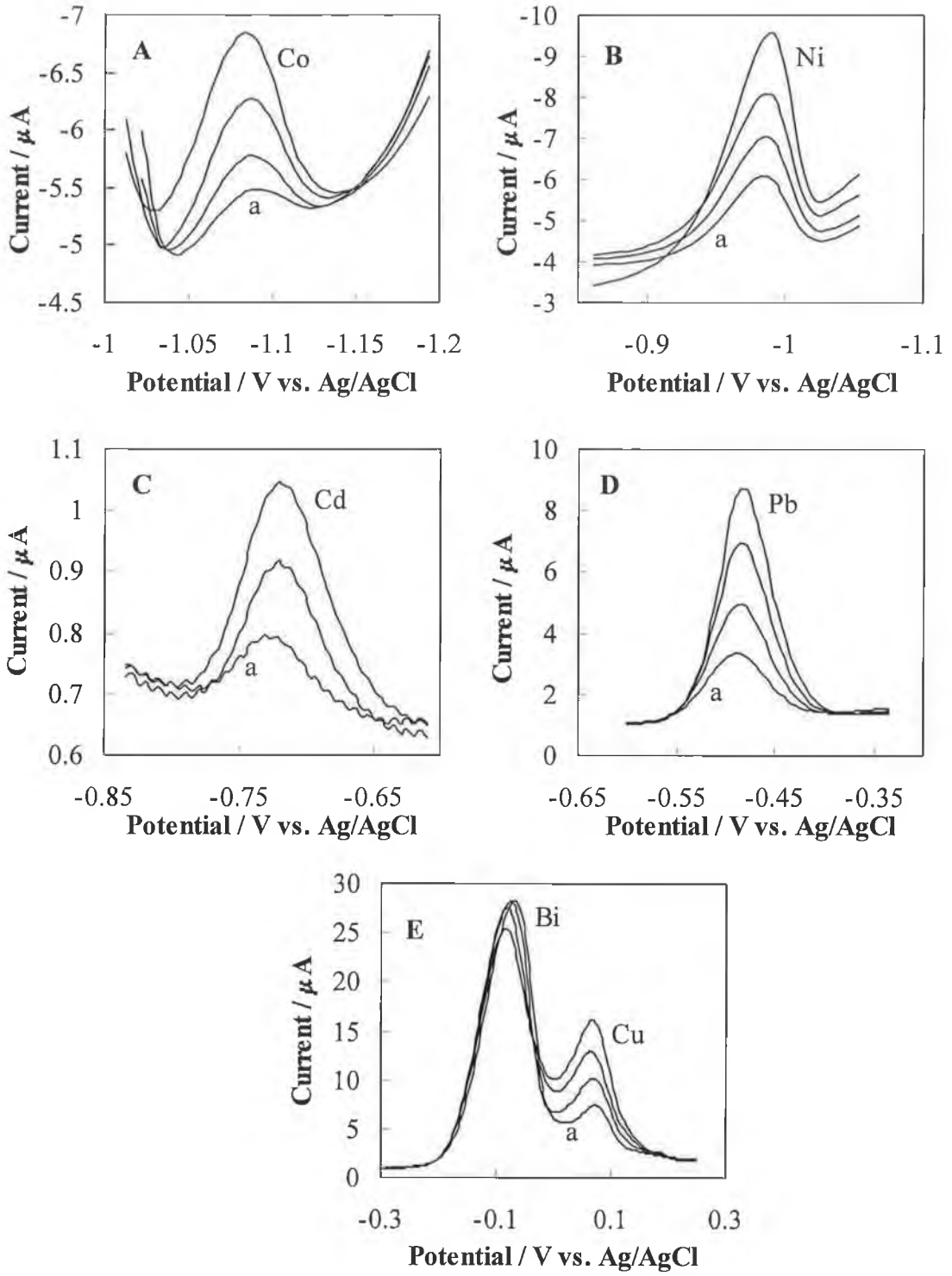

Figure 3.27: Cathodic adsorptive stripping voltammograms (A) Co and (B) Ni and anodic stripping voltammograms (C) Cd, (D) Pb and (E) Cu of (a) soil extract samples + standard additions of 5, 10 & 10 μg/L (A), 5 μg/L (B), 5 μg/L (C), 20 μg/L (D) 20 μg/L (E) 20 μg/L of the respective metal. A and B; LSV scan rate: 50 mV/s. C, D and E: SWV: frequency 20 Hz, potential step 5 mV, pulse amplitude 25 mV.

3.7.3 Comparison of Adsorptive and Anodic Stripping Voltammetry Measurement of Heavy Metals in Soil Extracts at BiFE with ICP-MS

Analysis was carried out on seven different soil samples – K1A, K2A, K3A, K4A, K5A, K6A and K7A. The results from each set of analyses are shown in Table 3.6 (A to G, with individual sample numbers also highlighted), in which data regarding the correlation data (equation of the line and correlation coefficient), dilution factor, and quantity of heavy metal determined using both voltammetry and ICP-MS are included.

A:

SAMPLE K1A Element	*Equation of Line; y =*	*r*[c]	*Inter-cept*	*Dilution Factor*	*Conc. µg/L*	*ICP-MS µg/L*
Cadmium	n.d.[#]	n.d.	n.d.	n.d.	n.m.*	1.38
Cobalt	0.0436x + 0.2869	0.995	6.58	2	13.16	9.69
Copper	0.0816x + 2.5821	0.999	31.64	2	63.28	44.04
Lead	0.0914x + 2.0350	0.999	22.26	2	44.52	72.54
Nickel	0.0822x + 1.6862	0.999	20.51	2	41.02	17.88

[c] correlation coefficient # not detected * not measured

B:

SAMPLE K2A Element	*Equation of Line; y =*	*r*	*Inter-cept*	*Dilution Factor*	*Conc. µg/L*	*ICP-MS µg/L*
Cadmium	n.d.	n.d.	n.d.	n.d.	n.d.	2.97
Cobalt	0.0676x + 0.3353	0.999	4.96	5	24.80	22.06
Copper	0.1152x + 4.5851	0.999	39.80	2	79.60	92.04
Lead	0.0834x + 3.6013	0.999	43.18	2	86.36	161.11
Nickel	0.1466x + 1.6409	0.999	11.19	5	55.95	40.45

C:

SAMPLE K3A Element	*Equation of Line; y =*	*r*	*Inter-cept*	*Dilution Factor*	*Conc. µg/L*	*ICP-MS µg/L*
Cadmium	0.0052x + 0.0182	0.997	3.50	2	7.00	5.58
Cobalt	0.0362x + 0.2479	0.997	6.85	10	68.50	43.13
Copper	0.0806x + 6.5439	1.000	81.19	2	162.38	150.38
Lead	0.0593x + 2.2880	0.999	38.58	4	154.32	251.34
Nickel	0.1425x + 2.0263	0.999	14.22	10	142.20	72.43

D:

SAMPLE K4A Element	*Equation of Line; y =*	*r*	*Inter-cept*	*Dilution Factor*	*Conc. µg/L*	*ICP-MS µg/L*
Cadmium	0.0227x + 0.1149	0.994	5.06	2	10.12	10.31
Cobalt	0.0809x + 0.3213	0.989	3.97	20	79.43	90.04
Copper	0.1454x + 6.0625	0.999	41.70	5	208.50	261.33
Lead	0.1235x + 4.8035	0.999	38.89	4	155.58	453.61
Nickel	0.1822x + 0.9415	0.999	5.17	20	103.35	144.85

E:

SAMPLE K5A Element	*Equation of Line; y =*	*r*	*Inter-cept*	*Dilution Factor*	*Conc. µg/L*	*ICP-MS µg/L*
Cadmium	0.0012x + 0.0091	0.993	7.58	2	15.16	13.79
Cobalt	0.0336x + 0.2124	0.987	6.32	20	126.40	124.50
Copper	0.1058x + 4.8375	0.996	45.72	5	228.62	288.08
Lead	0.0494x + 3.0960	0.996	62.67	2	125.34	471.74
Nickel	0.1289x + 1.2989	0.996	10.08	20	201.60	197.15

F:

SAMPLE K6A Element	*Equation of Line; y =*	*r*	*Inter-cept*	*Dilution Factor*	*Conc. µg/L*	*ICP-MS µg/L*
Cadmium	0.0063x + 0.0272	0.999	4.32	4	17.28	17.90
Cobalt	0.0315x + 0.2715	0.998	8.62	20	172.40	153.5
Copper	0.0925x + 6.1725	0.997	66.73	4	266.92	273.53
Lead	0.1093x + 7.0983	0.999	64.94	4	259.76	457.24
Nickel	0.1039x + 1.2656	0.998	12.18	20	243.60	236.65

G:

SAMPLE K7A Element	*Equation of Line; y =*	*r*	*Inter-cept*	*Dilution Factor*	*Conc. µg/L*	*ICP-MS µg/L*
Cadmium	0.0087x + 0.0530	0.999	6.09	4	24.36	22.83
Cobalt	0.0467x + 0.3708	0.999	7.94	20	158.8	176.7
Copper	0.1011x + 6.0425	0.999	59.77	4	239.08	261.58
Lead	0.0828x + 3.5563	0.998	42.95	4	171.80	447.94
Nickel	0.0941x + 1.3958	0.999	14.83	20	296.60	289.85

Table 3.6: Relevant data for determination of heavy metals in soil extracts (A) sample K1A, (B) sample K2A, (C) sample K3A, (D) sample K4A, (E) sample K5A, (F) sample K6A, (G) sample K7A.

From these results, it can be seen that the best correlation between the two methods appears to be for cadmium and cobalt. The method of least mean squares was used to evaluate the correlation between the two methods for these two metals; Figure 3.28 shows the results obtained in this comparison where "ideal" correlation is defined by a line of regression with a slope of 1 and an intercept of 0. Statistical tests performed on the data show that at the 95% significance level the slope and intercept for both cobalt and cadmium do not differ from the "ideal" values of 0 and 1, respectively (see inserts in Figure 3.28). Thus, the precision obtained with BiFE was correct but the 95% confidence bands show that the accuracy could be much better. While the correlation for nickel was good in some of the samples, e.g., K5A, K6A and K7A,

there was considerable disparity between the results for the other samples. The overall correlation between both techniques for lead was poor. This may be due to a more pronounced effect of dissolved organic matter in the samples on the quantification of lead in the samples. As well as the possible reasons listed in Section 3.8.1 for disparity in the results for nickel, another source of error may have been in dilution of the samples prior to analysis when both techniques were used. Any error introduced during the analysis would have been magnified when the dilution factor was taken into account.

As this was only a preliminary study, further optimisation of the voltammetric procedure (e.g. amount of Bi(III) ions in the plating solution for *in situ* measurements, deposition time and potential, etc.), for future use in such a study is recommended. An investigation into the causes of signal reduction in the ICP-MS should also be carried out. In addition, and most importantly, the effect of sample pretreatment (e.g. UV irradiation) on the measurements should be studied.

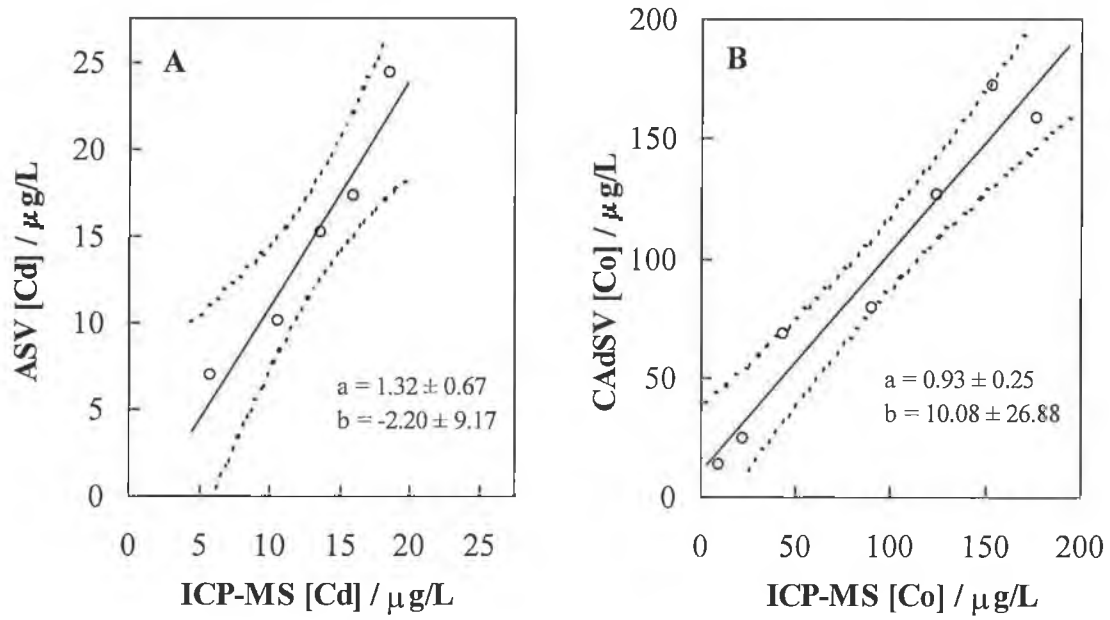

Figure 3.28: Comparison of results obtained for determination of cadmium (A) and cobalt (B) in soil extracts using stripping voltammetry at the BiFE and ICP-MS. The data were fitted on a line of regression $y = a \cdot x + b$ using the method of least mean squares. The dashed lines represent the 95% confidence bands.

3.7.4 Use of Voltammetric and ICP-MS Results for Determination of K_D and a_0 for Cadmium and Cobalt in Soil Extracts

As the correlation between voltammetric techniques and ICP-MS was best for cobalt and cadmium, examples illustrating the calculation of K_D and a_0 are shown for both of these heavy metals. Figure 3.29 and Figure 3.30 show plots of concentration of the respective heavy metal vs. the *V/m* ratio (A) and plots of reciprocal concentration vs. *V/m* ratio (B) for cadmium and cobalt, respectively. The lines in the graphs represent a plot of a combination of the data, while the symbols (■) and (●) represent the results obtained using ICP-MS and voltammetric techniques, respectively. From A in each case, a close correlation in the results is observed. The correlation coefficients (r) in Figure 3.29 and 3.30 (B), are 0.977 and 0.983 for cadmium and cobalt, respectively. Although these correlation coefficients are significantly different from ideal (r = 1), they do suggest a correlation between both techniques. It should be noted that any small difference in the concentrations obtained will be magnified in this plot, for example for a *V/m* ratio of 98.4 for cobalt, concentrations of 22.06 µg/L and 24.80 µg/L were determined using ICP-MS and AdSV, respectively. The difference here is only approximately 10 %, yet this is seen as a considerable difference in Figure 3.29 B. K_D and a_0 were calculated using Equation 3.5, whereby the slope of the plots in Figure 3.29 and 3.30 (B) is equal to $1/a_0$ and the intercept is equal to K_D/a_0. The calculated K_D values were. 8.9 and 4.6 mL/g for Cd and Co, respectively. This means that for a V/m ratio of say 10 mL/g, which is often used in extraction protocols, a (much) too low extractability of a_0 would have been found (for Co, 53% and for Cd, 68%). However, the *V/m* approach followed allowed the unambiguous determination of the maximal metal extractability from soil as 369 µg/g for Cd and 2597 µg/g for Co.

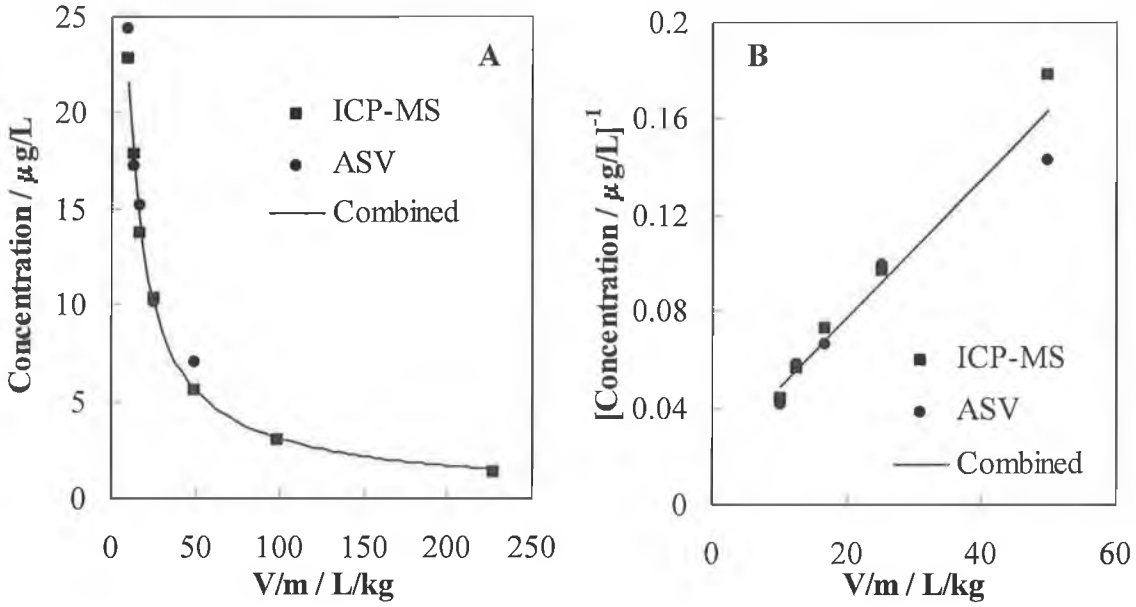

Figure 3.29: Comparison of results obtained for cadmium using ICP-MS and anodic stripping voltammetry at the BiFE for analysis of soil extracts. (A) plot of concentration obtained vs. volume to mass ratio; and (B) reciprocal concentration vs. volume to mass ratio.

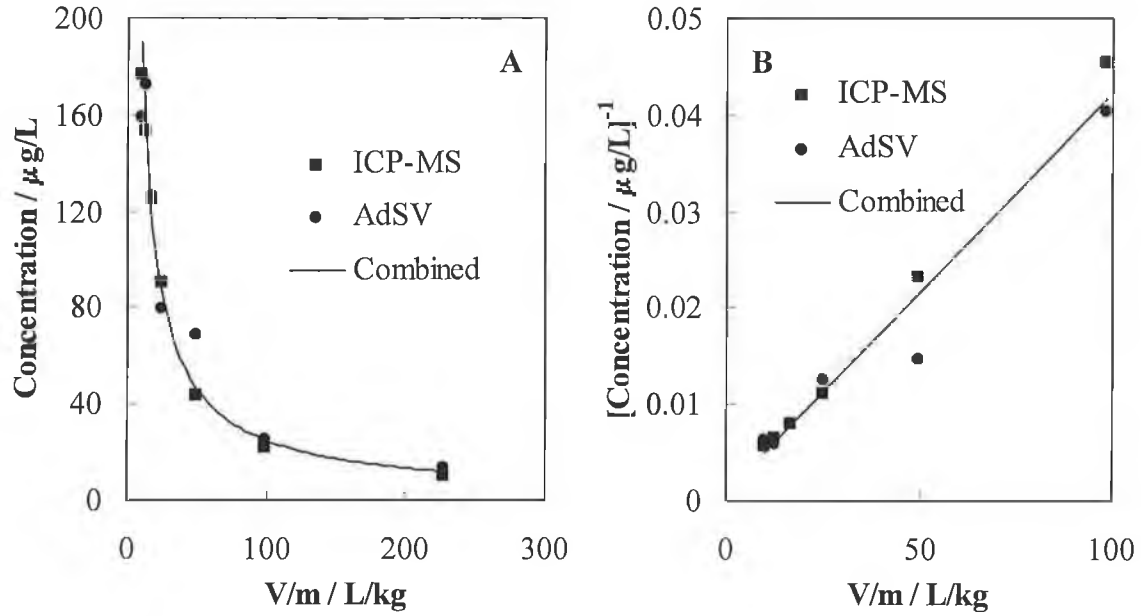

Figure 3.30: Comparison of results obtained for cobalt using ICP-MS and anodic stripping voltammetry at the BiFE for analysis of soil extracts. (A) plot of concentration obtained vs. volume to mass ratio; and (B) reciprocal concentration vs. volume to mass ratio.

3.8 Conclusions

This first part of this section of the work introduced the bismuth film electrode as a new electrode surface for cathodic adsorptive stripping voltammetry and potentiometric stripping analysis determination of trace levels of cobalt, and simultaneous measurement of trace cobalt and nickel. The BiFE was compared to its mercury counterpart, the mercury film electrode, whereby the performance of the BiFE was found to equal if not surpass that of the MFE, especially regarding the enhanced stripping signal for cobalt and significantly improved behaviour in the presence of dissolved oxygen.

Comparison of some of the available voltammetric and potentiometric techniques revealed that all were suitable for trace cobalt and nickel determination, with potentiometric stripping analysis providing the optimum resolution of the cobalt and nickel peaks. Interpretation of the cyclic voltammetry and PSA results revealed the irreversibility of the cobalt-DMG and nickel-DMG adsorption process, which is similar to behaviour previously observed at mercury electrodes for the same reaction.

The analytical performance of the BiFE for determination of trace cobalt and nickel was excellent, with limits of detection employing 60 s deposition of 0.08 μg/L for cobalt and 0.26 μg/L for nickel. Increasing the accumulation time will lead to even lower detection limits. The reproducibility of measurements at the BiFE was also excellent, with low r.s.d.s obtained for repeat measurements of low concentrations of cobalt and nickel. This represents a further advantage over MFE, with the possibility of using the BiFE for many measurements without the necessity for film regeneration / cleaning.

The BiFE was successfully employed in the measurement of trace amounts of nickel and cobalt in a number of low-volume artificial body fluid samples such as artificial saliva and synthetic sweat. The performance of the BiFE in comparison to ICP-MS for the measurement of five target heavy metals in soil extract samples was assessed, and the results of both sets of measurements used to determine the partitioning coefficient, K_D and the environmentally available (extractable) amount, a_0 of cadmium and cobalt in the soil samples, when 0.1 M HNO_3 was employed as the extractant.

3.9 References

1. A. Vercruysse, in *Techniques and Instrumentation in Analytical Chemistry – Volume 4, Part B Hazardous Metals in Human Toxicology*, ed. A. Vercruysse, Elsevier, Amsterdam, 1984, Ch. 1.
2. T.D. Luckey, B. Venugopal, *Metal Toxicity in Mammals 1, Physiologic and Chemical Basis for Metal Toxicity*, Plenum Press, New York, 1977, Ch. 1.
3. R.S. Young, *International Series of Monographs in Analytical Chemistry, Vol. 27: The Analytical Chemistry of Cobalt*, Pergamon Press, Oxford, 1966.
4. US EPA Technology Transfer Network Air Toxics Website, Cobalt Compounds: http://www.epa.gov/ttn/atw/hlthef/cobalt.html
5. http://www.hawaii.navy.mil/CNBDATA/n4/NPL.htm
6. Agency for Toxic Substances and Disease Registry (ATDSR), *2001 CERCLA Priority List of Hazardous Substances*: http://www.atsdr.cdc.gov/clist.html
7. Agency for Toxic Substances and Disease Registry (ATDSR), *Minimal Risk Levels (MRLs) for Hazardous Substances*: http://www.atsdr.cdc.gov/mrls.html
8. C.L. Lewis, W.L. Ott, N.M. Sine, *International Series of Monographs in Analytical Chemistry, Vol. 28: The Analysis of Nickel*, Pergamon Press, Oxford, 1966.
9. WHO Regional Office for Europe, *Air Quality Guidelines*, second ed. Copenhagen, 2000, Ch. 6.10 Nickel.
10. US EPA Technology Transfer Network Air Toxics Website, Nickel Compounds: http://www.epa.gov/ttn/atw/hlthef/nickel.html
11. R.F.M. Herber, in *Techniques and Instrumentation in Analytical Chemistry – Volume 15, Trace Element Analysis in Biological Specimens*, eds. R.F.M. Herber and M. Stoeppler, Elsevier, Amsterdam, 1994, Ch. 15.
12. US EPA Technology Transfer Network Air Toxics Website, Cadmium Compounds: http://www.epa.gov/ttn/atw/hlthef/cadmium.html
13. H.T. Delves and M. Stoeppler, in *Techniques and Instrumentation in Analytical Chemistry – Volume 15, Trace Element Analysis in Biological Specimens*, eds. R.F.M. Herber and M. Stoepler, Elsevier, Amsterdam, 1994, Ch. 17.

14. Agency for Toxic Substances and Disease Registry (ATDSR), *"Draft for Public Comment" Public Health Statement for Copper, CAS# 7440-50-8*, September 2002: http://www.atsdr.cdc.gov/toxprofiles/phs132.html
15. W.H. Nebergall, F.C. Schmidt, H.F. Holtzclaw, *General Chemistry*, 2nd edn., D.C. Heath and company, Boston, 1963, Ch. 40.
16. US EPA Technology Transfer Network Air Toxics Website, Lead Compounds: http://www.epa.gov/ttn/atw/hlthef/lead.html
17. U. Ewers, M. Turfels, E. Jerman, in *Techniques and Instrumentation in Analytical Chemistry – Volume 15, Trace Element Analysis in Biological Specimens*, eds. R.F.M. Herber and M. Stoepler, Elsevier, Amsterdam, 1994, Ch. 18.
18. D.A. Skoog, D.M. West, *Fundamentals of Analytical Chemistry*, second ed., Holt London Edition, Great Britain, 1971.
19. http://scientificsolutions1.com/ICPMSGuide.doc
20. M.D. Glascock, *An Overview of Neutron Activation Analysis, Missouri University Research Reactor*; http://www.missouri.edu/~glascock/naa_over.htm
21. R. Naginiene, O. Abdachmanovas, R. Kregzdyte, S. Ryselis, *Trace Elem. Electroly.* **19** (2002) 87.
22. N. Todorovska, I. Karadjova, T. Stafilov, *Anal. Bioanal. Chem.* **373** (2002) 310.
23. S. Turan, S. Saygi, O. Kilic, J. Trop, *Pediatrics* **47** (2001) 81.
24. J.C. Wataha, S.K. Nelson, P.E. Lockwood, *Dent. Mater.* **17** (2001) 409.
25. F.O. Omokhodion, J.M. Howard, *Clin. Chim. Acta*, **231** (1994) 23.
26. F. Baruthio, F. Pierre, *Biol. Trace Elem. Res.* **39** (1993) 21.
27. G. Samanta, D. Chakraborti, *Fres. J. Anal. Chem.* **357** (1997) 827.
28. M.E. Conti, *Food Res. Int.* **30** (1997) 343.
29. S. Kartikeyan, B. Vijayalekshmy, S. Chandramouleeswaran, T.P. Rao, C.S.P. Iyer, *Anal. Lett.* **30** (1997) 1037.
30. P. Sooksamiti, H. Geckeis, K. Grudpan, *Analyst* **121** (1996) 1413.
31. S. Hirata, Y. Ishida, M. Aihara, K. Honda, O. Shikino, *Anal. Chim. Acta* **438** (2001) 205.
32. J. Vogl, K.G. Heumann, *Fres. J. Anal. Chem.* **359** (1997) 438.
33. M.J. Duane, S. Facchetti, *Sci. Total Environ.* **172** (1995) 133.
34. C.C. Huang, M.H. Yang, T.S. Shih, *Anal. Chem.* **69** (1997) 3930.

35. J.C. Wasserman, A.M.G. Figueiredo, F. Pellegatti, E.V. Silva, *J. Geochem. Explor.* **72** (2001) 129.
36. J.M. Martin-Moreno, L. Gorgojo, R.A. Riemersma, J. Gomez-Aracena, J.D. Kark, J. Guillen, J. Jimenez, J.J. Ringstad, J. Fernandez-Crehuet, P. Bode, F.J. Kok, *Brit. J. Nutr.* **89** (2003) 673.
37. J. Versieck, L. Vanballenberghe, *Anal. Chem.* **63** (1991) 1143.
38. E.P. Achterberg, C. Braungardt, *Anal. Chim. Acta* **400** (1999) 381.
39. J. Wang, J. Lu, Ű.A. Kirgőz, S.B. Hočevar, B. Ogorevc, *Anal. Chim. Acta* **434** (2001) 29.
40. M. Panigati, M. Piccone, G. D'Alfonso, M. Orioli, M. Carini, *Talanta* **58** (2002) 481.
41. C. Locatelli, G. Torsi, *J. Electroanal. Chem.* **509** (2001) 80.
42. M.M. Ghoneim, A.M. Hassanein, E. Hammam, A.M. Beltagi, *Fres. J. Anal. Chem.* **367** (2000) 378.
43. R. Inam, G. Somer, *Food Chem.* **69** (2000) 345.
44. E. Fischer, C.M.G. van den Berg, *Anal. Chim. Acta* **385** (1999) 273.
45. J. Golimowski, B. Krasnodebska-Ostrega, *Fres. J. Anal. Chem.* **361** (1998) 65.
46. S. Jaenicke, R.M. Sabarathinam, B. Fleet, H. Gunasingham, *Talanta* **45** (1998) 703.
47. D. Sancho, M. Vega, L. Deban, R. Pardo, G. Gonzalez, *Analyst* **122** (1997) 727.
48. M.A. Baldo, C. Bragato, S. Daniele, *Analyst* **122** (1997) 1.
49. J. Wang, J. Lu, S.B. Hočevar, P.A.M. Farias, B. Ogorevc, *Anal. Chem.* **72** (2000) 3218.
50. S.B. Hočevar, B. Ogorevc, J. Wang, B. Pihlar, *Electroanalysis* **14** (2002) 1707.
51. G.U. Glechsig, O. Korbout, S.B. Hočevar, S. Thongngamdee, B. Ogorevc, P. Grűndler, J. Wang, *Electroanalysis* **14** (2002) 192.
52. J. Wang, J. Lu, S.B. Hočevar, B. Ogorevc, *Electroanalysis* **13** (2001) 13.
53. I. Švancara, R. Metelka, M. Stibůrková, G. Jansová, J. Seidlová, K. Vytřas, B. Pihlar, *Sci. Pap. Univ. Pardubice Ser. A* **8** (2002) 19.
54. P. Nangniot, *J. Electroanal. Chem.* **14** (1967) 197.
55. H. Eskilsson, C. Haraldsson, D. Jagner, *Anal. Chim. Acta* **79** (1985) 79.
56. M. Trojanowicz, W. Matuszewski, *Talanta* **36** (1989) 680.
57. Z.-Q. Zhang, H. Liu, H. Zhang, Y.-F. Li, *Anal. Chim. Acta* **333** (1996) 119.
58. A. Economou, P.R. Fielden, *Analyst* **118** (1993) 47.

59. E.P. Gil, P. Ostapczuk, *Fres. J. Anal. Chem.* **346** (1993) 952.
60. E.P. Gil, P. Ostapczuk, *Fres. J. Anal. Chem.* **346** (1993) 957.
61. R.I. Mrzljak, A.M. Bond, T.J. Cardwell, R.W. Cattrall, R.W. Knight, O.M.G. Newman, B.R. Champion, *Analyst* **119** (1994) 1057.
62. M. Cullen, S. Lancashire, *Analyst* **121** (1996) 75.
63. A. Economou, P.R. Fielden, *Talanta* **46** (1998) 1137.
64. M. Korolczuk, *Talanta* **53** (2000) 679.
65. E. Muñoz, S. Palmero, M.A. García-García, *Talanta* **57** (2002) 985.
66. J. Wang, J. Lu, *Electrochem. Commun.* **2** (2000) 390.
67. P.R.K. Reddy, S.J. Reddy, *Int. J. Environ. Anal. Chem.* **69** (1998) 287.
68. P. Gonzalez, V.A. Cortinex, C.A. Fontan, *Talanta* **58** (2002) 679.
69. J. Wang, J.Y. Wang, B.M. Tian, M.A. Jiang, *Anal. Chem.* **69** (1997) 1657.
70. E. Shams, *Anal. Lett.* **33** (2000) 465.
71. A. Safavi, E. Shams, *Talanta* **51** (2000) 1117.
72. A. Bobrowski, A.M. Bond, *Electroanalysis* **4** (1992) 975.
73. P. Suciu, M. Vega, L. Roman, *J. Pharm. Biomed. Anal.* **23** (2000) 99.
74. A.A. Ensafi, S. Abbasi, H.R. Mansour, I.M. Baltork, *Anal. Sci.* **17** (2001) 609.
75. S. Colin, E. Beche, R. Berjoan, H. Jolibois, A. Chambaudet, *Corros. Sci.* **41** (1999) 1051.
76. G. Sanna, M.I. Pilo, P.C. Piu, N. Spano, A. Tapparo, G.G. Campus, R. Seeber, *Talanta* **58** (2002) 979.
77. J. Wang, *Analytical Electrochemistry*, second ed., Wiley-VCH, New York, 2000.
78. Z. Galus, *Fundamentals of Electrochemical Analysis*, Ellis Horwood Limited, New York, 1976.
79. F. Ma, D. Jagner, L. Renman, *Anal. Chem.* **69** (1997) 1782.
80. R.L.W. Messer, L.C. Lucas, *Dent. Mater.* **16** (2000) 207.
81. G. Schmalz, P. Garhammer, *Dent. Mater.* **18** (2002) 396.
82. J.Y. Gal, Y. Fovet, M. Adib-Yadzi, *Talanta* **53** (2001) 1103.
83. E. Burguera, A.S. De Briceno, C.E. Rondon, J.L. Burguera, M. Burguera, P. Carrero, *J. Trace Elem. Med. Bio.* **12** (1998) 115.
84. W.Y. Jia, M.W. Beatty, R.A. Reinhardt, T.M. Petro, D.M. Cohen, C.R. Maze, E.A. Strom, M. Hoffman, J. *Biomed. Mater. Res.* **48** (1999) 488.
85. M. Kern, V.P. Thompson, *J. Dent.* **23** (1995) 47.

86. S. Colin, H. Jolibois, A. Chambaudet, M. Tireford, *Int. Biodeter. Biodegr.* **34** (1994) 131.
87. Ph. Quevauviller, *Trends Anal. Chem.* **17** (1998) 289.
88. V.H. Kennedy, A.L. Sanchez, D.H. Oughton, A.P. Rowland, *Analyst* **122** (1997) 89R.
89. A. Tessier, P.G.C. Campbell, M. Bisson, *Anal. Chem.* **51** (1979) 844.
90. J.T. van Elteren, *Anal. Chem.* Submitted.
91. J.T. Elteren, Z. Šlejkovec, R. Milačič, *Intern. J. Environ. Anal. Chem.* **83** (2003) 389.

4. AN ELECTROCHEMICAL MICROSENSOR FOR THE SELECTIVE DETERMINATION OF ASCORBIC ACID IN GASTRIC JUICE

4.1 Introduction

Ascorbic acid (AA), also known as vitamin C, is a γ-lactone that is synthesised by plants and almost all animals except primates and guinea pigs. It is approved for use as a dietary supplement and chemical preservative by the US Food and Drug Administration, and is on the FDA's list of substances generally recognized as safe [1]. It is widely found in fresh fruits and vegetables, with some typical examples given in Table 4.1 [2]. Its beneficial health effects were noticed as early as the sixteenth century in observations that citrus could have curative properties in sailors suffering from deficient wound healing [3]. Ascorbic acid was isolated in the late 1920s by Szent-Gyorgyi, and by the 1930s methods for its synthesis had been devised, making it widely available at low cost [4]. Today, ascorbic acid production is estimated at approximately 46,000 tonnes per year, with more than 20,000 tonnes being produced in Europe [5]. This amount, however, is negligible when compared to ascorbic acid of natural origin, e.g. approximately 89,250 tonnes of ascorbic acid are produced by grass alone each year in the United Kingdom!

The roles of ascorbic acid in the human body are manifold. It is necessary for the formation of collagen, an important protein used to make skin, scar tissue, tendons, ligaments, and blood vessels, and also functions as an antioxidant, blocking some of the damage caused by free radicals, toxic chemicals and pollutants such as cigarette smoke. Research has suggested that vitamin C may play an important role in the prevention of disorders such as heart disease, high cholesterol, high blood pressure, cancers (skin, cervical, breast and gastric), osteoarthritis, cataracts and macular degeneration. Ascorbic acid may also be important for boosting immune system function, maintaining healthy gums, slowing progression of Parkinson's disease, reducing the effects of sun exposure and healing burns and wounds [6]. Ascorbic acid has, therefore, been given tremendous consideration in biomedically-oriented research, due to which there is a strong need for sensitive, selective, and reliable methods for the direct measurement of ascorbic acid.

This chapter is concerned with the determination of ascorbic acid in gastric juice, hence further information regarding the functions of ascorbic acid in the human stomach is provided, in addition to a literature review of some current electrochemical (and other) methods used for quantifying ascorbic acid in both physiological and non-physiological matrices.

This chapter reports on a new all-solid microsensor suitable for determination of typical ascorbic acid concentrations in gastric juice. The microsensor is produced by modifying a substrate carbon cylinder fibre microelectrode (CFCME) with electrochemically deposited nickel oxide (galvanostatic) and ruthenium hexacyanoferrate (voltammetric) layers and a dip-coated protective membrane (cellulose acetate). The performance of the microsensor was studied in detail, with particular emphasis on stability, amperometric response and selectivity. Measurements were carried out in acidic media (0.01 mol/L HCl, pH 1.9), model gastric juice solution and real gastric juice, and revealed the suitability of the proposed microsensor for use in the selective measurement of ascorbic acid in gastric juice.

Foodstuff	*Approx. Conc. mg/kg*	*Foodstuff*	*Approx. Conc. mg/kg*
Acerola cherries	20,000	**Lemons**	450
Parsley	1,700	**Oranges**	360
Blackcurrants	1,400	**Tomatoes**	230
Green pepper	1,300	**Potatoes**	160
Green kale	1,100	**Mushrooms**	50

Table 4.1: Typical concentrations of ascorbic acid in common foodstuffs (adapted from [2]).

4.2 *Ascorbic Acid in the Human Body*

4.2.1 Structure and Oxidation Reaction

Ascorbic acid has a simple structure and is related to the C_6 sugars (see Figure 4.1). Its reducing properties stem from the reactive enediol group at C_2-C_3, while its acidity is related to the C_3 hydroxyl ($pK_a = 4.17$). Loss of the hydrogen atom above pH 4.17 leads to the ascorbate anion. Oxidation of ascorbic acid (or ascorbate anion) occurs in two steps; the first product is monodehydroascorbic acid, which is a relatively stable free radical (the extra electron is stabilised through the oxygens and the conjugated bonds). The second product is dehydroascorbic acid, which if not reduced (in the human body, via enzymes for example), undergoes irreversible hydrolytic ring cleavage to form diketogulonic acid and is lost from the ascorbic acid pool. Thus, the oxidation of ascorbic acid to diketogulonic acid involves the loss of two protons and two electrons.

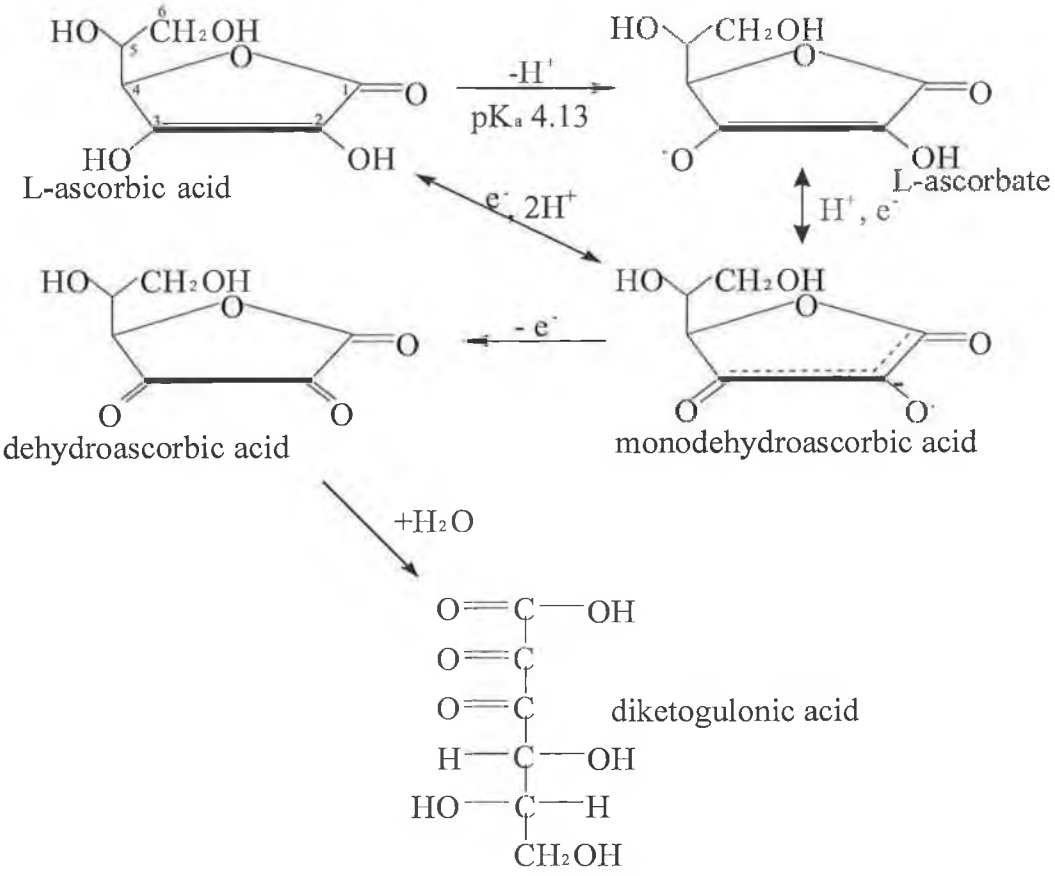

Figure 4.1: Structure and oxidation mechanism of ascorbic acid.

4.2.2 Physiological Roles and Levels in Gastric Juice

In addition to the numerous roles of ascorbic acid mentioned in the introduction, research has shown that ascorbic acid plays an important part in the prevention of gastric cancer. *H pylori* infection is recognised as an independent risk factor for gastric cancer and has been designated as a class 1 carcinogen by an International Agency of Research on Cancer-World Health Organisation committee [7 and references therein]. Infection inevitably leads to the development of chronic gastritis, and further to the development of gastric cancer. In *H. pylori* infection, there is a dramatic increase in levels of reactive oxygen species in the gastric mucosa, which may promote carcinogenesis in a variety of ways including direct DNA damage and generation of genotoxic products. Diets low in the antioxidant vitamins A, C and E are felt to increase the risk of developing gastric cancer and it seems likely that vitamin C exerts a protective effect against gastric carcinogenesis. It has been proven that in the normal stomach, ascorbic acid is secreted in high concentrations into gastric juice, with this secretion failing with the onset of acute *H. pylori* gastritis for example, Fraser *et al.* determined that gastric juice ascorbic acid concentration is lower in the presence of *H. pylori* infection [8].

It has also been suggested that ascorbic acid may be important in the prevention of gastric cancer through its ability to reduce nitrous acid and prevent the formation of carcinogenic *N*-nitroso compounds [9]. Under acidic conditions (such as those found in gastric juice), ascorbic acid reduces nitrite (from dietary sources) or related nitrosating species to nitric oxide and in the process is itself oxidised to dehydroascoric acid. Vermeer *et al.* showed that intake of ascorbic acid significantly reduced the amount of N-nitrosodimethylamine (NDMA) excreted in urine, suggesting that consumed ascorbic acid may reduce endogenous NDMA formation [10]. Under anearobic conditions, ascorbic acid converts the nitrite to nitric oxide and prevents nitrosation. However, in the presence of dissolved air, ascorbic acid is ineffective at preventing nitrosation due to the nitric oxide combining with oxygen to reform nitrite with this recycling of nitrite depleting the available ascorbic acid [11]. This process is illustrated in Figure 4.3.

The healthy stomach actively secretes ascorbic acid (at a rate of approximately 18 μmol/L per hour) and its concentration in fasting gastric juice is several times that in plasma [11]. The levels of ascorbic acid found in gastric juice are dependent on the

health of the individual, and will vary depending on conditions such as chronic gastritis, reflux gastritis, hypochlorhydria, and bacterial overgrowth in the stomach [12]. Choi *et al.* determined serum antioxidative vitamin levels (including ascorbic acid) obtained from blood samples taken from the stomachs of cancer patients and a control group [13]. The serum levels of ascorbic acid in the gastric carcinoma patients were less than one-fifth of the levels in normal healthy subjects, supporting the hypothesis that AA has an inverse association with gastric carcinoma. Table 4.2 shows the results obtained by two different groups regarding the concentrations of ascorbic acid in the human stomach.

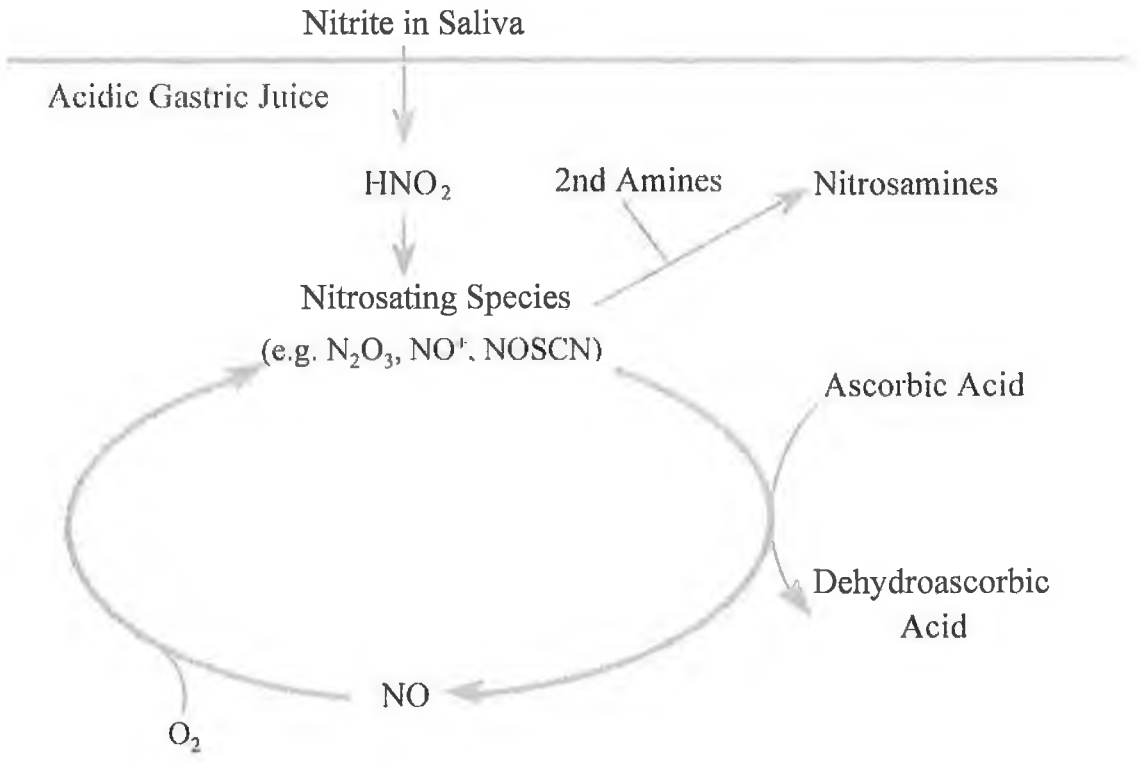

Figure 4.2: Schematic representation of chemical reactions occurring when nitrite enters acid gastric juice containing ascorbic acid and secondary amines (adapted from [11]).

Gastric Pathology	*Gastric Ascorbic Acid*[§] *μmol/L*			*Gastric Ascorbic Acid*[#] *μmol/L*		
	(a)	*(b)*	*(c)*	*(a)*	*(b)*	*(c)*
Normal	154	0-494	23	89	1-489	13
Chronic Gastritis	16	0-100	64	23	1-533	54
Reflux Gastritis	111	2-261	14	90	2-155	7
Ulcers without Chronic Gastritis	29	0-66	6			
Ulcers and Chronic Gastritis	30	3-534	26			

Table 4.2: Ascorbic acid concentration analysed according to gastric pathology; (a) median value, (b) range, (c) number of patients. [§]*[9],* [#]*[12].*

4.2.3 Significance of Ascorbic Measurement in Gastric Juice

Considering the importance of the role that ascorbic acid plays in the prevention of gastric cancer, there is a definite need for sensitive, selective, and reliable methods for its direct measurement in this environment. Conventional methods for detection of ascorbic acid in gastric juice involve quite a long and complicated procedure, for example, in several studies, after sampling, aliquots of gastric juice were frozen in liquid nitrogen (to be used within four weeks). The samples were then prepared for high performance liquid chromatography (HPLC) by passage through disposable columns of Sephadex for clean-up. The purified samples were then analysed by HPLC with detection by ultraviolet absorption at 270 nm [11,12,14]. The determination of ascorbic acid in gastric juice by HPLC with electrochemical detection was also described, although no details about the electrochemical parameters were provided [15]. Although reliable and sensitive, these chromatographic methods do not permit real-time analysis of ascorbic acid in gastric juice. The development of a microsensor suitable for direct determination of ascorbic acid therefore represents a simple, convenient, and inexpensive method for real-time analysis in gastric juice (and indeed in model solutions).

4.3 Metal Hexacyanoferrates

4.3.1 Functions as Electrode Modifiers

Metal hexacyanoferrates were mentioned briefly in Chapter One as a class of electrode modifier. In recent years they have received increased attention because of their numerous applications (which will be detailed in the next section). From a structural viewpoint, a metal hexacyanoferrate of general stoichiometric formula $A_xM_y[Fe(CN)_6]_z{\cdot}qH_zO$ (where M is a metal, A stands for a counterion, and x, y, z and q are stoichiometric coefficients) forms a rigid three-dimensional (almost cubic) framework of repeating –NC-Fe-CN-M-NC units [16]. This is illustrated in Figure 4.3. The properties (electrochemical and spectroscopic) of the respective metal-substituted hexacyanoferrate will depend on the choice of metal (M).

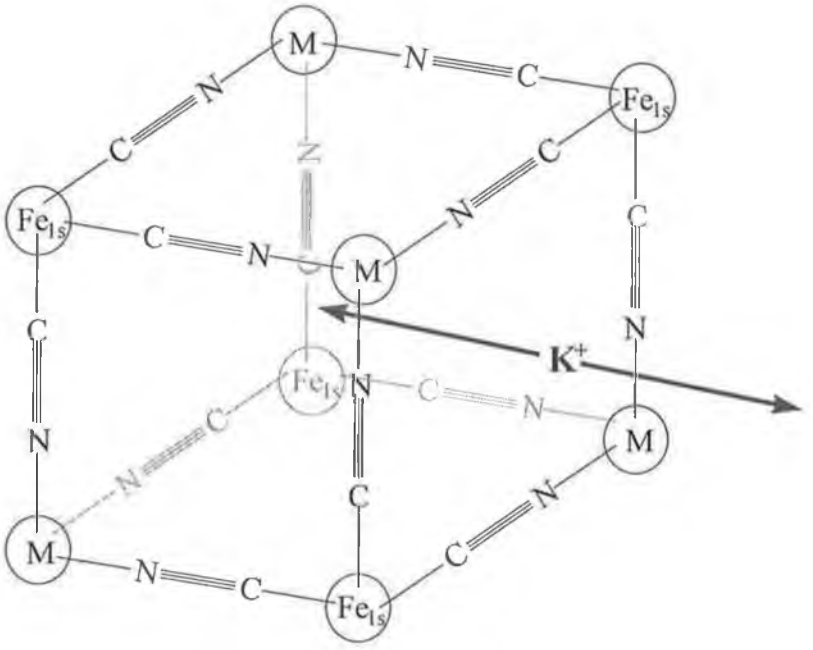

Figure 4.3: Schematic representation of metal hexacyanoferrate.

Modification of the electrode surface with these transition metal hexacyanoferrates is possible in four different ways:

(a) by immersing the electrode surface in a solution containing $Fe(CN)_6^{3-}$ and a transition metal ion and cycling the electrode over a certain potential range.

(b) by electrodeposition of the transition metal on the matrix and then electrochemical anodising of the resulting electrode in the presence of hexacyanoferrate as the derivatisation agent.

(c) by electrodeposition of a transition metal on the matrix and then chemical derivatisation of the resulting electrode in the presence of hexacyanoferrate.

(d) by immersing the transition metal electrode surface in a solution containing $Fe(CN)_6^{3-}$ and potentiostating the electrode at a convenient value [17].

In all cases, the insoluble transition metal hexacyanoferrate is formed by electrochemical or chemical oxidation of the transition metal and subsequent reaction with hexacyanoferrate.

One of the primary reasons for modification of an electrode surface with a metal hexacyanoferrate is the achievement of electrocatalysis, which consists of an acceleration of heterogeneous electron transfer of the target analyte, which is slow at the same potential at a bare electrode [18]. This process is different from mediation, where an immobilised redox couple generates heterogeneous electron transfer of a target redox analyte in solution that would occur just as readily at the same potential at a bare electrode if it were available i.e. electrocatalysis is accomplished by charge mediation but not all mediation results in electrocatalysis.

Slow reactions of many important analytes necessitate the application of a potential which exceeds their formal redox potentials in order that these reactions proceed at desirably high rates [18]. The acceleration of such kinetically-hindered electrode reactions by electrode-confined charge mediators permits the quantification of these analytes at less extreme potentials, as catalysed electrode reactions usually occur near the formal potential of the mediator. Through the application of less extreme potentials, both sensitivity and selectivity can be significantly improved when compared to unmodified electrodes. In addition, electrode fouling, which may occur as a result of direct electrochemical conversion of the analyte at more extreme potentials at the bare electrode, may also be decreased. Other advantages associated with the use of metal hexacyanoferrates as electrode modifiers include their cation-exchange capabilities, their ability to prevent corrosion, their unique spectro-electrochemical (electrochromic, thermochromic and ionchromic) and magnetic properties.

4.3.2 Some Applications of Metal Hexacyanoferrate-Modified Electrodes

Prussian Blue (PB), or ferric hexacyanoferrate, one of the most ancient coordination materials known, was discovered to form electroactive layers after electrochemical or chemical deposition onto an electrode surface [19]. Deposition of PB is usually carried out from aqueous solutions containing a mixture of ferric (Fe^{3+}) and ferricyanide ($[Fe^{III}(CN)_6]^{3-}$) ions, either spontaneously in an open-circuit regime, or by applying a reductive electrochemical driving force. Reduction of Prussian Blue results in the formation of Prussian White and an accompanying loss in colour. The transfer of electrons is compensated by the entrapment of cations (K^+, NH_4^+, Cs^+ or Rb^+) in the film. At high anodic potentials, Prussian Blue converts to its fully oxidised form (Prussian Yellow or Berlin Green). Probably the most popular electroanalytical application of PB modified electrodes is the selective determination of hydrogen peroxide by reduction in the presence of oxygen [19]. Indeed, Prussian Blue has been termed an "artificial peroxidase" due to its high activity and selectivity for hydrogen peroxide [20]. Its ability to electrocatalyse the reduction of H_2O_2 is seen in the electrochemical rate constant, which is higher for PB than for all other known H_2O_2 transducers (e.g., for 4 – 6 nmol/L/cm^2 of Prussian Blue, the electrochemical rate constant exceeds 0.01 cm/s (reduction) vs. 7 x 10^{-6} cm/s (oxidation) at platinum. The activity of Pt in H_2O_2 reduction is even lower). Hydrogen peroxide and glutamate were detectable at concentrations of 0.1 μmol/L (each) at an applied potential of –50 mV (vs. Ag/AgCl) at the Prussian Blue modified glassy carbon electrode [20]. A carbon fibre cone nanoelectrode modified by co-deposition of PB and glucose oxidase, and with an integrated reference electrode was applied for the determination of glucose in small sample volumes [21]. A Prussian Blue modified platinum microdisc electrode was shown to catalyse the oxidation of ascorbic acid, with an observed reduction in the overpotential for oxidation of 350 mV [22]. Flow injection amperometric detection at a PB film modified glassy carbon electrode provided a sensitive method for the oxidation of ascorbic acid, with a limit of detection of 2.49 μmol/L being achieved [23].

Following the discovery of the deposition and electroactivity of Prussian Blue, other metal hexacyanoferrates were deposited on various other electrode surfaces. These "Prussian Blue analogues" have been found to exhibit interesting properties and have been well-characterised by numerous groups, for example, mixed nickel-iron

hexacyanoferrates have been studied using abrasive stripping voltammetry [24], while scanning electrochemical microscopy was employed in the characterisation of cobalt hexacyanoferrate and nickel hexacyanoferrate deposited on gold and glassy carbon electrodes [25]. Other metal hexacyanoferrates that have been examined include cobalt hexacyanoferrate [26], nickel-cobalt hexacyanoferrate [16] and nickel-thallium hexacyanoferrate [27].

Nickel hexacyanoferrate modified electrodes have been widely used. One approach involved a metallic nickel and nickel hexacyanoferrate coated aluminium electrode, prepared by electroless deposition, which was used in the measurement of ascorbic acid down to levels of 2 μmol/L in pharmaceutical formulations [17,28]. The modified aluminium electrode catalyses the oxidation of ascorbic acid via surface layer mediated charge-transfer, with the oxidation process found to be independent of pH in the range 4–10. A nickel hexacyanoferrate modified microband gold electrode (0.1 μm x 1.0 cm) was employed in the catalytic oxidation of reduced nicotinamide adenine dinucleotide (NADH) [29]. Oxidation of NADH at conventional solid electrodes is highly irreversible and takes place at considerable overpotentials, resulting in electrode fouling. The nickel hexacyanoferrate modification layer considerably reduces this overpotential by ca. 340 mV, and permits determinations of NADH in the range 0.5 to 8.0 mmol/L. A nickel electrode chemically modified with an interfacial layer of nickel ferrocyanide was employed in the simultaneous sensing of sodium and potassium ions in aqueous solutions, human whole blood serum and human whole blood [30].

A cobalt hexacyanoferrate chemically modified electrode was employed in conjunction with microdialysis and liquid chromatography for the determination of glutathione and cysteine in rat brain, at concentrations of 2.5×10^{-4} mol/L and 1.0×10^{-6} mol/L, respectively, at an applied potential of +0.8 V [31]. A glassy carbon electrode, modified with the same inorganic layer was shown to provide a stable response for the oxidation of ascorbic acid [32]. The operational stability of ferrous (PB) and copper hexacyanoferrate modified platinum electrodes was investigated for the determination of hydrogen peroxide, with the latter providing the most stable, although lower, response [33]. A chromium hexacyanoferrate based electrode was employed in the determination of hydrogen peroxide [34]. However, the existence of such a layer has been disputed by Karyakin [18] (see Section 4.6.1). A mixed cobalt

and copper hexacyanoferrate modified carbon fibre microelectrode was used in the determination of hydrazine at low concentrations down to 0.5 μmol/L [35]. A graphite electrode, modified by mechanical immobilisation of copper hexacyanoferrate was used in the oxidation of ascorbic acid [36]. Oxidation of ascorbic acid was observed at both redox couples ($Fe(CN)_6^{4-}/Fe(CN)_6^{3-}$ and Cu^{+}/Cu^{2+}), with the former being employed in analytical determination of AA in pharmaceutical formulations due to its higher sensitivity. A screen-printed electrode modified with copper hexacyanoferrate and glucose oxidase, which showed a considerable decrease of the overvoltage for the reduction of enzymatically-liberated hydrogen peroxide, was employed in single-use glucose measurements [37].

Kulezsa's group have investigated the interesting concept of the formation of hybrid organic / inorganic films on a glassy carbon electrode and a gold covered foil in order to characterise the electrochemical and electrochromic features, respectively, of such films [38,39]. It was observed that during electrodeposition, alternate layers of polyaniline and nickel hexacyanoferrate were produced, with the resulting film showing reversible behaviour both electrochemically and electrochromically. Another interesting observation regarding metal hexacyanoferrates is the ability of ruthenium to stabilise polynuclear hexacyanometallate film electrodes [40,41]. Stabilisation was accomplished by cycling the metal (indium, nickel, cobalt or iron) hexacyanoferrate electrode in a solution containing ruthenium(III) chloride. Such further modified electrodes were found to exhibit better defined electrochemical and spectroscopic properties, improved redox rates and considerably enhanced stability.

4.4 Detection of Ascorbic Acid

The literature is replete with examples of the determination of ascorbic acid. Indeed, any preliminary search pertaining to ascorbic acid determination will certainly yield several thousand citations. Several excellent reviews describing the determination of ascorbic acid by various methods (high performance liquid chromatographic, photometric, non-spectrophotometric and flow injection methods) exist [42-45]. Obviously, it would be difficult to incorporate all of the literature relating to ascorbic acid in a brief literature survey such as this. Hence, only some of the more interesting

articles regarding the determination of ascorbic acid and published in recent years (1990 onwards) will be included.

4.4.1 Non-Electrochemical Methods

The accepted "gold standard" method of measuring ascorbic acid is by high performance liquid chromatography (HPLC) with ultraviolet (UV) or electrochemical (EC) detection [46 and references therein]. HPLC with UV detection (at 245 nm) was used to determine plasma ascorbic acid [46]. The method, as expected for HPLC, was sensitive and precise with good linearity and a limit of detection of 2 pmol/L, which was equivalent to a plasma concentration of 1.0 μmol/L. However, the use of such a method involved a quite complicated preparation procedure for the plasma samples. A similar method (HPLC with UV detection) was employed in the determination of ascorbic acid in serum samples from blood, which was collected from the stomach of cancer patients [13]. Again, this procedure involved complicated preparation (extraction, centrifugation, filtration, drying) and storage (at –70°C) of the samples. HPLC with a photo-diode detector (set at 243 nm) was employed in the identification and quantification of total vitamin C in fruit drinks [47]. This obviously represents a less complex matrix and hence these measurements are considerably less complicated. The procedure permitted detection of ascorbic acid down to concentrations of 0.5 μg/mL (2.84 μmol/L), with good reproducibility and a total analysis time of approximately 30 minutes. AA in beer was determined down to 0.2 mg/L using HPLC with electrochemical detection [48]. The electrochemical detection system consisted of a high efficiency porous graphite electrode (E_{app} = +40 mV) placed upstream of a glassy carbon amperometric electrode (E_{app} = +350 mV). The main advantages of using HPLC with either UV or EC detection include good sensitivity, accurate quantitative results, suitability for non-volatile or thermally fragile species and versatility. However, its distinct disadvantages involve the requirement for sample preparation (especially in the case of biological fluids), the quite low sample throughput and importantly, its inability to provide "real-time" results such as may be required in biological monitoring.

Titrations and spectrophotometric methods are also widely used in the determination of ascorbic acid. Indeed, titrimetric methods form one of the official methods and have been reported in different pharmacopoeias [43 and references

therein]. These involve the reduction of the blue coloured 2,6-dichlorophenol-indophenol dye to the colourless form upon addition of ascorbic acid. Vitamin C content in herbal juice (e.g. guava, lemon, sweet pepper) was quantified using direct titration with iodine, providing a simple and rapid method for AA determination with a limit of detection of 2.2 mg [49]. A sequential injection titration system based on the redox reaction between ascorbic acid and permanganate in acidic media was used in the determination of AA [50]. Detection is achieved by monitoring the decrease in colour intensity of permanganate (at 525 nm) upon reaction with ascorbic acid, and was applied in the measurement of AA in vitamin C tablets. A similar procedure was also carried out previously by the same authors [51]. In addition, they also performed flow injection conductometry, which was based on the neutralisation of ascorbic acid injected into a flowing ammonia solution yielding a change in conductivity.

A flow injection analysis (FIA) spectrophotometric method was developed for AA using its reducing action on Fe(III) in acidic medium and then following the spectrophotometric determination of the reduced iron by using 3-(2-pyridyl)-5,6-diphenyl-1,2,4-triazine-4′,4″-disulphonate as chromogenic reagent in pH 5.5 medium and monitoring the absorbance signal at 562 nm [52]. This procedure was sensitive with a limit of detection of 0.16 μmol/L and was employed in the determination of AA in pharmaceutical samples, urine and fruit juices. This method of indirect detection is often used in order to overcome the problem of interferences in the UV region. AA (down to 1.14 μmol/L) was determined in rat tissues using FIA spectrophotometric monitoring of the reaction of AA and iron(III)-2,2′-dipyridyl reagent and reading the absorbance at 510 nm [53]. These methods, although relatively simple and of low cost, are not, as mentioned for HPLC, suitable for real-time monitoring.

Gas chromatography-mass spectrometry (GC-MS) has also found some use in the determination of ascorbic acid. One group report the determination of ascorbate and dehydroascorbate in plant extracts, which involves their derivatisation with *tert.*-butyldimethylsilyl (TBDMS) to form TBDMS-ascorbate and TBDMS-dehydro-ascorbate, respectively, and analysis involving an isotope dilution assay using [$^{13}C_1$]ascorbate and [$^{13}C_1$]dehydroascorbate [54]. The limits of detection were 0.5 pg and 5 pg, respectively. Another GC-MS procedure involved the determination of AA in small (10 μL) volumes of plasma [55]. These methods are extremely selective and

allow determination of other components in sample matrices. However, disadvantages include the use of expensive equipment, the necessity for derivatisation, complicated sample preparation procedures and the inability to provide real-time measurements.

Ascorbic acid and uric acid were determined in blood from diabetic patients and from aqueous humour from patients with idiopathic acute anterior uveitis using capillary electrophoresis (CE) with UV detection (at 254 nm) [56]. CE was also used in the simultaneous analysis of the reduced and oxidised forms of ascorbate and glutathione in leaf tissues, with a detection limit of 28 μmol/L for AA [57]. These methods provide similar advantages to HPLC, but again, suffer from the same disadvantages.

4.4.2 Electrochemical Methods In Non-Physiological Media

As mentioned previously, due to the important role that ascorbic acid plays in human health, there exists a requirement, particularly in the food and pharmaceutical industries for reliable and simple techniques that would permit rapid monitoring of AA during production and quality control stages. Hence, numerous attempts have been made to develop a selective electrochemical sensor for AA determination in a variety of food and pharmaceutical based products. Electrochemical sensors are advantageous over the methods mentioned in Section 4.4.1 as they generally involve simple and inexpensive instrumentation and procedures, and offer selective determination of analytes without the need for difficult sample preparation (thus permitting analyses in complex matrices). In addition, low limits of detection can be achieved and in the case of microsensors, micro-volume and micro-location measurements are possible. A number of electrochemical methods involving the detection of ascorbic acid at metal-hexacyanoferrate modified electrodes were described in the previous section and hence will not be detailed here.

A copper-heptacyanonitrosylferrate film-modified carbon fibre microelectrode (CFME) (r = 5 μm to 20 μm), exhibiting good stability, was employed in the electrocatalysis of ascorbic acid in 0.1 mol/L KCl, with a decrease in overoxidation for AA of approximately 200 – 300 mV compared to a bare CFME [58]. It was determined that the overall process of oxidation changes from a diffusion controlled to a catalytic reaction controlled process with decreasing radius of the microelectrode.

Although hydrodynamic amperometry at +0.2 V provided a linear range of 8 x 10^{-6} mol/L to 2 x 10^{-3} mol/L, this sensor wasn't applied to any real samples. A screen-printed RuO_2 electrode was applied in the determination of AA at low operating potentials (100 mV vs. Ag/AgCl at pH 7.4) [59]. RuO_2 is commonly used in resistive pastes for screen-printing, and in this application, it shows selective oxidation of AA in the presence of uric acid and hydrogen peroxide. No limit of detection or application in a real sample was provided however.

Azide-based modifiers have been used in several applications as electrode modifiers. Amperometric detection of AA at +0.5 V (in pH 6.0 phosphate buffer) using a 1,5,8,12-tetraaza-2,4,9,11-tetramethylcyclotetradecinatonickel(II)-modified glassy carbon electrode provided a linear range of 5.0 x 10^{-7} mol/L to 1.0 x 10^{-3} mol/L and a detection limit of 4.7 x 10^{-7} mol/L [60]. The modified electrode was electroactive towards AA as the oxidation peak potential shifted 200 mV in the negative direction, while an increase in the peak current was also observed. This sensor was successfully applied in the determination of AA in beverages and was not affected greatly by the presence of interferents possibly found in such samples. A series of aza macrocyclic compounds were used to modify carbon paste electrodes [61]. Of these, 1,4,7-tritosyl-1,4,7-triazacyclononane, provided the best response and was used to assay the vitamin C content in multivitamin pharmaceutical preparations. Incorporation of zinc into the macrocyclic ring reduced the overpotential for AA oxidation by about 200 mV and an enhancement in peak current was observed, leading to a detection limit of 0.1 μg/mL (5.6 x 10^{-7} mol/L). The reaction was found to be initially diffusion controlled, but at faster scan rates the electron transfer became the rate-determining step, while the overall process was found to be typical of a catalytic process involving a chemical reaction followed by an electron transfer process. A CFME coated with an electrodeposited cobalt chelate of a tetra-*N*-methylpyridoporphyrazinocobalt was used in potentiometric detection of AA [62]. This modifier can be reduced electrochemically from its green aqueous acidic or neutral solution (Co(II)) at potentials more negative than approximately 400 mV (vs. SCE at pH 7) to form a purple electrically conducting film (Co(I)). This reaction can also be performed chemically by using an electron donor (AA in this case). Although the modified electrode is very stable, the overpotential for AA oxidation is only decreased by 80 mV and no increase in current is observed (although a low limit of

detection of 0.1 μmol/L is still achieved). Application of a Nafion® coating diminished the response to AA, but permitted the analysis of SH^- in the presence of AA.

Cobalt-based complexes have also been used in the modification of electrodes for the determination of ascorbic acid. A cobalt-salen (N,N'-bis(salicyclidene)-ethane-1,2-diamine) polymer modified electrode was observed to strongly electrocatalyse the oxidation of AA by causing a shift in the peak potential of AA approximately 400 mV in the negative direction (pH 6.8 phosphate buffer) [63]. This electrode was successfully applied in the measurement of AA in fruit juices. A carbon-epoxy composite electrode modified with the electron mediator cobalt phthalocyanine was used to determine AA in single- and multi-vitamin preparations [64]. The reaction was determined to be similar to that in [61]. Amperometric detection in pH 5 phosphate buffer (optimum pH) at an operating potential of +0.25 V (vs. SCE) provided a very low limit of detection of 0.65 ng/mL (3.69 nmol/L). Results obtained with the modified electrode compared favourably to those obtained using liquid chromatography with UV detection. The same modifier (cobalt phthalocyanine), was used in the modification of screen-printed electrodes [65]. The behaviour of this sensor towards ascorbic acid, glutathione and coenzyme A was investigated. For AA, amperometry at +0.30 V (vs. SCE at pH 5) provided a limit of detection of 5×10^{-8} mol/L, while the screen-printing process provided a reproducible electrode surface.

Casella and Guascito prepared a chemically modified electrode by electropolymerisation of aniline on a glassy carbon electrode, which showed good electrocatalytic properties towards ascorbic acid oxidation [66]. Although they determined that the maximum current response for AA was obtained at low pH (pH 1), they carried out further experiments at pH 5.4 in order to improve the stability of AA and to permit the usage of a lower operating potential for amperometric measurements. Flow injection measurements (at +350 mV) yielded a limit of detection of 1 μmol/L. Aniline was also used to modify glassy carbon and screen-printed electrodes for the measurement of AA in some pharmaceutical products (vitamin C tablets, cold / flu remedies) and fruit juices [67]. In contrast to [66], it was found that the optimum working buffer pH was between 6 and 7, with 6 chosen for further investigations. Also, a much lower operating potential of +100 mV was

applied here. Interestingly, the polyaniline layer was observed not only to act as a catalyst for the oxidation of ascorbic acid, but also as a permselective membrane.

Ferrocene and dimytristsoyl phosphatidylcholine (DMPC) in chloroform were cast onto a glassy carbon electrode and the resulting modified electrode exhibited good electrocatalytic activity for the oxidation of AA [68]. DMPC formed multi-bilayer films with ferrocene retained due to hydrophobic interaction. Ferrocene in the film exhibits a diffusion-controlled process, which implies that it acts as an electron shuttle between AA and the electrode. This modified electrode permitted the simultaneous determination of uric acid and AA, which have similar oxidation potentials at the bare GCE and hence the signals overlap. Another model of a biological membrane involved the casting of dipalmitoylphosphatidylcholine and rutin (a flavonoid glycoside, vitamin P) onto a glassy carbon electrode [69]. Rutin was observed to catalyse the oxidation of ascorbic acid, with a shift in the peak potential of approximately 100 mV in the negative direction compared to a bare GCE. The modification also permitted the simultaneous determination of ascorbic acid and uric acid.

Electropolymerisation of the amino acid glutamic acid at a glassy carbon electrode yielded a poly(glutamic acid) modified electrode which showed considerable catalytic effect towards AA oxidation, with a shift in peak potential of 400 mV in the negative direction obtained [70]. This modification was stable and at an applied potential of +0.30 V, the limit of detection was 4×10^{-8} mol/L. It was also possible to achieve a peak separation of 110 mV between dopamine and ascorbic acid. However, in this case equimolar concentrations of 1.5 mmol/L were employed, which differs considerably from real *in vivo* concentrations of dopamine (approximately 3000 fold less than AA). 3,4-Dihydroxybenzaldehyde was used to modify a glassy carbon electrode using two different techniques; electrochemical modification or modification by leaving the GCE in the modification solution at open circuit overnight, with the former being chosen as the optimum method [71]. A 250 mV shift in oxidation potential was achieved and the method employed in amperometric detection in flow injection analysis, with a limit of detection of 0.3 μmol/L. It was also possible to selectively determine AA in the presence of uric acid at this surface. A methylene green modified carbon paste electrode was shown to provide catalytic activity and stability towards AA oxidation in flow injection analysis by lowering the

oxidation overpotential by 400 mV [72]. The sensor was selective against a number of interferents, although cysteine and NADH did interfere due to their oxidation at the applied potential of 0.5 V. The limit of detection was 1 x 10^{-8} mol/L with a linear range from 5 x 10^{-7} mol/L to 1 x 10^{-3} mol/L. An indirect detection method based on the biamperometric detection of iodine, which was consumed upon reaction with AA in acidic medium [73]. The amount of iodine consumed in the redox reaction was proportional to the amount of AA in the sample (orange juice), and was detected at two (unmodified) platinum electrodes with a polarised potential of 100 mV applied between them.

The above examples are (mainly) based on the modification of carbon based electrodes. However, gold electrodes have also been widely used in the determination of ascorbic acid. Simple solid wire gold microdisc electrodes (core = 5 μm, o.d. = 15 μm) were used for the determination of vitamin C in fruit juices [74]. The microelectrodes were used in the determination of AA in buffered solutions, fruit juices and directly in fruit, with results comparing favourably with HPLC and iodometric results. However, the linear range was quite small (1 to 5 mmol/L) thus limiting these electrodes for usage in samples containing quite high concentrations of AA. A C_{60}-[dimethyl-(β-cyclodextrin)]$_2$ and Nafion® chemically modified electrode was prepared by solution casting on a gold electrode [75]. Reduction of the film in KOH solution resulted in a smoother and more homogeneous film (as determined by SEM) and a greatly improved response to AA, with a reduction in the overpotential of 350 mV, compared to a bare gold electrode. There was, however, a significant decrease in the peak potential (CV). The modified electrode was capable of selectively determining AA and dopamine, but as in [70], the concentration of dopamine (2 x 10^{-3} mol/L) was much higher than that typically observed in biological samples. No application to a real sample was provided.

A "self-doped" polyaniline layer was electrodeposited onto a gold microdisc electrode and the modified sensor used in the amperometric measurement of ascorbic acid in buffer solution (pH 7) at 0.1 V (vs. SCE) [76]. The film was prepared by the co-polymerisation of aniline and o-aminobenzoic acid, in which ionogenic groups, (COOH), were inserted into the polymer chain. The limit of detection was 2 μmol/L and the method was applied to the determination of AA in vitamin C tablets, with good correlation between the standard iodometric procedure obtained. A similar

procedure involving the electrochemical copolymerisation of 3,4-dihydroxybenzoic acid and aniline on a gold microdisc electrode was carried out by Sun *et al.* [77]. Again, the polymer was self-doped (with –COOH and –OH groups) and it exhibited stable electroactivity in neutral and weakly basic media. The overpotential for AA oxidation was reduced by 200 mV and a detection limit of 5×10^{-5} mol/L obtained with amperometry at +0.2 V in pH 7.0 buffer solution.

Platinum modified gold electrodes were prepared from conventional compact discs (CDs), by cutting the CDs into 12 slices, removing the protective polymeric films with nitric acid, and then applying a layer of electrodeposited platinum [78]. Thus prepared electrodes were much more sensitive to AA oxidation than the bare CD gold electrodes and were employed in the amperometric detection of AA (at +0.40 V in pH 4.0 medium) in flowing injection analysis, with a limit of detection of 7.8×10^{-8} mol/L. The procedure was applied to the determination of AA levels in some pharmaceutical formulations and compared well to the standard iodometric titration method. The same group applied an array of gold microelectrodes, obtained from an electronic integrated circuit chip, and modified by electrodeposition of platinum, palladium or a mixture of platinum + palladium, in conjunction with multivariate calibration for flow injection amperometric simultaneous determination of ascorbic acid, dopamine, epinephrine and dipyrone [79]. Each of the modified microelectrodes gave a response to each of the four analytes, with +0.5 V chosen as the optimum operating potential for amperometric analysis. The method was successfully applied in the simultaneous determination of all four analytes in buffered medium. Gold electrodes modified with cationic self-assembled monolayers of 2,2′-dithiobisethane-amine (CYST) and 6,6′-dithiobishexaneamine (DTH) were used in the determination of AA at levels down to 0.3 μmol/L [80]. The oxidation of AA at both modified electrodes occurred at potentials approximately 450 mV less negative than at the bare electrode, while the oxidation current was highest at the CYST modified gold electrode. It was also possible to employ this sensor in the simultaneous determination of AA and dopamine.

A batch injection analysis system employing an automatic mercury electrode in the amperometric mode at +0.23 V vs. Ag/AgCl in pH 4.8 acetate buffer solution was used for the determination of ascorbic acid in packed / canned tropical fruit juices, with a detection limit of 2.5 μmol/L [81]. A sessile mercury drop electrode

was used in flow injection amperometric determination of ascorbic acid at +0.19 V (vs. SCE) in pH 5.5 acetate buffer [82]. This electrode was also capable of simultaneously determining AA and dopamine. Although mercury electrodes can be used to determine AA, there are very few recent reports (1990 onwards) of AA determination at such electrodes. This is probably due to the difficulty in handling mercury electrodes, its well-known toxicity, and the inability to carry out *in vivo* analysis with these electrodes.

4.4.3 Electrochemical Methods in Physiological Media

Urinary ascorbate reflects recent dietary intake. Excretion in healthy individuals is estimated at > 50 mg/day [83]. Many electrochemical methods have been developed for measuring AA in urine. A glassy carbon electrode modified with diphenyl amine was used in the determination of AA in (diluted) urine samples at levels down to 0.2 mg/L (1.14 μmol/L) [84]. A conventional, unmodified rotating glassy carbon electrode in square wave or differential pulse mode was used for the simultaneous determination of AA and uric acid in urine [85]. Dilution of the urine sample was found to exert a significant effect on the potential for AA (and uric acid) oxidation e.g., for DPV at pH 5.1, in pure electrolyte (0.2 mol/L acetate buffer), E_p (AA) = 181 mV, in 1:205 diluted urine, E_p (AA) = 188 mV, 1:20 dilution E_p (AA) = 258 mV. The detection limit in urine was found to be 3 μmol/L.

A similar array of gold microelectrodes to those in [79], and modified with palladium, was employed in flow injection analysis-amperometric determination of ascorbic and uric acids in urine [86]. An operating potential of +0.55 V (vs. Ag/AgCl in 0.05 mol/L monochloroacetic acid) was chosen for AA measurements and a linear range of 0.44 to 2.64 mg/L (2.50 to 15.0 μmol/L) and a sensitivity of 53.2 nA·L/mg were obtained. Glutamic acid was used in the covalent modification of a glassy carbon electrode [87]. The modified electrode was used in the simultaneous determination of ascorbic acid and uric acid, and was observed to exhibit a strong electrocatalytic effect on both analytes, reducing their oxidation overpotentials by approximately 0.2 V and 0.3 V, respectively. The detection limit for ascorbic acid was 0.92 μmol/L and the sensor was successfully applied in AA measurements in diluted urine (1:8.8 dilution).

Ascorbic acid concentrations in the brain are believed to be in the order of 100 to 500 μmol/L [88]. AA has a range of general antioxidant and specific neurochemical functions, and can function as a cofactor for the enzymatic conversion of dopamine to norepinephrine by dopamine-β-hydroxylase. Hence, its concentration and secretion have been studied extensively. Direct electrochemical methods (*in vivo* voltammetry) provide the most convenient tools for these studies, and generally involve the use of carbon paste or carbon fibre electrodes. The former have been found advantageous over the latter in *in vivo* measurements in brain, as the presence of lipids in the sample could reverse poisoning caused by protein [89]. The lipid molecules appeared to have a cleaning effect on the carbon paste electrodes (CPEs) by removing pasting oil and adsorbed proteins from the surface of the electrode. It should be noted that the carbon fibre electrodes employed in this work were unmodified (just activated). The same group carried out characterisation of CPEs *in vitro* for simultaneous amperometric measurement of changes in oxygen and ascorbic acid concentrations *in vivo* [90]. Lipid treated CPEs (prepared by contact of the CPE with brain tissue) were found to be selective (*in vitro*) for AA and O_2 measurements, while *in vivo* (in rat brain) experiments were successful in monitoring the response of the rat (in terms of changes in AA and O_2 in the brain) to the "tail pinch" stimulus. Extracellular brain ascorbate was determined *in vivo* in rats using a carbon paste electrode held at an operating potential of +250 mV [91]. The CPE was attached to a microdialysis probe (total diameter 0.8 mm) through which various concentrations of AA were infused. The sensor responded to changes observed when the rats were stimulated (moving) and to additions (perfusions) of ascorbate solution. Ascorbic acid (and some other analytes) were monitored in patients suffering from two different forms of epilepsy using *in situ* microvoltammetry at a carbon paste microelectrode [92]. AA was determined in only one of the patients at a concentration of 0.1 μmol/L.

Carbon fibre electrodes, due particularly to their small size, have also been widely used in *in vivo* analyses. A poly(sulphosalicyclic) acid modified CF electrode (d = 15 μm) was used for determining AA (and 5-hydroxyindole-3-acetic acid) in rat striatum [93]. *In vitro* experiments using DPV showed the electrocatalytic effect of the modification layer on ascorbic acid oxidation, by reducing the oxidation overpotential to –0.03 V (vs. Ag/AgCl at pH 7.4). AA concentration in *in vivo*

measurements was 215 ± 5 μmol/L. Cahill and Wightman monitored the simultaneous secretion of ascorbate and catecholamine from individual bovine medullary cells using two CF electrodes, one untreated and encased in polymer and the other treated by electrochemical oxidation [94]. The untreated CF and treated sensors were held at +0.65 V and +0.05 V (both vs. SSCE) and were used for the detection of catecholamine and ascorbate, respectively. Experiments with the medullary cells revealed that both analytes are released from different cell compartments.

The above examples deal with analyses in urine and brain fluid only. Despite a thorough search of the literature, there does not seem to be any report of a sensor (macro- or micro-) for direct determination of ascorbic acid in gastric juice.

4.5 Selective Determination of Ascorbic Acid in Gastric Juice at a Nickel Oxide,Ruthenium Hexacyanoferrate-Modified Carbon Fibre Cylinder Microelectrode

4.5.1 Experimental

4.5.1.1 Apparatus

Cyclic voltammetric and amperometric measurements were performed using a modular electrochemical system (Autolab, Eco Chemie, The Netherlands), equipped with a potentiostat PGSTAT10 and driven by GPES 4.8 software (Eco Chemie). For bulk voltammetric experiments, a bare or metal-hexacyanoferrate modified carbon fibre cylinder microelectrode (CFCME) (7 μm in diameter) served as the working electrode, with an Ag/AgCl(satd. KCl) and a platinum wire acting as the reference and auxiliary electrodes, respectively. A glassy carbon electrode was used as substrate for optical microscopy. A laboratory-made glassy carbon disc electrode with removable GC disc served as substrate for SEM and AFM experiments. A laboratory-made dip-coating device was employed for coating of the modified carbon fibre with cellulose acetate.

Scanning electron microscopy (SEM) with energy dispersive x-ray analysis (EDX) experiments were performed using a Hitachi S 3000N Scanning Electron

Microscope (Hitachi, Japan), equipped with a Link Isis Energy Dispersive Spectrometer (Oxford Instruments, UK). Atomic force microscopy (AFM) was carried out employing a Digital Instruments Dimension 3100 Atomic Force Microscope (Veeco).

4.5.1.2 Reagents and Solutions

Ascorbic acid, nickel(II) sulfate-hexahydrate, iron(III) nitrate-nonahydrate, cobalt(II) nitrate-hexahydrate and glucose were obtained from Kemika (Zagreb, Croatia). Chromium(III) nitrate-nonahydrate was obtained from Merck. Ruthenium(III) chloride was obtained from Sigma (Germany), while potassium hexacyanoferrate (III) was obtained from Fluka (Buchs, Switzerland). Potassium hexacyanocobaltate was obtained from Aldrich (Dorset, UK). 5% Nafion® in lower aliphatic alcohol solution and cellulose acetate were purchased from Aldrich (Milwaukee, USA). Protein standard, lyophilized (1.32 mg/mL protein) was obtained from Bio-Rad, California, USA. All chemicals employed in this work were of analytical-grade purity and were used as received. Gastric juice was obtained from a healthy volunteer. Water used to prepare all solutions was first de-ionized and then further purified via a Milli-Q unit (Millipore, Bedford, MA, USA).

Ascorbic acid standard solutions (0.1 mol/L) were prepared daily by appropriate dilution and were stored in a refrigerator when not in use.

4.5.1.3 Fabrication of Carbon Fibre Cylinder Microelectrodes

The carbon fibres were initially cleaned by sonication for 5 minutes each in acetone, 1:1 (v/v) nitric acid and in de-ionised water. The carbon fibres were then left to dry in air and stored in a closed box. A cleaned single carbon fibre (7 μm in diameter, 2-3 cm in length, Goodfellow Co., Oxford, UK) was attached to a copper wire using silver paint (SPI Supplies, West Chester, PA, USA) and inserted into a glass capillary tube (7 cm in length, Euroglass, Ljubljana, Slovenia). A fine-pulling technique employing a microelectrode puller (PP-830, Narishige, Tokyo, Japan), was applied for a stepwise thinning of the glass capillary with a concurrent direct sealing of the glass / fibre interface leaving 2-4 mm of the carbon fibre protruding at the pulled end. Following the pulling step, the stem end of the glass capillary was sealed by casting a drop of non-conducting epoxy resin. Finally, the exposed carbon fibre was cut using a

microsurgical scalpel blade (approximately 200-500 μm) to a length of approximately 1 mm. The resulting CFCMEs were inspected optically using an inverted microscope (Eclipse, Nikon, Tokyo, Japan) and electrochemically (in 1 x 10^{-3} mol/L ferricyanide in 0.1 mol/L KCl solution). Such prepared CFCMEs were stored in a sealed box prior to use. Figure 1.16 in Chapter One shows a schematic of a CFCME, two photographs of the CFCME and an SEM micrograph of the junction between the carbon fibre and the glass housing.

4.5.1.4 Modification of CFCMEs with Metal Hexacyanoferrates

Prior to modification, a CFCME was electrochemically pretreated in acetone and 1:1 (v/v) nitric acid and finally in 0.1 mol/L KCl solution by cycling between 0 and +1.0 V at a scan rate of 100 mV/s until a steady state current-voltage profile was obtained. The CFCME was thoroughly rinsed with doubly de-ionised water after each step and was then ready for use.

Preliminary experiments involved the deposition of mixed metal hexacyanoferrates on the CFCMEs. Iron-chromium hexacyanoferrate was grown on a CFCME in a 0.1 mol/L KCl solution containing 5 x 10^{-4} mol/L potassium hexacyanoferrate (III), 1 x 10^{-4} mol/L iron(II) nitrate and 1 x 10^{-4} mol/L chromium(III) nitrate by a continuous scanning of the potential between 0 and +1.0 V at a scan rate of 100 mV/s until the desired number of coatings were achieved. Iron-chromium (1-3) hexacyanoferrate was deposited using the above solution, but with a $Cr(NO_3)_3$ concentration of 3 x 10^{-4} mol/L.

Iron-nickel hexacyanoferrate, iron-ruthenium hexacyanoferrate and cobalt-ruthenium hexacyanoferrate were deposited from 0.1 mol/L solutions containing 5 x 10^{-4} mol/L $K_3Fe(CN)_6$ and 1 x 10^{-4} mol/L of the respective salts (Fe; $Fe(NO_3)_3$, Ni; $NiSO_4$, Ru; $RuCl_3$ and Co; $Co(NO_3)_2$) in 1:1 ratios. Deposition of iron-ruthenium hexacyanocobaltate was accomplished using a solution consisting of 5 x 10^{-4} mol/L $K_3Co(CN)_6$, 1 x 10^{-4} mol/L $Fe(NO_3)_3$ and 1 x 10^{-4} mol/L $RuCl_3$. The same electrochemical procedure as above was applied.

4.5.1.5 Modification of CFCMEs with NiO,RuHCF and Variants

For the two step deposition of nickel oxide,ruthenium hexacyanoferrate (NiO,RuHCF), the CFCME was galvanostatically activated by immersion in 1.14 mol/L $NiSO_4.6H_2O$ in 1.18 mol/L H_3BO_3 aqueous solution and application of a current of 0.4 μA for 10 s (corresponding to an applied current of 0.002 A/cm^2), whereupon the potential observed was approximately 2.3 V. The ruthenium hexacyanoferrate (RuHCF) film was electrochemically grown on the nickel oxide modified CFCME in a modification solution consisting of 0.1 mol/L KCl containing 4×10^{-3} mol/L HCl, 2×10^{-4} mol/L $K_3[Fe(CN)_6]$, and 1×10^{-4} mol/L $RuCl_3$ by cycling the potential between 0.0 and +1.0 V at a scan rate of 100 mV/s until a desired coverage was obtained (22 CV runs unless otherwise stated).

The nickel oxide modified electrode was obtained by performing the first stage of the previous method (i.e. galvanostatic activation alone). Nickel hexacyanoferrate (NiHCF) (a), RuHCF (b) and nickel-ruthenium hexacyanoferrate (NiRuHCF) (c) were obtained by cycling the CFCME in a solution consisting of 0.1 mol/L KCl containing 4×10^{-3} mol/L HCl, 2×10^{-4} mol/L $K_3[Fe(CN)_6]$, and 1×10^{-4} mol/L $RuCl_3$ (a) or 1×10^{-4} M $NiSO_4$ (b) or both in a 1:1 ratio (c) and applying the same electrochemical procedure as above .

4.5.1.6 Further Modification of NiO,RuHCF-Modified Electrode

Nafion® or cellulose acetate protective membranes were progressively developed on the surface of the NiO,RuHCF modified CFCME by immersing the modified CFCME several times into a 1% Nafion® alcoholic solution or 1:1 (v/v) cyclohexanone-acetone solution containing 1% cellulose acetate, respectively, using a laboratory made dip-coating device (speed of dipping = 0.034 cm/s). After each dipping, the tip was allowed to dry in air at room temperature for approximately 10 minutes. Six layers of cellulose acetate were employed for the determination of ascorbic acid in gastric juice.

4.6 *Results and Discussion*

4.6.1 Some Preliminary Results for Ascorbic Acid Oxidation at Metal Hexacyanoferrate Modified CFCMEs

The interesting and positive results obtained for various analytes at metal hexacyanoferrate modified electrodes (Section 4.3), and the apparent requirement for a sensor suitable for direct measurements of ascorbic acid in gastric juice (Section 4.2.3), prompted an investigation on the development of such a sensor based on these modification layers. Although many such layers were tested in this study, none approached the desired properties of a sensor for ascorbic acid in acidic medium. Some of the preliminary results obtained in this study are presented in this section. One such layer consisted of iron and chromium hexacyanoferrate (FeCrHCF), which is shown in Figure 4.4 A, in addition to the response of ascorbic acid at this modified CFCME (Figure 4.4 B).

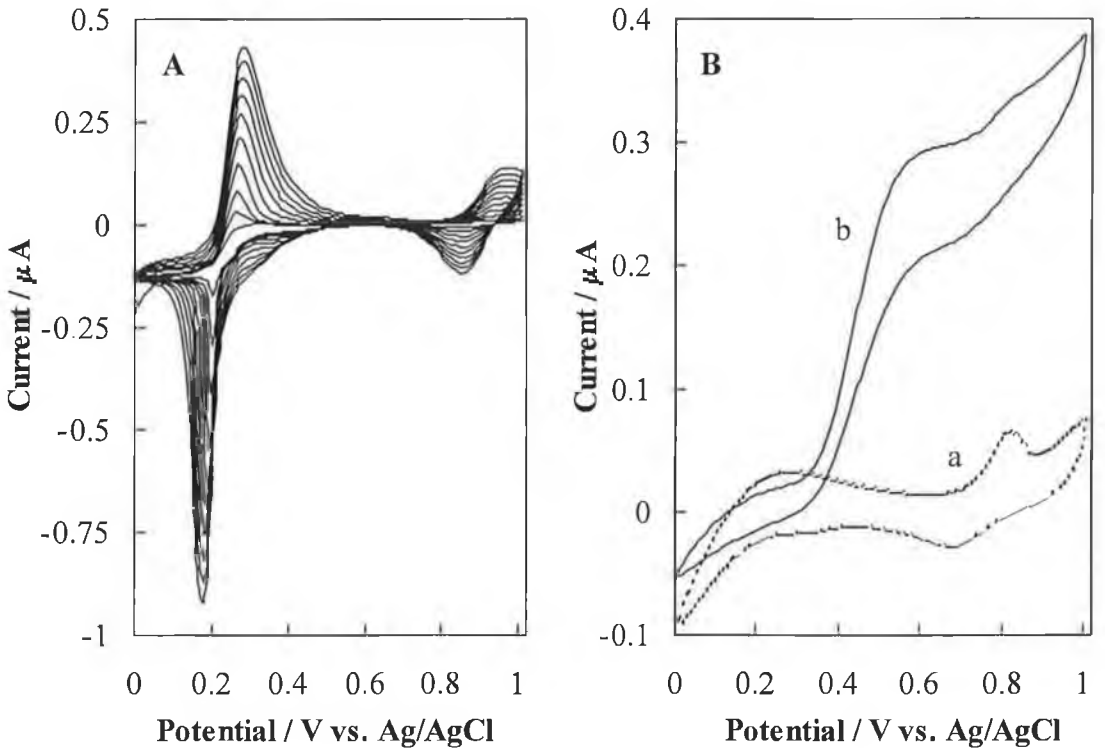

Figure 4.4: (A) Repetitive cyclic voltammograms at the CFCME in a solution containing 0.1 mmol/L $Fe(NO_3)_3$ + 0.1 mmol/L $Cr(NO_3)_3$ + 0.5 mmol/L $K_3(FeCN)_6$ in 0.1 mol/L KCl; scan rate 100 mV/s; scan range 0.0 to +1.0 V; and (B) Cyclic voltammograms of (a) 0.01 mol/L HCl and (b) a + 1 mmol/L ascorbic acid.

Although chromium hexacyanoferrate has been reported for the determination of hydrogen peroxide [34], this existence of such a layer has been disputed by Karyakin [19], who claimed that it was more likely that Prussian Blue layers had been synthesised during the deposition step. It seems likely that this has also occurred in the experiments here, as the redox couples present at approximately +0.25 V and +0.90 V (Figure 4.4 A) were quite similar to those found for PB (both in terms of potential and peak shape) [19]. In addition, it has been found that Cr^{3+} ions do not give any appreciable precipitate with either ferricyanide or ferrocyanide ions [19]. And, since during deposition in this case, the applied potential was always higher than 0 V, Cr^{3+} cannot be reduced to Cr^{2+} as the $Cr^{3+/2+}$ redox potential is –0.6 V. Ascorbic acid was, as expected (considering reports of its measurement at PB modified electrodes [23]), oxidisable at this surface (Figure 4.4 B), but there was no reduction in the overpotential for the oxidation reaction and hence, this surface was deemed to show no advantage over the performance of a bare carbon fibre electrode.

During investigations involving the mixed metal hexacyanoferrates, the ratios of the various metals in the deposition solution were also varied in order to assess if this offered any advantage (i.e. reduction in oxidation overpotential) for determination of ascorbic acid. Figure 4.5 shows an example of such an experiment, in which the ratio of iron to chromium was changed to 1:3. It was obvious here that the formation of the film was somewhat different to that in Figure 4.4. The well-defined couple at approximately +0.25 V in Figure 4.4 has been replaced by a different, ill-defined couple with a mid-potential of approximately +0.16 V. The other couple was similar in shape to that obtained in Figure 4.4, although the mid potential shifted to approximately +0.70 V. However, this film was still similar to that of Prussian Blue, and suggested that just as in the previous case, Prussian Blue and not iron-chromium hexacyanoferrate was deposited. It seemed that an increased level of chromium in the solution exerted some effect upon the deposition of the film, possibly by incorporation of some small amount of the smaller chromium ions (Cr = 0.65 Å; Fe = 0.75 Å) into the film structure. The oxidation potential for ascorbic acid actually increased with this film (Figure 4.5 B), which is undesirable as interference from other components in gastric juice would be correspondingly increased.

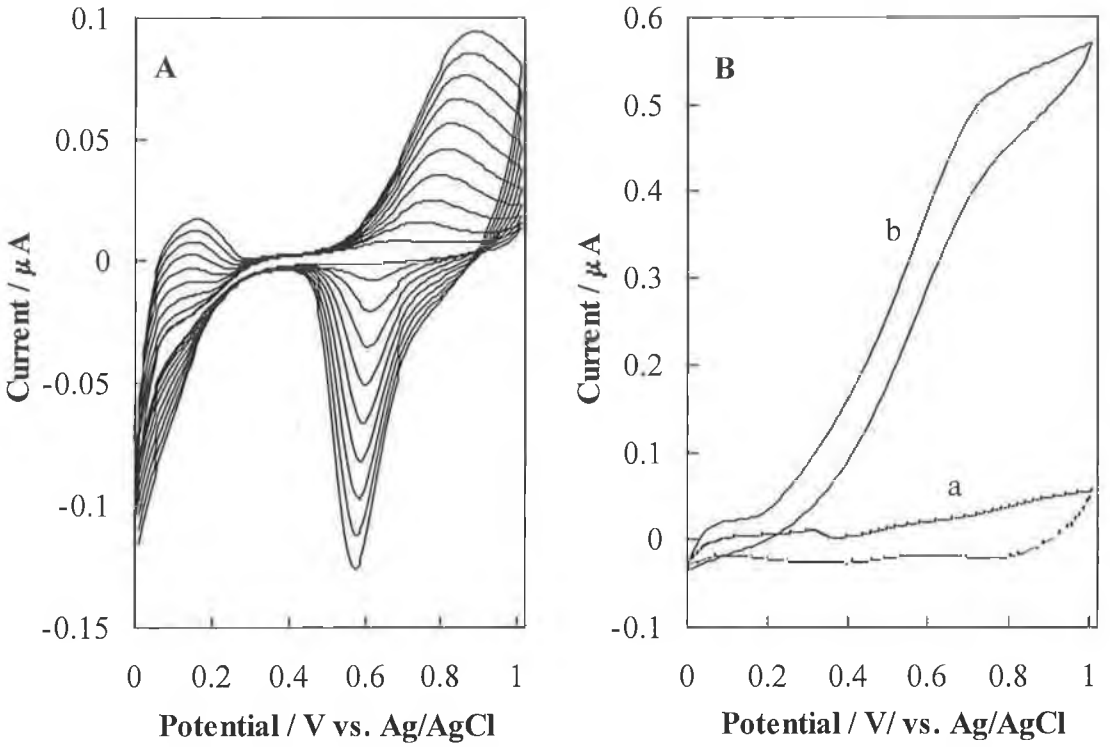

Figure 4.5: (A) Repetitive cyclic voltammograms at the CFCME in a solution containing 0.1 mmol/L $Fe(NO_3)_3$ + 0.3 mmol/L $Cr(NO_3)_3$ + 0.5 mmol/L $K_3(FeCN)_6$ in 0.1 mol/L KCl; scan rate 100 mV/s; scan range 0.0 to +1.0 V; and (B) Cyclic voltammograms of (a) 0.01 mol/L HCl and (b) a + 1 mmol/L ascorbic acid.

As mentioned in Section 4.3, electrodes modified with nickel hexacyanoferrate layers have found applications in the detection of several analytes (ascorbic acid, potassium cations). Reddy *et al.* reported the electrochemical behaviour of mixed iron-nickel hexacyanoferrates on a graphite electrode, in which they determined that mixed crystals of Fe-Ni hexacyanoferrate were formed, with the nitrogen-coordinated iron being replaced by nickel in the lattice [24]. Figure 4.6 shows the deposition of an iron-nickel hexacyanoferrate film, and the oxidation of ascorbic acid at this electrode. The shape of the cyclic voltammogram in Figure 4.6 A reveals that it is likely that a film other than Prussian Blue has been deposited. The formal potentials of the largest couple – at approximately +0.67 V for a 1:3 mixture of Fe:Ni and +0.78 V for 1:1 Fe:Ni (Figure 4.6 A inset), correspond to those obtained by Reddy at +0.64 V and +0.74 V, respectively. The slight differences in potential may be attributed to differences in the modification solutions, or to the use of different electrode surfaces (graphite and carbon fibre).

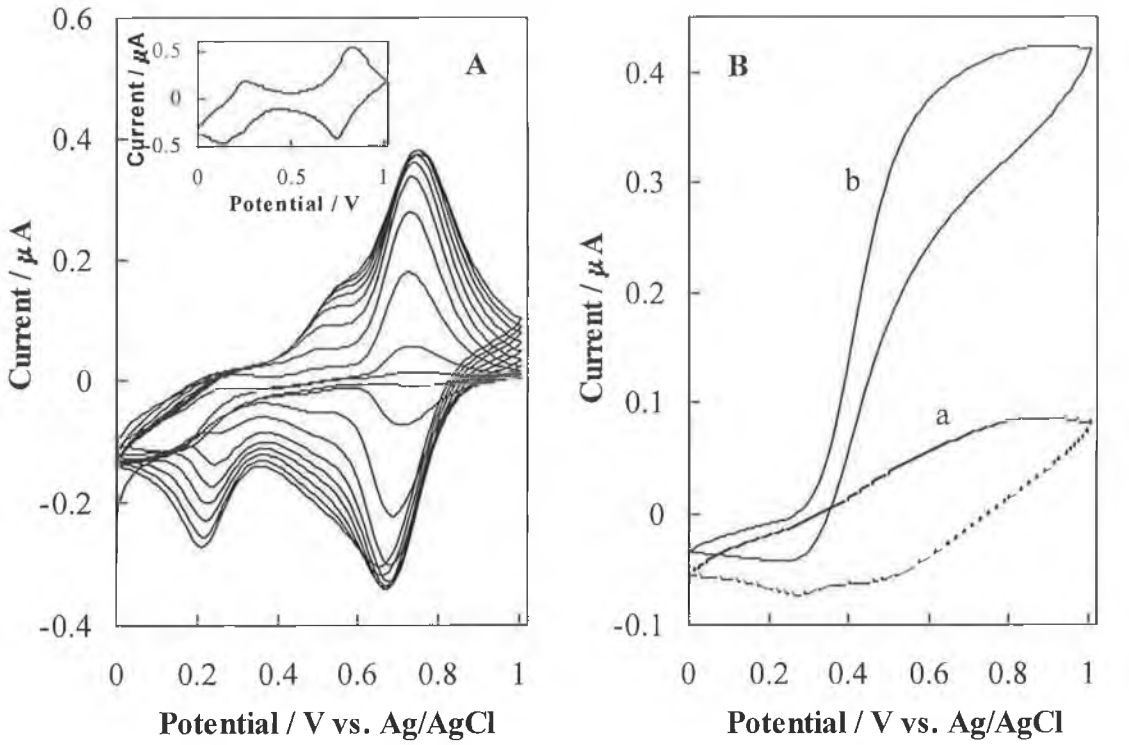

Figure 4.6: (A) Repetitive cyclic voltammograms at the CFCME in a solution containing 0.1 mmol/L $Fe(NO_3)_3$ + 0.3 mmol/L $NiSO_2$ + 0.5 mmol/L $K_3(FeCN)_6$ in 0.1 mol/L KCl; scan rate 100 mV/s; scan range 0.0 to +1.0 V; inset: 10^{th} cycle at the CFCME of a solution containing 0.1 mmol/L $Fe(NO_3)_3$ + 0.1 mmol/L $NiSO_2$ + 0.5 mmol/L $K_3(FeCN)_6$ in 0.1 mol/L KCl; scan rate 100 mV/s; scan range 0.0 to +1.0 V; and (B) Cyclic voltammograms of (a) 0.01 mol/L HCl and (b) a + 1 mmol/L ascorbic acid at Fe:Ni (1:3) HCF modified CFCME.

From Figure 4.6, it was evident that besides having Fe and Ni in definite ratios, there also existed a certain amount of pure Prussian Blue, as evidenced by the electrochemical response of low-spin iron of PB separate from the signal for the mixed compound. No such couple was present in a cyclic voltammogram of nickel hexacyanoferrate (not shown). In addition, it was observed that increasing the proportion of nickel in the film caused a peak at approximately +0.55 V, with a corresponding decrease in the oxidation signal at approximately +0.29 V. This may be due to the replacement of this low-spin iron by nickel ions as they have similar ionic radii (Fe 0.75 Å, Ni 0.78 Å). Figure 4.6 B shows results obtained for ascorbic acid oxidation at an iron-nickel hexacyanoferrate (in a 1:3 ratio) modified CFCME.

This modification layer did not produce any shift in the overpotential for ascorbic acid oxidation, although it was evident that the modified CFCME was active towards AA.

Figure 4.7 A shows repetitive cyclic voltammograms obtained during the formation of iron-ruthenium hexacyanoferrate. Such a film was previously reported by Cataldi *et al.* [95]. However, it seems that the film displayed in Figure 4.7 did not correspond to iron-ruthenium hexacyanoferrate, as the cyclic voltammograms differed considerably from those found in [95].

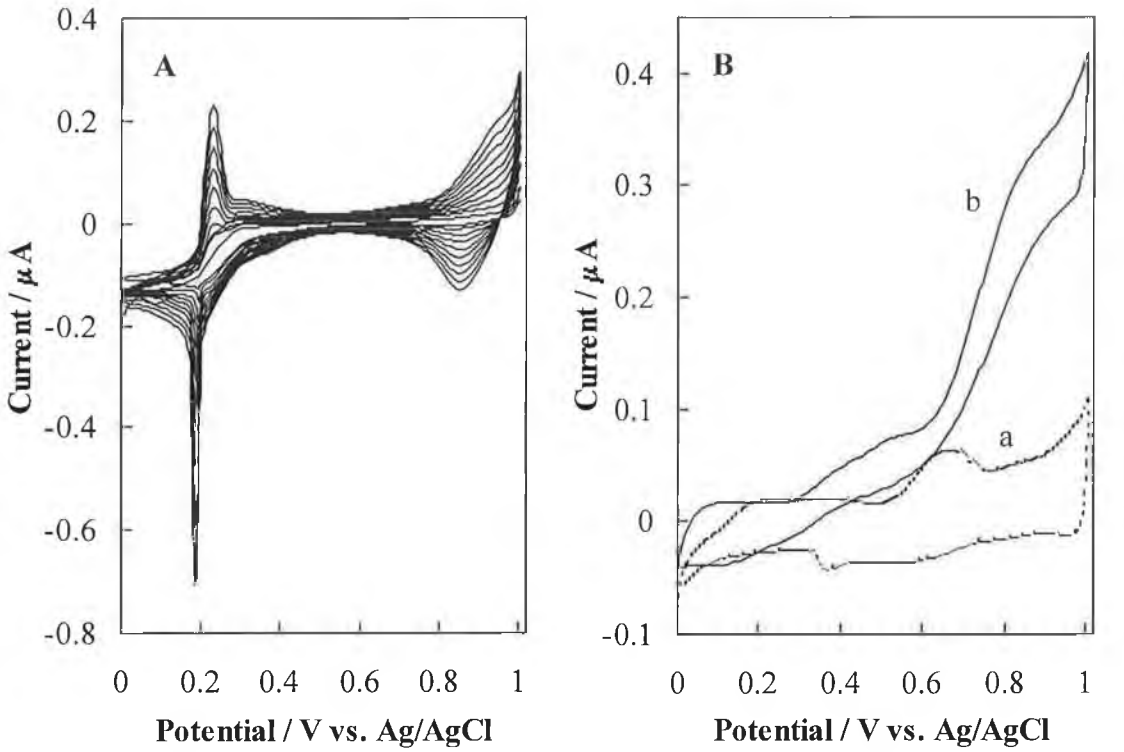

Figure 4.7: (A) Repetitive cyclic voltammograms at the CFCME in a solution containing 0.1 mmol/L $Fe(NO_3)_3$ + 0.1 mmol/L $RuCl_3$ + 0.5 mmol/L $K_3(FeCN)_6$ in 0.1 mol/L KCl; scan rate 100 mV/s; scan range 0.0 to +1.0 V; and (B) Cyclic voltammograms of (a) 0.01 mol/L HCl and (b) (a) + 1 mmol/L ascorbic acid.

This difference may be attributed to the different potential ranges employed during cycling and differences in the pH of the deposition solution (it was probable that the solution employed in Figure 4.7 A was not sufficiently acidic, leading to hydrolysis of the ruthenium ions). It may assumed, however, that the deposited film was not solely pure Prussian Blue from the presence of a feature at approximately +0.30 V, which is absent in PB and also the difference in the redox couple at +0.89 V. In addition, the

markedly different behaviour of ascorbic acid at this film, compared to that at pure Prussian Blue, confirmed the presence of a mixed-metal hexacyanoferrate film. It is possible that Fe ions (0.75 Å) have been replaced to some extent by the smaller Ru ions (0.65 Å). Again, as with the other films, no shift in the overpotential for AA oxidation is observed at this particular modification layer.

Although cobalt hexacyanoferrate (CoHCF) modified electrodes have been used in the determination of a variety of analytes (e.g., ascorbic acid, glutathione), their stability has been disputed and ruthenium has been employed in their stabilisation [41]. The resulting ruthenium-modified CoHCF thin film electrode was shown to be extremely stable. Mixed metal hexacyanoferrates incorporating cobalt as one of the metal ions have also been reported, e.g., cobalt-copper [35], nickel-cobalt [96]. Considering these reports, the possibility of using a ruthenium-cobalt hexacyanoferrate (RuCoHCF) modified electrode for the determination of ascorbic acid under acidic conditions was investigated, the results of which are displayed in Figure 4.8.

The cyclic voltammograms of the RuCoHCF film exhibited remarkably similar behaviour to that observed for CoHCF films reported by several authors. The presence of two redox couples at approximately +0.51 V and +0.70 V were comparable to those found by Chen [97] of +0.49 V and +0.61 V (the supporting electrolyte here was KNO_3). The shapes of the CVs were also very similar to those obtained by Vittal *et al.* for a cobalt hexacyanoferrate + CTAB modified electrode [96]. Considering the similarity between CoHCF and the proposed RuCoHCF film, it seems likely that no Ru (or only a small amount) was incorporated into the lattice. The couple observed at approximately +0.23 V in the first scan may be attributable to the reduction of $Fe^{III}(CN)_6^{3-}$ in aqueous solution. The resulting $Fe^{II}(CN)_6^{4-}$ then reacts with Co^{2+} (or possibly Ru^{2+}) to yield a deposit of cobalt (II) hexacyanoferrate on the electrode surface, this process being repeated during each successive scan (as seen by the disappearance of the couple at approximately +0.23 V and the growth of the other redox peaks). The resulting film shows a strong electrocatalytic effect for the oxidation of ascorbic acid, as evidenced by the enhancement of the anodic current and simultaneous decrease in the cathodic current. Similar to the other films reported here, the film exerted no effect on the overpotential for the oxidation reaction. The redox couple present at approximately +0.85 V may be due to the second couple in

Figure 4.8 A. The potential shift may be caused by the difference in pH of the working solution.

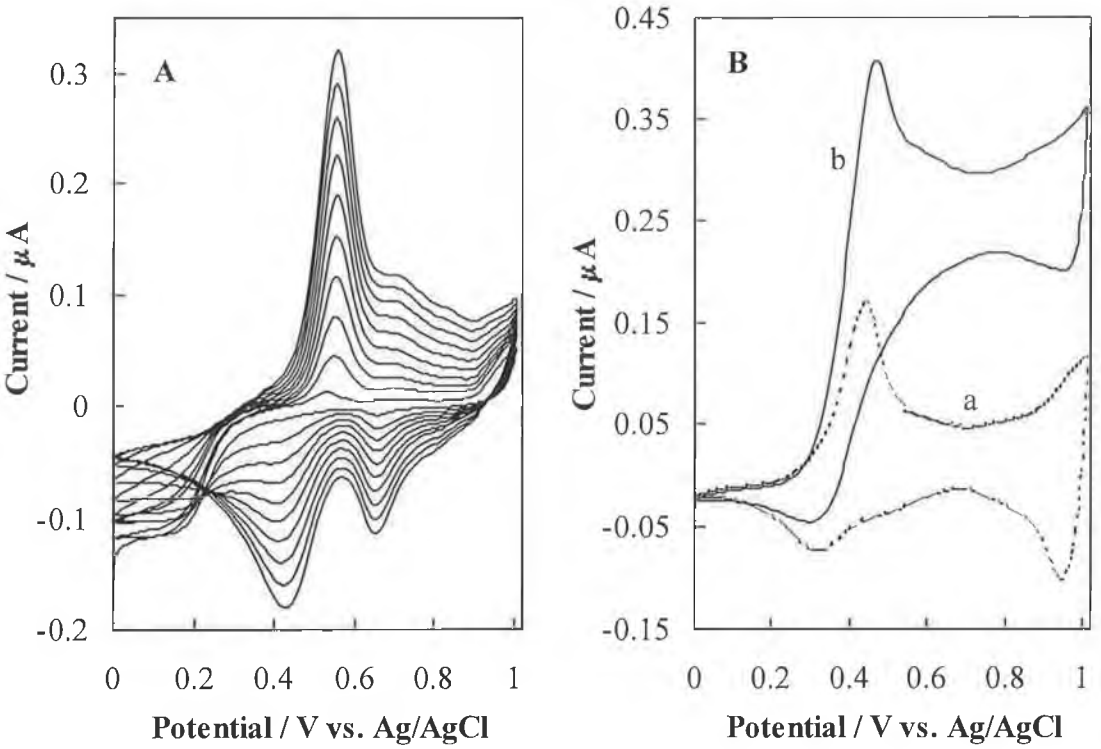

Figure 4.8: (A) Repetitive cyclic voltammograms at the CFCME in a solution containing 0.1 mmol/L $RuCl_3$ + 0.1 mmol/L $Co(NO_3)_2$ + 0.5 mmol/L $K_3(FeCN)_6$ in 0.1 mol/L KCl; scan rate 100 mV/s; scan range 0.0 to +1.0 V; and (B) Cyclic voltammograms of (a) 0.01 mol/L HCl and (b) (a) + 1 mmol/L ascorbic acid.

The possibility for modification of the CFCME with a different metal hexacyanometalate was also considered. Here, an attempt was made to deposit a mixed metal hexacyanocobaltate (HCCo) film, again with a view to reducing the overpotential for ascorbic acid oxidation. The results are displayed in Figure 4.9. It is evident from this figure that little or no deposition of the iron-ruthenium hexacyanocobaltate film occurred, as there was no film growth upon successive cycling of the CFCME in the modification solution. In addition, the behaviour of AA at the CFCME was almost identical to that observed for a bare carbon fibre electrode, indicating again, that no film was deposited. Further experiments employing hexacyanocobaltate were abandoned and films based on hexacyanoferrate further investigated.

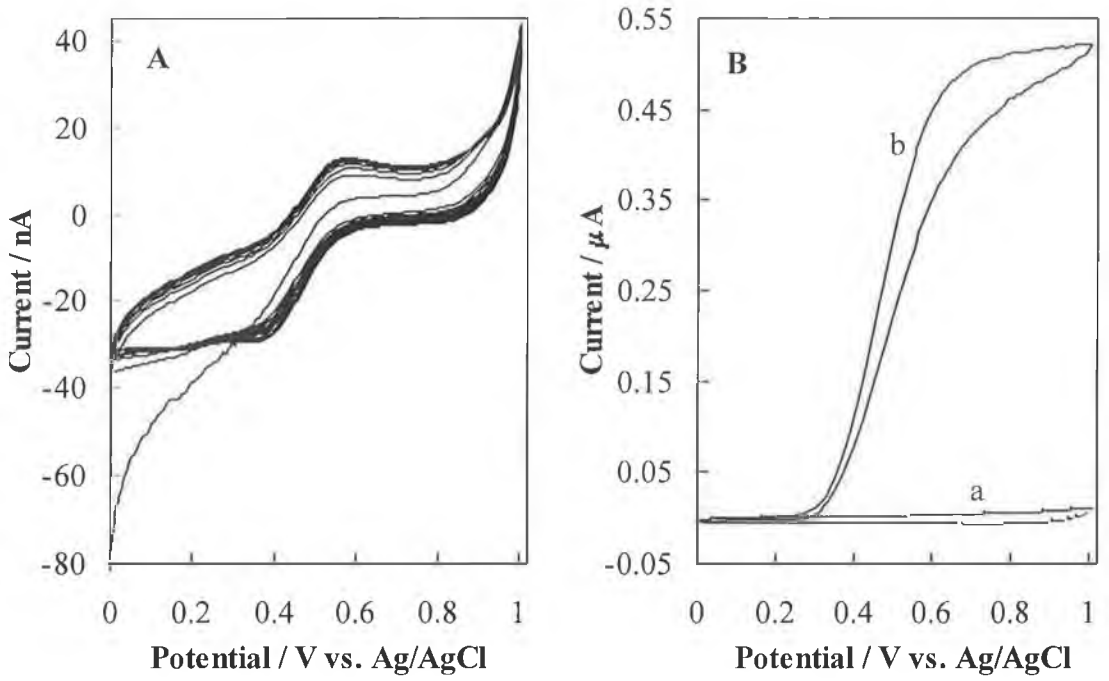

Figure 4.9: (A) Repetitive cyclic voltammograms at the CFCME in a solution containing 0.1 mmol/L $Fe(NO_3)_3$ + 0.1 mmol/L $RuCl_3$ + 0.5 mmol/L $K_3Co(CN)_6$ in 0.1 mol/L KCl; scan rate 100 mV/s; scan range 0.0 to +1.0 V; and (B) Cyclic voltammograms of (a) 0.01 mol/L HCl and (b) (a) + 1 mmol/L ascorbic acid.

An alternative method for the formation of a mixed metal hexacyanoferrate film was investigated, which involved the deposition of the metals in separate steps. An interesting procedure was employed by Sinha *et al.*, in which they found that several species of the form $[M(CN)_5L]^{n-}$ (M = Fe, Ru) could be immobilised on a Ni electrode under either anodising electrochemical or chemical conditions, producing surfaces with a high degree of stability [98]. Considering this and the positive results obtained with nickel-based metal hexacyanoferrate electrodes [17,28,30], an investigation into the use of a mixed metal hexacyanoferrate consisting of ruthenium hexacyanoferrate deposited on a nickel-based electrode for the oxidation of ascorbic acid, was prompted.

4.6.2 Preparation and Optimisation of NiO,RuHCF Modified Microsensor

As mentioned in the previous section, the mixed nickel oxide,ruthenium hexacyanoferrate film was deposited onto a CFCME in two separate steps. A clean CFCME was galvanostatically activated in nickel solution, while the RuHCF layer

was subsequently applied using multiscan cyclic voltammetry. In order to verify that this procedure provided the optimum modification layer considering the response to ascorbic acid oxidation, various other modification layers consisting of one or both of the components (Ni and RuHCF) were tested for their response to 1 x 10^{-3} mol/L AA. These results are presented in Figure 4.10, where the letters (a)-(e) represent the signals obtained when: (a); the procedure as outlined in Section 4.5.1.5 was employed, (b); NiHCF was deposited using multiscan cyclic voltammetry, (c); the electrode was galvanostatically activated in Ni alone, (d); only RuHCF was deposited using multiscan CV and (e); Ni and RuHCF were co-deposited from the same solution using multiscan cyclic voltammetry.

From these results, it is evident that nickel hexacyanoferrate (Figure 4.10, b) provided quite a well-defined response to AA, which was as expected from the literature [28]. This layer also provided a slight shift (approximately 20 mV) in the overpotential for AA oxidation. The type of layer is proposed to catalyse the oxidation of AA via surface layer mediated charge-transfer [17]. Considering the strong response obtained at the CFCME modified with this layer, it was assumed that the film electrocatalyses the oxidation of AA. A layer of galvanostatically deposited nickel oxide (Figure 4.10, c) also provided a well-defined signal, with a half-wave potential of approximately +0.30 V, which was considerably shifted from that of a bare carbon fibre (+0.44 V). This may be due to the high electrical conductivity of nickel (146 1/mohm-cm). When compared to their corresponding blank voltammograms (not shown), it was evident that there was a response to AA at both the RuHCF and NiRuHCF modified CFCMEs, but this response was clearly ill-defined in the potential range used, in contrast to layers (a) – (c). The process at approximately 0 V is possibly attributable to hexacyanoferrate deposited on the surface of the carbon fibre, with the shift in potential due to the more acidic medium. It can be clearly seen that the NiO,RuHCF modification layer provides the optimum response for the oxidation of AA, with a less positive half-wave potential compared to the other layers and a more clearly defined signal, especially when compared to the electrodes modified with ruthenium hexacyanoferrate and ruthenium-nickel hexacyanoferrate deposited in a single step. In addition, when compared to the bare CFCME, a decrease in the overpotential of AA oxidation of approximately 185 mV was observed, with an accompanying increase in signal (Figure 4.11).

As described in earlier sections, metal hexacyanoferrates are known to exhibit electrocatalytic behaviour. In this case, it is assumed that the NiO,RuHCF film provides a suitable catalytic surface for the oxidation of ascorbic acid. As for Prussian Blue, it is assumed that the metal hexacyanoferrate film is not permeable to the rather large ascorbic acid molecules, with the reaction process being controlled by mass transfer of a solute in solution to the film-solution interface and by electron exchange cross-electron transfer at the film-solution interface [22]. The shift in the potential for ascorbic acid oxidation at the modified CFCME for approximately 185 mV compared to the bare CFCME shows that the nickel oxide,ruthenium hexacyanoferrate layer can catalyse the oxidation of AA. A thorough electrochemical and spectroscopic investigation and characterisation of the nickel oxide,ruthenium hexacyanoferrate film (and the other layers investigated here), which is beyond the scope of this work, would be required in order to determine the exact electrocatalytic properties of the film.

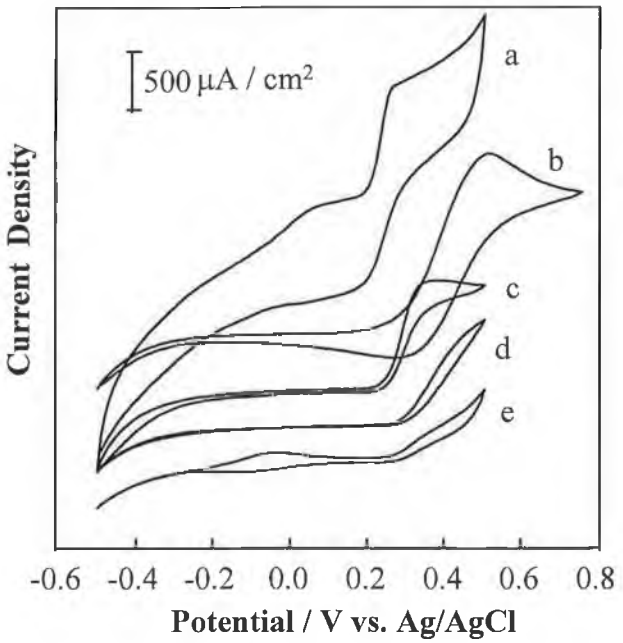

Figure 4.10: Cyclic voltammograms of 1 x 10^{-3} mol/L ascorbic acid in 0.01 mol/L HCl (pH 1.9) at CFCMEs modified with: (a) NiO,RuHCF, (b) NiHCF, (c) NiO, (d) RuHCF, (e) NiRuHCF; deposition solution compositions in text; no. of CV coatings (a) 22, (b) – (e) 25; scan rate 100 mV/s.

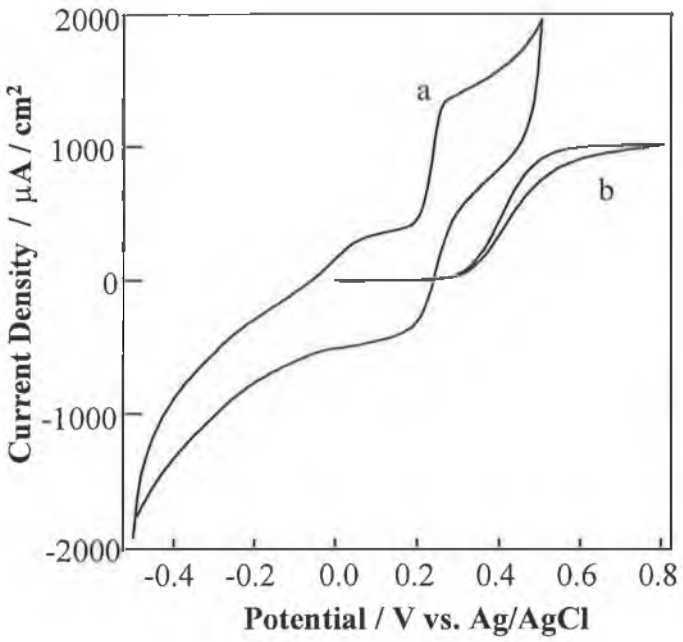

Figure 4.11: Cyclic voltammograms of 1 x 10^{-3} mol/L ascorbic acid in 0.01 mol/L HCl (pH 1.9) at (a) a NiO,RuHCF modified CFCME and (b) a bare CFCME. Operating parameters as in Figure 4.10.

In tandem with the previous experiments to determine that a two-step modification procedure for the NiO,RuHCF layer provided the optimum signal for ascorbic acid oxidation, this layer itself was optimised with respect to the oxidation of 1 x 10^{-3} mol/L AA. This optimisation was carried out in relation to the time of galvanostatic activation in the nickel solution and the thickness of the RuHCF layer, which is defined in terms of the number of CV runs. Figure 4.12 A shows the relative response to 1 x 10^{-3} mol/L AA with respect to galvanostatic activation time (25 layers of RuHCF were applied here). From this Figure, 10 s and 15 s provided the optimum signal for ascorbic acid oxidation. While there was a response when 2 s and 5 s deposition were used, it was likely that the amount of nickel oxide coverage was inadequate here, and hence not enough nickel oxide for the ruthenium hexacyanoferrate layer to deposit onto. At higher deposition times of 25 s and 40 s, the signal decreased significantly. Two possible reasons for this are a "too thick" nickel oxide layer or damage to the carbon fibre electrode caused by holding it at the high applied galvanostatic current for too long. In further experiments a deposition time of 10 s was chosen.

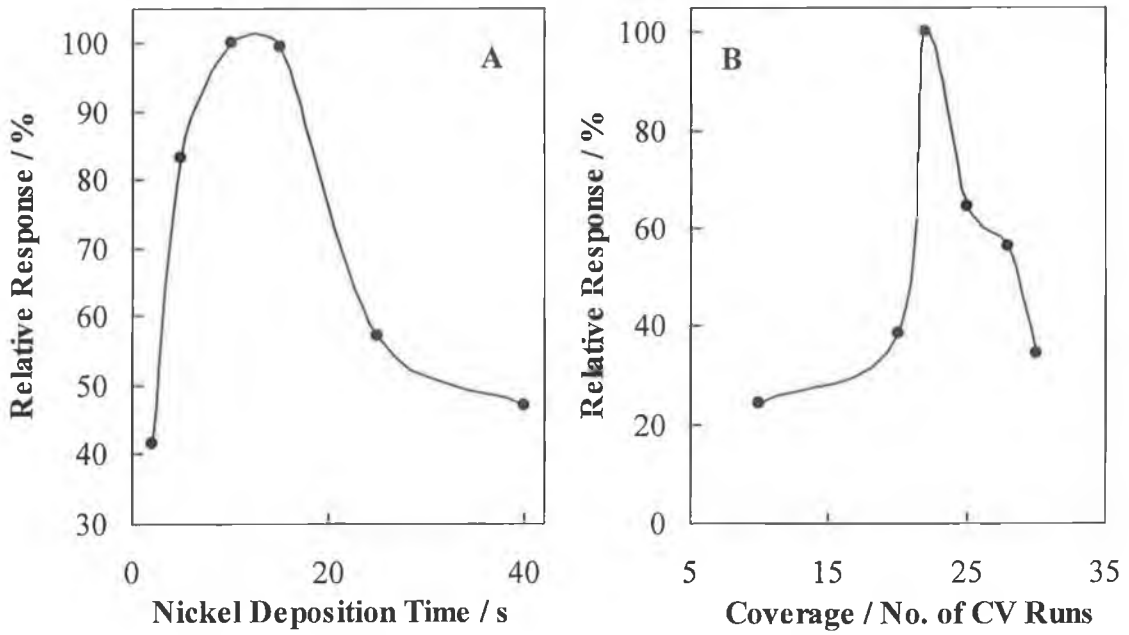

Figure 4.12: Optimisation of the NiO,RuHCF film. (A) Effect of nickel oxide deposition time and (B) Coverage / thickness of the RuHCF layer on the response to 1 x 10^{-3} mol/L ascorbic acid in 0.01 mol/L HCl; 25 layers of RuHCF in A; 10 s nickel deposition in B.

Figure 4.12 B shows the relative effect of the thickness of RuHCF on the oxidation of 1 x 10^{-3} mol/L AA. The nickel deposition time was 10 s. Here, it was apparent that 22 layers provided the optimum response to AA, with thinner or thicker films yielding lower anodic peak currents for the oxidation of AA. Similar behaviour has been observed at a CoHCF film for AA oxidation [29]. It was postulated that the thinner films do not provide a sufficient number of catalytic sites to handle the available supply of AA, while the thicker ones may form a resistive barrier to the delivery of electrons to the active sites. Considering the similarity in behaviour, it was assumed that this was also the case here. Based on these results, 10 s of galvanostatic activation and 22 layers of RuHCF were employed in subsequent experiments.

4.6.3 Preliminary Characterisation of NiO,RuHCF Modified Microsensor

As a preliminary investigation into the properties of the NiO,RuHCF modification layer, a brief spectroscopic study was carried out. The first simply involved taking optical photographs of the different layers. The results of this are shown in Figure 4.13.

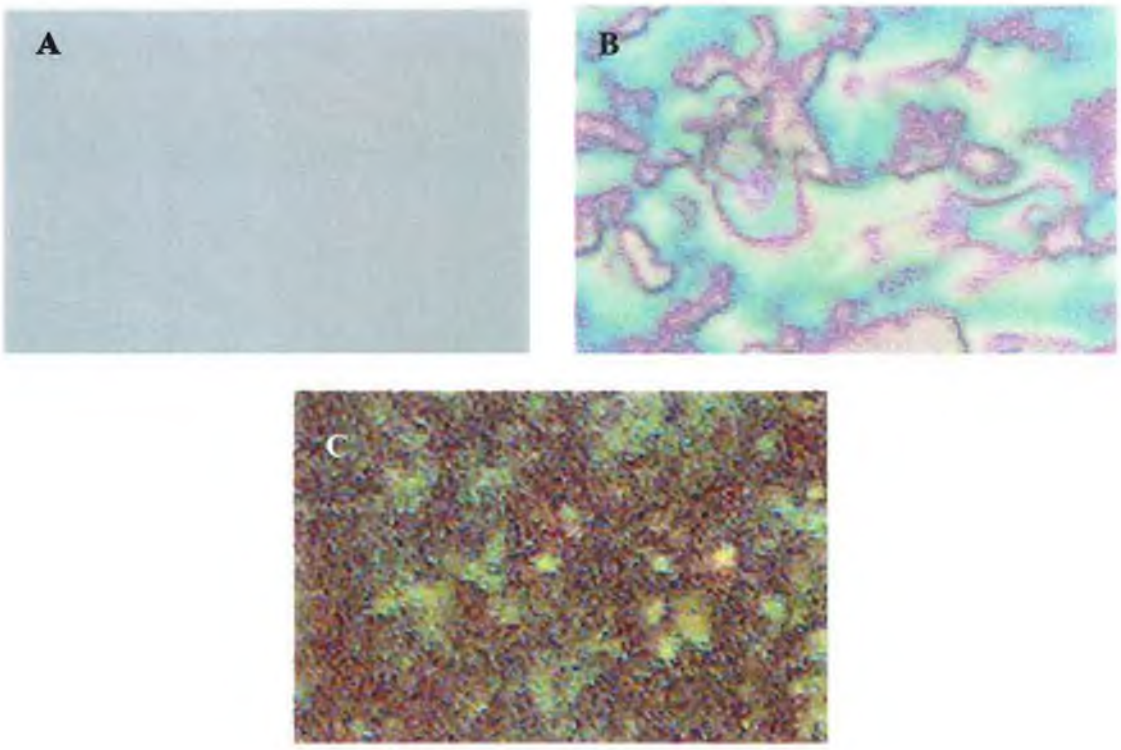

Figure 4.13: (A) Bare glassy carbon electrode, (B) Galvanostatically deposited nickel oxide layer, (C) B + RuHCF layer. Magnification x 400.

A bare glassy carbon electrode was used as the substrate electrode here rather than a carbon fibre in order to permit easier visualisation of the modification layers. Figure 4.13 A shows a typical optical photograph of a bare glassy carbon electrode, as a comparison between the bare electrode surface and the modified electrode. Part B shows an optical photograph of the galvanostatically deposited nickel oxide layer. This layer was green in colour and was present in what seemed quite a thick layer on the GC electrode surface. From Figure 4.13 C, it appeared that a composite layer of both components was formed as the structure was different from that in B, and also the colour indicated that it was a composite, with the lighter green areas originating from the nickel oxide layer and the darker from the ruthenium hexacyanoferrate layer.

The green colour of the nickel layer in the photograph above led to the belief that in fact nickel oxide (NiO) was deposited. Nickel metal is white in colour, while nickel oxide is green [99]. In addition, application of a positive current will lead to deposition of the metal oxide – if a negative current is applied the metal itself is reduced and deposited on the surface. Further evidence of the formation of a nickel oxide layer was provided upon analysis of the film surface with atomic force microscopy (AFM) and scanning electron microscopy (SEM). Figure 4.14 A and B display AFM and SEM micrographs of the nickel oxide layer, respectively. From the SEM micrograph in particular, cracks in the surface are visible. The film here is almost identical to that of a nickel oxide film (on HOPG) reported by Häring *et al.* [100], supporting the theory that nickel oxide is deposited during the galvanostatic deposition step. EDX spectra of this film revealed the presence of nickel (K_α, L_α and K_β lines) and oxygen, supporting the presence of a nickel oxide layer. Some sulphur (SK_α) was also present. This was attributed to sulphur in the nickel sulphate salt used in the deposition solution.

Figure 4.15 A and B display AFM and SEM micrographs of the nickel oxide,ruthenium hexacyanoferrate layer. The surfaces here are markedly different from those obtained for nickel oxide. The cracks are no longer visible, suggesting that cycling in the ruthenium hexacyanoferrate has "covered" them up. It is possible that cycling the nickel oxide surface at positive potentials in the solution containing ruthenium hexacyanoferrate caused the formation of oxide bridges leading to NiO,RuHCF. As the surface is not uniform in appearance, it is likely that some nickel oxide (and possibly some RuOHCF) is also present on the surface. EDX spectra of this surface revealed the presence of Ru(L_α), Ni(K_α) and Fe(K_α), supporting the presence of the nickel oxide, ruthenium hexacyanoferrate layer.

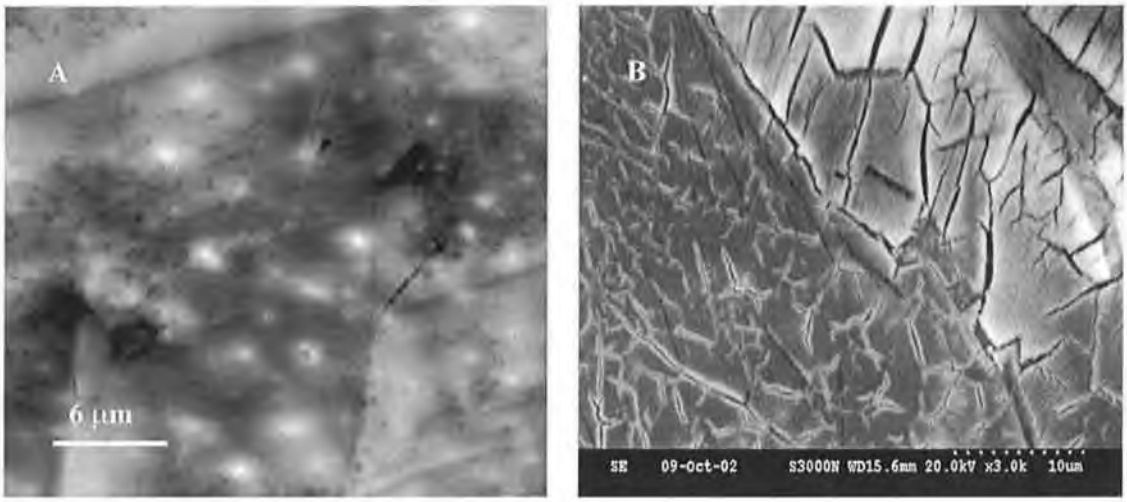

Figure 4.14: (A) Atomic force microscopy and (B) Scanning electron microscopy images of galvanostatically deposited nickel oxide layer.

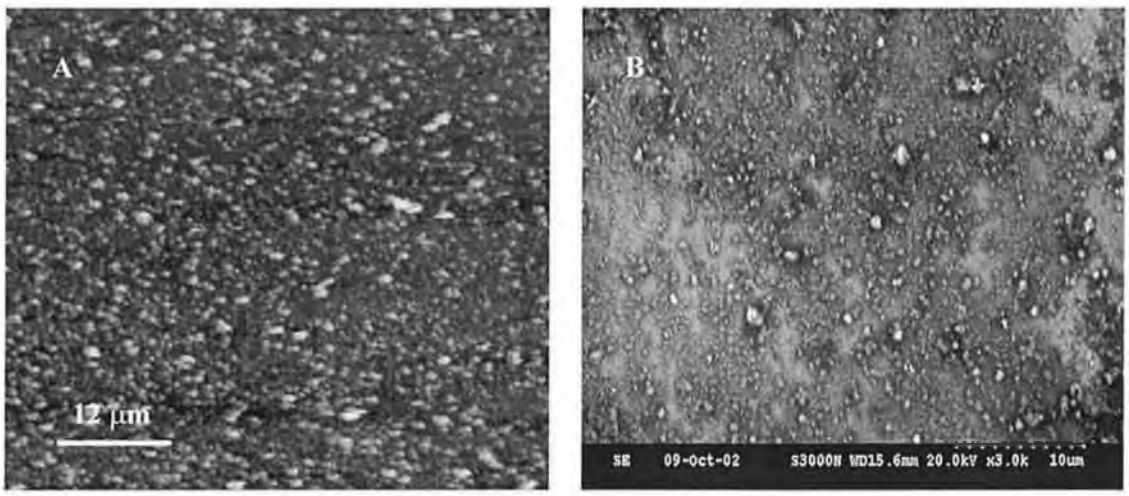

Figure 4.15: (A) Atomic force microscopy and (B) Scanning electron microscopy images of nickel oxide,ruthenium hexacyanoferrate layer.

4.6.4 Electrochemical Oxidation of Ascorbic Acid at the NiO,RuHCF Modified Microsensor

A cyclic voltammogram of ascorbic acid oxidation at the NiO,RuHCF modified carbon fibre is displayed in Figure 4.11. The process occurring at approximately +0.06 V was assumed to be due to hexacyanoferrate in the film. The nature of the processes occurring upon oxidation of ascorbic acid at the NiO,RuHCF layer were investigated by varying the scan rate in the range 5 to 150 mV/s. The results of this experiment are shown in Figure 4.16. Figure 4.16 A illustrates the dependence of current on the scan rate for 1 x 10^{-3} mol/L ascorbic acid. The relationship was not linear. However, the dependence of current on the square root of the scan rate (Figure 4.16 B) revealed a distinct linear relationship (r = 0.996). These results indicated that the reaction is controlled by diffusion. In contrast, the current response for the process at approximately +0.06 V was linearly dependent (r = 0.999) on the scan rate (Figure 4.16 A inset). This suggests that this process is a function of some redox active species confined to the surface of the electrode.

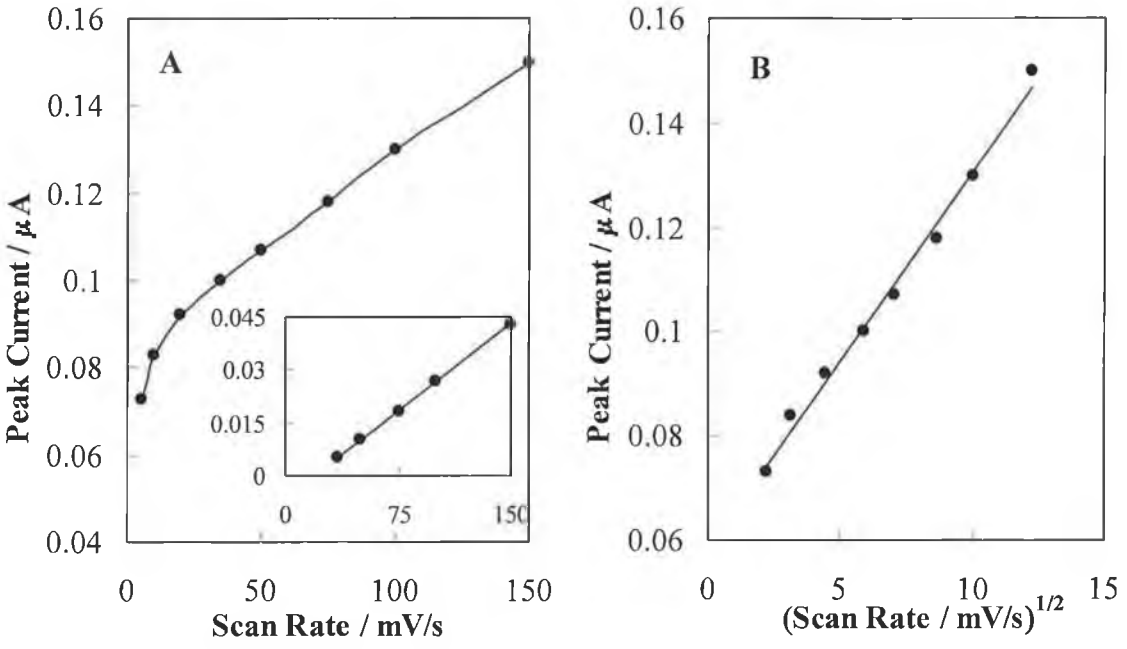

Figure 4.16: (A) Influence of scan rate and (B) influence of square root of scan rate on oxidation of 1 x 10^{-3} mol/L ascorbic acid in 0.01 mol/L HCl; (A) inset; influence of scan rate on process at approximately +0.06 V.

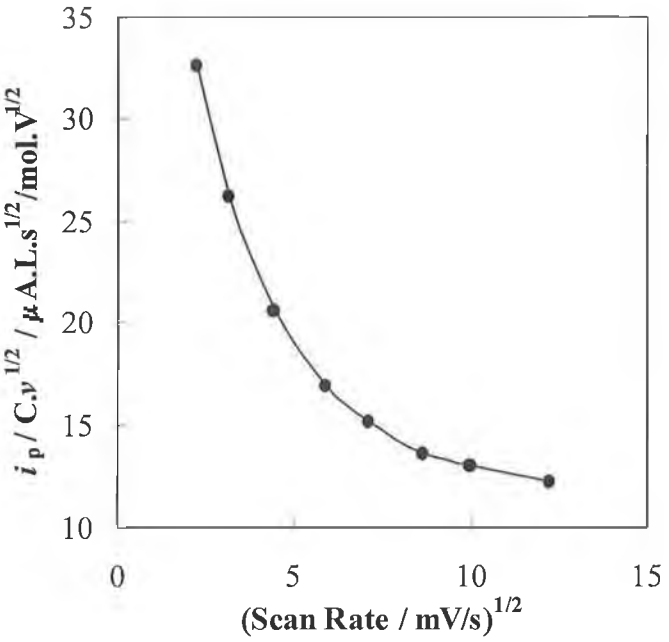

Figure 4.17: Current function vs. $v^{1/2}$ for 1 x 10^{-3} mol/L ascorbic acid in 0.01 mol/L HCl at the NiO,RuHCF modified CFCME.

With regard to the oxidation of ascorbic acid, a plot of $i_p/Cv^{1/2}$ (current function) vs. $v^{1/2}$, where C is the concentration of ascorbic acid (mol/L) and v is the scan rate (mV/s), exhibited a negative slope (see Figure 4.17), which is typical of a catalytic process involving a chemical reaction followed by an electron transfer process [64]. These results suggested that the electrocatalysis of ascorbic acid at the NiO,RuHCF layer also involved some chemical reaction.

4.6.5 Potential Effect on the Response of the Microsensor

While cyclic voltammetry is extremely useful and unique in elucidating the processes occurring at the working electrode, its analytical use is rather limited due to its inability to determine low levels of analytes. In addition, considering the rather unusual shape of the cyclic voltammogram for AA oxidation at the NiO,RuHCF modified microsensor, it would most likely be difficult to carry out any calibration using CV. For determination of low levels of analytes, pulsed techniques such as SWV and DPV are used. However, in measurements such as this modified microsensor is tailored for, amperometry is the most suitable electroanalytical technique, as this method permits "real-time" determination of levels of the target analyte. The most important operating parameter in amperometric measurements is

the applied potential, hence in any study the optimum operating potential must be obtained. In order to determine the optimum operating potential for amperometric measurements of ascorbic acid at the modified microsensor, the influence of the applied potential on the oxidation of ascorbic acid was investigated and a hydrodynamic voltammogram obtained. The polarized potential was observed to exert a significant effect upon the response of the NiO,RuHCF microsensor to AA.

Figure 4.18 demonstrates the influence of the polarized potential on the amperometric response to the addition of 50 μmol/L AA to 0.01 mol/L HCl solution. At a potential lower than +0.20 V (vs. Ag/AgCl), no response was observed. The current was observed to increase sharply from +0.275 V to +0.30 V and more slowly from +0.30 V to +0.35 V, clearly making this latter range sufficiently positive for AA oxidation. Although the current increased significantly at +0.40 V, it was observed that upon subsequent additions of AA (not shown), the current response decreased and became non-linear, possibly due to electrode fouling by the oxidation products of AA. The corresponding background current at this potential (+0.40 V) was also considerably higher than that at lower operating potentials. Since the possibility of interference from other electroactive components increases at higher potentials and background current will increase at higher potentials, the optimum potential selected was +0.30 V vs. Ag/AgCl. This potential also corresponds to an inflection point in the voltammogram, which is desirable for improved stability in current measurements [64]. Interestingly, the application of a potential of +0.30 V to a bare carbon fibre cylinder electrode for the oxidation of ascorbic acid produced no response, illustrating again the positive effect of the NiO,RuHCF layer on the overpotential for AA oxidation.

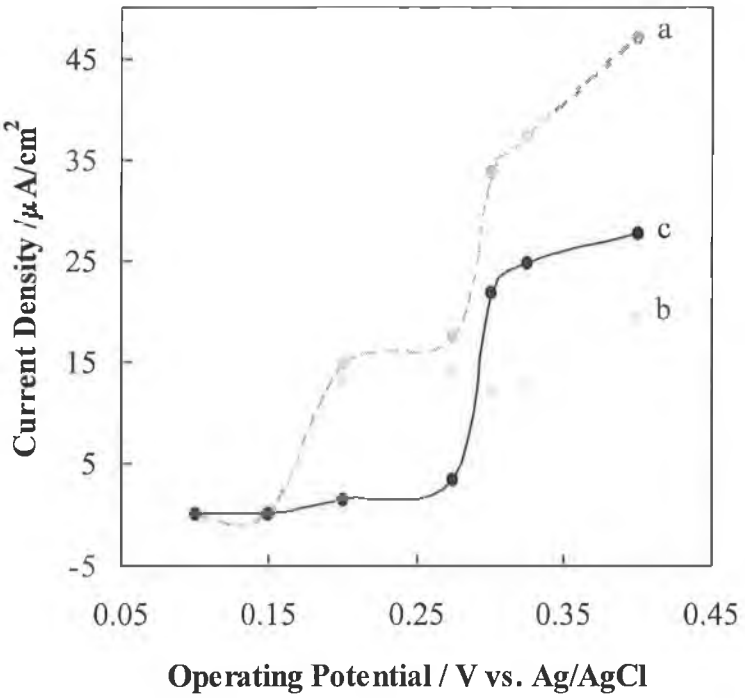

Figure 4.18: Hydrodynamic voltammogram for 50 μmol/L ascorbic acid at a NiO,RuHCF modified carbon fibre cylinder microelectrode (25 layers) in stirred 0.01 mol/L HCl; (a) signal obtained; (b) corresponding signal background; (c) signal minus background.

4.6.6 Analytical Performance of the NiO,RuHCF Modified Microsensor Under Acidic Conditions

Following selection of the optimum operating potential of +0.30 V, the performance of the NiO,RuHCF modified CFCME was tested under amperometric conditions. A preliminary experiment to verify the response of the microsensor to different concentrations of ascorbic acid was performed, with the results illustrated in Figure 4.19. From this figure, it is evident that the microsensor responded rapidly to the addition of varying concentrations of AA, with an almost immediate response of the microsensor upon addition of ascorbic acid to the working solution. After addition of the ascorbic acid, the current quickly stabilised and remained so until the next addition. The background contribution was very low, as evidenced by the smooth currents following the additions. Also included in this figure (inset) is a plot of the current response vs. the concentration of ascorbic acid added to the working solution ($r = 0.999$).

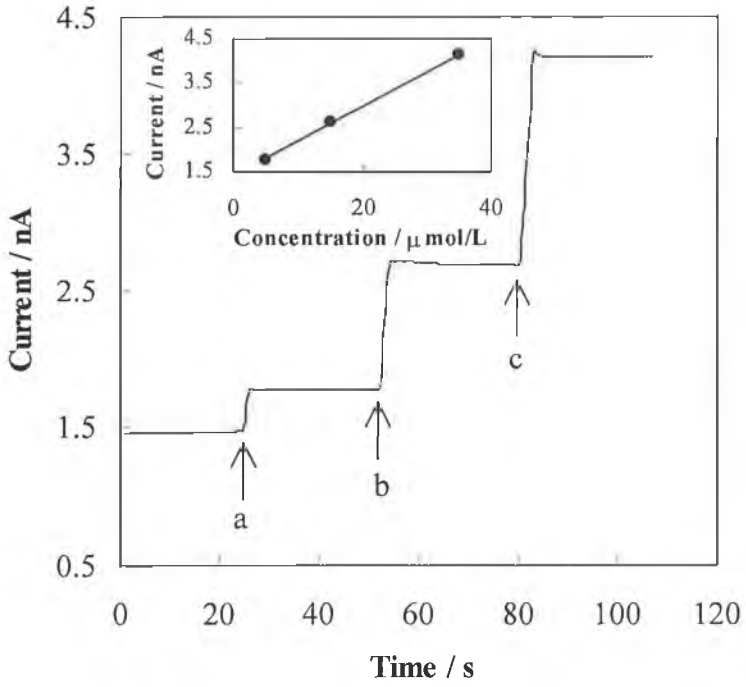

Figure 4.19: Typical amperogram at +0.30 V for additions of (a) 5 μmol/L, (b) 10 μmol/L and (c) 20 μmol/L of ascorbic acid to a stirred 0.01 mol/L HCl solution (pH 1.9) at a NiO,RuHCF (25 layers) modified CFCME. Inset: corresponding data.

The analytical performance of the NiO,RuHCF modified microsensor in determination of ascorbic acid in 0.01 mol/L HCl was very good. Employing the amperometric mode at an operating potential of +0.30 V, the signal-to-concentration relationship for increasing ascorbic acid concentration was linear over the range of 10 – 1610 μmol/L (n = 22), with a slope of 0.12 μA•L/μmol and a correlation coefficient (r) of 0.999. Figure 4.20 shows the amperogram from this experiment, with the inset displaying the corresponding calibration curve. From these results, it is evident that the NiO,RuHCF microsensor provides detection possibilities over the entire range of ascorbic acid levels encountered in human gastric juice. The reproducibility of ascorbic acid measurements at the NiO,RuHCF was quite good. Employing amperometry (at +0.30 V), the residual standard deviations (r.s.d.) for 6 consecutive additions of 10 μmol/L, 100 μmol/L and 300 μmol/L ascorbic acid to 0.01 mol/L HCl were 5.05 %, 4.06 % and 4.88 %. The slightly higher than expected r.s.d. obtained for the 300 μmol/L additions may have been due to some saturation of the microsensor surface, as the concentration here is quite high. The limit of detection

(based on S/N = 3) was calculated to be 1.53 μmol/L, which is consistent with experiments (not shown) in which even 2 μmol/L ascorbic acid elicited a response at the microsensor. The between-electrode reproducibility, considering the entire procedure, was also quite good. For 10 μmol/L and 100 μmol/L ascorbic acid measured at 5 different modified CFCMEs, the r.s.d.s were 8.97 % and 6.90 %, respectively. These calibration data reveal the excellent performance of the NiO,RuHCF modified microsensor and suggest its potential applicability in measurements of gastric juice ascorbic acid levels.

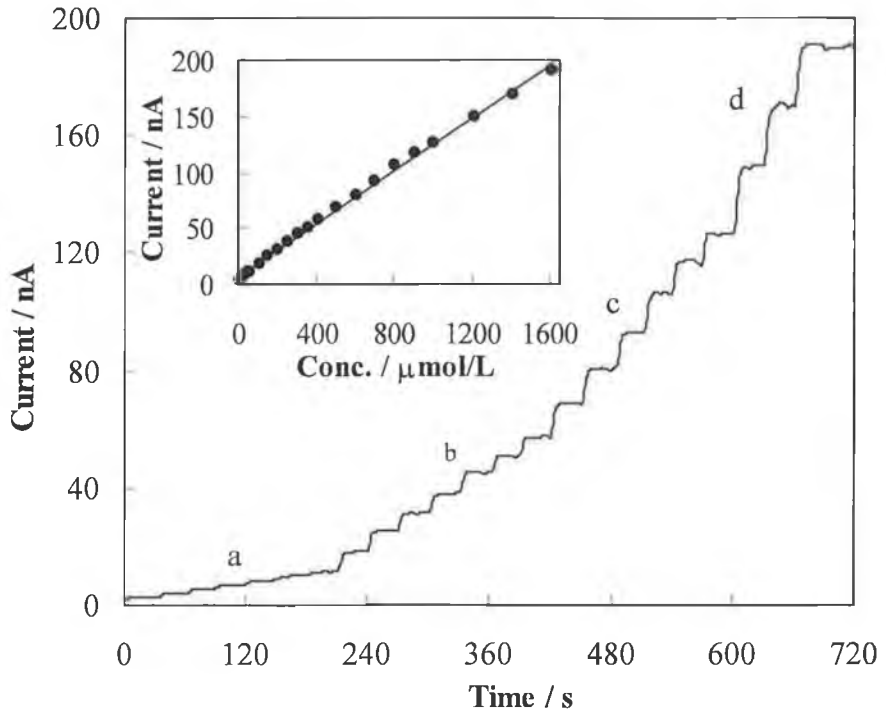

Figure 4.20: Increasing increments of ascorbic acid to 0.01 mol/L HCl; (a) 6 x 10 μmol/L, (b) 7 x 50 μmol/L, (c) 6 x 100 μmol/L, (d) 3 x 200 μmol/L; operating potential +0.30 V; inset: corresponding calibration curve.

Another interesting feature of the modified microsensor is its operational behaviour over time compared to that of the bare carbon fibre cylinder microelectrode. Figure 4.21 shows an amperogram obtained at a bare CFCME upon addition of 20 μmol/L increments of ascorbic acid to 0.01 mol/L HCl. While the current was observed to increase rapidly upon addition of ascorbic acid, the increase was not linear. After the third addition, upon addition of more AA, the current was observed to decrease from

its initial value, with this decrease becoming more marked as the number of additions increased. In comparison, at the modified microsensor (see Figure 4.20 above), there was no such tailing off in current when increasing amounts of ascorbic acid were added to the working solution. Indeed, after the final (10^{th}) addition of 20 μmol/L AA, the current at the bare CFCME was observed to tail off quite rapidly. For comparative purposes, the corresponding response of the modified microsensor is included in Figure 4.21 (*). Here, the current remains at the same initial level over the same period of time in which the current at the bare CFCME diminishes considerably.

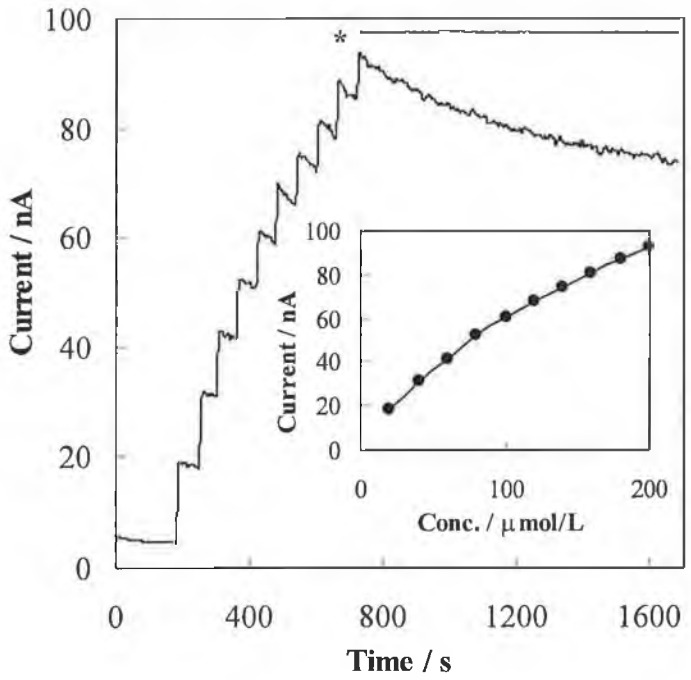

*Figure 4.21: Consecutive 20 μmol/L additions of ascorbic acid to 0.01 mol/L HCl at the bare CFCME; * corresponding response at the NiO,RuHCF modified CFCME; inset: corresponding data; operating potential +0.50 V.*

The response of the NiO,RuHCF modified microsensor over a prolonged period of use was also tested. The modified microsensor was first tested over 6 hours employing amperometry at +0.30 V, by periodically adding 20 μmol/L increments of ascorbic acid, under stirring conditions, to 0.01 mol/L HCl. 20 μmol/L AA was chosen as a concentration which related closely to the amount of ascorbic acid secreted by the human stomach (18 μmol/L per hour). Following this, the

microsensor was stored overnight in 0.01 mol/L HCl, tested the following day over a period of 2 hours, stored again overnight in 0.01 mol/L HCl, tested the following day over a period of 2 hours, stored again overnight in 0.01 mol/L HCl and tested again for 1 hour. This represents a total working time of 11 hours, with the total elapsed time from the first measurement to the last of 75 hours. After a further 67 hours storage in 0.01 mol/L HCl, the response was poor, and characterised by a very high background signal. The r.s.d. for 112 measurements of 20 μmol/L ascorbic acid over this entire time (i.e. 75 hours) was 16.08 %. This is quite good reproducibility for a relatively low concentration of ascorbic acid, indicating that the modified microsensor can be used in direct measurements of AA under acidic conditions such as those encountered in gastric juice over a prolonged period. Considering the above results with the bare CFCME, in which the signal decreased significantly over a short period of time, the modified microsensor offers a further advantage (in addition to the reduction in overpotential for ascorbic acid oxidation) in AA detection.

4.6.7 Performance of the NiO,RuHCF Modified Microsensor in Model Solution and Real Gastric Juice

The gastrointestinal system consists of the gastrointestinal tract and associated glandular organs that produce secretions. The major physiological functions of the gastrointestinal system are to digest foodstuffs and absorb nutrient molecules into the blood stream [101]. The gastrointestinal system carries out these functions by *motility* (movements that mix and circulate the gastric contents and propel them along the tract), *secretion* (processes by which the glands associated with the tract release water and substances into the tract), *digestion* (the process by which food and large molecules are chemically degraded to produce smaller molecules that can be adsorbed across the wall of the gastrointestinal tract), and *absorption* (the processes by which nutrient molecules are absorbed by cells that line the gastrointestinal tract and enter the bloodstream). The process which is of greatest interest in any determination of a compound in the gastrointestinal system is secretion, as this process will potentially secrete substances that may interfere with the desired analytical signal. Hence, in a study such that described here, it was necessary to test the NiO,RuHCF modified microsensor in a "model solution", in order to determine whether the microsensor would ultimately be employable in a real gastric matrix.

The major secretions of the stomach are hydrochloric acid, pepsins (enzymes), intrinsic factor (a glycoprotein), mucus (carbohydrate), bicarbonate (salt), while other substances present may include proteins, sugars, other salts and hormones [101]. Obviously, the health and diet of an individual will influence the composition of the gastric matrix, although these substances may be considered as the primary components present in the stomach. With these substances in mind, the following were considered in the "model solution";

- *Thiocyanate;* the concentration of the thiocyanate anion in saliva is approximately 1 mmol/L and even higher in smokers, and it may be secreted directly into gastric juice. Thiocyanate is a powerful catalyst of the nitrosation of secondary amines by nitrite under acidic conditions, and its delivery into the acidic environment of the stomach has therefore been regarded as a potentially important source of endogenous formation of carcinogenic nitroso compounds [11].
- *Glucose*; the exact concentration of glucose in the stomach is difficult to determine. Its level in blood is in the mmol/L range, so it was decided to use a concentration of 2 mmol/L in the model solution.
- *Protein solution*; varying concentrations of protein were used in this study, with the upper level used being 20%.
- *Sodium nitrite*. As mentioned in the first part of this chapter, ascorbic acid reacts with (is oxidised by) nitrite in the stomach. Hence, $NaNO_2$ was added in order to demonstrate the reaction of ascorbic acid with NO_2 and illustrate the concurrent reduction in current signal at the NiO,RuHCF modified CFCME.

In order to determine the possibility of interference of the above compounds with the detection of ascorbic acid at the NiO,RuHCF modified carbon fibre cylinder microelectrode, the cyclic voltammetric response of the microsensor to potassium thiocyanate, glucose and sodium nitrite was investigated. The resulting cyclic voltammograms are shown in Figure 4.22. Figure 4.22 A shows the response obtained when 1 mmol/L of KSCN was added to the supporting electrolyte of 0.01 mol/L HCl. While an oxidation response at ca. +0.60 V was evident, this was not expected to interfere with the signal for ascorbic acid oxidation achieved at an amperometric operating potential of +0.30 V. The response of the NiO,RuHCF microsensor to 2 mmol/L glucose is shown in Figure 4.22 B. Glucose elicited almost no response in the employed range, and hence was not expected to interfere with AA

determination at +0.30 V. It was also determined that nitrite (1 mmol/L $NaNO_2$) exhibited no oxidation response at the operating potential employed for amperometric determination of AA. There was a reduction process at approximately –0.4 V, but this was not expected to interfere at the employed potential of +0.30 V.

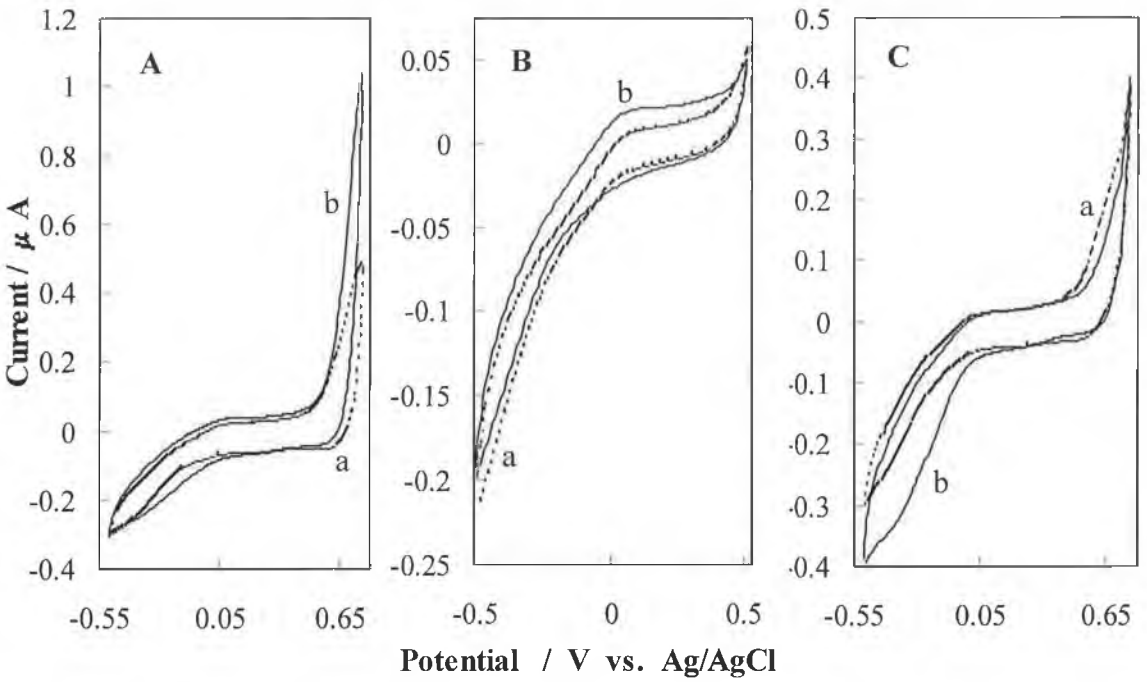

Figure 4.22: Cyclic voltammograms of substances in "model solution" experiments; (a) 0.01 mol/L HCl, (b) a + additions of (A) 1 mmol/L KSCN; (B) 2 mmol/L glucose; (C) 1 mmol $NaNO_2$ at NiO,RuHCF modified; scan rate 100 mV/s.

Figure 4.22 illustrated that the constituents considered as composing a "model solution" for gastric juice elicited no response at a potential of +0.30 V. A preliminary amperometric experiment was carried out in order to determine if the "model solution" components were electroactive under amperometric conditions at +0.30 V. The results of this are shown in Figure 4.23, in which the addition of 1 mmol/L potassium thiocyanate (at 30 s), 2 mmol/L glucose (at 60 s) and 10 % standard protein solution (at 90 s) failed to induce any change in signal at the NiO,RuHCF modified CFCME. In contrast, addition of ascorbic acid into the model solution at μmol/L levels generated a strong response at the microsensor. Addition of a large excess (~ 17 times) of $NaNO_2$ resulted in a rapid and sharp reduction in the current for AA, which was due to reaction between the ascorbic acid and the nitrite,

with the nitrite being converted to nitric oxide and the ascorbic acid simultaneously being oxidised to dehydroascorbic acid.

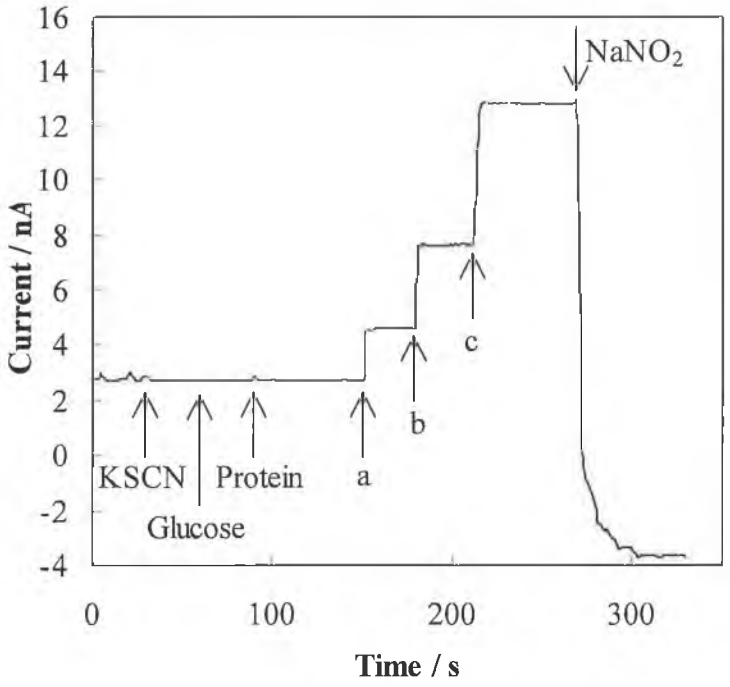

Figure 4.23: Typical amperogram for additions of 1 mmol/L potassium thiocyanate, 2 mmol/L glucose and 10 % standard protein solution to 0.01 mol/L HCl, with subsequent additions of (a) 10 µmol/L, (b) 20 µmol/L, (c) 40 µmol/L ascorbic acid, and 1.2 mmol/L sodium nitrite; operating potential: +0.30 V; arrows indicate the time of addition.

It is also interesting to note that oxidation of the ascorbic acid to dehydroascorbic acid was not the sole reaction which took place in this experiment. Following addition of the excess $NaNO_2$, the signal not only diminished to the level corresponding to 0.01 mol/L HCl (i.e. background signal), it decreased further, possibly due to the reduction of NO (a product of the reaction between AA and $NaNO_2$). Reduction of NO has been reported on PB-modified ITO electrodes at potentials of ca. +0.1 V (vs. Ag/AgCl) in pH 2 solution [102]. Such a reduction may also occur at the metal hexacyanoferrate modified electrode employed in this work, with the difference in potentials being accounted for by a number of factors (e.g. different electrode substrate materials, composition of modifier, supporting electrolyte, etc.)

Following this preliminary experiment, in which it was determined that the model solution components were inactive under the employed conditions, this type of experiment was expanded upon. 1 mmol/L KSCN, 2 mmol/L glucose and 10 % protein were added to 0.01 mol/L HCl. 10, 20 and 40 μmol/L ascorbic acid were subsequently added to this solution under stirring conditions at an applied potential of +0.30 V, with each addition resulting in a sharp increase in the observed current. Following this, 50 μmol/L $NaNO_2$ was added. The results of this experiment are shown in Figure 4.24. As expected, addition of 50 μmol/L $NaNO_2$ caused the current to decrease, rapidly at first and then more slowly. 40 μmol/L AA was then added, with the current decreasing immediately after the initial increase. This was due to AA reacting with NO_2. A further 50 μmol/L of $NaNO_2$ was then added to the solution and the current was observed to diminish even further. Ascorbic acid was added again in 6 additions of 40 μmol/L, whereupon in each case, the current was observed to decrease rapidly to the baseline level following the initial increase due to AA addition. It is also of interest to note that the magnitude of the current response to 40 μmol/L ascorbic acid after addition of NO_2 to the AA containing solution is diminished. It was assumed that this was either due to (i) fouling of the electrode due to the presence of protein in the solution or (ii) catalysis of the reaction between AA and NO_2 in the presence of KSCN, which is known to catalyse this reaction [11]. The second was thought to be more likely and subsequent experiments (not shown) proved that the presence of KSCN in the solution caused this type of behaviour. This type of experiment could be potentially useful in monitoring the effect of KSCN on the catalysis of the reaction between ascorbic acid and nitrite.

A further experiment to monitor the reaction between ascorbic acid and NO_2 was carried out. In order to correctly monitor the exact reaction, the model solution components were omitted from the working solution. In this experiment, 5 additions of 40 μmol/L ascorbic acid were added to the supporting electrolyte of 0.01 mol/L HCl. As seen from Figure 4.25, upon each addition, the current, as expected, was observed to increase rapidly and sharply. Upon addition of 100 μmol/L $NaNO_2$, the current was observed to decreased quickly initially, with the reaction gradually slowing. Three further additions of 40 μmol/L AA caused the current to increase again, with addition of 200 μmol/L $NaNO_2$ again causing a reduction in the current response. Addition of 200 μmol/L $NaNO_2$ resulted in a much larger initial decrease in

the current when compared to 100 μmol/L $NaNO_2$. Following this addition, the reaction was allowed to proceed for a considerably longer time (9 min vs. 2 min for 100 μmol/L $NaNO_2$). During this time, the current was observed to decrease to the baseline level, indicating that ascorbic acid and nitrite continued to react even after a considerable time. Further addition of AA again results in an increase in the current.

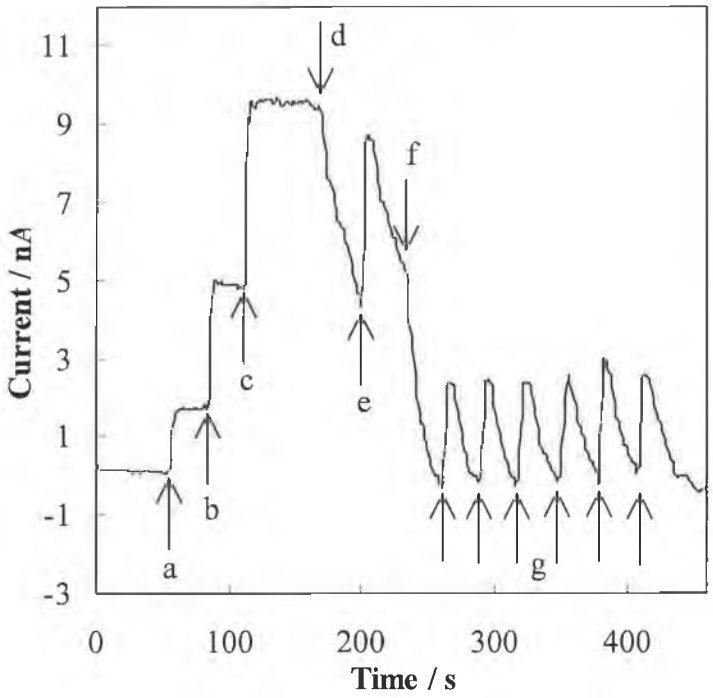

Figure 4.24: Effect on NO_2 on ascorbic acid oxidation signal; addition of (a) 10 μmol/L AA, (b) 20 μmol/L AA (c) 40 μmol/L AA, (d) 50 μmol/L $NaNO_2$ (e) 40 μmol/L AA, (f) 50 μmol/L $NaNO_2$ and (g) 6 x 40 μmol/L AA to a solution of 0.01 mol/L HCl containing 1 mmol/L KSCN, 2 mmol/L glucose and 10 % protein solution; operating potential +0.30 V.

It was noticed that after addition of 100 μmol/L $NaNO_2$, the average current for the subsequent AA additions was reduced by approximately 20-25 %, when compared to the initial five additions. Considering this decrease, it was expected that upon addition of 200 μmol/L $NaNO_2$, a further decrease in the current for AA would be observed. However, this did not occur. It was assumed that upon addition of 100 μmol/L $NaNO_2$, 2 minutes was not enough time for the reaction to go to completion, and hence subsequent amounts of AA added were immediately consumed

in the reaction between AA and $NaNO_2$. This theory is supported by the fact that upon addition of a further 200 μmol/L, with a period of 9 minutes left between this and the subsequent AA additions, the average current for 40 μmol/L AA was the same as that of the AA additions after the first addition of 100 μmol/L $NaNO_2$. These results suggest the potential applicability of the modified microsensor in monitoring the reaction between ascorbic acid and nitrite under acidic conditions.

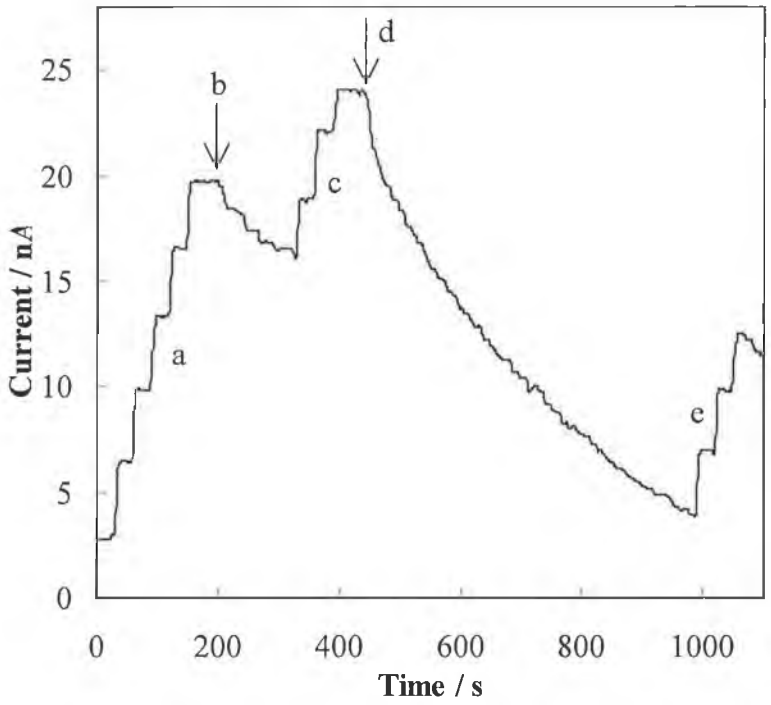

Figure 4.25: Effect on NO_2 on ascorbic acid oxidation signal; addition of (a) 5 x 40 μmol/L AA, (b) 100 μmol/L $NaNO_2$, (c) 3 x 40 μmol/L AA, (d) 200 μmol/L $NaNO_2$ (e) 3 x 40 μmol/L AA to a solution of 0.01 mol/L HCl; operating potential +0.30 V.

The above results have indicated the potential applicability of the NiO,RuHCF modified CFCME in determination of ascorbic acid under acidic conditions, especially over a prolonged period. However, in considering future use in real gastric medium, it becomes evident that the microsensor must be protected from fouling by macromolecular components present in the gastric juice matrix. The simplest way of protecting the microsensor surface from fouling is to apply a protective membrane layer. In this study, Nafion® and cellulose acetate were considered as possible protective coverings. Nafion® is a perfluorinated polymer that contains small

proportions of sulfonic or carboxylic ionic functional groups, and is often applied in *removing* ascorbic acid interferences when detecting other analytes with similar oxidation overpotentials, e.g. nitric oxide [103]. These measurements are usually at approximately neutral pH, where ascorbic acid is in the negatively charged ascorbate anion form and hence is repelled from the negatively charged Nafion® film. However, at the acidic pH employed in this work, neutrally charged ascorbic acid was expected to pass through the Nafion® membrane. Cellulose acetate is derived from natural cellulose and has been used as a protective electrode coating [104].

The NiO,RuHCF modified microsensors were further modified with either Nafion® or cellulose acetate membranes using a laboratory-made dip-coating device. Following application of the respective protective membranes, a simple experiment was carried out to investigate which membrane was more suitable for further study. In these measurements, successive increments of ascorbic acid were made to a working solution of 0.01 mol/L HCl and the response of the modified microsensor monitored. From a comparison of both sets of results, it was determined that cellulose acetate was more suitable for ascorbic measurements in acidic medium than Nafion®. At low concentrations of ascorbic acid (10 μmol/L additions), the cellulose acetate covered microsensor exhibited a more favourable performance over that of the Nafion® covered microsensor. In addition, at higher concentrations, the background current at the Nafion® covered microsensor was slightly higher than at the cellulose acetate covered CFCME. The response time upon addition of AA to the working solution at the Nafion® coated microsensor was also slightly slower, possibly due to some repulsion of the ascorbic acid. Hence, a cellulose acetate membrane (6 layers of cellulose acetate) was employed in subsequent measurements.

Further to the investigations in model solution described above (Figure 4.24 and Figure 4.25), the cellulose acetate covered NiO,RuHCF modified CFCME was applied in measurement of AA in a model gastric juice solution containing a high concentration of protein. As the purpose of this experiment was to determine the behaviour of the NiO,RuHCF modified microsensor covered with a protective membrane, KSCN was replaced with NaCl in order to permit investigation without any interference from the KSCN catalysed reaction of ascorbic acid with nitrite. The model solution was composed of 1 mmol/L NaCl, 2 mmol/L glucose and 20 % protein solution. Four additions of 20 μmol/L ascorbic acid were made to this

solution, followed by 100 μmol/L $NaNO_2$, with this sequence repeated after 5 minutes. Figure 4.26 shows the results obtained for this experiment. Even in the presence of a high concentration of protein solution, the response of the microsensor was good, with the current remaining steady after each addition of ascorbic acid. Fouling of the microsensor surface by proteins present in the solution was prevented by the presence of the cellulose acetate protective membrane. From this figure, one can see that the results were similar to those obtained Figure 4.25. Again, a possible reason for the disparity between the currents obtained for the ascorbic acid additions may have been due to insufficient time for the reaction to complete. It is also possible that the presence of the membrane caused some hindrance to ascorbic acid reaching the electrode surface.

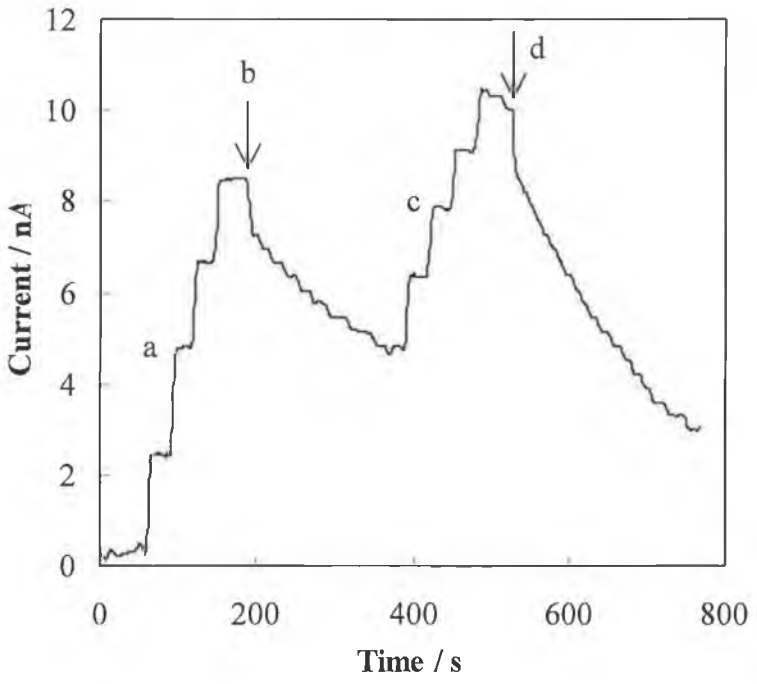

Figure 4.26: Response of cellulose acetate membrane covered NiO,RuHCF modified microsensor to addition of (a) 4 x 20 μmol/L AA, (b) 100 μmol/L $NaNO_2$, (c) 4 x 20 μmol/L AA and (d) 100 μmol/L $NaNO_2$ to a solution containing 1 mmol/L NaCl, 2 mmol/L glucose and 20 % protein; operating potential +0.30 V.

The above experiments revealed the potential for use of the modified microsensor in acidic and model solution media. However, in order to prove the microsensor's suitability for application in real gastric juice medium experiments, it was necessary

to determine the performance of the microsensor in this medium. Figure 4.27 shows cyclic voltammograms of increasing concentrations of ascorbic (0 to 3 mmol/L in 0.5 mmol/L increments) to a solution of 1:1 (v/v) gastric juice / 0.01 mol/L HCl. From this figure, it is evident that the NiO,RuHCF modified microsensor responds well even in a medium composed of real gastric juice. The redox process at approximately 0 V was more pronounced here than that in Figure 4.11. It is possible here that there was some interaction between the macromolecular components of the gastric juice matrix and the NiO,RuHCF film, thus implying the necessity for application of the cellulose acetate membrane as described in the previous results.

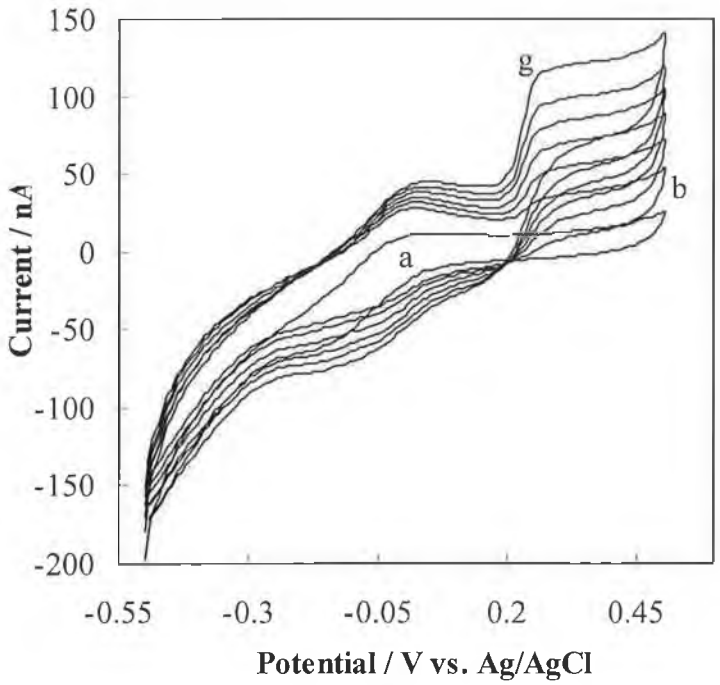

Figure 4.27: Cyclic voltammograms of (a) 50/50 gastric juice / 0.01 mol/L HCl and (b) – (g) a + increasing increments of 0.5 mmol/L ascorbic acid; scan rate 100 mV/s.

Further evidence for the necessity of a protective covering was obtained upon determinations of ascorbic acid in pure gastric juice matrix. Figure 4.28 A shows an amperogram obtained at the NiO,RuHCF modified microsensor without a protective membrane covering, upon addition of 4 x 20 μmol/L, 6 x 100 μmol/L and 2 x 200 μmol/L ascorbic acid to pure gastric juice matrix. The response here, especially at the lower concentrations was very poor and ill-defined. At higher concentrations of 100 μmol/L, the current increase was quite well-defined, but the

increase became non-linear. This was attributed to fouling of the microsensor surface with macromolecular components present in the gastric juice. In stark contrast, the analytical performance of the cellulose acetate covered NiO,RuHCF modified microsensor was greatly improved. An amperogram displaying its response upon addition of 6 x 20 μmol/L, 6 x 50 μmol/L and 5 x 100 μmol/L amounts of ascorbic acid to pure gastric juice is shown in Figure 4.28 B. While the current response upon most additions was good, some "bumps" in the amperogram could be attributed to disturbance of the solution upon insertion of the pipette tip into the gastric juice. In such cases, due to the opaque nature of the solution, and small working solution volume of 2 mL, addition of ascorbic acid was somewhat difficult, and it was likely that the pipette tip approached the microsensor surface thus disturbing the double layer around the microsensor.

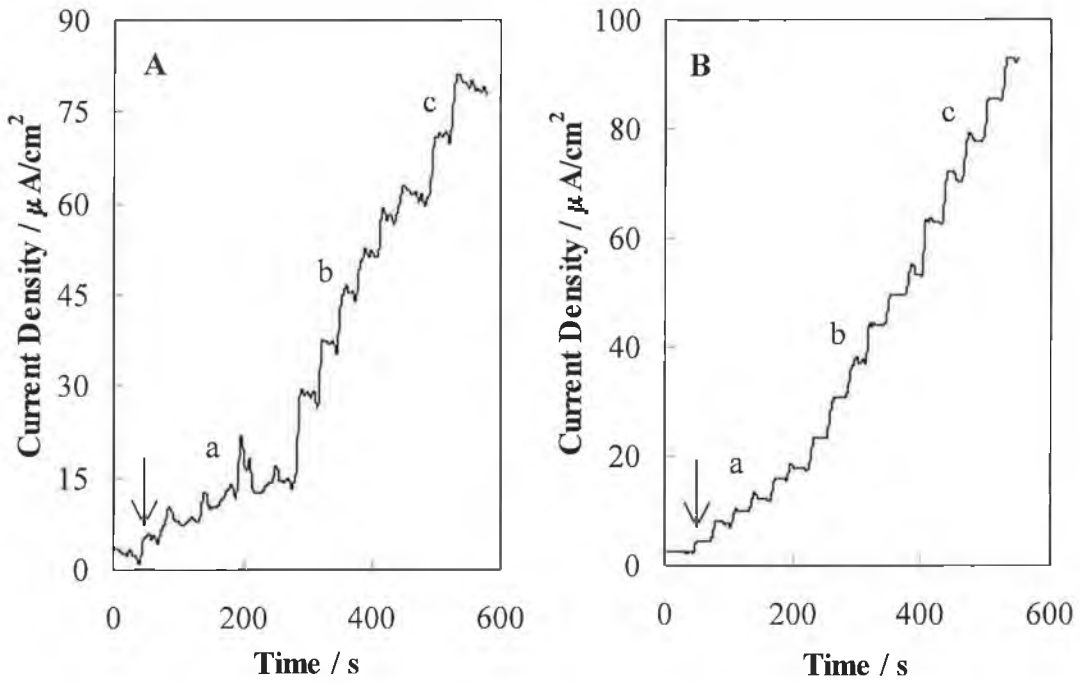

Figure 4.28: (A) Amperogram at NiO,RuHCF modified microsensor for additions of (a) 4 x 20 μmol/L, (b) 6 x 100 μmol/L and (c) 2 x 200 μmol/L ascorbic acid to pure gastric juice (pH 2.8) and (B) amperogram at NiO,RuHCF modified microsensor covered with a protective cellulose acetate membrane for additions of (a) 6 x 20 μmol/L, (b) 6 x 50 μmol/L and (c) 5 x 100 μmol/L ascorbic acid to pure gastric juice (pH 2.8); operating potential +0.30 V. Arrows indicate time of first addition.

As it is difficult to see the correlation between the current and concentration of ascorbic acid in Figure 4.28 B, Figure 4.29 shows the corresponding data for this figure. The calibration curve for increasing ascorbic acid concentration was linear over the range of 20 to 420 μmol/L, with a slope of 0.02 μA•L/μmol and a correlation coefficient of 0.999. At higher concentrations, there was a deviation in linearity. This may have been due to some inhibition of access of high concentrations of ascorbic acid to the electrode surface by the cellulose acetate membrane. The results shown in Figure 4.28 and Figure 4.29 indicate the possibility of employing the NiO,RuHCF modified CFCME with a protective cellulose acetate membrane in measurements of ascorbic acid in gastric juice.

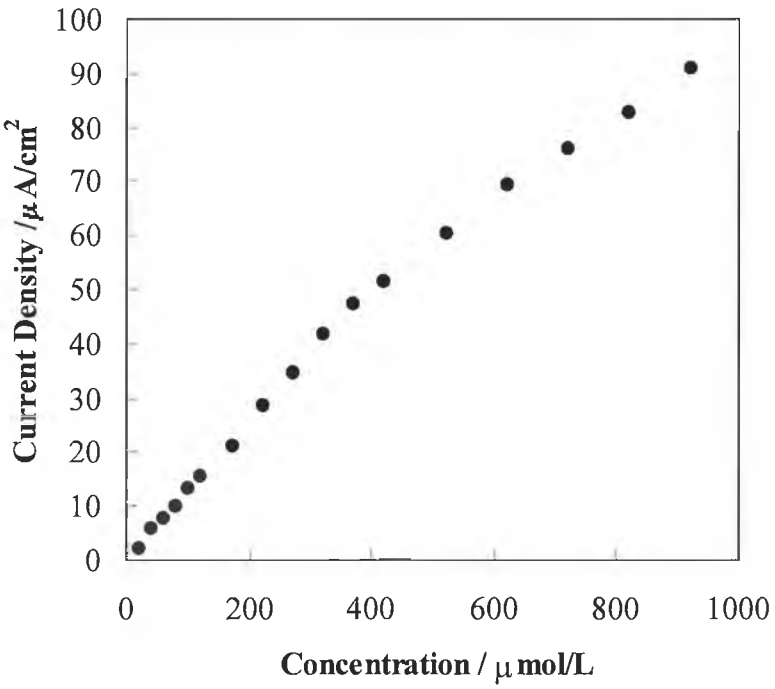

Figure 4.29: Data corresponding to Figure 4.28 B.

4.7 Conclusions

This Chapter introduced the nickel oxide,ruthenium hexacyanoferrate (NiO,RuHCF) modified carbon fibre cylinder microelectrode (CFCME) as a microsensor for the determination of ascorbic acid in gastric juice. The Chapter opened with a description of ascorbic acid and its functions and roles in the prevention of gastric cancer. A literature review provided insights into the techniques commonly used in the measurement of ascorbic acid in a variety of media. Metal hexacyanoferrates as electrode modifiers were also introduced, and some details regarding their application in determining a variety of substances described.

In the first part of the Results and Discussion section, some preliminary results concerning the application of CFCMEs modified with various mixed metal hexacyanoferrates in the oxidation of ascorbic acid in acidic medium were provided. The most favourable results were obtained for a CFCME, which was first galvanostatically activated in nickel solution and then cycled in a solution containing ruthenium hexacyanoferrate. This microsensor provided a decrease in overpotential for ascorbic acid oxidation of approximately 185 mV when compared to that of the bare CFCME. In addition, in contrast to the bare carbon fibre, the modified microsensor exhibited favourable behaviour with respect to the signal-to-concentration ratio, with a wide linear range, and stable response over time.

The modified microsensor was further modified with a cellulose acetate protective membrane to prevent fouling of the surface of the microsensor with macromolecular components present in gastric juice matrix. This microsensor was then successfully applied in the determination of μmol/L levels of ascorbic acid in model gastric juice and real gastric juice medium.

4.8 References

1. http://ntp-server.niehs.nih.gov/htdocs/LT-Studies/TR247.html
2. SIDS Data Set on L-Ascorbic Acid (Vitamin C): http://www.chem.unep.ch/irptc/sids/volume4/part1/ascorbic/sidsdata.html
3. I.P. Ronchetti, D. Quaglino, G. Bergamini, in: *Subcellular Biochemistry, vol. 25: Ascorbic Acid: Biochemistry and Biomedical Cell Biology*, J.R. Harris (ed.), Plenum Press, New York, 1996.
4. K.A. Head, *Alternative Medicine Review* 3 (1998) 174.
5. OECD High Production Volume Chemicals Programme – Phase 3, *SIDS Initial Assessment Report, L-Ascorbic acid CAS No. 50-81-7*: http://www.chem.unep.ch/irptc/sods/volume4/part1/ascorbic/oecd_rep.html.
6. http://www.healthandage.com/html/res/com/ConsSupplements/VitaminCAscorbicAcidcs.html
7. M. Hayat, S. Everett, *Nutrition* **15** (1999) 402.
8. A.G. Fraser, G.A. Woollard, *J. Gastroen. Hepatol.* **14** (1999) 1070.
9. C.J. Schorah, G.M. Sobala, M. Sanderson, N. Collis, J.N. Primrose, *Amer. J. Clin. Nutr.* **53** (1991) 287S.
10. I.T.M. Vermeer, E.J.C. Moonen, J.W. Dallinga, J.C.S. Kleinjans, J.M.S. van Maanen, *Mutat. Res.-Fund. Mol. M.* **428** (1999) 353.
11. A. Moriya, J. Grant, C. Mowat, C. Williams, A. Carswell, T. Preston, S. Anderson, K. Iijima, K.E.L. McColl, *Scand. J. Gastroentero.* **37** (2002) 253.
12. G.M. Sobala, C.J. Schorah, M. Sanderson, M.F. Dixon, D.S. Tompkins, P. Godwin, A.T.R. Axon, *Gastroenterology* **97** (1989) 97.
13. M.A. Choi, B.S. Kim, R. Yu, *Cancer Letters* **136** (1999) 89.
14. M.J. Sanderson, C.J. Schorah, *Biomed. Chromatogr.* **2** (1987) 197.
15. A.J. Waring, C.J. Schorah, *Clin. Chim. Acta* **275** (1998) 137.
16. P.J. Kulesza, M.A. Malik, J. Skorek, K. Miecznikowski, S. Zamponi, M. Berrettoni, M. Giorgetti, R. Marassi, *J. Electrochem. Soc.* **146** (1999) 3757.
17. M.H. Pournaghi-Azar, H. Razmi-Nerbin, *J. Electroanal. Chem.* **456** (1998) 83.
18. IUPAC, *Pure Appl. Chem.* **70** (1988) 1301.
19. A.A. Karyakin, *Electroanalysis* **13** (2001) 813.
20. A.A. Karyakin, E.E. Karyakina, *Sens. Actuators B* **57** (1999) 268.

21. X. Zhang, J. Wang, B. Ogorevc, U.E. Spichiger, *Electroanalysis* **11** (1999) 945.
22. S. Dong, G. Che, *J. Elecroanal. Chem.* **315** (1991) 191.
23. S.S.L. Castro, V.R. Balbo, P.J.S. Barbeira, N.R. Stradiotto, *Talanta* **55** (2001) 249.
24. S.J. Reddy, A. Dostal,. F. Scholz, *J. Electroanal. Chem.* **403** (1996) 209.
25. S. Sauter, G. Wittstock, *J. Solid State Electrochem.* **5** (2001) 205.
26. S.M. Chen, *Electrochim. Acta* **43** (1998) 3359.
27. J. Kukulka-Walkiewicz, J. Stroka, M.A. Malik, P.J. Kulesza, Z. Galus, *Electrochim. Acta* **46** (2001) 4057.
28. M.H. Pournaghi-Azar, H. Razmi-Nerbin, B. Hafezi, *Electroanalysis* **14** (2002) 206.
29. C.X. Cai, H.X. Ju, H.Y. Chen, *Anal. Chim. Acta* **310** (1995) 145.
30. D.R. Coon, L.J. Amos, A.B. Bocarsly, P.A. Fitzgerald Bocarsly, *Anal. Chem.* **70** (1998) 3137.
31. G. Shi, J.Lu. X. Fang, F. Xu, W. Sun, L. Jin, K. Yamamoto, S. Tao, J. Jin, *Anal. Chim. Acta.* **391** (1999) 307.
32. C.X. Cai, K.H. Xue, S.M. Xu, *J. Electroanal. Chem.* **486** (2000) 111.
33. R. Garjonyte, A. Malinauskas, *Sens. Actuators B* **56** (1999) 93.
34. M.S. Lin, T.F. Tseng, W.C. Shih, *Analyst* **123** (1998) 159.
35. J.W. Mo, B. Ogorevc, X. Zhang, B. Pihlar, *Electroanalysis* **12** (2000) 1.
36. D.R. Shankaran, S.S. Narayanan, *Fres. J. Anal. Chem.* **364** (1999) 686.
37. J. Wang, X. Zhang, *Anal. Lett.* **32** (1999) 1739.
38. P.J. Kulesza, K. Miecznikowski, M.A. Malik, M. Galkowski, M. Chojak, K. Caban, A. Wieckowski, *Electrochim. Acta* **46** (2001) 4065.
39. P.J. Kulesza, K. Miecznikowski, M. Chojak, M.A. Malik, S. Zamponi, R. Marassi, *Electrochim. Acta* **46** (2001) 4371.
40. T.R.I. Cataldi, G.E. De Benedetto, *J. Electroanal. Chem.* **458** (1998) 149.
41. T.R.I. Cataldi, G. De Benedetto, A. Bianchini, *J. Electroanal. Chem.* **471** (1999) 42.
42. B. Berthelemy, *Analusis* **24** (1996) 95.
43. S.P. Arya, M. Mahajan, P. Jain, *Anal. Sci.* **14** (1998) 889.
44. S.P. Arya, M. Mahajan, P. Jain, *Anal. Chim. Acta* **417** (2000) 1.
45. M.C. Yebra-Biurrun, *Talanta* **367** (2000) 367.

46. W.Y. Chung, J.K.O. Chung, Y.T. Szeto, B. Tomlinson, I.F.F. Benzie, *Clin. Biochem.* **34** (2001) 623.
47. N. Furusawa, *Food Control* **12** (2001) 27.
48. D. Madigan, I. McMurrough, M.R. Smyth, *Anal. Commun.* **33** (1996) 1.
49. L. Suntornsuk, W. Gritsanapun, S. Nilkamhank, A. Paochom, *J. Pharm. Biomed. Anal.* **28** (2002) 849.
50. N. Lenghor, J. Jakmunee, M. Vilen, R. Sara, G.D. Christian, K. Grudpan, *Talanta* **58** (2002) 1139.
51. K. Grudpan, K. Kamfoo, J. Jakmunee, *Talanta* **49** (1999) 1023.
52. A. Molina-Díaz, I. Ortega-Carmona, M.I. Pascual-Reguera, *Talanta* **47** (1998) 531.
53. T. Kleszczewski, E. Kleszczewska, *J. Pharm. Biomed. Anal.* **29** (2002) 755.
54. G. Wingsle, T. Moritz, *J. Chromatogr. A* **782** (1997) 95.
55. J.C. Deutsch, J.A. Butler, A.M. Marsh, C.A. Ross, J.M. Norris, *J. Chromatogr. B* **726** (1999) 79.
56. M.L. Cheng, T.Z. Liu, F.J. Lu, D.T.Y. Chiu, *Clin. Biochem.* **32** (1999) 473.
57. M.W. Davey, G. Bauw, M.V. Montagu, *J. Chromatogr. B* **697** (1997) 269.
58. Z. Gao, A. Ivaska, T. Zha, G. Wang, P. Li, Z. Zhao, *Talanta* **40** (1993) 399.
59. J. Wu, J. Suls, W. Sansen, *Electrochem. Commun.* **2** (2000) 90.
60. Z.U. Bae, J.H. Park, S.H. Lee, H.Y. Chang, *J. Electroanal. Chem.* **468** (1999) 85.
61. V.S. Ijeri, P.V. Jaiswal, A.K. Srivastava, *Anal. Chim. Acta* **439** (2001) 291.
62. P. Janda, J. Weber, L. Dunsch, A.B.P. Lever, *Anal. Chem.* **68** (1996) 960.
63. G.D. Liu, Z.Q. Li, S.S. Huan, G.L. Shen, R.Q. Yu, *Anal. Lett.* **33** (2000) 175.
64. S.A. Wring, J.P. Hart, *Anal. Chim. Acta* **229** (1990) 63.
65. S.A. Wring, J. P. Hart, L. Bracey, B.J. Birch, *Anal. Chim. Acta* **231** (1990) 203.
66. I.G. Casella, M.R. Guascito, *Electroanalysis* **9** (1997) 1381.
67. P.J. O'Connell, C. Gormally, M. Pravda, G.G. Guibalt, *Anal. Chim. Acta* **431** (2001) 239.
68. H. Wang, Z. Wu, J. Tang, R. Teng, E. Wang, *Electroanalysis* **13** (2001) 1093.
69. J. Tang, Z. Wu, J. Wang, E. Wang, *Electroanalysis* **13** (2001) 1315.
70. A.M. Yu, H.Y. Chen, *Anal. Chim. Acta* **344** (1997) 181.
71. Z. Gao, K.S. Siow, A. Ng, Y. Zhang, *Anal. Chim. Acta* **343** (1997) 49.
72. A.M. Yu, C.X. He, J. Zhou, H.Y. Chen, *Fres. J. Anal. Chem.* **357** (1997) 84.

73. M. Cheregi, A.F. Danet, *Anal. Lett.* **30** (1997) 2625.
74. A.M. Farrington, N. Jagota, J.M. Slater, *Analyst* **119** (1994) 233.
75. M. Wei, M. Li, N. Li, Z. Gu, X. Zhou, *Electroanalysis* **14** (2002) 135.
76. J.J. Xu, D.M. Zhou, H.Y. Chen, *Fres. J. Anal. Chem.* **362** (1998) 234.
77. J.J. Sun, D.M. Zhou, H.Q. Fang, H.Y. Chen, *Talanta* **45** (1998) 851.
78. R.A.A. Muñoz, R.C. Matos, L. Angnes, *Talanta* **55** (2001) 855.
79. R.C. Matos, L. Agnes, M.C.U. Araújo, T.C. B. Saldanha, *Analyst* **125** (2000) 2011.
80. C.R. Raj, K. Tokuda, T. Ohsaka, *Bioelectrochem.* **53** (2001) 183.
81. A. DeDonato, J.J. Pedrotti, I.G.R. Gutz, *Electroanalysis* **11** (1999) 1124.
82. A.G. Fogg, A.M. Summan, M.A. Fernández-Arciniega, *Analyst* **110** (1985) 341.
83. http://www.inform.umd.edu/EdRes/Colleges/AGNR/Depts/NutritionFood Science/Course_Information/NFSC450/week_11
84. A. Bagheri, F. Emami, M.R. Nateghi, *Anal. Lett.* **30** (1997) 2023.
85. E.M. Strochkova, Y.I. Tur'yan, I. Kuselman, A. Shenhar, *Talanta* **44** (1997) 1923.
86. R.C. Matos, M.A. Augelli, C.L. Lago, L. Angnes, *Anal. Chim. Acta* **404** (2000) 151.
87. L. Zhang, X. Lin, *Analyst* **126** (2001) 367.
88. R.D. O'Neill, *Analyst* **119** (1994) 767.
89. D.A. Kane, R.D. O'Neill, *Analyst* **123** (1998) 2899.
90. J.P. Lowry, M.G. Boutelle, R.D. O'Neill, M. Fillenz, *Analyst* **121** (1996) 761.
91. M. Miele, M. Fillenz, *J. Neurosci. Meth.* **70** (1996) 15.
92. S.V. Pacia, W.K. Doyle, P.A. Broderick, *Brain Res.* **899** (2001) 106.
93. W. Zhang, X.N. Cao, Y.Z. Xian, Q. Xu, S. Zhang, L.T. Jin, *Anal. Chim. Acta* **458** (2002) 337.
94. P.S. Cahill, R.M. Wightman, *Anal. Chem.* **67** (1995) 2599.
95. T.R.I. Cataldi, A.M. Salvi, D. Centonze, L. Sabbatini, *J. Electroanal. Chem.* **406** (1996) 91.
96. R. Vittal, H. Gomathi, G.P. Rao, *J. Electroanal. Chem.* **497** (2001) 47.
97. S.M. Chen, *J. Electroanal. Chem.* **521** (2002) 29.
98. S. Sinha, B.D. Humphrey, A.B. Bocarsly, *Inorg. Chem.* **23** (1984) 203.
99. *Handbook of Chemistry and Physics*, 80th Edition, ed. D.R. Lide, CRC Press, Boca Raton, 1999.

100. P. Häring, R. Kötz, G. Repphun, O. Haas, H. Siegenthaler, *Appl. Phys. A* **66** (1998) S481.

101. H.C. Kutchai, *Physiology*, 4th Edn., Ed. R.M. Berne *et al.*, Mosby Inc., St. Louis, Missouri (1998) Ch. 37-39.

102. K.C. Pan, C.S. Chuang, S.H. Cheng, Y.O. Su, *J. Electroanal. Chem.* **501** (2001) 160.

103. X. Zhang, Y. Kislyak, J. Lin, A. Dickson, L. Cardosa, M. Broderick, H. Fein, *Electrochem. Commun.* **4** (2002) 11.

104. M.I. Prodromidis, S.M. Tzouwara-Karayanni, M.I. Karayannis, P.M. Vadgama, *Analyst* **122** (1997) 1101.

5. CONCLUDING REMARKS AND SUGGESTIONS FOR FUTURE WORK

5.1 Introduction

Electroanalytical techniques, which are concerned with the interplay between electrical quantities such as current, potential or charge, and chemistry, have found widespread use in a vast range of applications, including industrial quality control, environmental monitoring, food testing and biomedical analysis. From its discovery over 200 years ago in Italy by Galvani, overwhelming advances (some of which have been described in Section 1.1) have been made in the field. Advances in recent decades such as the development of micro- and ultramicro-electrodes, progress in the methods of electrode modification, the coupling of biological components and electrochemical transducers, the synthesis of ionophores and receptors of molecular size, and the development of ultratrace voltammetric techniques and high-resolution scanning probe microscopies have lead to a substantial increase in the popularity of electroanalysis, and to its expansion into new areas and fields [1]. Its popularity can also be attributed to its attractive advantages, such as selectivity and sensitivity, inexpensive equipment, ample choice of working electrode materials, and ability to attain real-time measurements.

However, despite these apparent advantages, there seems to be a dearth in the use of such techniques in certain analytical laboratories in which routine analysis is performed. Indeed, consultation with colleagues in the pharmaceutical industry (7 different companies) revealed that the only applications in which electrochemistry plays a role in the laboratory are in conventional pH probes, conductivity detectors and coulometric Karl Fischer titrations. Considering the aforementioned advantages associated with electroanalytical procedures, why are they not more popular in routine analysis? There are several possible reasons for this. One of the primary reasons is surely the incorrect perception that such procedures are difficult to perform. Another reason lies in the properties of the most commonly employed electrode materials such as platinum, gold, glassy carbon and mercury. The limitations of the former three are primarily the necessity for electrode maintenance i.e. electrode cleaning by electo-chemical, chemical or manual polishing means. Although eminently suitable for

numerous applications for which solid electrodes are inappropriate, such as stripping analysis, mercury electrodes present a potentially serious hazard due to the toxic nature of mercury and its salts. Indeed, many countries are currently attempting to prohibit the use of mercury as an electrode material, component of dental amalgams, constituent of thermometers, etc.

In order to encourage the use of electroanalytical techniques in industries such as the pharmaceutical industry, it seems that much work is required to promote the advantages associated with such methods and to adequately train analysts in the understanding of electroanalytical theory and use of electroanalytical instrumentation. In addition, and perhaps most importantly, it is necessary to develop electroanalytical procedures that are simple to perform and employ convenient, easy to maintain and non-toxic electrode materials. The work described here attempts to address such matters, with relatively simple techniques employing non-toxic electrode materials being used to detect a range of substances of biomedical and environmental significance.

5.2 Chapter Two

The introduction of the bismuth film electrode (BiFE) as a new solid electrode material represents a step forward in the electrochemical detection of reducible organic compounds such as the nitrophenols. Such compounds are commonly detected oxidatively or reductively at bare glassy carbon electrodes or cathodically at mercury electrodes. The problems associated with these electrode materials include the requirement for regular regeneration of the glassy carbon electrode surface to remove adsorbed products from the electrode surface, and the toxic and inconvenient nature of mercury. The bismuth film electrode overcomes the drawbacks associated with the glassy carbon electrode by providing an electrode surface that is simply and conveniently renewed employing electrochemical means i.e., through simple electrochemical deposition and removal of the bismuth film, hence obviating the need for tedious electrode polishing. The properties of the BiFE with particular regard to the electrochemical reduction of the herbicide bromofenoxim and the nitrophenols,

closely resemble those of the mercury electrode, indicating that non-toxic bismuth represents a suitable replacement for mercury as an electrode material.

While the BiFE has been demonstrated as a suitable electrode material for the determination of nitrophenols in bulk voltammetric and flow injection-amperometric detection measurements, with low limits of detection achieved in both cases, it has yet to be applied in a real sample matrix. To further investigate the possibility of employing the BiFE in routine detection of nitrophenols, the system should be applied in the analysis of a real sample such as ground water, river water, or a soil extract. Such a study should first involve examination of the electrochemical behaviour of the nitrophenols at the BiFE in the presence of potential interferents including other reducible compounds potentially present in such samples, heavy metals, surfactants etc. in bulk voltammetric measurements. The next step should be an examination of nitrophenol behaviour at the BiFE in non-aqueous media, such as those commonly used in solid phase extraction and liquid chromatographic methodologies, again in the presence of potential interferents. Finally, the entire system i.e. the bismuth film preparation-measurement-electrode regeneration cycle should be tested using a real sample containing measurable levels of the nitrophenols. Another possibility is the coupling of the bismuth film electrode detection system to a liquid chromatography system to investigate the compatibility of the two.

The cathodic electrochemical detection of substances such as bromofenoxim, which are detectable solely at mercury electrodes, represents a further interesting avenue in the applications of the BiFE. Considering the interesting preliminary results obtained for the reduction of bromofenoxim at the BiFE, it would be interesting to more thoroughly investigate the behaviour of such compounds at the BiFE, thereby replacing toxic mercury electrodes.

5.3 Chapter Three

As mentioned in the previous section, the bismuth film electrode represents a potential complete replacement for toxic mercury electrodes. Nowhere is this more evident than in the application of the BiFE in the stripping analysis of heavy metals. Recent literature has shown that the BiFE is comparable and even superior to the

mercury electrode in the anodic stripping analysis of heavy metals such as lead, cadmium, zinc and copper. This work presents the adsorptive stripping voltammetric and potentiometric stripping analysis of trace cobalt and nickel in some low volume body fluids at the BiFE. In addition, the BiFE is employed in the determination of cobalt, nickel, lead, cadmium and copper in a number of soil extract samples, with the results obtained compared to those obtained using inductively coupled plasma-mass spectrometry (ICP-MS).

The behaviour of the BiFE in the determination of trace cobalt and nickel regarding operating parameters such as accumulation potential and time and analytical parameters such as linear range and limit of detection closely approximated that of the mercury film electrode (MFE). The BiFE revealed its superiority over the MFE in its behaviour towards dissolved oxygen. At the MFE, a distinct peak due to oxygen was observed in non-deoxygenated solution. In contrast, the presence of dissolved oxygen elicited no response at the BiFE. This fact represents an advantage over the MFE considering the possibility of employing the BiFE in on-site monitoring of heavy metals in, for example river water or biological fluids, as there is no requirement for sample deoxygenation. While the BiFE was successfully applied in the determination of trace cobalt and nickel in some low-volume body fluids, it would be interesting to apply the BiFE in a clinical study in order to assess its feasibility in measuring these trace elements in biological samples. The effects of interference from potential interferents present in such matrices should also be investigated.

Regarding the measurement of cobalt, nickel, lead, cadmium and copper in the soil extract samples, some further study is certainly necessary. The most important parameter to be investigated is the effect of UV treatment of the sample solutions in order to break down any dissolved organic matter present in the matrix. Such a step would surely improve the accuracy of measurements – both electroanalytical and ICP-MS. However, the preliminary results provided in this work indicate that the BiFE is indeed a suitable electrode surface for the determination of heavy metals in environmental matrices. The possibility of employing the BiFE to measure heavy metals "on site" is certainly an interesting concept. Such a determination would involve relatively simple and portable equipment – a laptop and a hand-held potentiostat – and would provide detection capabilities not possible with a large unwieldy instrument such as an ICP-MS or atomic absorption spectrometer.

5.4 *Chapter Four*

Considering the abundance of literature regarding the role of ascorbic acid (AA) in the prevention of gastric cancer, and the profusion of publications concerning the electrochemical detection of ascorbic acid, it is somewhat remarkable that a thorough search of the literature by the author revealed no electroanalytical methods for the direct determination of AA in gastric juice. The methods currently employed for measurement of AA levels in gastric juice involve a complicated sampling, storage and analysis procedure using HPLC with UV detection, hence the proposed microsensor represents a considerable advantage permitting real-time analysis of ascorbic acid in gastric juice. The nickel oxide,ruthenium hexacyanoferrate modification layer provided a reduction in overpotential for AA oxidation of approximately 185 mV when compared to the bare carbon fibre cylinder microelectrode (CFCME). In addition, the modified microsensor response was stable over a prolonged period of use in acidic solution, in contrast to the bare CFCME. The analytical parameters of linear range and limit of detection revealed the suitability of the modified CFCME for use in detection of AA at levels usually encountered in gastric juice. In addition, application of a cellulose acetate protective membrane permitted the use of the proposed microsensor in determination of low μmol/L quantities of ascorbic acid in real gastric juice. While the proposed microsensor was found to be suitable for direct measurements in gastric juice, the next step in this study requires an investigation into the possibility of its employment in a study such as that carried out in the field of gastric cancer research. This should involve tailoring the microsensor to permit its insertion into the gastric cavity. It would also be necessary to compare results obtained for ascorbic acid levels in gastric juice using the microsensor with another technique such as HPLC with UV detection.

5.5 *Other Interesting Concepts Considered in the Work*

In addition to the work described above, some other projects were initiated, with a view to developing suitable electrodes and sensors for the determination of some substances of environmental and biomedical significance. The first of these involved

the development of a modified microsensor for the selective determination of ascorbic acid in plant cells. The proposed microsensor was based on the coating of an over-oxidised poly(1,2)-phenylenediamine film on a carbon fibre cylinder microelectrode. This microsensor had previously been proved to be suitable for the simultaneous determination of ascorbic acid and dopamine at physiological levels [2]. This film selectively accumulates dopamine, while repelling ascorbic acid, hence permitting the determination of dopamine in the presence of a large excess of ascorbic acid. It was envisioned that varying the deposition parameters of the overoxidised poly(1,2)-phenylenediamine film would lead to different film properties, thereby permitting selective AA determination in plant cells. While some preliminary experiments were carried out in this direction, certain problems were encountered, which necessitated postponement of further work in this direction. Future work in order to determine whether the overoxidised poly(1,2)-phenylenediamine film is a suitable modification layer for AA determination in plant cells remains an interesting concept.

Inorganic nanotubes, which have received attention in recent literature [3-7], were employed as electrode modifiers in a preliminary study. The nanotubes (MoS_2) were suspended in solution of dimethylformamide (for self-assembly) or Nafion® (for dip-coating and drop-casting). Gold, carbon fibre and glassy carbon electrodes were modified by self-assembly, dip-coating and drop-casting, respectively. The behaviour of the modified electrodes was examined in two well-known redox systems - iron hexacyanoferrate and ruthenium hexamminechloride. As expected the electrodes showed activity towards these couples, but the results were inconclusive. In addition, the response of the nanotube modified electrodes to H_2O_2 and dopamine was investigated. The most interesting results were obtained with the gold electrodes modified with a self-assembled monolayer(s) of nanotubes. Two sharp peaks were observed in a solution of 0.1 mol/L KCl, which were attributed to some rapid redox system present on the electrode surface. At a glassy carbon electrode modified by drop-casting 10 μL of nanotube-containing suspension onto the electrode surface, some activity towards H_2O_2, which was not evident at the bare or just Nafion® modified electrode, was observed.

The results presented suggested that MoS_2 nanotubes may find some use as inorganic electrode modifiers in future work. It was considered that the concentration of nanotubes in the Nafion® and DMF solutions was too low at 1 mg/L, and that a

concentration of at least 10 mg/L would be necessary to properly characterise their electrochemical behaviour and electroanalytical properties. As this was just a preliminary study, much further work is required in these directions.

5.6 Conclusions

On successful completion of the work described in this chapter, it is envisaged that the proposed techniques could be used in the determination of a wide variety of analytes – reducible compounds, heavy metals and ascorbic acid in environmental and biological matrices. The techniques described are easy to perform and involve the use of relatively inexpensive equipment when compared to instrumental techniques such as ICP-MS or AAS. It is hoped that this work and others in the same vein will lead to further promotion of the advantages of electroanalytical techniques and result in their increased use in analytical laboratories carrying out both routine analysis and research.

5.7 References

1. J. Wang, *Analytical Electrochemistry*, second ed., Wiley-VCH, New York, 2000.
2. J.-W. Mo, B. Ogorevc, *Anal. Chem.* **73** (2001) 1196.
3. M. Remškar, A. Mrzel, Z. Škraba, A. Jesih, M. Ceh, J. Demšar, P. Stadelmann, F. Lévy, D. Mihailovič, *Science* **292** (2001) 479.
4. E. Furimsky, *Appl. Catal A: Gen.* **208** (2001) 251.
5. M. Remškar, Z. Škraba, P. Stadelmann, F. Lévy, *Adv. Mater.* **12** (2000) 814.
6. M. Remškar, A. Mrzel, A. Jesih, F. Lévy, *Adv. Mater.* **14** (2002) 680.
7. V. Kralj-Iglič, M. Remškar, G. Vidmar, M. Fošnarič, A. Iglič, *Phys. Lett. A* **296** (2002) 151.